EPFL

Thèse n° 7331

Motion planning for CAVs in mixed traffic, a study on roundabouts

Présentée le 24 avril 2020

à la Faculté des sciences et techniques de l'ingénieur
Groupe SCI STI DG
Programme doctoral en génie électrique

pour l'obtention du grade de Docteur ès Sciences

par

Ezequiel GONZÁLEZ DEBADA

Acceptée sur proposition du jury

Prof. M. Bierlaire, président du jury
Dr D. Gillet, directeur de thèse
Dr N. Fouquet, rapporteur
Dr F. Nashashibi, rapporteur
Prof. A. M. Alahi , rapporteur

École polytechnique fédérale de Lausanne

2020

Acknowledgment

First, I wish to express my gratitude to my supervisor, Denis Gillet, for the continuous support and the endless patience he showed while dealing with the most insecure version of myself. I still remember our first interview, and how surprised I felt that he saw enough potential in that younger me to offer him the Ph.D position that puts me here today.

I am very grateful to the international chair Drive-For-All, which co-funded this Ph.D. thesis with the support of the PSA Group, Safran, and Valeo.

I want to thank Arnaud de la Fortelle for his guidance and his excellent body of research, which inspired my very first baby steps. My sincere thanks also go to David Allard, Frederic Large, and Nicolas Fouquet, who put a considerable amount of time and effort into making our collaboration pay off and encouraged me to consider more realistic and practical aspects of the problem I studied.

I wish to thank every person that has passed by REACT during these years, as I believe this thesis is somewhat the result of having been exposed to such a wide variety of people and personalities. I would like to recognize the invaluable support of Laleh Makarem, who had to bear with me during the very first and steepest part of the professional and personal learning curve I went through. Thanks to Chus, Andrii, Wissam, Alex, and Maria, who showed me that sleeping is overrated, running makes you free, our bodies can handle an unthinkable amount of stress, complaining out loud sometimes helps, if complaining does not work a cold beer is not a bad plan B (sometimes it is an excellent plan A), and that no amount of sugar is ever enough. Thanks to all students that I was lucky to supervise, who made me push my limits and explore aspects that I could not have explored otherwise. I would like to specially mention to Adeline Ung, who helped me to get into one of the technical contributions that glues this thesis together.

I feel especially grateful to Juan Carlos, for his priceless help during the tough writing process, and for keeping me motivated in the hard last months of this journey. Also, I want to thank him for being there along with André, Clarisse, and Vânia, always ready to talk just about anything, spend quality time out of the office's walls, and feeling like family when the blood one is so far.

Thanks to my lifelong friends, Andrea, Sonia, and Helena, willing to skype for as long as it takes, and travel as far as we need to for the sake of keeping our friendship alive and my psychological health in line.

Thanks to my family, especially to my parents and sister, for believing in me and not losing faith. It is their support and the thought of failing them what gets me going in the hardest moments.

Last but foremost, thanks to my beloved wife Raquel for holding strong during this psychologically extreme adventure, for being understanding and supportive, and bringing me on track anytime I got off it. Thanks for everything you did to make me stay on my feet and for reminding me that there are way more important things that these pages put together.

Résumé

Bien que le fait de conduire puisse paraître anodin pour des conducteurs expérimentés, l'automatisation de cette simple tâche s'avère être beaucoup plus complexe en réalité. De manière générale, une telle complexité provient de la nécessité 1) d'être constamment en état d'alerte par rapport à son environnement et de prédire la manière dont il évolue dans un futur proche, 2) d'identifier et planifier les trajectoires possibles et pertinentes avec un certain degré d'anticipation, et 3) d'agir sur les actionneurs du véhicule, tels que le volant, le frein et l'accélérateur, afin de mener à bien les manoeuvres envisagées. Ces trois tâches clés représentent les thèmes de recherche principaux concernant la conduite autonome, à savoir la perception et la prédiction de l'environnement, la planification des trajectoires et le contrôle du véhicule.

Dans cette thèse, je traite des défis qui relèvent de la planification des trajectoires et des problèmes de décision de haut-niveau pour les véhicules automatisés connectés et dotés de systèmes de communication (CAVs) dans du trafic dit mixte, i.e. où cohabitent des conducteurs, des véhicules automatisés connectés (CAVs), et également des véhicules automatisés non connectés (AVs). Par ailleurs, bien que les travaux proposés aspirent à être valables dans tout contexte, leur évaluation est réalisée dans le cadre de ronds-points, étant donné qu'une grande partie des difficultés rencontrées dans la planification des trajectoires se retrouvent dans ce type d'intersections. En effet, les ronds-points constituent un scénario de test particulièrement idéal de par la complexité et la dynamique du trafic à l'intérieur de ceux-ci, de la présence d'incertitude élevée sur les intentions des véhicules et son impact sur les performances de coordination, et également de l'influence significative que représente les occultations causées par les véhicules et autres obstacles de l'environnement sur le processus de décision.

Dans cette dissertation, je présente une nouvelle approche concernant la manière dont l'espace autour de l'ego véhicule est représenté et décrit pour le module de planification de trajectoires. En particulier, contrairement aux méthodes classiques de planification basées sur la détection et l'évitement d'obstacles/objets, je m'intéresse à une alternative plutôt basée sur l'identification et l'exploitation des intervalles vides/libres, qui se révèlent être une stratégie plus pertinente dans la prise en compte d'occultations et d'autres incertitudes liées à la perception.

Les solutions pour la planification de trajectoires sont fondées sur des modèles et inspirées de la manière dont les conducteurs semblent décider de leurs actions au volant. Elles cherchent à prendre des décisions assurant non seulement sécurité mais également efficacité sans devoir explicitement explorer toutes les possibilités de trajectoires. Ainsi, je propose une représentation plutôt abstraite et à faible dimension des manoeuvres (de conduite) permettant de caractériser l'espace de solution du problème de décision à un haut niveau, qui est ensuite exploitée par une variété de stratégies de prise de décisions.

La structure de planification exposée ici traite de quatre approches de planification principales. Tout d'abord, une conduite purement réactive aux intervalles est formulée, ce qui constitue un solide point de comparaison malgré sa simplicité. Puis, une méthode de prise de décisions fondée sur des modélisations de trafic microscopique pour les CAVs dans des scénarios complètement connectés est étudiée, où le but est de permettre aux CAVs d'accomplir leurs manoeuvres ciblées tout en améliorant la qualité du trafic global à travers une coopération explicite basée sur la communication entre les véhicules. Ensuite, en atténuant l'hypothèse de connectivité entre véhicules, le problème d'assurer la coopération de véhicules automatisés non connectés (AVs) avec des véhicules standards à travers un pseudo mécanisme de coopération implicite est traitée. En outre, une stratégie prédictive-réactive de planification prenant en considération de plus longues durées de prédictions du trafic, qui potentiellement, peuvent être plus ou moins erronées est présentée. Finalement, la pertinence de certains des résultats théoriques est évaluée dans un contexte plus réaliste, notamment en appliquant les méthodes présentées sur des données réelles fournies par nos partenaires industriels.

Cette dissertation introduit de nouveaux concepts et méthodes pour aborder la complexité de la planification de trajectoires dans un trafic mixte, et traite de ses principaux défis grâce à une structure de planificateur polyvalente et à des stratégies pragmatiques de prise de décisions basées sur des modèles, ouvrant ainsi la voie à des solutions davantage réalisables, efficaces et fiables.
Keywords—automated vehicles, motion planning, decision-making, intelligent vehicles, connected automated vehicles, traffic coordination, trajectory planning, self-driving car, cooperative driving, uncertainty-aware planning, occlusion-aware planning, interaction-aware motion planning, intelligent transportation systems.

Abstract

DRIVING is a very challenging task to automatize despite how naturally and efficiently it may come to experienced human drivers. The complexity stems from the need to (i) understand the surrounding context and forecast how it is likely to evolve, (ii) plan maneuvers with a certain level of anticipation despite the uncertainty of the future traffic state, and (iii) act on the throttle and the steering wheel so that the planned motions are accurately executed. These three tasks match the fundamental research topics concerning autonomous driving, namely *perception* and *prediction*, *motion planning*, and *control*.

In this thesis, I study challenges related to motion planning and high-level decision-making for connected automated vehicles (CAVs) in mixed traffic. That is for CAVs that coexist with human drivers, other CAVs, and unconnected automated vehicles (AVs). Moreover, even though I intend to formulate the proposed methods in such a way that they are context agnostic, their assessment is carried out in roundabout scenarios, as all major problems a motion planner must address are somehow present at these intersections. Roundabouts are ideal testing scenarios due to the complexity of the traffic interaction and overall traffic dynamics, the impact that the uncertainty concerning the surrounding vehicles' driving intent has on the coordination performance, as well as the strong influence that dynamic occlusions of the surrounding space caused by nearby vehicles and environmental elements have on the decision-making process.

I propose a novel approach concerning how an AV's surrounding space is represented and described, which brings benefits to the motion planning module. Specifically, unlike the classical planning approach based on *object detection and avoidance*, I study an alternative planning strategy based on *free space identification and exploitation*, which is shown to be a more suitable mechanism to account for occlusions and other perception uncertainties.

My motion planning solutions are model-based and are inspired by the way human drivers seem to make decisions. I intend to formulate strategies whereby safe, yet efficient decisions can be made without the need of explicitly exploring all possible sequences of accelerations that the automated vehicle can follow. Instead, I propose a low-dimensional and rather abstract driving maneuver representation that enables me to characterize the solution-space of the decision-making problem at a rather high-level, which can then be exploited by a wide variety of decision-making strategies.

In particular, in this thesis I make use of the novel motion planning framework I propose to address four significant planning aspects. Firstly, a purely reactive gap-acceptance behavior is formulated, which represents an appropriate baseline behavior despite its simplicity. Afterward, I investigate a microscopic traffic-model-based decision-making approach for CAVs in fully connected scenarios, aiming at enabling CAVs to perform their targeted maneuvers while improving the overall traffic quality through communication-based cooperation. Then, I relax the connectivity assumption and address the challenge of making AVs cooperate with other unconnected vehicles through a

so-called implicitly cooperative mechanism. Furthermore, I tackle the design of a predictive-reactive planning strategy aimed to take into account longer traffic predictions, and the possibility of them being wrong. Finally, the suitability of some of the proposed theoretical results is assessed in a more realistic setup, where the methods are applied to a real data set provided by our industrial partners.

This dissertation provides new ideas and methods to address the complexity of motion planning in mixed traffic. Specifically, I tackle the problem through a versatile motion planning framework and a set of pragmatic model-based decision-making strategies, paving the way towards feasible, efficient, and more reliable solutions.

Keywords—automated vehicles, motion planning, decision-making, intelligent vehicles, connected automated vehicles, traffic coordination, trajectory planning, self-driving car, cooperative driving, uncertainty-aware planning, occlusion-aware planning, interaction-aware motion planning, intelligent transportation systems.

Contents

1 Introduction **23**
- 1.1 Introduction to autonomous driving . . . 24
- 1.2 State of the art . . . 25
  - 1.2.1 Motion planning and control . . . 25
  - 1.2.2 Motion planning and surrounding traffic . . . 26
  - 1.2.3 Motion planning and perception . . . 28
- 1.3 Scope and research questions . . . 29
- 1.4 Methodology . . . 31
- 1.5 Thesis structure . . . 31

2 Problem Formulation and Preliminaries **33**
- 2.1 Problem formulation . . . 33
  - 2.1.1 Notation . . . 35
- 2.2 Simulation platform . . . 35
  - 2.2.1 Simulation environment architecture . . . 36
  - 2.2.2 Definition of simulated roundabout geometry . . . 37
  - 2.2.3 Definition of simulated traffic configuration . . . 39
  - 2.2.4 Definition of vehicles' simulated behavior . . . 39
  - 2.2.5 Simulation engine . . . 40
  - 2.2.6 Analysis tools . . . 42
- 2.3 Traffic scenario . . . 42
  - 2.3.1 Roundabouts . . . 42
  - 2.3.2 Incoming traffic . . . 44
  - 2.3.3 Outgoing traffic . . . 45
  - 2.3.4 Scenario-labeling process . . . 46
- 2.4 Performance assessment . . . 46
  - 2.4.1 Traffic evolution . . . 47
  - 2.4.2 Traffic performance metrics . . . 49
- 2.5 Conclusions . . . 52

3 Perception Models **53**
- 3.1 Related work . . . 54
- 3.2 Perception post-processing . . . 56
  - 3.2.1 Object detection and classification . . . 56
  - 3.2.2 Dynamic occupancy grid . . . 57
  - 3.2.3 Gaps inference . . . 62

3.2.4 Perception models . . . 63
3.3 Results . . . 64
3.3.1 Dynamic occupancy grid evolution . . . 64
3.3.2 Probably-free gaps . . . 67
3.4 Conclusions . . . 67

4 Motion Planning **71**
4.1 Planning architecture . . . 73
4.2 Route planning . . . 74
4.3 Tactical planning . . . 75
4.3.1 Driving maneuver description . . . 75
4.3.2 Set of maneuver candidates . . . 77
4.4 Maneuver planning . . . 79
4.4.1 Self-serving planning submodule . . . 81
4.4.2 Cooperative planning submodule . . . 81
4.5 Trajectory planning . . . 82
4.5.1 Reactive approach . . . 82
4.5.2 Optimization-based approach . . . 83
4.6 Conclusions . . . 85

5 Reactive Self-Serving Planning **87**
5.1 Related work . . . 87
5.2 Problem formulation and assumptions . . . 88
5.3 Reactive maneuver planner . . . 89
5.3.1 Reactive maneuver target . . . 90
5.3.2 Maneuver target safety . . . 90
5.3.3 Gap-acceptance decision map . . . 91
5.3.4 Maneuver selection and scoring . . . 92
5.3.5 Planner outputs . . . 93
5.4 Results . . . 94
5.4.1 Decision-making . . . 94
5.4.2 Single traffic scenario . . . 94
5.4.3 Traffic coordination performance . . . 97
5.5 Conclusions . . . 101

6 Communication-Based Planning **105**
6.1 Related work . . . 107
6.2 Problem formulation and assumptions . . . 108
6.3 Planning approach . . . 109
6.3.1 Reachable maneuver target candidates . . . 110
6.3.2 Feasible virtual vehicle state . . . 111
6.3.3 Safe Virtual Vehicle insertion . . . 113
6.3.4 Traffic-model-based maneuver target scoring . . . 114
6.3.5 Maneuver selection . . . 116
6.3.6 Planner outputs . . . 116
6.3.7 Maneuver safety . . . 117
6.4 Results . . . 117

6.4.1 Decision-making examples . . . 118
6.4.2 Single traffic scenario . . . 119
6.4.3 Traffic coordination performance . . . 125
6.5 Conclusions . . . 126

7 Implicitly Cooperative Planning 129
7.1 Related work . . . 130
7.2 Problem formulation, assumptions, and preliminaries . . . 132
7.3 Gap-acceptance criterion . . . 132
7.4 Yielding maneuver planner . . . 134
7.4.1 Yielding trajectory . . . 135
7.4.2 Expected evolution of the front limit of the gap . . . 136
7.4.3 Feasibility of the yielding maneuver . . . 137
7.4.4 Minimum effort yielding maneuver . . . 138
7.4.5 Yielding maneuver scoring . . . 138
7.4.6 Maneuver selection and planner output . . . 140
7.5 Results . . . 140
7.5.1 Decision-making . . . 141
7.5.2 Single traffic scenario . . . 141
7.5.3 Traffic coordination performance . . . 144
7.6 Conclusions . . . 149

8 Predictive-Reactive Self-Serving Planning 151
8.1 Related work . . . 152
8.2 Assumptions and problem formulation . . . 153
8.3 Planning approach . . . 154
8.3.1 Safely reachable maneuver targets . . . 155
8.3.2 MT safety w.r.t. observed gaps . . . 160
8.3.3 Maneuver selection . . . 162
8.3.4 Planner output . . . 163
8.4 Results . . . 163
8.4.1 Safe approaching behavior . . . 164
8.4.2 Decision-making . . . 164
8.4.3 Single traffic scenario . . . 166
8.4.4 Traffic coordination performance . . . 169
8.5 Conclusions . . . 173

9 Application 177
9.1 Experimental setup and data set . . . 177
9.2 Application implementation description . . . 178
9.2.1 Scene processing . . . 180
9.2.2 Approaching roundabout . . . 182
9.2.3 Perception information . . . 182
9.2.4 Decision-making . . . 182
9.3 Results . . . 183
9.3.1 Perception post-processing . . . 183
9.3.2 Gap inference . . . 185

9.3.3 Decision-making . . . 185
9.4 Conclusions . . . 189

10 Conclusions **195**
10.1 Overview . . . 195
10.1.1 Perception model . . . 196
10.1.2 Motion planning architecture . . . 197
10.1.3 Gap-acceptance decision map . . . 197
10.1.4 Self-serving planning method . . . 198
10.1.5 Validation . . . 199
10.2 Contributions . . . 199
10.3 Future work . . . 200

A Appendix **201**
A.1 Car-following . . . 201
A.1.1 Safe car-leading and following constraint . . . 201
A.1.2 Maximum safe following speed . . . 202
A.1.3 Minimum safe leading speed . . . 202
A.1.4 Set of safe car-following states . . . 203
A.1.5 Set of safe car-leading states . . . 203
A.1.6 Set of safe car-following states between two vehicles . . . 203
A.2 Reachable states . . . 203
A.2.1 Speed transition auxiliary operators . . . 204
A.2.2 Time-constrained reachable distance . . . 204
A.2.3 Time-constrained reachable speed . . . 205
A.2.4 Distance-constrained reachable speed . . . 205
A.2.5 Distance-constrained arrival time . . . 206
A.2.6 Time-distance-constrained reachable speed . . . 206
A.2.7 Set of reachable states . . . 207
A.2.8 Set of time-constrained reachable distances . . . 207
A.2.9 Set of time-constrained reachable speeds . . . 208
A.2.10 Set of time-constrained reachable states . . . 208
A.2.11 Set of distance-constrained arrival times . . . 208
A.2.12 Set of time-distance-constrained reachable speed . . . 208
A.3 Maneuver targets . . . 208
A.3.1 Set of reachable maneuver targets . . . 208
A.3.2 Set of safe car-following maneuver targets . . . 208
A.3.3 Set of safely reachable maneuver targets . . . 209
A.3.4 Envelope set of reachable maneuver targets . . . 211

List of Figures

2.1 Main tasks involved in automated driving 35
2.2 Roundabout microscopic traffic simulator architecture. 36
2.3 Examples of automatically-created roundabout geometries. 37
2.4 Illustration of the process to manually create a roundabout layout. 38
2.5 Implementation of the simulated vehicles' behavior. 40
2.6 Visualizations of our microscopic-traffic simulator. 41
2.7 Simulation visualization for debugging proposes. 41
2.8 Three-dimensional representation of the trajectories of a set of vehicles driving through a certain roundabout. 43
2.9 Two roundabout scenarios illustrating the roundabout geometry we consider. . . . 44
2.10 Normal distributions used to sample the distance that the vehicles are likely to drive inside the roundabout. 46
2.11 Examples of origin-destination patterns randomly drawn. 47
2.12 Three-dimensional representation of the trajectories followed by a set of vehicles driving through a roundabout. Time is represented in the vertical axis. 47
2.13 Time-distance diagram representation. 48
2.14 Time-distance representation of the traffic circulating inside a two-lane roundabout. 49
2.15 Time-distance representation of the traffic approaching the depicted roundabout by two incoming lanes. 50

3.1 Dynamic occupancy grid configuration to represent the circulatory lanes and illustration of the identification process of the occluded cells. 58
3.2 Identification of three relevant subsets of cells. 59
3.3 Illustration of the probably-free gaps inference process 63
3.4 Traffic scenario illustrating the considered static obstacle and the position form which it observes the scenario. 64
3.5 Evolution of the occupancy probability of the circulatory lane when the ego vehicle can detect the surrounding vehicles perfectly. 65
3.6 Evolution of the occupancy probability of the circulatory lane when the scene is observed from Ⓐ. 66
3.7 Evolution of the occupancy probability of the circulatory lane when the scene is observed from Ⓑ. 68
3.8 Example of probably-free gaps extracted for a certain configuration of the surrounding traffic. Case 00. 69
3.9 Example of probably-free gaps extracted for a certain configuration of the surrounding traffic. Cases 01-04 and observer positioned at Ⓐ. 69

3.10 Example of probably-free gaps extracted for a certain configuration of the surrounding traffic. Cases 01-04 and observer positioned at Ⓑ. 70

4.1 Illustration of the motion planning task. 72
4.2 Considered planning submodules composing our motion planner. 74
4.3 Lane-graph representation of a two-lane roundabout. 77
4.4 Illustration of two eligible maneuver candidates to perform a merging maneuver into a two-lane roundabout 78
4.5 The proposed maneuver planning architecture. 80
4.6 Illustration of the convexification process used to formulate the original non-linear safety constraint as a set of linear inequalities. 85
4.7 A speed profile generated for a specific set of parameters with the proposed trajectory planning strategy. 86

5.1 Representation of the so-called gap-acceptance decision map. 92
5.2 Examples of the decision resulting from the application of the proposed self-serving reactive maneuver planner in a set of five traffic scenes. 95
5.3 Circulating vehicles' time-distance trajectory resulting from the proposed reactive planning strategy in a low-density traffic scenario. 98
5.4 Approaching vehicles' time-distance trajectory resulting from the proposed reactive planning strategy in a low-density traffic scenario. 98
5.5 Histograms characterizing the vehicles' trajectory resulting from the proposed reactive planning strategy in a low-density traffic scenario. 98
5.6 Circulating vehicles' time-distance trajectory resulting from the proposed reactive planning strategy in a medium-density traffic scenario. 99
5.7 Approaching vehicles' time-distance trajectory resulting from the proposed reactive planning strategy in a medium-density traffic scenario. 99
5.8 Histograms characterizing the vehicles' trajectory resulting from the proposed reactive planning strategy in a medium-density traffic scenario. 99
5.9 Circulating vehicles' time-distance trajectory resulting from the proposed reactive planning strategy in a high-density traffic scenario. 100
5.10 Approaching vehicles' time-distance trajectory resulting from the proposed reactive planning strategy in a high-density traffic scenario. 100
5.11 Histograms characterizing the vehicles' trajectory resulting from the proposed reactive planning strategy in a high-density traffic scenario. 100
5.12 Generation of the batch of simulated traffic scenarios. 101
5.13 Boxplots characterizing the overall impact of the reactive planner on vehicles' overall travel speed distribution and fairness. 102
5.14 Boxplots characterizing the overall impact of the reactive planner on vehicles' arrival delay distribution and fairness. 102
5.15 Boxplots characterizing the overall impact of the reactive planner on intersection's throughput. 102

6.1 Illustration of the problem tackled by the communication-based planning and representation of the virtual vehicle interaction mechanism. 106
6.2 Representation of the traffic scene used along this chapter to illustrate some steps of the planning process. The ego vehicle is represented by the green vehicle. 110

6.3 Illustration of three sets of reachable maneuver targets along with its envelope set. 111
6.4 Three sets of reachable maneuver targets and their corresponding set of virtual insertion states. . . . 112
6.5 Set of reachable maneuver targets, and virtual insertion states corresponding to the highlighted maneuver targets. . . . 112
6.6 Finite set of all reachable virtual insertion states and the subset of those that are safe w.r.t. the observed gaps. . . . 114
6.7 Representation of the quality score assigned to a set of safe and reachable virtual insertion states. . . . 116
6.8 Examples of the decision made by the explicitly cooperative maneuver planner in different scenarios. . . . 120
6.9 Circulating vehicles' time-distance trajectory resulting from the proposed explicitly cooperative planning strategy in a low-density traffic scenario. . . . 122
6.10 Approaching vehicles' time-distance trajectory resulting from the proposed explicitly cooperative planning strategy in a low-density traffic scenario. . . . 122
6.11 Histograms characterizing the vehicles' trajectory resulting from the proposed explicitly cooperative planning strategy in a low-density traffic scenario. . . . 122
6.12 Circulating vehicles' time-distance trajectory resulting from the proposed explicitly cooperative planning strategy in a medium-density traffic scenario. . . . 123
6.13 Approaching vehicles' time-distance trajectory resulting from the proposed explicitly cooperative planning strategy in a medium-density traffic scenario. . . . 123
6.14 Histograms characterizing the vehicles' trajectory resulting from the proposed explicitly cooperative planning strategy in a medium-density traffic scenario. . . . 123
6.15 Circulating vehicles' time-distance trajectory resulting from the proposed explicitly cooperative planning strategy in a high-density traffic scenario. . . . 124
6.16 Approaching vehicles' time-distance trajectory resulting from the proposed explicitly cooperative planning strategy in a high-density traffic scenario. . . . 124
6.17 Histograms characterizing the vehicles' trajectory resulting from the proposed explicitly cooperative planning strategy in a high-density traffic scenario. . . . 124
6.18 Generation of the batch of simulated traffic scenarios. . . . 126
6.19 Boxplots characterizing the overall impact of the explicitly cooperative planner on vehicles' overall travel speed distribution and fairness. . . . 127
6.20 Boxplots characterizing the overall impact of the explicitly cooperative planner on vehicles' jerk distribution and fairness. . . . 127
6.21 Boxplots characterizing the overall impact of the explicitly cooperative planner on intersection's throughput. . . . 127

7.1 Illustration of the addressed traffic scenario. . . . 132
7.2 Illustration of the example scenario used to illustrate the implicitly cooperative maneuver planner . . . 133
7.3 Illustration of the *gap-acceptance decision map* corresponding to the merging trajectory a circulatory vehicle would presume approaching vehicles apply. . . . 134
7.4 Decision map of the presumed merging trajectory, and the evolution of a gap whose limits move at constant speed. . . . 135
7.5 Example of the evolution of the gap in the example scenario, when the maximum cooperative deceleration is applied. . . . 137

7.6 Example of the evolution of the gap in the example scenario, when the minimum cooperative deceleration feasible is applied. 138
7.7 Representation of the yielding decision-making mechanism in five different scenarios. 142
7.8 Circulating vehicles' time-distance trajectory resulting from the proposed implicitly cooperative planning strategy in a low-density traffic scenario. 145
7.9 Approaching vehicles' time-distance trajectory resulting from the proposed implicitly cooperative planning strategy in a low-density traffic scenario. 145
7.10 Histograms characterizing the vehicles' trajectory resulting from the proposed implicitly cooperative planning strategy in a low-density traffic scenario. 145
7.11 Circulating vehicles' time-distance trajectory resulting from the proposed implicitly cooperative planning strategy in a medium-density traffic scenario. 146
7.12 Approaching vehicles' time-distance trajectory resulting from the proposed implicitly cooperative planning strategy in a medium-density traffic scenario. 146
7.13 Histograms characterizing the vehicles' trajectory resulting from the proposed implicitly cooperative planning strategy in a medium-density traffic scenario. 146
7.14 Circulating vehicles' time-distance trajectory resulting from the proposed implicitly cooperative planning strategy in a high-density traffic scenario. 147
7.15 Approaching vehicles' time-distance trajectory resulting from the proposed implicitly cooperative planning strategy in a high-density traffic scenario. 147
7.16 Histograms characterizing the vehicles' trajectory resulting from the proposed implicitly cooperative planning strategy in a high-density traffic scenario. 147
7.17 Generation of the batch of simulated traffic scenarios. 148
7.18 Boxplots characterizing the overall impact of the implicitly cooperative planner on vehicles' overall travel speed distribution and fairness. 149
7.19 Boxplots characterizing the overall impact of the implicitly cooperative planner on vehicles' jerk distribution and fairness. 149
7.20 Boxplots characterizing the overall impact of the implicitly cooperative planner on intersection's throughput. 149

8.1 The ego vehicle approaching a two-lane roundabout, which is partially occluded by the surrounding vehicles and the roundabout island. 152
8.2 Illustration of three sets of reachable maneuver targets and states, given a specific initial state. 156
8.3 Illustration of the construction process of the set of safely-reachable maneuver targets w.r.t. moving obstacles ahead. 157
8.4 Illustration of the construction process of the set of safely-reachable maneuver targets w.r.t. road markings. 159
8.5 Illustration of the model used to approximate the probably-free gaps' occupancy transition probability. 161
8.6 Examples of the set of safe ϵ-approaching states, and safe ϵ-reachable MTs for five different scenarios. Every raw correspond to a different example, and for each of them, the same information than the one provided in Fig. 8.4 is included. 165
8.7 Examples of the maneuver target that would be chosen by the proposed strategy in a set of six different scenarios. 167
8.8 Circulating vehicles' time-distance trajectory resulting from the proposed predictive-reactive planning strategy in a low-density traffic scenario. 170

8.9 Approaching vehicles' time-distance trajectory resulting from the proposed predictive-reactive planning strategy in a low-density traffic scenario. 170
8.10 Histograms characterizing the vehicles' trajectory resulting from the proposed predictive-reactive planning strategy in a low-density traffic scenario. 170
8.11 Circulating vehicles' time-distance trajectory resulting from the proposed predictive-reactive planning strategy in a medium-density traffic scenario. 171
8.12 Approaching vehicles' time-distance trajectory resulting from the proposed predictive-reactive planning strategy in a medium-density traffic scenario. 171
8.13 Histograms characterizing the vehicles' trajectory resulting from the proposed predictive-reactive planning strategy in a medium-density traffic scenario. 171
8.14 Circulating vehicles' time-distance trajectory resulting from the proposed predictive-reactive planning strategy in a high-density traffic scenario. 172
8.15 Approaching vehicles' time-distance trajectory resulting from the proposed predictive-reactive planning strategy in a high-density traffic scenario. 172
8.16 Histograms characterizing the vehicles' trajectory resulting from the proposed predictive-reactive planning strategy in a high-density traffic scenario. 172
8.17 Generation of the batch of simulated traffic scenarios. 173
8.18 Boxplots characterizing the overall impact of the predictive-reactive planner on vehicles' overall travel speed distribution and fairness. 174
8.19 Boxplots characterizing the overall impact of the predictive-reactive planner on vehicles' jerk distribution and fairness. 174
8.20 Boxplots characterizing the overall impact of the predictive-reactive planner on intersection throughput. 174

9.1 Map of the scenario where the experiments take place. 179
9.2 Trajectory traces of the experimental vehicle while crossing the two roundabouts in the scenario. Note that both roundabouts are two-lane roundabouts. 180
9.3 Examples of the speed and acceleration merging profiles registered in each of the roundabouts in the scenario. 180
9.4 Representation of the two roundabouts in the experimental scenario, along with the fitted occupancy grid, and the considered environmental obstacles. 182
9.5 Samples of the evolution of the dynamic occupancy grid representing the occupancy state of the circulatory lanes, in four different scenarios. 184
9.6 Cases 1-3, for which the state of the dynamic occupancy grid, the extracted probably-free inter vehicle gaps, and the frame of the on-board camera footage are shown. . 186
9.7 Cases 4-6, for which the state of the dynamic occupancy grid, the extracted probably-free inter vehicle gaps, and the frame of the on-board camera footage are shown. . 187
9.8 Cases 7-9, for which the state of the dynamic occupancy grid, the extracted probably-free inter vehicle gaps, and the frame of the on-board camera footage are shown. . 188
9.9 Illustration of the reactive maneuver planner output for two merging maneuvers in the data set. Examples 1-2. 191
9.10 Illustration of the reactive maneuver planner output for two merging maneuvers in the data set. Examples 3-4. 192
9.11 Illustration of the reactive maneuver planner output for two merging maneuvers in the data set. Examples 5-6. 193

10.1 Thesis structure 195

10.2 Illustration of probably-free gaps in a simulated and real scenario 196
10.3 Comparison of the introduced gap-acceptance decision map, and the yielding maneuver approach 197
10.4 Summary of the proposed self-serving maneuver planners. 198
10.5 Summary of the comparison scheme used to assess the proposed strategies. 199

List of Tables

3.1 Transition probabilities 60
3.2 Sensor model 61
3.3 Design parameters 65

4.1 Parameters used in simulation 85

5.1 Design parameters 94
5.2 Intersection throughput and fairness metrics 96
5.3 Driver agent used in our simulation study 97
5.4 Simulation batch scenario configuration 97

6.1 Driver agents used in our simulation study 118
6.2 Design parameters 118
6.3 Example traffic scores 119
6.4 Intersection throughput and fairness metrics 119
6.5 Simulation batch scenario configuration 125

7.1 Design parameters 138
7.2 Driver agents used in the experiments 141
7.3 Example yielding scores 141
7.4 Intersection throughput and fairness metrics 143
7.5 Simulation batch scenario configuration 148

8.1 Driver agents used in our simulation study 163
8.2 Design parameters 163
8.3 Safe ϵ-reachable MTs scenarios 164
8.4 Safe ϵ-reachable MTs scenarios 166
8.5 Intersection throughput and fairness metrics 168
8.6 Simulation batch scenario configuration 169

Acronyms

ADAS Advanced driving assitance systems
AI Artificial intelligence
ASS Active safety systems
AV Automated vehicle
CAV Connected automated vehicle
CF Car-following
DOG Dynamic occupancy grid
DSDM Decision spot driving maneuver
FOV Field of view
GPS Global positioning system
IDM Intelligent driver model
ID Identifies
ITS Intelligent transportation systems
IV Intelligent vehicles
LIDAR Light detection and ranging
MDP Markov decision process
ML Machine learning
MOBIL Minimizing the overall braking induced by lane change
MPC Model predictive control
MT Maneuver target
POMDP Partially observable Markov decision process
QP Quadratic program
SCF Safe car-following
SCL Safe car-leading
V2I Vehicle to infrastructure communication
V2V Vehicle to vehicle communication
V2X Vehicle to vehicle/infrastructure communication
VIS Virtual insertion state
VP Virtual platoon
VV Virtual vehicle

1 Introduction

AUTONOMOUS vehicle technology is meant to profoundly transform transportation by providing new methods to achieve not only a more efficient but also a safer use of the existing and future transportation infrastructure [81]. Automated and autonomous vehicles have the potential to outperform human-drivers by making more efficient decisions as a consequence of having access to more and better contextual information, as well as profiting from a deeper understanding of the complex traffic dynamics and phenomena [79]. New and revolutionary services may arise thanks to this technology [80], and other existing ones would undoubtedly undergo drastic changes, and face new and unprecedented competition. Overall, one could expect roads to become safer and more efficiently-used thanks to this technology, while the driving experience becomes more comfortable and exciting for human beings. However, for the futuristic scene just described to become a reality, many open challenges need to be solved, some of which are addressed in this dissertation.

In this thesis, we study the process through which a connected automated vehicle decides how to behave in the few seconds that follow (the so-called motion planning problem) while driving in mixed traffic. That is while coexisting with other CAVs, human drivers, and unconnected automated vehicles (AVs). Overall, two distinct sets of contributions are made in this work. On the one hand, we reflect on the additional challenges that the mixed traffic condition imposes on the motion planning solution. Explicitly, we discuss some specific aspects of the motion planning architecture itself, the general planning framework, as well as the type of information that the perception systems should provide. On the other hand, built upon our proposed planning framework, we formulate methods to perform self-serving and cooperative maneuvers, targeting different interaction mechanisms.

Even though we aim to formulate context-agnostic planning strategies, they will be validated and assessed using roundabout scenarios, as all major challenges a motion planner must address are somehow present at these complex intersections. For instance, navigating at roundabouts is affected by the uncertainty concerning the surrounding vehicles' driving intent (due to the lack of traffic lights explicitly granting the right of way), the complex traffic interaction and phenomena resulting from its particular geometry, and the occlusions caused by not only nearby vehicles but also environmental elements.

In the remainder of this chapter, we will put our research into perspective w.r.t. the state of the art and provide the context needed to understand the considerations from which the proposed

methods emerge. Specifically, we will start by providing an introduction to autonomous driving in Section 1.1, which will be followed, in Section 1.2, by a discussion concerning the state of the art and the works that more strongly inspired our research. Then, we will further characterize, in Section 1.3, the scope of this thesis as well as the research topics we address. We subsequently describe the methodology used in our study in Section 1.4 and conclude the chapter in Section 1.5 by presenting the structure of the thesis and the topics treated in the following chapters.

1.1 Introduction to autonomous driving

Driving is an extremely challenging task despite how naturally it might come to human beings. As in many other fields related to robotics and artificial intelligence, it is precisely the process of designing a system that performs specific tasks autonomously what makes us grasp the real complexity of the tasks themselves. Replicating complex human behaviors and skills is particularly challenging, and the process often inspires a very intense sense of amazement regarding the capacity of the human brain.

The task of driving is one that has to be learned, which allows us to grasp the intuition behind the most significant challenges in autonomous driving. Specifically, as any inexperienced driver could recall, the difficulty of driving is caused by the need to (i) understand what is happening in the surroundings and predict how it is likely to evolve, (ii) plan the future behavior so that specific goals are safely reached despite the uncertain evolution of the surrounding traffic, and (iii) act on the throttle and the steering wheel so that the planned motions are accurately executed. These three major tasks lead to the fundamental research topics concerning autonomous driving, namely *perception* and *prediction*, *motion planning*, and *control*. These topics are of such a complexity that they are typically studied individually, and hence often built upon assumptions regarding the capabilities and performance of the modules carrying out the remaining tasks.

The challenge of designing efficient strategies to address the problems mentioned above comes not only from the complexity of the tasks themselves but also from the impact they have between each other. It is straightforward to acknowledge, for instance, the effect that perception accuracy would have on the quality of the plans that can be made, and these, in turn, on the performance with which the low-level controllers are able to execute such motion plans. It is important to note that, although slightly less intuitive, the impact between tasks does also propagate upwards. Indeed, inaccurate control solutions may lead the vehicle to situations where planning comfortable and effective motions becomes more challenging. Similarly, ineffective plans can make the vehicle adopt states from which it is exceptionally challenging to perceive the surroundings properly.

As happens with inexperienced drivers, who, over time, become more capable of performing complex maneuvers more efficiently and with less effort, different degrees of expertise can be identified in the context of autonomous driving, corresponding to the so-called automation levels [10]. There are five levels of automation defined in such a way that the level of engagement expected from the human driver decreases as the autonomy level increases. Vehicles that have active safety systems (ASS) and basic driving assistance systems would belong to levels 1-2. Advanced driving assistance systems (ADAS) able to drive fully autonomously in specific scenarios such as highways would fall within the levels 3-4, and a vehicle that does not require their passengers to engage in the driving task would be categorized as level 5. For the sake of consistency, vehicles are only said to be *autonomous* if they are level 5. Otherwise, we prefer the term *automated* vehicles.

From a theoretical perspective, the assumptions made regarding the traffic scene and the vehicles' capabilities have a significant influence on the nature of the challenges and solutions that are

studied by different researchers. It is evident that to solve the challenges that AVs are meant to face in the early stages of their deployment, realistic traffic scenarios need to be considered. Nonetheless, the enormous potential of autonomous driving technology encourages researchers in the field to anticipate more futuristic traffic scenarios and develop solutions that fit them in order to motivate their vision and somehow steer the future of autonomous mobility. In this sense, a rather widespread assumption that is often used in the literature involves considering the availability of vehicle-to-vehicle (V2V) and/or vehicle to infrastructure (V2I) communication[1].

Assuming communication capabilities enables researchers to envision new tools and interaction mechanisms that AVs could use and, although it does not necessarily change the true nature of the problem, it often comes along slightly different assessment criteria. Indeed, realistic assumptions regarding the vehicles' capabilities and traffic scenarios are more inclined to result in research concerning safe and self-focused navigation, while assuming communication encourages the study of strategies oriented to improve the overall traffic performance.

The topic we address in this thesis is motion planning, and our discussion will hover, from now on, around such matter—the reader is kindly referred to [4, 44, 88] for extensive reviews on the topics of vehicle perception, prediction, and control.

1.2 State of the art

An efficient way of understanding the main research topics in motion planning is regarding motion planning from a rather abstract level, and in conjunction with the entities and systems that surround it. Particularly, motion planning can be seen as a module that affects and is affected by, (i) the low-level control systems, (ii) the surrounding traffic, and (iii) the perception layer. The ultimate objective is indeed developing planning strategies that account for all such interactions as well as possible. However, the complexity of doing so is such, that works in the literature typically focus on one of those interactions at a time, while imposing minimum levels of performance on the remaining ones.

In the following sections, we discuss some of the trends and families of methods used in the state of the art concerning motion planning. Specifically, we start by briefly reviewing works focused on the motion planning problem disregarding the limitations and interaction stemming from the surrounding modules, and continue by gathering those works in the literature focused on some of such interactions. It is worth noting that despite the increase in popularity of data-driven solutions, we are mostly interested in model-based approaches, which are hence the ones we focus on in this section.

Let us also point out that in this section, we will focus on providing an overview of the family of methods that are exploited in the literature to address a specific set of motion planning problems. It will be in Section 1.3, where the content of this thesis is put into perspective w.r.t. the state of the art and the gaps we study. Moreover, the subsequent chapters will include a dedicated *related work* section, where studies better related to the specific strategies we propose are discussed.

1.2.1 Motion planning and control

The dimension of motion planning that has been the most studied to date concerns its relationship with the control layer. This aspect has been mainly explored from the motion planning towards the control systems, i.e., regarding how to generate trajectories that can be followed by the control

[1]The term V2X is often used to refer to both V2V and V2I capabilities.

layer with accuracy.

Works falling in this category might as well address the collision avoidance problem considering the surrounding obstacles either to be static or to follow a trajectory that is independent of the AV's actions. Thus, the motion planning problem at this stage could be reduced to trajectory planning, or, as it is usually tackled, the combination of path planning and velocity planning [40].

The variety of existing methods to address such a problem is vast, but luckily, very informative reviews exist that provide a very comprehensive view of the state of the art. For instance, two very informative reviews are [25, 69] which, although they focus on methods to address the path planning problem, the discussed approaches are as well suitable for trajectory planning. They start by identifying different stages within the motion planning problem: global planning, behavioral planning, and local planning. They identify four major classes of methods

- Graph search: where the surrounding space is represented by a grid, from which paths are generated by applying graph searching algorithms that visit the different states in the grid. The main representatives of this family of methods are the Dijkstra algorithm and the A-start algorithm (and the endless proposed variations of such methods).
- Sampling-based planners: based on randomly sampling the state space, looking for connectivity inside it, until a feasible path is found. Methods that are mainly represented by PRM and RRT.
- Interpolation curve planners: where paths are built by roughly setting key locations that want to be traversed, and then generating new points in between while regarding curve continuity, and kinetic and dynamic feasibility.
- Numerical optimization planners: based on obtaining a path to follow, by minimizing/maximizing a specific cost/quality function while imposing constraints on the solution space.

The works included in such reviews are regarded from the control and collision avoidance standpoint, but not considering challenges from imperfect perception, or the interaction with the surrounding vehicles.

1.2.2 Motion planning and surrounding traffic

Concerning the motion planning problem and the interaction with the surrounding traffic, two primary trends can be found in the literature. On the one hand, a broad set of studies focuses on the so-called *traffic coordination* or *cooperative driving* problem, where motion planning solutions are often built on the assumption of having perfect information available. In this context, existing works typically assume V2X communication. On the other hand, considering a more realistic setup, a second general group of studies address the motion planning in scenarios where the surrounding vehicles' behavior is uncertain.

Traffic coordination

Interestingly, early research concerning IVs regarded the problem of motion planning under the assumption of V2V communication. We believe that such a research topic emerged in the early stages of autonomous vehicle technology due to two main reasons. On the one hand, such a research topic was a natural extension of the traffic and intersection management problem extensively studied in the field of *intelligent transportation systems* (ITS) [34]. On the other hand, for the *intelligent vehicles* (IV) community, assuming inter-vehicle communication allowed as well a straightforward

extension of more classic trajectory planning solutions, which could then be complemented with the assumption of perfectly knowing the surrounding vehicle's state and intent.

It is worth stressing that the connectivity assumption changes the scenario to the extent that it would deserve its own category. The problem of motion planning when considering inter-vehicle communication is often referred to in the literature as the traffic coordination, or the cooperative motion planning problem.

The so-called optimal coordination problem [34] can be easily formulated as the problem of optimizing the aggregated value of a specific cost function for every vehicle in the scenario, subject to safety and comfort constraints. Nonetheless, the combinatorial nature of the problem demands the application of heuristics and approximations to find feasible near-optimal solutions. Such a need for heuristics and approximations to tackle the problem is precisely what leads to the broad set of approaches that can be found in the literature. For a more in-depth discussion in this sense, the reader is kindly referred to [34], where a very understandable introduction to the problem and the types of existing solutions is provided.

In summary, two fundamental features characterize the different families of solutions concerning the body of work on traffic coordination. On the one hand, families of *centralized* and *decentralized* solutions can be found in the literature in such a way that (borrowing the criterion in [74]) a planning/coordination strategy is considered to be centralized if it includes a central agent that performs at least one task. On the other hand, the exploited methods can roughly be classified considering whether they rely on heuristics or optimization-based methods to determine the crossing sequence of the vehicles through the intersections and/or the sequence of accelerations they need to apply to drive forward while respecting the assigned priorities safely.

Centralized communication-based solutions involve a central agent or intersection manager in charge of guaranteeing that the crossing sequence of the vehicles through the intersection is safe and efficient [21, 59]. Presuming this architecture, existing works differ on the strategies followed by the vehicles to make their requests, for instance: self-serving criteria where every vehicle wants to cross as soon as possible [21], decisions based on rather macroscopic properties of the surrounding traffic [95], mechanisms whereby vehicles first form platoons whose leader negotiates the crossing maneuver of the whole platoon [38], or simply based on arrival-time heuristics [77].

Another very popular approach is considering that the intersection manager would directly decide the most appropriate crossing sequence, which would then be broadcast to the vehicles that should optimize their trajectory so that the imposed crossing time-window is met. In this direction, studies mainly differ on the cost function of their optimal-trajectory planning problem, which could, for instance, aim to maximize intersection throughput [94], minimize the time vehicles stay in the intersection area simultaneously [43], or optimize multi-objective criteria combining comfort, risk, speed considerations [14], etc.

Decentralized communication-based planning solutions assume, on the other hand, that all calculations are done by the cars themselves and often consider the crossing sequence to be given by ad-hoc heuristics [13, 23, 52]. Concerning existing approaches, behavioral policies can be found where the crossing order emerges from the designed behavior, and where methods such as virtual vehicles, fuzzy logic [58, 67], or critical/invariant sets [9, 28, 29, 73] are used. Moreover, works can as well address the problem by first designing a heuristic whereby every vehicle calculates the priority of every road participant in the scenario, i.e. the crossing order, and then generate a suitable state trajectory—for instance using potential fields [53] or optimization-based strategies [6, 7, 54].

Uncertainty-aware motion planning

An additional aspect worth studying is the one that relates the motion planning performance with the uncertain behavior of the surrounding traffic. Traditionally, from the motion planning standpoint, the surrounding traffic has been regarded as a set of moving obstacles with predefined and fixed plans, with which collisions should be avoided while pursuing the local objectives. However, real planning challenges arise when, to efficiently plan trajectories, the future state of the traffic or the possible reaction of surrounding road agents need to be taken into account.

Studies on interaction-aware motion planning try to provide strategies for an AV to plan its motion while considering the reaction that could be expected from the surrounding vehicles. Such research topic is considered crucial at cluttered situations where the reaction of surrounding vehicles becomes critical to optimal decision-making, and simplistic assumptions regarding surrounding road participants become insufficient [78]. Similarly, when motions want to be optimally planned over long planning horizons, the uncertainty concerning the future state of the surrounding traffic needs to be considered.

Unlike the coordination problem, where V2X communication was presumed to allow the vehicles to have a perfect knowledge concerning surrounding vehicles reactions, uncertainty-aware motion planners do not rely on communication.

Differences between existing methods addressing uncertainty-aware motion planning emerge at different levels of the solution. On the one hand, we can differentiate two first categories regarding whether the proposed method is only meant to trigger maneuvers reactively [26, 37], or rather plan trajectories over a relatively long planning horizon [33, 45, 90]. The former is indeed a particular case of the latter. However, reducing the decision-making problem to a decision that needs to be taken *now* and is to be executed *now* simplifies the task and can indeed be addressed with rather simple behavioral policies. In this sense, reactive decision-makers consider interactivity by approximating the uncertain reaction that the instantaneous decision will induce in the surrounding traffic. In contrast, longer-term planning approaches aim to exploit an approximated knowledge of how surrounding vehicles make and execute tactical decisions to increase the probability of the AV performing the maneuver successfully.

Within the studies treating the problem of uncertainty-aware long-term planning, different levels of complexity can as well be found depending on how the decision-making is understood, and the specific planning framework that is exploited. Concerning the decision-making modeling itself, two well-differentiated trends can be observed: (i) one where a finite set of trajectories are provided to the decision-maker for it to decide which is the best one to pursue [45, 90, 91], and (ii) another one where the problem is seen as a sequence of decisions concerning the acceleration to apply at every time step in the planning horizon (for instance [33]). Approaches following the first trend benefit from shorter computational times even for a relatively large set of maneuver candidates but suffer from the fact that the solution space is often oversimplified. On the contrary, problems considering every planning step to be a decision-making instance typically rely on probabilistic decision-making frameworks as Markov decision processes (MDPs) to precisely model the decision-making problem. However, such a powerful modeling framework comes at the cost of raising the complexity of finding the optimal solution, ultimately having to rely on heuristics and simplifications to solve the problem.

1.2.3 Motion planning and perception

The interaction of the motion planning module and the perception system is not a widely studied one, and a large proportion of existing works on motion planning assume that they have a reasonable

good representation of the environment. However, the need for motion planning strategies that are able to generate safe and efficient trajectories despite perception inaccuracies and occlusions has recently caught the attention of part of the community.

In particular, a very recent trend can be observed in the IV community towards the study of safe motion planning in the presence of occlusions and other perception inaccuracies. Once again, existing solutions differ not only on the specific methods used to tackle motion planning in itself but also on the models that exploit to integrate the occlusion information within the planning framework. Generally speaking, three major families of model-based solutions can be observed.

A relatively popular approach to address this type of problem consists in reusing rather general trajectory planning solutions but considering a set of phantom vehicles positioned in the occluded area [83, 98]. By doing this, any planning solution able to account for probabilistic predictions would also be able to provide a solution in occluded scenes.

A second relevant approach would consist in assuming the geometry of the occluded region to be known (often justified with the availability of high-resolution maps), and then imposing dedicated constraints in the trajectory planning so that the resulting trajectory allows the vehicle to approach the occluded region carefully enough. In a way, these studies (e.g. [62, 68, 97]) rely on the fact that, whereas occlusions do have a substantial impact when long planning horizons are considered, the closer the vehicle gets to the occluded regions, the better the visibility will become. Thus, a possibly efficient solution would consist in driving in such a way that a safe emergency maneuver could be performed if a vehicle emerges from the occluded regions.

Furthermore, the methods used for interaction-aware motion planning when modeled as a sequence of decision-making instances can as well be applied to occlusion-aware motion planning [5, 32, 63]. The process would nonetheless require a model of how the occlusion is expected to evolve in the future, which is a tractable task only for relatively simple architectural occlusions.

1.3 Scope and research questions

This dissertation focuses on some open challenges related to motion planning for CAVs and its interaction with the perception layer and the surrounding traffic. As was discussed in the previous section, such a broad problem covers a large set of research topics and challenges. Thus, in this section, we aim to clearly state the scope of our research as the aspects studied in this thesis address several specific gaps in the existing state of the art.

First and foremost, driving autonomously in mixed traffic scenarios entails problems related to the specific methods used to interact with the different types of vehicles in the surroundings, as well as the orchestration of such processes to compose a unique motion planning solution. To date, this is an unsolved problem that has been disregarded in the literature and requires novel motion planning architectures. In this thesis, we tackle this challenge by designing a common planning framework that allows formulating motion planning solutions and their implicit decision-making process regardless of the specific interaction mechanism it is built upon, thereby facilitating their integration.

A novel approach is proposed to address motion planning, which aims to provide a more suitable framework to allow motion planning strategy to generate safe plans in occluded scenes naturally. Specifically, unlike the classical planning approach based on surrounding *objects detection and avoidance*, we study an alternative one based on *free space identification and exploitation*, which is shown to be a very suitable strategy to account for occlusions and other perception uncertainties.

In what concerns the interaction between CAVs (also referred to as the cooperative planning

problem), we can identify the need for communication-based interaction mechanisms that are less communication-intensive yet sufficiently efficient. In this sense, we formulate a V2V interaction mechanism that does not require the vehicles to be continuously broadcasting their intent and is meant to enable vehicles to altruistically cooperate with surrounding vehicles rather than compete for shared resources. Moreover, despite the freedom and flexibility that inter-vehicle communication provides to the decision-makers, very few works consider the impact of the vehicle's decision on the overall traffic performance, which is an aspect that we also integrate in our proposed solution.

Concerning the interaction with surrounding unconnected vehicles, we identify two interesting gaps in the literature. On the one hand, whereas interaction-aware planning has been extensively addressed in the literature so that an AV can profit from the expected reaction of the surrounding vehicles, the dual interpretation of the problem has not. That is, not much attention has been paid to the problem of making AVs able to facilitate the surrounding vehicle's maneuver without the use of communication. In this context, we address the design of a so-called implicitly cooperative motion planner, which aims to reach cooperation with surrounding vehicles by changing the context instead of explicitly communicating the cooperation intent. On the other hand, the lack of communication entails a significant level of uncertainty concerning the detection of surrounding vehicles and their future intent, which makes the task of safely planning motions with long planning horizons remarkably challenging. Novel methods are needed to generate reasonably efficient motion plans in this context, in a computationally efficient way. We address such a challenge by defining the decision-making solution space in such a way that a broad set of maneuver candidates can be evaluated w.r.t. the uncertainty of the future traffic state without the need to intensively explore explicit sequences of accelerations.

Additionally, in what concerns the evaluation of the proposed planning strategies, we borrow practices not only from the field of IVs but also from the field of ITS. Interestingly, in the IVs field, planning strategies are traditionally regarded and assessed from an AV's standpoint. Contrary, in the field of ITS (where the traffic management problem has been traditionally studied) the objective is to improve the overall traffic performance instead. The analysis of our proposed strategies lies somewhere in between those two approaches. This practice emerges from the idea that autonomous driving strategies should not only care about the local objectives of the AV itself but also, up to some extent, act to maintain an efficiently coordinated traffic situation. Therefore, we will evaluate the capacity of our planning methods to perform the maneuvers of interest, along with the change concerning the overall traffic dynamics that could be expected from them.

Additionally, even though we aim to provide a rather general discussion of the topics mentioned above, we will validate our strategies in roundabout scenarios, which are marginally used in the literature compared to other traffic scenes despite their complexity.

Summarizing, this thesis will address the following aspects concerning motion planning:

- context representation for safer motion planning and decision-making under occlusions,
- motion planning architecture and decision-making modeling to support the coexistence of different interaction mechanisms,
- simple yet efficient reactive planning strategy for AVs,
- novel interaction mechanism for CAVs based on meaningful yet non-intensive communication,
- communication-based cooperative planning strategy for CAVs,
- implicitly cooperative motion planning method for AVs without communication capabilities,
- predictive-reactive planning method enabling AVs to plan ahead and profit from medium and long term traffic predictions while remaining safe.

1.4 Methodology

The research topics discussed in Section 1.3 are addressed through the design of model-based planning strategies, which are assessed following a simulation-based methodology. Whichever specific topic we study, we start by analyzing the particularities of the problem being treated, continue hypothesizing about a possible model-based strategy that could address them, and finalize formalizing, implementing, and evaluating the strategy in simulation.

Concerning the evaluation of the strategies, their performance is compared to a straightforward and reactive baseline behavior at two different levels. Firstly, we study the effect the strategies have on the individual vehicles' trajectory by analyzing their travel speed. Then, we evaluate the impact the strategy has on the overall traffic coordination performance by quantifying, in a broad set of simulated scenarios, the measured intersection throughput.

In our analysis, we aim at quantifying not only the average improvement of the considered metrics but also how well they are distributed among the set of drivers in the scenario. In a way, we do so to evaluate the fairness of the traffic evolution, i.e. whether all vehicles in the scenario make similar use of the shared resources.

In an attempt to avoid evaluating the performance of the strategies based on the particularities of a single traffic scenario, the evaluation is done by analyzing the average effect of the proposed methods across a broad set of simulated scenarios covering a wide variety of traffic configurations. Specifically, within such a set of simulations, we include instances with different traffic inflow volume, distribution among the incoming legs of the roundabout, and randomly drawn origin-destination patterns.

Finally, the baseline reactive behavior is validated on a real data set provided by our industrial partners. Such results will further validate the suitability of more advanced planning strategies measured relative to the baseline.

1.5 Thesis structure

This dissertation is structured as follows. We start in Chapter 2 by formalizing the problem, introducing some definitions and notation, the simulation platform we exploit, as well as discussing aspects concerning the assessment and representation of the results.

In Chapter 3, we discuss the information that the perception layer is expected to provide to the motion planner, as well as the method we propose to generate it. Specifically, we therein describe a strategy to extract probably-free inter-vehicle gaps by exploiting a dynamic occupancy grid representation of the surrounding space. The proposed context description represents the foundation upon which a novel motion planning workflow is later built.

In Chapter 4, we formalize our proposed motion planning architecture. Specifically, we: (i) identify the challenges concerning motion planning in mixed traffic scenarios, (ii) present a motion planning architecture suitable to tackle the challenge, and (iii) describe a planning method enabling high-level decision-making without the explicit exploration of all sequences of accelerations that can be followed.

In Chapters 5-8, we present novel planning methods that are, respectively, reactive, explicitly cooperative, implicitly cooperative, and predictive-reactive, thereby addressing the coexisting interaction mechanisms we presume to be available in mixed traffic conditions. Specifically, in Chapter 5, we formalize a reactive decision-making approach and introduce a novel and intuitive graphical representation of the reactive gap-acceptance mechanism. Afterward, in Chapter 6, we

conceptualize a new communication-based interaction mechanism for CAVs and formulate an explicitly cooperative planning strategy built upon it. Moreover, in Chapter 7, we present the notion of implicitly cooperative maneuvers, and design and assess a strategy suitable to perform yielding maneuvers without the need to communicate. Then, we design in Chapter 8 a predictive-reactive planning strategy whereby longer planning horizons can be used without sacrificing safety, despite the uncertainty of the future traffic state.

Furthermore, the baseline behavior is validated w.r.t. a real data set in Chapter 9. Our conclusions and further remarks are subsequently gathered in Chapter 10, where the body of this dissertation ends.

2 Problem Formulation and Preliminaries

In this dissertation, we investigate novel strategies to address the motion planning problem of a CAV driving through a roundabout in mixed traffic. Such a problem is regarded from the perspective of different interaction mechanisms that may coexist due to the heterogeneous technical capabilities of the vehicles surrounding the CAV of interest (often referred to as the *ego vehicle*). In this chapter, we begin by formalizing the traffic scenario we consider, the problem we tackle, as well as some assumptions that are common to all our proposed strategies regardless of the interaction mechanism upon which they are built. Additionally, for the sake of clarity, we introduce as well some elementary notions and terminology that will be exploited in all of the following chapters. It is worth stressing that, as we consider automated vehicles with communication capabilities, we will as well formalize the specific communication-based interaction mechanism we presume available to them. Moreover, we address an early challenge that comes up when designing motion planning strategies that are validated using roundabout scenarios, which concerns the assessment process. Specifically, we describe our simulation platform, the process exploited to generate the simulated traffic configurations, as well as the techniques used to evaluate and visualize the resulting behavior.

The chapter is structured as follows. In Section 2.1, we formalize the general problem in hand, along with the presumed communication-based interaction mechanism to be exploited by CAVs and some initial notations. The simulation platform we exploit in our study is briefly described in Section 2.2. The discussion concerning the creation of the traffic scenarios we use in the assessment stage is addressed in Section 2.3. Then, in Section 2.4 we discuss our approach to tackle some challenges regarding the evaluation and representation of the simulation results. Finally, in Section 2.5, some conclusions are presented.

2.1 Problem formulation

In this thesis, we consider the so-called motion planning problem for a CAV. That is, letting x generally denote the state of the ego vehicle, we aim to design strategies whereby, at a given time t and with a certain planning sampling time h, a state trajectory

$$x^T(t) = \{x(t), x(t+h), \cdots, x(t+T)\} \tag{2.1}$$

over a planning horizon T is generated, which represents how the vehicle should move so that its local objectives are achieved. Trajectories are assumed to be generated in a receding horizon fashion, i.e. they are continuously updated with a certain planning frequency, whereby the vehicle can adequately react to changes in the traffic context. Moreover, trajectories $x^T(t)$ are required to be (i) feasible concerning the vehicle's kinematics and dynamics, (ii) collision-free regarding the surrounding vehicles, and (iii) efficient in the way they utilize the surrounding roads and the inter-vehicle gaps.

The challenge is studied in a context where the ego vehicle shares the road with other CAVs, AVs, and human drivers (also referred to as *mixed traffic*). Such a circumstance imposes some particularities concerning the type of information that is available to the ego vehicle, and the mechanisms it can rely on to execute its maneuvers and interact with the surrounding vehicles. On the one hand, being surrounded by unconnected vehicles entails uncertainty concerning the vehicles' intent and state, thus requiring the ego vehicle to be able to perform traffic predictions and properly evaluate the safety probability of the motion it plans. On the other hand, when surrounded by other CAVs, the ego vehicle would be expected to have a dedicated communication-based interaction mechanism whereby the real driving intent of surrounding CAVs would be known. Thus, the ego vehicle could share its intent and issue cooperative requests to guarantee the safety of the maneuvers it is about to execute.

Regarding the dedicated communication-based interaction mechanism, we envision a scenario where CAVs can make cooperative requests, and/or reserve inter-vehicle gaps they plan to occupy in the foreseeable future. To do so, CAVs would create virtual vehicles (VVs) at the *reserved* locations, to which surrounding CAVs would then appropriately react. The idea is based on the working principle of the lane change indicators. For instance, picture a situation where a vehicle drives in a highway and plans to make a lane change. When the lane change indicators are turned on, surrounding vehicles willing to cooperate automatically behave as if there was a vehicle positioned in parallel to the vehicle trying to change lanes, i.e. in the position the vehicle plans to occupy. V2V communication could indeed be exploited to extend such an interaction mechanism if vehicles were allowed to explicitly point to the position they plan to occupy in the targeted traffic stream, which can be communicated through the creation of a virtual vehicle in the targeted location.

The presumed mixed traffic scenario also has an interesting impact on the perception capabilities of the ego vehicle. Indeed, the ego vehicle could be assumed to receive information from other CAVs concerning their driving intent, destination, and/or state, seeing its regular perception capabilities extended due to the inter-vehicle communication. Nonetheless, while driving surrounded by unconnected cars, the perception capabilities should be assumed to be affected by detection and estimation inaccuracies, as well as occlusions caused not only by the surrounding vehicles but also by other environmental elements.

Furthermore, as was mentioned in the introduction, although we aim to propose general methods to address the described problem, our ultimate goal is to make vehicles drive efficiently and safely through roundabouts. Interestingly, many navigation challenges are condensed in this type of traffic intersection, which makes it an excellent test bench for motion planning strategies. Specifically, (i) the traffic dynamics in roundabouts is complex and peculiar due to the circular geometry of the circulatory lanes, (ii) the fact that surrounding vehicles' intent is uncertain has an important impact on the efficiency of the decisions made, and (iii) occlusions pose important challenges as vehicles often have a partially occluded view of the precise regions that need to be accounted for to make a safe merging decision.

Regarding the solution we seek to formulate, several assumptions are adopted concerning the

Figure 2.1 – Representation of the main tasks involved in automated driving.

format and its desirable features. Firstly, we formulate planning strategies from the standpoint of a single CAV, meaning that if several CAVs were simultaneously at the intersection, each of them would independently run the solution we propose. Moreover, concerning the architecture of the automated driving system, we presume a clear separation between *perception*, *motion planning*, and *control* (see Fig. 2.1). That is, contextual information is first provided by the perception layer, the motion planner generates then feasible state trajectories, which are finally followed by a control module that applies the necessary control signal. Furthermore, whereas different assumptions will be made concerning the performance of the perception layer, the control layer is presumed to be able to accurately follow the trajectories our strategies generate.

2.1.1 Notation

Regarding some common notation we use throughout the coming chapters, let us begin by introducing how the state of the ego vehicle, and other surrounding obstacles, is represented and denoted. Generally speaking, the state of a vehicle in the scene will be denoted as $q = (p, \dot{p})$, which contains the vehicle's position and orientation $p = (p_x, p_y, \psi)$, as well as its derivative. Moreover, the control signal $u \in \mathbb{R}_{[a_\mathrm{m}, a_\mathrm{M}]}$ is assumed to represent its longitudinal acceleration (with a_m and a_M being the minimum and maximum accelerations).

From the standpoint of the ego vehicle, it is useful to represent the surrounding objects' state and the ego vehicle's future state, using a Frenet-Serret reference frame related to a certain path of reference π. Such a state representation is denoted as $x_\pi = (p_\pi, \dot{p}_\pi)$, with $p_\pi = (s, d, \theta_e)$ representing the vehicle's position through the distance s along the path where the projection of the vehicle is, the lateral distance d to it, and the heading deviation w.r.t. the path's orientation. Furthermore, we frequently make use of a reduced state $x = (s, v)$ (with $v \coloneqq \dot{s}$) representing the state of the vehicle's projection on the path of reference.

Furthermore, since the formulated strategies are to be used in a receding horizon fashion, we can consider, without loss of generality, the current time and the ego vehicle's position as a reference. Thus we consider $s_0 = 0$, and $t_0 = 0$ at each iteration, thereby absolute distances s and times t can be equivalently expressed as distance differences δ and time intervals τ. Consequently, we will often write (τ) when referring to $(t_0 + \tau)$, and δ instead of $s_0 + \delta$.

Moreover, let us point out that the term *agent* is exploited in this thesis to generally refer to the algorithm dictating the behavior of a certain vehicle.

2.2 Simulation platform

Our intent to evaluate the proposed planning strategies in simulation is motivated by two main reasons. Firstly, some of the strategies we aim to study are based on rather strong assumptions concerning the performance of the perception systems that current technology would not be able to provide. Yet their study is of interest as such presumed performance is likely to materialize in the

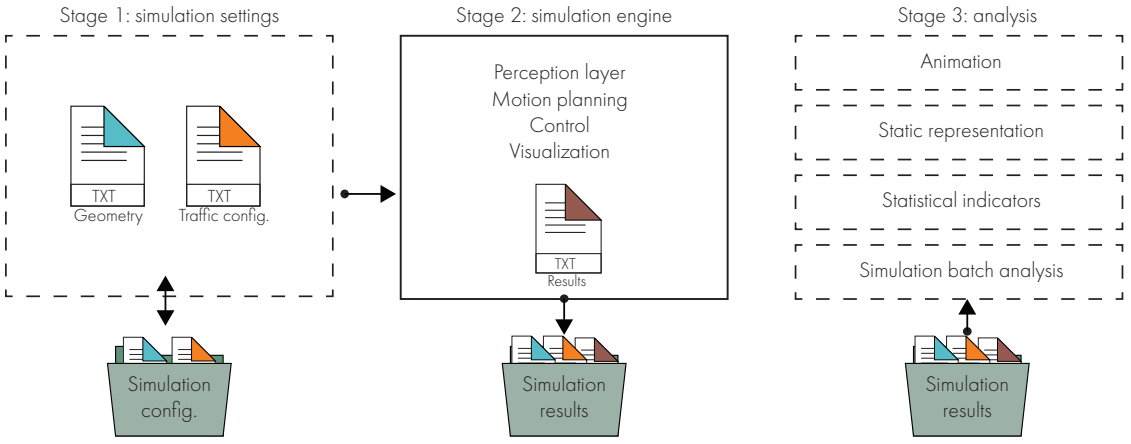

Figure 2.2 – Roundabout microscopic traffic simulator architecture.

future. For this reason, we require a testing platform that enables us to impose a minimum level of performance concerning the vehicles' sensing and control capabilities. Moreover, we are interested in quantifying the impact that behavioral policies might have on the overall traffic evolution. Thus, we require an evaluation method whereby our behavioral strategies can be implemented on a high number of vehicles.

As a consequence, simulation-based analysis emerges as the most viable solution to carry out our investigation. The problem, however, is that by the time this project started, no available microscopic-traffic simulation platform was found to meet all our needs. Thus, the theoretical study we present in this dissertation is built upon a dedicated Matlab-based roundabout microscopic-traffic simulation platform that we developed, which is briefly described below.

2.2.1 Simulation environment architecture

A fundamental aspect we considered when designing the simulation platform concerns the reproducibility of the traffic scenarios and the flexibility of the overall environment. To achieve such objectives, we implemented a simulation framework with the architecture shown in Fig. 2.2.

The implemented architecture is modular in such a way that the provided modules can be run independently if needed.

The *simulation setting* stage aims to unequivocally define a traffic scenario by making use of two independent text files defining the intersection geometry and the traffic configuration. High-level functions were developed to generate such configuration files from Matlab. Nonetheless, one could potentially modify such text files, by hand or programmatically, to control every detail of the simulation.

The *simulation engine* takes as input the geometry and traffic configuration information and simulates the behavior of every single vehicle until the last one exits the roundabout. Broadly speaking, placeholders are provided to adapt the vehicle's behavior at the perception, planning, and control level.

A set of *analysis* tools are as well developed to facilitate the numerical assessment of the simulations' result. Basic functionalities to retrieve and visualize saved simulation results are included.

Moreover, we designed tools to visualize the saved results as animation so that the resulting

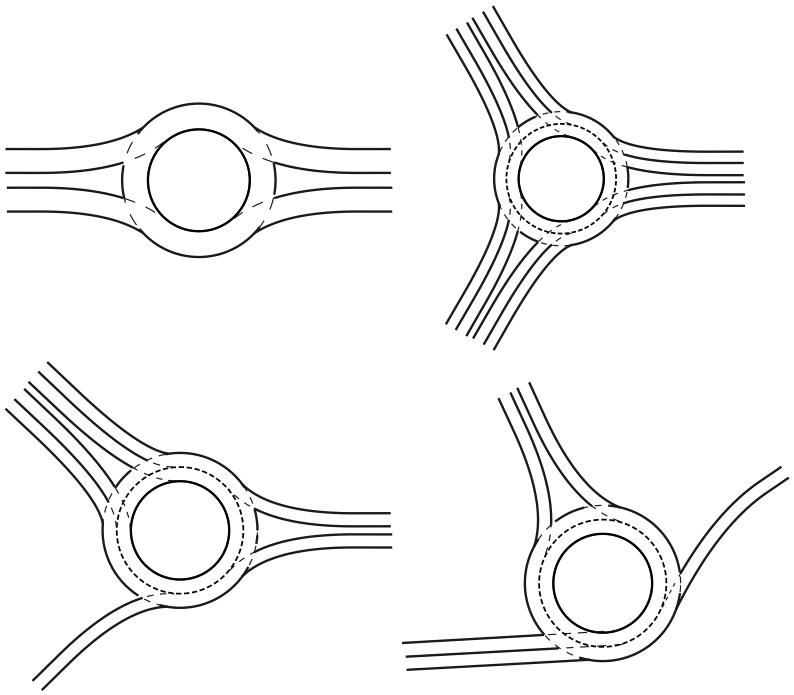

Figure 2.3 – Four examples of roundabout geometries that can be automatically generated with our simulation platform. Among examples we have varied the number of circulatory lanes, the number of legs, and the number of incoming and outgoing lanes in each leg.

traffic behavior could be qualitatively evaluated in a straightforward way. Among others, we developed tools to create videos out of simulation results, represent two simulation results at once in case several behaviors are to be compared, etc.

Finally, let us point out that a particularly interesting feature our simulator supports, is the easy creation, simulation, and assessment of large simulation batches. To do so, we developed not only high-level wrapper functions, but also some policies to structure, at a directory-level, the results of every single simulation within the set composing the analysis.

2.2.2 Definition of simulated roundabout geometry

In the coming Section 2.3, we will discuss aspects concerning the roundabout's geometry that are essential for the understanding of the theoretical results shown in this thesis. Thus, let us focus in this section on the flexibility our simulation platform provides concerning the generation of roundabout layouts.

Generally speaking, two main mechanisms are considered for the creation of the roundabout geometries.

Automatically generated roundabout geometry

Firstly, we provide an automated process to create hypothetical roundabout layouts (see Fig. 2.3), which allows us to generate complete roundabout geometries by the definition of a handful set of parameters. Specifically, it is only required to set the value of

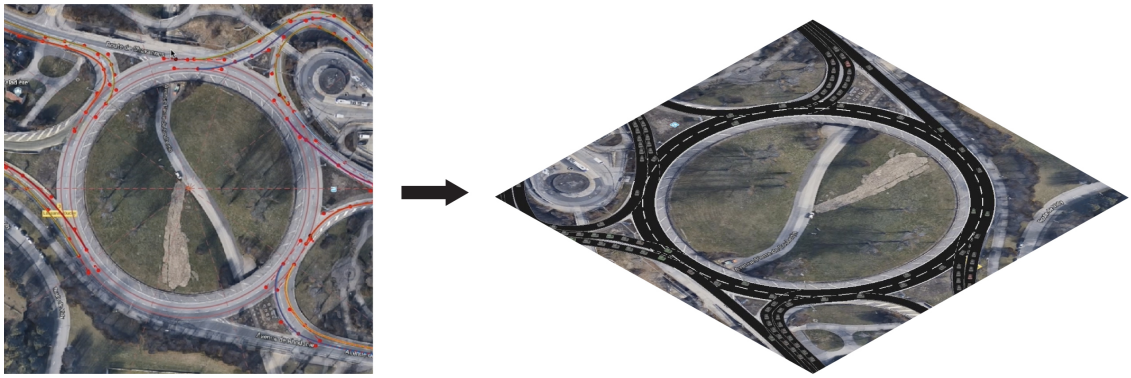

Figure 2.4 – Illustration of the process to manually create a roundabout layout. On the left-hand side, the top view of the roundabout and a set of Bézier curves defined by the user. On the right-hand side, screenshot of a simulation based on the resulting geometry. Roundabout image obtained from `maps.google.com`

- the inner radius of the roundabout,
- the extension of the roundabout area,
- the number of circulatory lanes,
- the number of legs,
- the number of incoming lanes in each leg,
- the number of outgoing lanes in each leg.

The parameters listed above are the main ones considered, but lower-level parameters can as well be edited to control the automatic creation process we implemented.

Even though the process is automatized, it provides a great flexibility concerning the variety of geometries that can be created in this way (see Fig. 2.3 for some examples).

Custom roundabout layout

Our automatic geometry generation process has some limitations despite its practicality. Such limitations mainly concern the specific definition of the geometry of the incoming and outgoing lanes, as well as the specific location where they merge into the circulatory lanes.

To address cases where the geometry of a real roundabout has to be replicated and simulated, we implemented a family of functions allowing the manual definition of roundabout layouts.

The process begins by obtaining an image of the top view of the roundabout of interest. Once the image is saved, its location is passed to a function in our simulation toolbox, which triggers an assisted procedure to define every single lane worth simulating.

Circulatory lanes are always considered to be perfectly circular, thus the algorithm starts by asking to indicate the center of the roundabout. Then, circles for the outer and inner roundabout's radii have to be fitted. Subsequently, the roundabout area is defined, which represents the extension that delimits the simulated scenario. Finally, the user has to define the incoming and outgoing lanes geometry one by one (an illustration of the process can be seen in Fig. 2.4).

During the process, the user defines the geometry of the lanes by creating and editing Bézier curves' control points. Once the process is completed, a geometry structure containing the control points of the defined curves is generated and saved for future use.

2.2.3 Definition of simulated traffic configuration

The traffic configuration details that are relevant for the motion planning assessment we exploit in this thesis are discussed in Section 2.3. Nonetheless, let us briefly discuss, in this section, the possibilities our simulation tool gives us in this regard.

As done with the creation process of roundabout layouts, we developed high-level functions to easily create the configuration structure defining the traffic to be simulated. Typically, one only needs to set

- the number of vehicles to include in the simulation,
- a set of parameters controlling the probability distributions used to randomly draw the origin and destination of every vehicle, and
- a set of IDs defining the vehicle's behavior.

Further parameters, as kinematic limits, vehicle's size, etc can as well be controlled. However, we will not describe here the full list of manipulable characteristics for the sake of brevity.

It is worth noting that all the features set automatically can be, nonetheless, manually redefined. That is the case, for instance, of the origin-destination pattern. By default, we apply the strategy that will be presented in Sections 2.3.2-2.3.3 to generate the vehicle's origin and destination. Nonetheless, as the result of the provided function is a configuration structure, the user is free to manipulate those as he/she pleases.

2.2.4 Definition of vehicles' simulated behavior

The behavior of the vehicles in our simulation is implemented as the combination of three sets of submodules, shown in Fig. 2.5.

Two submodules are first expected to define the perception capabilities of the vehicle. In our implementation, they are intended to separate the object-detection from the context-representation tasks, but any other distribution of tasks could also be implemented. By providing two differentiated submodules, we provide a physical separation between functionalities. As a result, if we develop two different object detection models, and two strategies for context representation, one could potentially combine those options to generate up to four different and complete perception layers.

Concerning the planning stage, four submodules compose the motion planning task, which allow to differentiate between driving stages. Such a practical division was implemented so that we could focus on the study of one driving stage at a time. For instance, if we were to develop a new merging policy, we could first duplicate the baseline behavior and then work only on the merging planning behavior while having the guarantee that the behavior at the remaining driving stages stays stable.

Finally, vehicles implement as well a dedicated low-level control layer. In our specific case, however, we assume that the control layer is capable of following the planned trajectory perfectly.

Interestingly, our simulation environment allows the development of new behaviors without the need to modify the main simulation loop. Specifically, we use additional data structures to specify the connection between a perception/planning/control ID, and the name of the submodule it represents. Then, by properly setting such a set of IDs in the simulation configuration file, the simulation loop can dynamically identify the behavioral function that needs to be called for every single vehicle.

Moreover, it must be noted that although such a set of placeholders are provided to define the vehicle's behavior, one could potentially manipulate them to implement different architectures if

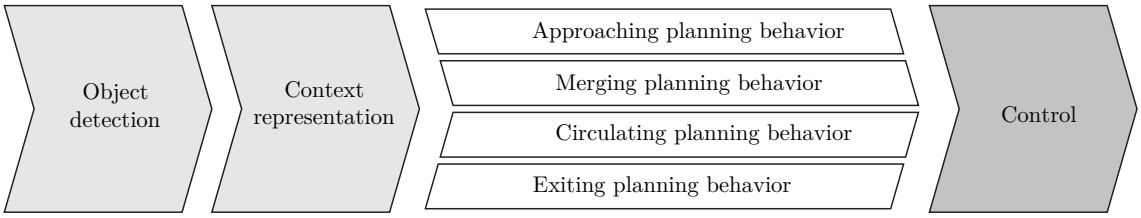

Figure 2.5 – Implementation of the simulated vehicles' behavior.

needed. In an extreme case, where an end-to-end solution wanted to be tested, one could potentially call a unique function from every provided submodule to do so.

2.2.5 Simulation engine

The *simulation engine* initializes simulations using the previously created geometry and configuration files, simulates traffic under those initial conditions, and dumps the configuration information as well as vehicle's trajectory in a specified directory.

In summary, this module implements a double-loop structure. A first simulation loop iterating over time, and a second inner loop iterating over the vehicles.

Given the control actions, and the model of the vehicles to be considered, the state of all vehicles is updated at the end of every time-iteration. The vehicle's motion model is given by a set of differential equations, which are integrated using `ode45` between simulation time steps.

When the simulation ends, the engine dumps into a set of `.mat` files the vehicles' trajectory and an additional set of macroscopic traffic indicators for future analysis. The vehicle's saved trajectory is sampled according to a certain driven distance interval. By doing so, as opposed to sampling the trajectories over time, we make the number of points representing the vehicles' trajectory only dependent on the path they follow and not on the speed profile.

We will not get into the details concerning how the numerical simulation is implemented. Instead, let us present some of the higher-level features implemented.

Contextual information In our main simulation loop, we have accounted for basic contextual calculations that might be required by most planning strategies, so that they do not need to be recalculated for every vehicle.

Specifically, we perform, only once at every sampling time, calculations concerning the identification of the vehicles that are merging/circulating/exiting, the headway and follow-up headway distances for every vehicle in the simulation, etc.

Visualization Concerning the simulation visualization, we intended to make the graphical interface of our simulations as meaningful and clean as possible. Two main visualization options were developed, (i) a practical two-dimensional representation of the traffic scenario, and (ii) a more appealing three-dimensional representation for demonstration proposes (see Fig. 2.6).

Debugging One of the main motivations to develop a dedicated simulation platform, was having the flexibility to debug the behavioral policies graphically. Thus, the simulation loop was designed to enable us to visualize, in real time, the paths, the decisions, and any other information of interest (see Fig. 2.7).

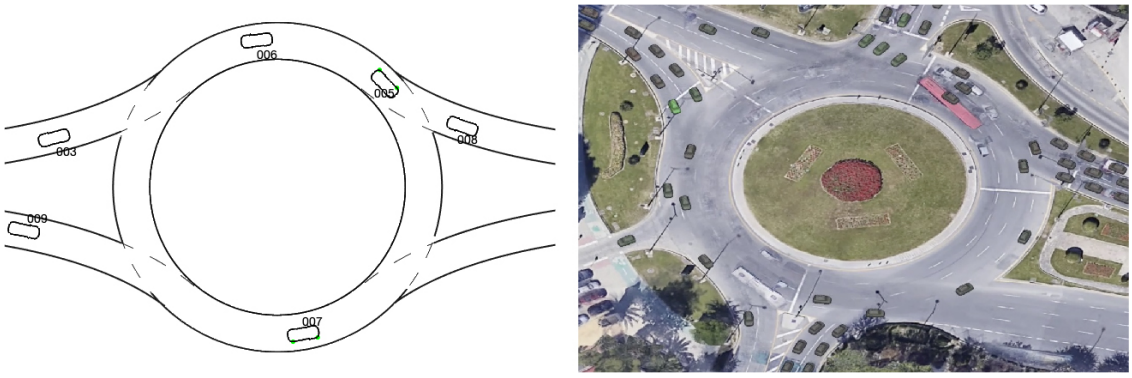

Figure 2.6 – Examples of the two on-line visualizations options our simulation environment supports. On the left-hand side, a two dimensional on-line representation. On the right-hand, a three dimensional view with the real image the roundabout's geometry is extracted from placed in the background.

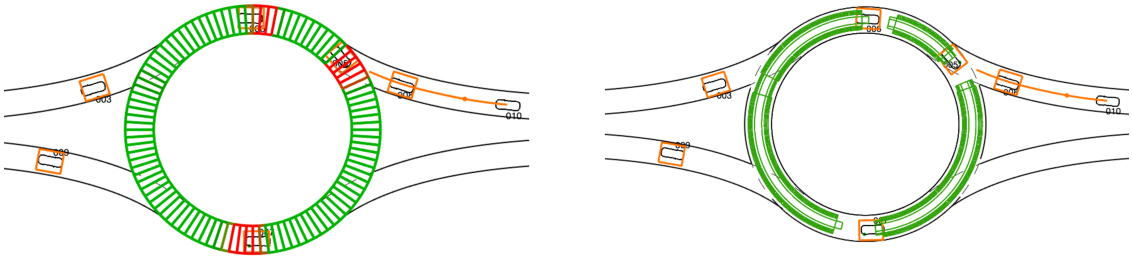

Figure 2.7 – On the left-hand side, debugging view where the path of the vehicle of interest, the objects it detects, and the state of the intersection it perceives is shown. On the left-hand side, an additional debugging representation showing the inter-vehicle gaps the pinned vehicle observes are shown.

This feature turned out to be very useful as, along with the debugging tools provided by Matlab, allowed us to stop and analyze the state of the decision-making policies at any point, and for any particular vehicle we chose.

Queue management As the dimension of the intersection area is set independently to the number of vehicles to be simulated, a method to deal with virtual queues is needed. In particular, every time that a vehicle is to appear in the scenario, the existence of vehicles in its leg is first checked and the vehicle appearance is delayed if needed.

The queue management was implemented so that the order in which the vehicles are set to appear is preserved. Moreover, arrival delays do not only affect the appearance of a vehicle in the roundabout area but also the density of the traffic that will appear in the future. Generally speaking, we propagate the traffic congestion beyond the roundabout area by the appropriate manipulation of the arrival events.

2.2.6 Analysis tools

The *analysis module* provides tools to retrieve, format, visualize and analyze the past simulation results.

Low-level functions to load the results of a determined simulation given the directory, and the ID of the simulation of interests were as well coded. Such low-level functions, would enable the user to design more complex analysis in an easy way.

In general, as the high-resolution vehicle's trajectory is saved along with the structures of the traffic configuration and intersection geometry information, the variety of analysis and representations that can be carried out is endless (see Fig. 2.8 for a three-dimensional representation, provided by one of our functions, of the traffic evolution in three scenarios). Some of the analysis that are possible to performed with our simulation environment will be shown through the thesis, but many more analysis are possible.

2.3 Traffic scenario

In this section, we address some aspects related to the creation of the traffic scenarios that will be used through this thesis to evaluate the proposed planning strategies. Specifically, three main aspects will be discussed:

- the basic geometry of the roundabouts considered,
- how the incoming traffic flow is created (i.e. how the vehicles' origin and arrival time are set),
- and the process used to randomly draw the destination of the vehicle in the scenario.

Additionally, we will present a scenario-labeling strategy to convey the information needed to fully characterize the simulated scenarios compactly.

2.3.1 Roundabouts

In this section, we begin by describing the geometry of the roundabout scenarios we consider in our study. A roundabout, denoted as $\mathcal{R}$, is defined as a tuple

$$\mathcal{R} = \{p_{\mathcal{R}}, r_{\mathcal{R}}, L_{\text{in}}, L_{\text{out}}, \mathcal{L}_{\text{circ}}, \mathcal{L}_{\text{in}}, \mathcal{L}_{\text{out}}\} \tag{2.2}$$

containing

- the position $p_{\mathcal{R}} \in \mathbb{R}^2$ of the roundabout's center,
- the radius $r_{\mathcal{R}} \in \mathbb{R}$ of the innermost circulatory lane boundary,
- a pair of sets $L_{\text{in}} = \{1, \cdots, n_{L_{\text{in}}}\}, L_{\text{out}} = \{1, \cdots, n_{L_{\text{out}}}\}$ of incoming and outgoing legs, and
- the sets $\mathcal{L}_{\text{circ}} = \{1, \cdots, n_{\mathcal{L}_{\text{circ}}}\}$, $\mathcal{L}_{\text{in}} = \{1, \cdots, n_{\mathcal{L}_{\text{in}}}\}$, $\mathcal{L}_{\text{out}} = \{1, \cdots, n_{\mathcal{L}_{\text{out}}}\}$ of, respectively, circulatory, incoming, and outgoing lanes.

The geometry of the lanes conforming the roundabout is assumed to be known, and the ego vehicle is presumed to be able to localize itself in the intersection perfectly. The circulatory lanes are considered to be perfectly circular, and the roundabout scenes we use in our study will be balanced, i.e. they will have the same number of incoming and outgoing legs and lanes ($n_{\mathcal{L}_{\text{in}}} = n_{\mathcal{L}_{\text{out}}}$). Moreover, incoming and outgoing lanes are radial to the roundabout itself, with a smooth transition

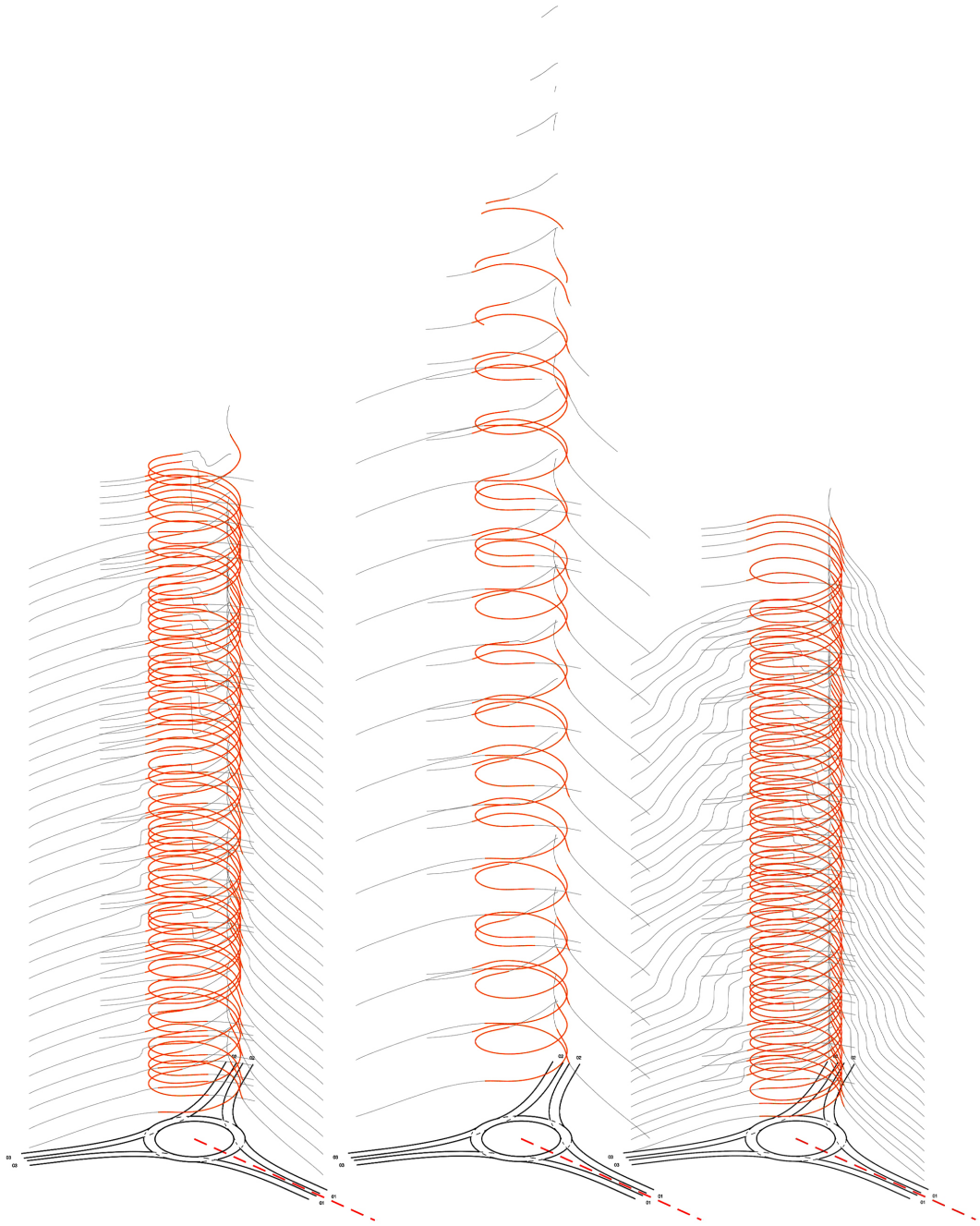

Figure 2.8 – Three-dimensional representation of the trajectories of a set of vehicles driving through a certain roundabout. A common geometry but different traffic configurations are used on the three instances shown. Time is represented in the vertical axis.

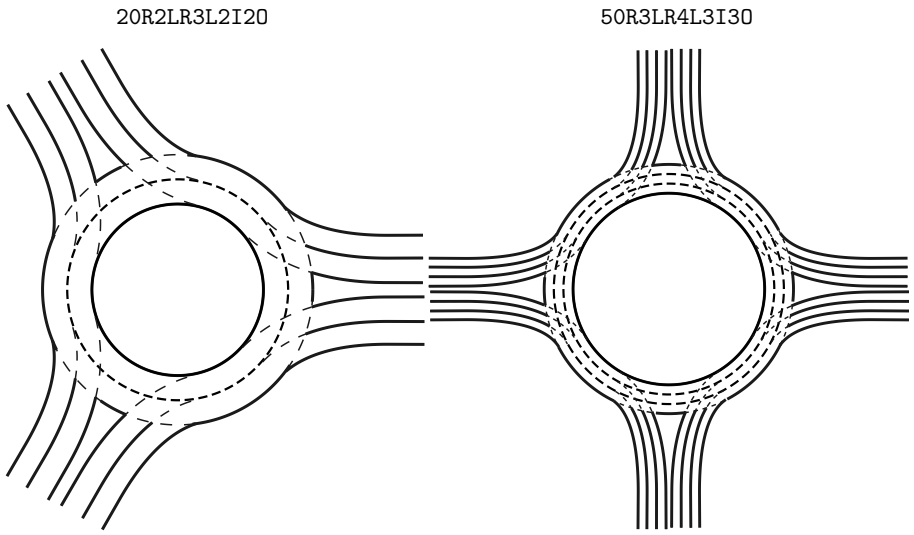

Figure 2.9 – Two roundabout scenarios illustrating the roundabout geometry we consider. On the left-hand side, a 20R2LR3L2I2O roundabout. On the right-hand side, a 50R3LR4L3I3O roundabout.

connecting such lanes to the circulatory ones. Furthermore, only a finite circular region around the roundabout itself will be considered in our simulations, which is referred to as the *roundabout area*.

Given the considerations mentioned above, a $r_{\mathcal{R}}$ Radius $n_{\mathcal{L}_{\text{circ}}}$ Lanes Roundabout, with $n_{L_{\text{in}}}$ Legs, $n_{\mathcal{L}_{\text{in}}}$ Incoming lanes, and $n_{\mathcal{L}_{\text{out}}}$ Outgoing lanes can be labeled as $r_{\mathcal{R}}\texttt{R}n_{\mathcal{L}_{\text{circ}}}\texttt{LR}n_{L_{\text{in}}}\texttt{L}n_{\mathcal{L}_{\text{in}}}\texttt{I}n_{\mathcal{L}_{\text{out}}}\texttt{O}$. For instance, the roundabouts depicted in Fig. 2.9 would be simply denoted as 20R2LR3L2I2O (20m radius, 2-lanes roundabout, 3 legs, 2 incoming lanes, 2 outgoing lanes) and 50R3LR4L3I3O, respectively.

2.3.2 Incoming traffic

For the incoming traffic to be fully characterized, we need to specify the total number of vehicles included in the simulations, along with the level of congestion of the traffic heading towards the roundabout, and how it is distributed among the incoming lanes. Such information can be encapsulated in three parameters:

- $n_{\mathcal{N}}$: the total number of vehicles in the scene, also represented by the cardinality of the set $\mathcal{N} = \{1, \cdots, n_{\mathcal{N}}\}$ of all vehicles in the scene,
- Q_{I}: representing, in vehicles per hour (veh/h), the total traffic volume moving towards the scene (also referred to as *traffic inflow*),
- $\beta = \{\beta_1, \cdots, \beta_{n_{L_{\text{in}}}}\}$: a vector gathering weights β_i related to the traffic flow approaching the intersection by the incoming leg i, in such a way that the higher the weight, the higher the proportion of Q_{I} that approaches the intersection by the leg i.

From such parameters, the vehicles' arrival time and origin are generated as follows. Firstly, the traffic inflow q_i approaching the roundabout by the leg i, in [vehs/h], is calculated as

$$q_i = \frac{\beta_i}{\sum_j^{n_{L_{\text{in}}}} \beta_j} Q_{\text{I}}. \tag{2.3}$$

Then, the time interval between vehicles arriving at the roundabout area by every incoming leg i would be assumed to follow a Poisson distribution $\text{Pois}(\lambda_i)$ with its parameter

$$\lambda_i = 3600/q_i \tag{2.4}$$

representing the average arrival time interval (in s) between vehicles in leg i. Then, for every origin $o \in L_{\text{in}}$, a vector

$$\tau_o^{\text{a}} = \left(\tau_{o,0}^{\text{a}}, \tau_{o,1}^{\text{a}}, \cdots, \tau_{o,n_{\mathcal{N}}}^{\text{a}}\right) \tag{2.5}$$

of possible arrival times would be generated, whose elements are calculated as

$$\tau_{o,i}^{\text{a}} = \tau_{o,i-1}^{\text{a}} + \text{Pois}(\lambda_o). \tag{2.6}$$

Consequently, the theoretical arrival time t_i^{ta} of every vehicle $i \in \mathcal{N}$ in the simulation will simply correspond to the $n_{\mathcal{N}}$ smallest arrival times generated across possible legs. Moreover, the specific incoming lane they approach by would be obtained by randomly choosing a lane within the leg corresponding to the arrival time.

It is worth noting that the actual arrival time of the vehicles in the scenarios may get delayed if queues that extend to the limit of the roundabout area are formed.

In the following chapters, for the sake of compactness, we will typically use the notation $n_{\mathcal{N}}\texttt{V}-Q_{\texttt{I}}\texttt{Q}[\beta_1, \cdots, \beta_{n_{L_{\text{in}}}}]$ to provide the full information concerning the incoming traffic configuration. For instance, the label `100V-1500Q[1 1 1]` would represent a simulation of 100 vehicles, driving towards a roundabout at a rate of 1500 vehs/h, and equally distributed among the three legs of a roundabout.

2.3.3 Outgoing traffic

The traffic flow leaving the roundabout area is dependent on the behavioral policy the vehicles are assumed to follow. However, the way in which the vehicles in the scene get assigned a destination must be discussed.

The destination of every vehicle in the scene is chosen by randomly drawing the distance the vehicle is likely to drive inside the roundabout, and then selecting the closest destination to such a distance. Specifically, given an origin $o \in \mathcal{L}_{\text{in}}$ and the circulatory lane $c = \texttt{circ}(o) \in \mathcal{L}_{\text{cir}}$ it merges into, and denoting as $\texttt{Len}(c) : \mathcal{L}_{\text{cir}} \to \mathbb{R}^+$ the length of a circulatory lane c, we consider the distance δ the vehicle is likely to drive to be a random variable (r.v.) following a normal distribution $\mathcal{N}(\mu(c), \sigma(c))$, with

$$\mu(c) = \frac{c}{2n_{\mathcal{L}_{\text{cir}}}}\texttt{Len}(c), \qquad\qquad \sigma(c) = \frac{\texttt{Len}(c)}{5}. \tag{2.7}$$

That is, the more inner the circulatory lane the vehicle merges into, the longer it is expected to drive inside the roundabout (see Fig. 2.10 for a representation of the distributions used in the example scenario).

Once a distance δ_i for every vehicle $i \in \mathcal{N}$ has been drawn, we proceed to identify the outgoing leg whose exiting spot is the closest to the targeted distance, and then randomly select a specific lane within the leg as the vehicle's destination.

In Fig. 2.11, a sample of the origin-destination pattern resulting from this process is shown for

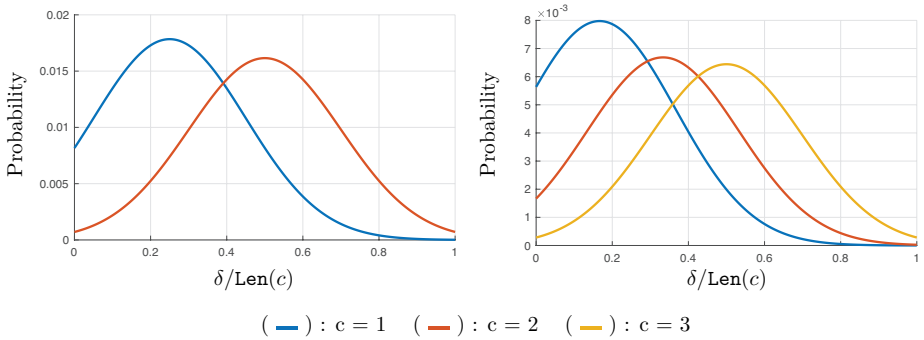

Figure 2.10 – Normal distributions used to sample the distance that the vehicles are likely to drive inside the roundabout, which depends on the circulatory lane c they merge into. The results shown correspond to the two scenarios depicted in Fig. 2.9, and in the horizontal axis we represent the ration between the driven distance and the roundabout's length (i.e. value 1 represents a distance equal to the roundabout length). Note how, the inner the circulatory lane the vehicle merges to (c), the longer they are expected to drive.

the two geometries presented in Fig. 2.9. Notice how those vehicles approaching the intersection by an incoming lane that merges into the innermost and outermost circulatory lanes are unlikely to take, respectively, the first and last exit of the roundabout w.r.t. their origin.

2.3.4 Scenario-labeling process

Given the considerations described in the previous sections, the sub-labels proposed to specify certain aspects of the scenario configuration can be concatenated to fully characterize the scenarios themselves. In particular, we will use the notation

$$\texttt{X}_1\texttt{RX}_2\texttt{LRX}_3\texttt{LX}_4\texttt{IX}_5\texttt{O} - \texttt{X}_6\texttt{V} - \texttt{X}_7\texttt{Q[X}_8, \cdots, \texttt{X}_{7+\texttt{X}_3}\texttt{]} \tag{2.8}$$

to embed the information concerning the roundabout geometry ($\texttt{X}_1\texttt{RX}_2\texttt{LRX}_3\texttt{LX}_4\texttt{IX}_5\texttt{O}$) and the incoming traffic configuration ($\texttt{X}_6\texttt{V} - \texttt{X}_7\texttt{Q[X}_8, \cdots, \texttt{X}_{7+\texttt{X}_3}\texttt{]}$) directly in the simulation's name.

2.4 Performance assessment

In this section, we discuss some challenges that arise at the time of evaluating the performance of our planning methods in the described roundabout scenarios, as well as how we tackle them. On the one hand, we illustrate the challenges encountered to represent in a meaningful way the trajectories followed by the vehicles in the traffic scenario of interest, and briefly describe the strategy we adopt. On the other hand, we present the method we exploit to evaluate the overall traffic coordination performance resulting from the application of our strategies and propose a set of traffic performance metrics that will appear throughout the thesis.

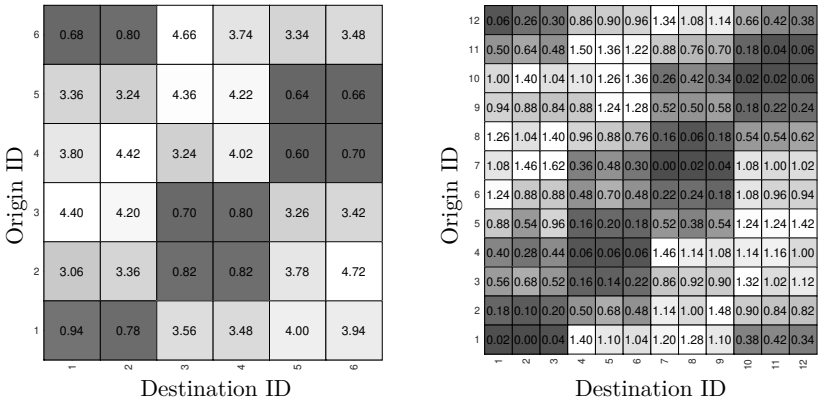

Figure 2.11 – Examples of two random instances of origin-destination patterns drawn for the two scenarios shown in Fig. 2.9, and a incoming traffic configuration `5000V-[1 1 1]` and `5000V-[1 1 1 1]`, respectively. The value shown in every cell (o, d), corresponding to an origin o and a destination d, shows the percentage of vehicles that were assigned to drive from o to d.

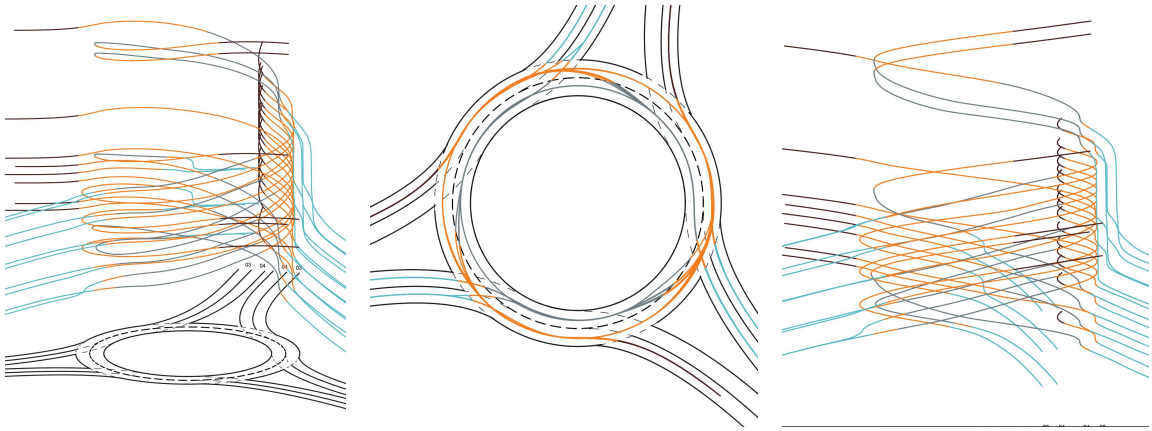

Figure 2.12 – Three-dimensional representation of the trajectories followed by a set of vehicles driving through a roundabout. Time is represented in the vertical axis.

2.4.1 Traffic evolution

One of the first challenges we face when trying to analyze the vehicles' evolution over time in roundabout scenarios concerns its visualization. Indeed, due to the intersection's geometry, a clear representation of the vehicles' trajectory is challenging to achieve, as can be observed in Fig. 2.12 where several perspectives of a three-dimensional view of the vehicles' trajectory are shown. The type of features one could expect to analyze by visualizing the vehicles' trajectory (such as whether vehicles collide or how smoothly they move forward) can hardly be observed, since trajectories are contained in non-parallel curved planes. Thus, an alternative representation approach is needed.

Traffic flow time-distance diagram

Let us begin by describing the basics upon which our approach to represent traffic evolution at roundabouts is built. Specifically, the so-called time-distance diagram.

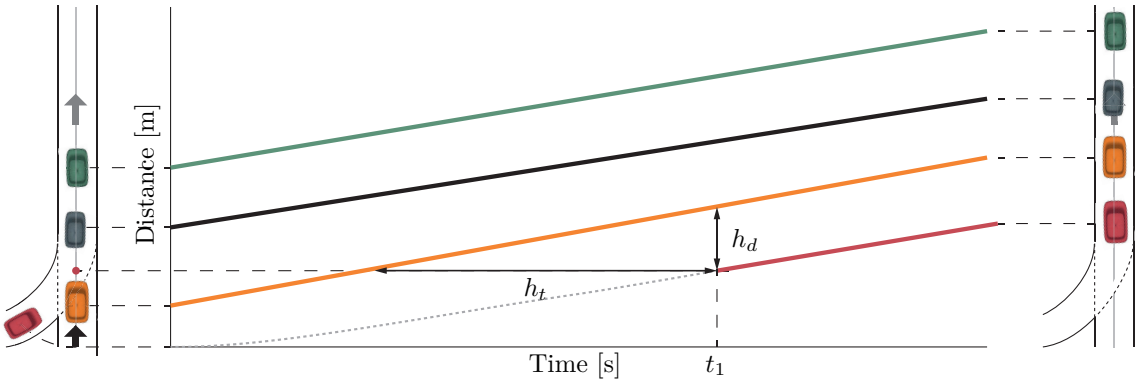

Figure 2.13 – Time-distance diagram representation.

The time-distance diagram of a traffic flow refers to a two-dimensional representation of the trajectory described by a set of vehicles along a common path (see Fig. 2.13).

In such representation, the slope of the trajectories represents the speed of the vehicle in such a way that, the more horizontal the trajectory, the lower the speed at which the vehicle drives.

From the diagram one could as well extract the distance headway h_d, and time headway h_t between two vehicles. The distance headway h_d represents the physical distance between two vehicles, and would be extracted from the time-distance diagram by choosing a time of interest, drawing a vertical line, and measuring the separation between the vehicle's trajectory. The time headway h_t shows the time interval separating two successive vehicles, and can be obtained by similarly measuring the distance between trajectories, this time in the horizontal direction. Furthermore, collisions in such a diagram would be represented by crossing trajectories.

The diagram does allows us to represent the trajectory of vehicles that merge into the path of reference as well. In such a case, however, the vehicle's trajectory would appear at some specific time. Consider, for instance, the red vehicle's trajectory in Fig. 2.13. Such a trajectory begins at the time the vehicle merges into the straight road, i.e. t_1. For the sake of giving some further continuity to the representation, we sometimes represent as well, with dashed gray lines, the trajectory of the vehicle's projection on the main road when it is positioned in a different lane.

In Fig. 2.13, we have illustrated the evolution of four vehicles along a straight path. Nonetheless, the same representation could be used to illustrate the traffic evolution along a path of arbitrary geometry as long as it is common to all the considered vehicles.

Representation of traffic at roundabouts

The strategy we exploit in this thesis to represent the traffic evolution in roundabouts is based in the time-distance representation described above. Specifically, it consists in splitting the lanes composing the roundabout (mainly the approaching and circulatory lanes) and then representing time-distance diagrams of the traffic at each of those lanes. Notice that, in multi-lane roundabouts, every circulatory lane would as well require a dedicated time-distance diagram.

The distance represented in such diagrams needs to be measured w.r.t. a common reference location. For the case of circulatory lanes, it will typically be the position where the horizontal axis passing through the center of the roundabout intersects the right-hand side of the circulatory lanes (which is illustrated in Fig. 2.14 by a dashed red line). When the vehicles' merging trajectory is

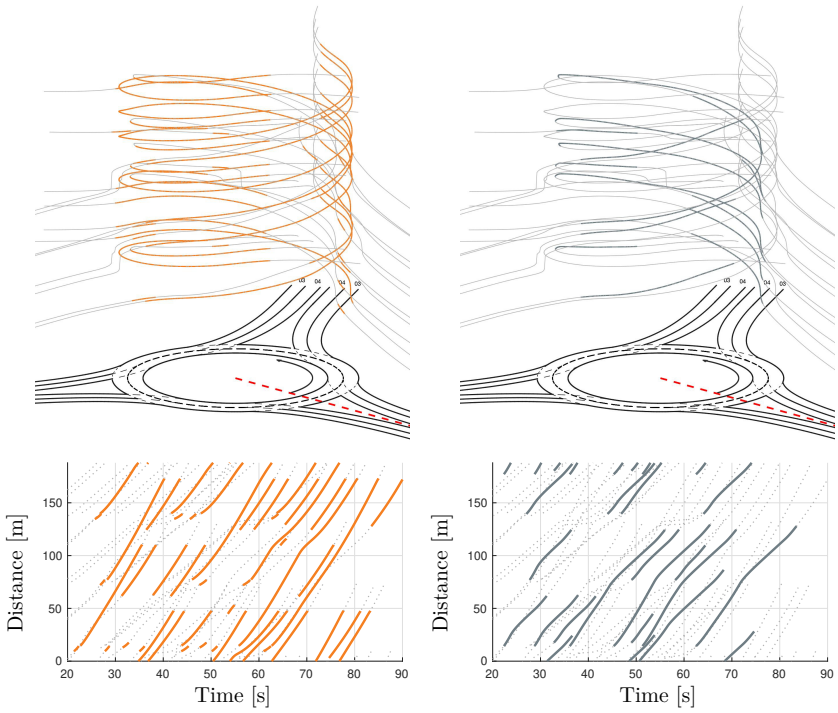

Figure 2.14 – At the top, a three-dimensional representation of the trajectory of the vehicles circulating in the roundabout's outermost (left-hand side) and innermost (right-hand side) circulatory lane. At the bottom, their equivalent two-dimensional representation as time-distance diagram. The dashed red line represents the spot in the circulatory lane which is used as the distance reference.

represented, the distance is referred to the position of their merging spot. It is nonetheless worth stressing that the absolute value of the represented distance is not critical to qualitatively understand the traffic evolution, for which only the relative position between the trajectory traces is relevant.

Moreover, due to the circular geometry of the circulatory lanes of the roundabout, the vertical axis of the time-distance diagram is represented between zero (referred to some reference spot) and the length of the roundabout. As a result, vehicles' trajectory often disappear at the top and appear at the bottom when vehicles drive through the location of reference.

Furthermore, when the focus of the representation is the merging traffic, we use, as commented above, a similar approach. Note however that, in this case, the traffic approaching by every incoming *lane* must be represented separately. Furthermore, we could additionally represent a small portion of the trajectory of those vehicles that circulate around the decision spot of the incoming lane being analyzed (represented by (—) in Fig. 2.15) to provide additional collision avoidance information.

2.4.2 Traffic performance metrics

For the sake of comparing the effects that different motion planning strategies have on the overall traffic coordination performance, we require appropriate quality metrics. Three main groups of metrics can be differentiated: those aiming to quantify the characteristics of the vehicles' trajectory, those characterizing the fairness with which the vehicles make use of the traffic intersection, and those providing information about the overall intersection performance.

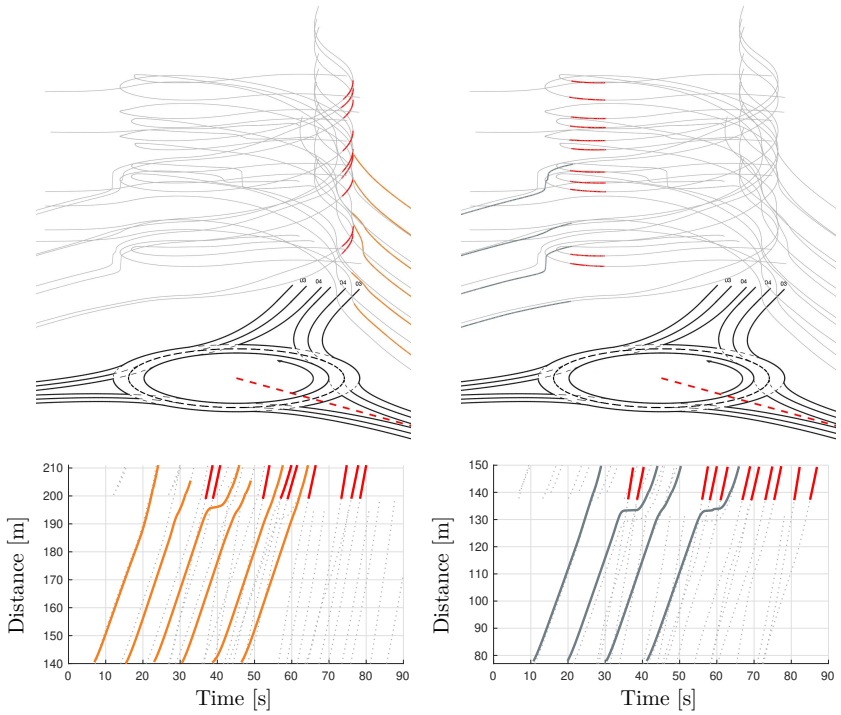

Figure 2.15 – Time-distance representation of the traffic approaching the depicted roundabout by two incoming lanes. On the left-hand side, the time-distance representation of the trajectories of the vehicles approaching the roundabout by the first leg. On the right-hand side, time-distance representation of trajectory of the vehicles approaching the roundabout by the third leg.

Let us begin by pointing out that every vehicle $i \in \mathcal{N}$ included in the scenario would have, once the simulation is over, the following set of properties:

- $\mathbf{t}_i = \{(k_i^{\mathrm{a}} + k)h_{\mathrm{sim}} : k \in [0, 1, \cdots, N_i]\}$: the set of simulated time instances at which the vehicle is within the roundabout area, where $h_{\mathrm{sim}} = 0.05$s is the chosen simulation sampling time, k_i^{a} shows the simulation time step in which the vehicle i first appears in the scenario, and N_i represents the number of time steps the vehicle requires to drive through the roundabout,
- $t_i^{\mathrm{a}} \coloneqq k_i^{\mathrm{a}} h_{\mathrm{sim}}$: the vehicle's arrival time to the roundabout area (which might differ from the theoreticla arrival time t_i^{ta} if the incoming lane the vehicle i approaches by saturates and the appearance of the vehicle in the scenario needs to be delayed),
- $t_i^{\mathrm{f}} \coloneqq (k_i^{\mathrm{a}} + N_i)h_{\mathrm{sim}}$: the time the vehicle disappears from the roundabout area,
- $\mathbf{v}_i = \{v_i(t) : t \in \mathbf{t}_i\}$: the sequence of speeds the vehicle experiences as it moves through the scenario,
- $\mathbf{a}_i = \{a_i(t) : t \in \mathbf{t}_i\}$: the set of accelerations applied by the vehicle over the simulation.

Vehicles' trajectory features

From such a set of information, we can extract the following indicators concerning the trajectory of every vehicle i:

- travel time $\mathtt{TT}_i = t_i^{\mathrm{f}} - t_i^{\mathrm{a}}$,

- travel speed $\texttt{TS}_i = s_i^{\text{od}}/\texttt{TT}_i$,
- delay $\texttt{D}_i = t_i^{\text{a}} - t_i^{\text{ta}}$,
- overall travel speed $\texttt{OTS}_i = s_i^{\text{od}}/(\texttt{TT}_i + \texttt{D}_i)$,
- average speed $\texttt{V}_i = \texttt{Mean}\{\mathbf{v}_i\}$, and
- average jerk $\texttt{J}_i = \texttt{Mean}\{\mathbf{a}_i^2\}$.

In the previous definitions, the operator

$$\texttt{Mean}(\{x_1, \cdots, x_n\}) = \frac{1}{n}\sum_{k=1}^{n}(x_k) \tag{2.9}$$

is used to represent the mean of a certain sequence.

The analysis of the distribution of the metrics listed above would, therefore, provide information concerning the characteristics that a vehicle could expect its trajectory to have as it moves through the scenario.

Note that the travel speed is calculated using the theoretical distance between the origin and the destination of the ego vehicle instead of the distance driven by it. This subtlety is considered for the sake of capturing the possibility of vehicles missing their exit in multi-lane roundabouts and being forced to drive around the roundabout one extra time. Similarly, the vehicles' travel speed only takes into account the time it takes the vehicles to drive from their origin to their destination from the time they appear in the roundabout area. However, it does not capture the fact that the vehicle's arrival time might have been delayed. To capture such a phenomenon, we introduced the so-called *overall travel speed*, calculated by considering the vehicle travel time as well as its arrival delay.

Traffic fairness

An additional set of metrics can be extracted from the previously-mentioned distributions to represent how balanced the resulting traffic evolution is. In a way, such a fairness metric could be thought to be related to the variance of the distributions, measuring how narrow or wide the distributions are. However, the variance in itself would not take into account the mean value of the distributions, and, intuitively, a variance of 1s^2 for the distribution of vehicles' delay would represent a fairer situation the higher the delays were on average. For this reason, we will use the fairness index proposed by Jain et al. in [35], formulated as

$$\texttt{Fairness}(\{x_1, \cdots, x_n\}) = \frac{\left(\sum_{k=1}^{n} x_k\right)^2}{n\sum_{k=1}^{n} x_k^2}, \tag{2.10}$$

to quantify the fairness with which the previous metrics are distributed among the agents. As an example, let us consider three hypothetical vehicles in a certain scenario, and three different cases where their average speeds are, respectively,

$$\texttt{V}^{(i)} = \{15, 15, 15\} \qquad \texttt{V}^{(ii)} = \{15, 10, 15\} \qquad \texttt{V}^{(iii)} = \{5, 0, 5\}. \tag{2.11}$$

In those cases, the aforementioned fairness index would return

$$\texttt{Fairness}(\texttt{V}^{(i)}) = 1, \qquad \texttt{Fairness}(\texttt{V}^{(ii)}) = 0.97, \qquad \texttt{Fairness}(\texttt{V}^{(iii)}) = 0.66, \tag{2.12}$$

where cases (ii) and (iii) are successfully assigned different fairness values, despite of them having the same variance.

Overall traffic performance

Moreover, to evaluate the overall traffic coordination performance we analyze, on the one hand, the total intersection throughput, measured in vehs/h and calculated as

$$\texttt{TH} = \frac{|\mathcal{N}|}{\max_{i\in\mathcal{N}} t_i^{\mathrm{f}} - \min_{i\in\mathcal{N}} t_i^{\mathrm{a}}} 3600 \ . \tag{2.13}$$

On the other hand, we analyze the distribution of throughput values (in vehs/h) calculated in intervals of 15min, which, letting

$$\mathcal{N}_{[t_1,t_2]} = \left\{ i \in \mathcal{N} : t_i^{\mathrm{f}} \in [t_1, t_2] \right\} \tag{2.14}$$

be the subset of vehicles within $\mathcal{N}$ whose exit time is within the time window $[t_1, t_2]$, $\underline{t}^{\mathrm{a}} = \min_{i\in\mathcal{N}} t_i^{\mathrm{a}}$ be the time at which the first vehicle appears in the scenario, and $\overline{t}^{\mathrm{f}} = \max_{i\in\mathcal{N}} t_i^{\mathrm{f}}$ be the time at which the last vehicle in the scenario exits the roundabout area, can be calculated as

$$\texttt{TH}_{15} = \left\{ |\mathcal{N}_{[t_1,t_1+15]}| \frac{3600}{15} : t_1 = \underline{t}^{\mathrm{a}} + k15, k \in \left[0, \left\lfloor \overline{t}^{\mathrm{f}}/15 \right\rfloor\right] \right\}. \tag{2.15}$$

The analysis of the sequence $\texttt{TH}_{15}$ is expected to provide information concerning the continuity with which the vehicles drive through the intersection.

2.5 Conclusions

In this chapter, we have addressed some common aspects concerning the strategies that will be presented in the upcoming chapters of this thesis. We started formalizing the problem we address, describing the communication-based interaction mechanism that CAVs are assumed to have available, as well as introducing some initial notations. Then, the specific roundabout geometry we use, as well as the process we follow to generate the traffic in our simulations, were described along with a scenario-labeling strategy that allows us to provide complete information of the scenario in a very compact way. Finally, problems concerning the representation of the simulation results have been addressed, some solutions proposed, and the performance metrics used to quantify the performance of the proposed strategies have been explained.

It is worth stressing that the aspects discussed in this chapter are meant to properly characterize the simulation study we carry out in this thesis. However, the strategies that will be proposed in the coming chapters are, in general, applicable to a broader set of traffic scenarios and, specifically, to roundabouts with different geometries from the ones used in our simulation study.

3 Perception Models

Perception is a crucial part of automated vehicles technology as it is the pillar upon which the understanding of the surrounding traffic scene is built, decisions are made, and future motions are planned. The perception layer can be thought of as the interface through which the ego vehicle understands the real world. Hence, its role is to synthesize and provide reliable and high-quality information to the motion planner, which will use it to generate safe and efficient motion plans. In this chapter, we discuss some aspect of the perception systems that have a strong influence on the motion planning strategy. Namely, the format in which the ego vehicle's surrounding space is described, as well as the method we follow to obtain such a description from the output of more traditional approaches.

Generally speaking, the perception module of an AV should be engineered in such a way that enough information is provided to the motion planner for it to generate safe trajectories to follow. In this sense, a widespread practice is assuming that such information consists of a set of observed surrounding objects. In this way, the motion planner can focus on generating plans that are collision-free (a practice that is herein referred to as the *object-detection and avoidance* approach). Moreover, depending on the specific motion planning problem under study, the set of observed objects might be considered to be incomplete because of the presence of occluded objects, or the state of the detected ones uncertain due to detection inaccuracies.

Occlusions pose a particularly interesting challenge, as the lack of detection in the mentioned approach means, a priori, the absence of an obstacle, which would be an unsafe conclusion in occluded scenes. As a consequence, occlusions are typically addressed in this sense by identifying the occluded region and then taking into account the possible existence of an obstacle in such a region with the worst possible state. However, to date, studies following this rationale run into rather cumbersome solutions where additional difficulties arise in scenarios with highly dynamic and transient occlusions. Among other reasons, because such dynamic occlusions would still need to be modeled and would potentially require creating virtual vehicles (VVs) in each of them for the sake of imposing safety on the planned motions.

The aspects discussed above concerning the object-detection and avoidance models, along with the specific traffic scenario we study, motivate the investigation of an alternative approach. Specifically, we explore a dual representation of the environment referred to as *free-space identification and exploitation*, whereby the surrounding free space is represented as a set of probably-free inter-vehicle gaps as opposed to as a set of objects that should be avoided.

This chapter motivates and describes in detail the gap-based perception approach we envision, which will enable the motion planner (that will be formalized in Chapter 4) to systematically and more naturally generate trajectories in the presence of perception uncertainty and/or occlusions. We do not intend to tackle the perception problem understood as the problem of performing detections and extracting meaning out of the low-level sensors. Instead, we aim to formulate a post-processing layer to generate a more suitable description of the partially occluded surrounding space, which is to be used by the decision-making modules proposed in the remainder of this thesis.

The chapter is structured as follows. We begin by discussing in Section 3.1 some relevant research by which this chapter is inspired. In Section 3.2, we present the considered general perception approach, as well as some specific variations that will be used in the simulation analyses carried out in the coming chapters. Some results are shown in Section 3.3 so that the type of information that could be expected from the proposed method is better characterized. Subsequently, conclusions and final remarks are gathered in Section 3.4.

3.1 Related work

The objective of this chapter is describing the context representation our proposed motion planners exploit. Specifically, we seek to come up with a representation of the surrounding space that, if properly used by the motion planners, naturally allows our strategies to handle occlusions. Thus, we begin in this section by reviewing some existing works addressing occlusion-aware motion planning.

Motion planning under occlusions is a significant challenge for AVs that is recently attracting a great deal of attention in the literature. Occlusions have a substantial impact on motion planning as they severely affect the object detection capabilities, requiring the motion planner to integrate additional considerations to preserve safety, yet navigating as efficiently as possible. Such a challenge represents a rather hot research topic in the IV community, and many studies in this direction have arisen in the last years.

A common practice in the literature consists in accounting for phantom vehicles in the occluded regions, which are then integrated within preexisting trajectory planners for the sake of planning while considering the worst-case scenario. For instance, Sahin Tas Ömer et al. address in [83] the problem of motion planning at an intersection in the presence of occlusions caused by static environmental elements like buildings. They consider uncertainty on the ego vehicle's position as well as on the estimated position of surrounding vehicles, and incorporate occlusions within the planning strategy by considering phantom vehicles that sit at the border of the field of view. They propose a simple maneuver planner which, built on the *intelligent driver model* (IDM) for trajectory prediction, makes comprehensible merging decisions. Constraints are also added to the trajectory planner to impose, when needed, a safety distance with the yield marking and/or the vehicle ahead.

Recently, stochastic motion planning framework based on Markov Decision Processes (MDPs) have emerged as a promising approach to address decision-making under uncertainty, which is also applicable to occlusion-aware planning. In that direction, Naumann et al. investigate in [63] the motion planning problem at crossroads whose visibility is affected by a surrounding building. The authors aim at imposing safety while considering comfort yet avoiding over-conservative behaviors. They present a scenario-based discussion of safety and elaborate on the constraints to be dynamically imposed on the planned trajectories depending on the specific way the scene evolves. The presented ideas concerning the safety considerations to take into account when planning safe motions are of great interest. However, the strategy is difficult to generalize due to the fact that it only addresses static occlusions that can be inferred from detailed maps, and assumes that the ego vehicle would

only evaluate the decision to be made when there is no vehicle ahead of it and before the conflicting zone.

Constantin Hubmann et al. in [32] handle occlusions by modeling the problem as a POMDP, which includes the surrounding vehicles' route as hidden states and the potential existence of phantom vehicles on the occluded areas. A particularly interesting feature of their work is that they integrate within the POMDP the expected evolution of the field of view (FOV) over time, resulting in trajectories from which the quality of the FOV is preserved.

Bouton et al. address an over-simplified motion planning problem at a T-join using POMDPs in [5]. The study focuses on the computational issues associated with POMDPs and makes use of a so-called *utility function decomposition* technique to approximate the solution by combining the utility functions resulting from individually considering every agent in the scene. As they rather focus on the method to approximate the POMDP solution, they integrate strong assumptions to the traffic scenario such as the total knowledge of surrounding vehicles and pedestrian paths, and questionably use a single belief state to represent an arbitrary number of agents/vehicles in the occluded zones. Moreover, they only consider occlusions caused by static elements as buildings, and neglect other perception inaccuracies as missed tracked objects.

Reachability-based methods often used to address the problem of safety verification [1], can also be exploited to formulate safe motion planning strategies in occluded scenes. Naget et al. proposed, in [62], a motion planning strategy (based on the *generalized label correcting* method [70]) built on the notion of intent-aware dynamic shadow regions. Their strategy consists in approximating the set of reachable states of all possible hidden agents by explicitly taking into account the agent class. The approach takes into account computational delays and guarantees passive motion safety [50], and is evaluated regarding safety with respect to pedestrians. Nonetheless, the application of the proposed strategy to dynamically occluded scenarios is not discussed.

Piotr F. Orzechowski et al. in [68] extend the reachable set approach presented in [2] to account for initial state intervals, which are then used for the safety verification of trajectories in the presence of occlusions. The strategy does not consider, however, the possible reaction that surrounding vehicles could potentially exhibit to the ego vehicle's decisions, and always treat occlusions as areas that are thought to be occupied. Even though such work-flow fits the over-conservative estimation approach of [2] and is a valid strategy to guarantee safety, the proposed formulation could not profit from any estimation concerning the state of the occluded areas. Moreover, from the motion planning standpoint, the strategy is only used to verify that trajectories are safe and steer them towards the fail-safe maneuvers if needed, but the use of the proposed method to impose safety by design is not discussed.

Other studies propose strategies whereby vehicles drive by keeping available an emergency maneuver to safely react to a vehicle potentially located in the occluded regions. In this sense, Yoshihara et al. in [97] present a model-based strategy to safely approach blind intersections which relies on a Frenet frame trajectory planner [92] to generate candidate trajectories whose safety is later verified. They do not study collision avoidance nor decision-making but address the formulation of the maximum speed that would allow the ego vehicle to brake before the intersection as a function of its position along the approaching lane. In the process, they take into account the specific geometry of the occluded region, which makes the generalization of the strategy difficult especially to scenes where the exact shape of the occluded region is not known a priori.

Finally, data-driven methods have also been proposed to learn, from real data, the behavioral constraints that should be applied so that safety is guaranteed in the presence of occlusions. Yoichi Morales et al. in [60], make use of inverse reinforcement learning to imitate the driving style of

expert drivers when approaching a blind crossing intersection in a residential area. As the strategy uniquely takes as inputs the relative position of the ego vehicle with respect to the intersection, it replicates the safe approaching behavior but does not perform any decision-making, safety check, nor would it be able to avoid collisions with surrounding moving obstacles.

All mentioned studies regard the occlusion-aware motion planning problem from an *object detection and avoidance* standpoint, and apply different methods to generate safe motions despite the possible existence of undetected obstacles in the occluded regions. To do so, most existing works rely on a precise model of the evolution of the occluded region, and the consideration of virtual obstacles in the occluded regions. In general, existing studies scale up poorly to situations where the surroundings of the ego vehicle are dynamically occluded by moving objects. In this chapter, we set the basis to address the problem of planning under occlusions by proposing an alternative representation of the surrounding free space, which will be shown to represent a more suitable method to address the motion planning task in such conditions.

3.2 Perception post-processing

In this chapter, we propose a perception post-processing strategy to generate more suitable information for the motion planning module to create safe trajectories in a more natural manner. Overall, we expect the perception module to provide an information set $\mathcal{I} = \{\mathcal{O}_{\text{obs}}, \mathcal{G}_{\text{obs}}\}$ containing not only a set $\mathcal{O}_{\text{obs}} = \left\{\mathcal{O}_i, \cdots, \mathcal{O}_{n_{\mathcal{O}_{\text{obs}}}}\right\}$ of observed obstacles, but also a set $\mathcal{G}_{\text{obs}} = \left\{\mathcal{G}_i, \cdots, \mathcal{G}_{n_{\mathcal{G}_{\text{obs}}}}\right\}$ of probably-free inter-vehicle gaps. On the one hand, perceived surrounding objects $\mathcal{O} \in \mathcal{O}_{\text{obs}}$ are assumed to be characterized by their state $q_{\mathcal{O}}$, which includes the obstacle's position and speed. On the other hand, gaps $\mathcal{G} \in \mathcal{G}_{\text{obs}}$ are characterized by their extended state $q_{\mathcal{G}} = (q_{g_{\text{F}}}, q_{g_{\text{R}}}, \text{P}(E_{\mathcal{G}}), l_{\mathcal{G}})$, containing the states $q_{g_{\text{F}}}$ and $q_{g_{\text{R}}}$ of, respectively, the gap's front and rear limits, the probability $\text{P}(E_{\mathcal{G}})$ of the gap being currently empty, and the lane $l_{\mathcal{G}}$ the gap belongs to. In this section, we aim to present a suitable method to generate such a set of information.

Broadly speaking, we start by discussing different possible assumptions concerning the set of detected objects, continue by describing how to use such detections to maintain a dynamic occupancy grid (DOG) representation of the surrounding space, and conclude by presenting a method to extract probably-free inter-vehicle gaps from such a grid.

The method concerning the maintenance of the dynamic occupancy grid is heavily based on existing literature, namely [64, 84]. Although we introduced some minor changes and improvements in the process, most of the equations presented in this regard were obtained from such studies. Therefore, this chapter's contribution resides in the exploitation of an existing DOG representation method to infer a suitable high-level representation of the surrounding free space, but not the DOG technique itself.

3.2.1 Object detection and classification

Let us begin by discussing the assumptions leading to the construction of the set $\mathcal{O}_{\text{obs}}$ of surrounding obstacles that the ego vehicle is expected to observe successfully. In general, and considering that the ego vehicle could potentially have communication capabilities, the set $\mathcal{O}_{\text{obs}}$ could be seen as the aggregation $\mathcal{O}_{\text{obs}} = \mathcal{O}_{\text{V}} \cup \mathcal{O}_{\text{W}}$ of two sets of obstacles: a set $\mathcal{O}_{\text{V}}$ of detected surrounding real vehicles and a set $\mathcal{O}_{\text{W}}$ of surrounding VVs. On the one hand, concerning the set $\mathcal{O}_{\text{V}}$, we will generally consider two main cases:

- Perfect detection: the ego vehicle is assumed to perceive all vehicles in the scenario, without

exception.

- Occluded detection: the ego vehicle is assumed to perceive only those vehicles on sight, therefore losing track of those vehicles in occluded regions.

On the other hand, the set $\mathcal{O}_{\mathrm{W}}$ of surrounding VVs would contain all those VVs that are created by surrounding CAVs whose path intersects with the ego vehicle's (also referred to as conflicting CAVs). Two cases could be differentiated:

- Connectivity: if the ego vehicle is assumed to have communication capabilities (that is, if it is a CAV), it would have full access to such a set.
- Non-connectivity: if the ego vehicle is considered not to be able to communicate, such a set would be empty.

The aforementioned sets of objects can, for practical reasons, be further split into several subsets that will provide a more detailed description of the context. In particular, we propose two different classifications: (i) one where the vehicles are divided according to the driving stage at which they are regarding the task of driving through a roundabout, and (ii) a second one splitting the detected objects with respect to whether the ego vehicle has the capacity of cooperating with them.

Firstly, the sets $\mathcal{O}_{\mathrm{k}}$ (with $k = \{\mathrm{V}, \mathrm{W}, \mathrm{obs}\}$) can be split into the following subsets:

- $\mathcal{O}_k^{\mathrm{A}}$: the subset of vehicles approaching the roundabout, i.e. those within $\mathcal{O}_k$ that are out of the roundabout's circulatory road, facing its center, and with enough distance to the outermost boundary to gently stop before it,
- $\mathcal{O}_k^{\mathrm{M}}$: the subset of vehicles merging into the roundabout, which includes the objects within $\mathcal{O}_k$ that are out of the roundabout, facing it, and without time to brake before its boundary,
- $\mathcal{O}_k^{\mathrm{C}}$: the subset of vehicles circulating inside the roundabout and sufficiently aligned with the circulatory lanes, and
- $\mathcal{O}_k^{\mathrm{E}}$: the subset of vehicles exiting the roundabout, i.e. those that are in a circulatory lane yet oriented sufficiently outwards to be considered as being about to exit it.

Although the previous classification has been generally addressed, consistently with the proposed use of VVs in our context, all vehicles within $\mathcal{O}_{\mathrm{W}}$ should be on the circulatory roads.

An additional way of dividing the set $\mathcal{O}_k$ (with $k \in \{\mathrm{V}, \mathrm{W}, \mathrm{obs}\}$) of obstacles is by differentiating between the set $\mathcal{O}_{k,\mathrm{C}}$ of those that surround the ego vehicle, have less priority, and might profit from the ego vehicle's cooperation, and the set $\mathcal{O}_{k,\mathrm{NC}}$ of those that do not. In the discussed traffic scenario, this classification would allow the ego vehicle to identify not only the subset of obstacles behind which it must safely drive, but also those that might be trying to merge or change lanes in front of the ego vehicle and would, therefore, benefit from a cooperative action coming from it.

3.2.2 Dynamic occupancy grid

The second step we consider necessary to efficiently tackle the motion planning problem consists in maintaining a DOG representation of the surrounding space. Specifically, we propose tue use of a DOG to represent the state of the circulatory lanes, which is maintained by fusing high-level information concerning the detected surrounding objects, as well as a sensor model.

In this section, we briefly present and illustrate the procedure we implement to do so, which is, as mentioned in the introduction, heavily based on [64, 84].

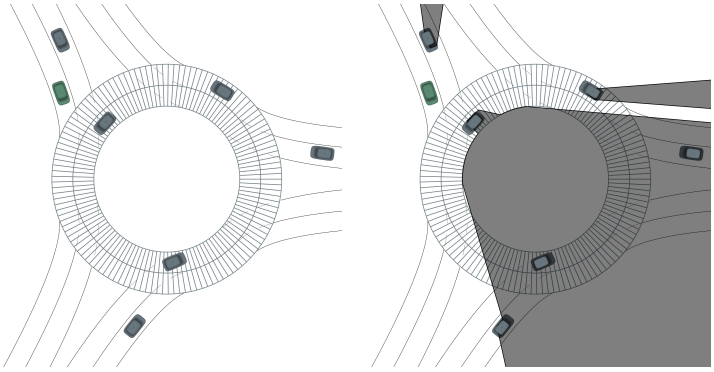

Figure 3.1 – On the left-hand side, a grid representing the circulatory lanes. On the right-hand side, an illustration of the identification process of the occluded cells.

Grid initialization

The term dynamic occupancy grid makes reference to a family of methods whose objective is to estimate the probability distribution of the occupancy states and velocities of a finite set of discrete cells representing the surrounding space of an agent. Existing methods make use of Bayesian filtering [20, 36] and, generally speaking, comprise two steps whereby the occupancy and velocity distribution of every cell is first predicted (given the prior knowledge and a certain transition model), and it is then corrected given the new sensor measurements.

Although DOGs could be used to represent the surrounding space disregarding the geometry of the nearby roads, we will construct a grid to exclusively represent the state of the circulatory lanes (see Fig. 3.1).

Specifically, the set $\mathcal{C}$ of all cells in the grid would be the result of aggregating the set of cells assigned to every circulatory lane, i.e.

$$\mathcal{C} = \cup_{l \in \mathcal{L}_{\text{circ}}} \mathcal{C}_l, \tag{3.1}$$

with $\mathcal{C}_l = \{0, 1, \cdots, n_{\mathcal{C}_l} - 1\}$ being the set of cells used to represent the circulatory lane l. Every cell $c \in \mathcal{C}_l$ would represent the set of polar positions

$$\mathcal{P}_c = \{(\theta_c, \rho_c) : \theta \in [c\Delta\theta, (c+1)\Delta\theta), \rho \in [\rho_{l,1}, \rho_{l,2})\}, \tag{3.2}$$

where the limits $\rho_{\mathtt{L}(c),1}$ and $\rho_{\mathtt{L}(c),2}$ are the boundaries of the circulatory lane $\mathtt{L}(c)$ the cell belongs to, and $\Delta\theta = \frac{2\pi}{n_{\mathcal{C}_l}}$ is the angular sector the cell covers.

Labeling cells

Before addressing the procedure to maintain the occupancy and speed probability distribution of the grid's cells, let us identify several sets of cells that will require special treatment.

Firstly, we denote by $\mathcal{C}_{\text{occl}} \subseteq \mathcal{C}$ the subset of cells that are occluded by the surrounding objects, which is constructed by first approximating the ego vehicle's field of view, and then identifying the cells that are out of such a region. The process is illustrated in Fig. 3.2.

The second set worth identifying is the subset $\mathcal{C}_{\text{occ}} \subseteq \mathcal{C}$ of cells that should be occupied given the set $\mathcal{O}_{\text{obs}}$ of detected obstacles (see Fig. 3.2). Note that when those vehicles within the occluded

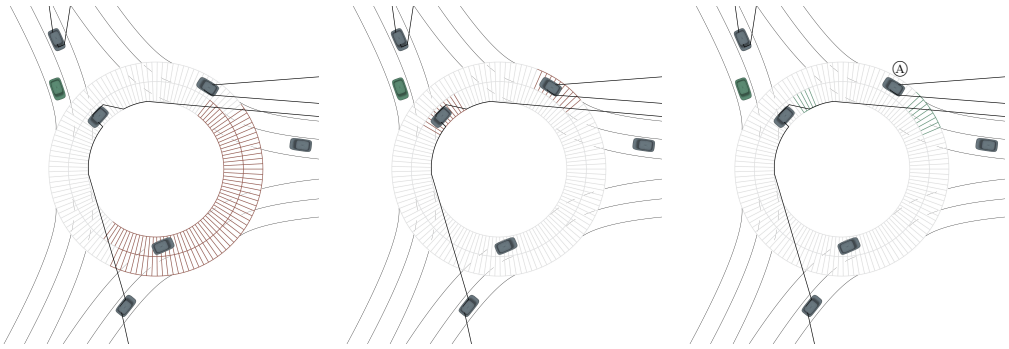

Figure 3.2 – Identification of three relevant subsets of cells. On the left-hand side, the set of occluded cells. At the center, the set of occupied cells. On the right-hand side, the set of cells that must be free for the detected obstacles to be driving safely.

regions are assumed not to be detected, the intersection $\mathcal{C}_{\text{occ}} \cap \mathcal{C}_{\text{occl}}$ should be empty.

Moreover, the traffic scene is further processed to identify the subset $\mathcal{C}_{\text{free}}$ of cells that, given the set of detected vehicles and assuming they are driving safely, must be free. In particular, the identification of such a set of cells results from assuming that the set $\mathcal{O}_{\text{obs}}^{\text{C}}$ of surrounding detected objects in the circulatory lanes must have a minimum free distance ahead and behind for them to be driving safely. Similarly, for the set $\mathcal{O}_{\text{obs}}^{\text{M}}$ of obstacles to be merging safely, a sufficiently large free space must exist in the circulatory lane. These assumptions allow us to infer the state of some cells that are occluded, as is the case in the scene depicted in Fig. 3.2, where the detection of vehicle Ⓐ would indicate that there is a small portion of the occluded area that must be free.

Speed and occupancy probability distribution

Once the relevant subsets of cells have been identified, we can proceed to approximate the occupancy and velocity probability distributions of every cell. The process is based on applying a Bayes Filter along with the information concerning the cells' state and their confidence.

The Bayes Filter [36] addresses the problem of estimating the probability distribution $\mathrm{P}(X|Z)$ (also known as the posterior probability) of the state X of a system, given the observations Z. In our setup, such a task can be seen as that of approximating the probability distribution

$$\mathrm{P}(V, O|Z, C) \tag{3.3}$$

where

- C is the index of the cell whose probability distribution the previous expression refers to,
- Z represents the sensor measurement,
- $V \in \{v_1, \cdots, v_n\}$ is a random variable representing the speed of the cell, which can take a finite set of speed values,
- $O \in \{\text{occ}, \text{emp}\}$ is a random variable representing the occupancy state of the cell (*occ*, and *emp* standing for *occupied* and *empty*).

The posterior probability can be equivalently expressed as

$$\mathrm{P}(V, O|Z, C) = \frac{\mathrm{P}(V, O, Z, C)}{\mathrm{P}(Z, C)} \tag{3.4}$$

if the definition of conditional probability is taken into account. Furthermore, by applying marginalization and letting

- A denote the index of a theoretical antecedent cell, and
- O^- represent the occupancy state of the antecedent cell,

the posterior probability can be reformulated as

$$\mathrm{P}(V, O|Z, C) = \frac{\sum_{A,O^-} \mathrm{P}(CAZOO^-V)}{\sum_{A,O,O^-,V} \mathrm{P}(CAZOO^-V)}. \tag{3.5}$$

That is, in terms of the joint probability of all the variables of interest. Then, the process can be tackled by quantifying such a joint distribution, which can be decomposed by applying the chain rule, Bayes' rule, and accounting for dependency assumptions as

$$\mathrm{P}\big(CAZOO^-V\big) = \mathrm{P}(A)\mathrm{P}(V|A)\mathrm{P}(C|V, A)\mathrm{P}\big(O^-|A\big)\mathrm{P}\big(O|O^-\big)\mathrm{P}(Z|O, V, C). \tag{3.6}$$

The terms in Eq. (3.6) have the following interpretation:

- $\mathrm{P}(A)$ is the probability distribution of all possible antecedents of a cell c, which will be chosen to be uniform.
- $\mathrm{P}(V|A)$ is the distribution over all possible velocities of a certain antecedent of the cell c, which is updated at every iteration.
- $\mathrm{P}(C|V, A)$ is a distribution that explains if the cell c is reachable from $A = a$ with a velocity $V = v$. In a discrete space, this distribution is

$$\mathrm{P}(C|V, A) = \begin{cases} 1 & \text{if } c_x = a_x + v_x h \wedge c_y = a_y + v_y h \\ 0 & \text{otherwise} \end{cases}. \tag{3.7}$$

- $\mathrm{P}(O^-|A)$ is the distribution over the occupancy state, in the previous sampling time, of the antecedent cells.
- $\mathrm{P}(O|O^-A)$: is the conditional distribution over the occupancy of the current cell, which depends on the occupancy state of the previous cell. It is defined by the transition probabilities in Tab. 3.1.

Table 3.1 – Transition probabilities

	$A \in \mathcal{C}\backslash\mathcal{C}_{\text{occl}}$		$A \in \mathcal{C}_{\text{occl}}$	
	$O^- = occ$	$O^- = emp$	$O^- = occ$	$O^- = emp$
$\mathrm{P}\big(\mathbf{O} = \mathbf{occ}\|\mathbf{O}^-, \mathbf{A}\big)$	$1 - \epsilon_{\text{t,noccl}}$	$\epsilon_{\text{t,noccl}}$	$1 - \epsilon_{\text{t,occl}}$	$\epsilon_{\text{t,occl}}$
$\mathrm{P}\big(\mathbf{O} = \mathbf{emp}\|\mathbf{O}^-, \mathbf{A}\big)$	$\epsilon_{\text{t,noccl}}$	$1 - \epsilon_{\text{t,noccl}}$	$\epsilon_{\text{t,occl}}$	$1 - \epsilon_{\text{t,occl}}$

Note that this term changes w.r.t. the original publication as it depends on the type of the antecedent cell. Specifically, we aim to apply two different transition models depending on

whether the antecedent cell is occluded or not. The rationale behind this is the following. This transition probability models how much we rely on the occupancy of the previous cell to estimate the state of the current one. When it comes to visible cells, the transition probability enables us to compensate for problems concerning losing track of visible objects, but we mainly rely on the sensor information. On the occluded regions, however, from where no information can be acquired using the on-board sensors, the transition probability controls how the state of the cells at the border of the occluded area (or even the previous state if the occlusion is dynamic) gets propagated through the occluded region. These two essentially different effects motivate differentiating between two transition models, in such a way that the prior knowledge can be further propagated in the occluded region than in the visible one.

- $\mathrm{P}(Z|O,V,C)$ is the conditional distribution over the sensor measurements, i.e. the sensor model, which depends on the cell's state and is used to perform the correction stage of the Bayesian filter. The sensor signal we consider consists of the labels assigned to the cells as a result of the high level detected obstacles the perception system provides. The sensor signal

$$Z_c = \begin{cases} free & \text{if } c \in \mathcal{C}_{l,free} \\ occ & \text{if } c \in \mathcal{C}_{l,occ} \backslash \mathcal{C}_{l,ocl} \end{cases} \tag{3.8}$$

represents the high-level cell information extracted from the observed obstacles. As such characterization might be subject to uncertainty, we consider the sensor model in Tab. 3.2.

Table 3.2 – Sensor model

	$C \in \mathcal{C}\backslash\mathcal{C}_{\text{occl}}$		$C \in \mathcal{C}_{\text{occl}}$	
	$O^- = occ$	$O^- = emp$	$O^- = occ$	$O^- = emp$
$\mathrm{P}(\mathbf{Z_c} = \mathbf{free}\|\mathbf{O},\mathbf{V},\mathbf{C})$	$\epsilon_{\text{z,free}}$	$1-\epsilon_{\text{z,free}}$	0.5	0.5
$\mathrm{P}(\mathbf{Z_c} = \mathbf{occ}\|\mathbf{O},\mathbf{V},\mathbf{C})$	$1-\epsilon_{\text{z,occ}}$	$\epsilon_{\text{z,occ}}$	0.5	0.5

By considering the decomposition of the joint distribution and the meaning of its terms listed above, the numerator of Eq. (3.5) can be rewritten as

$$\sum_{A,O^-} \mathrm{P}\big(CAZOO^-V\big) = \mathrm{P}(Z|O,V,C)\left(\sum_{A,O^-} \mathrm{P}(A)\mathrm{P}(V|A)\mathrm{P}(C|V,A)\mathrm{P}\big(O^-|A\big)\mathrm{P}\big(O|O^-\big)\right), \tag{3.9}$$

where the prediction and estimation stages can be identified as: (prediction) calculating the term

$$\sum_{A,O^-} \mathrm{P}(A)\mathrm{P}(V|A)\mathrm{P}(C|V,A)\mathrm{P}\big(O^-|A\big)\mathrm{P}\big(O|O^-\big), \tag{3.10}$$

and (correction) modifying such a prediction by multiplying by $\mathrm{P}(Z|O,V,C)$.

The described process is typically addressed by first computing the estimation, i.e. the terms

$$\alpha(occ, v_k) = \sum_{A,O^-} \mathrm{P}(A)\mathrm{P}(v_k|A)\mathrm{P}(C|V,A)\mathrm{P}\big(O^-|A\big)\mathrm{P}\big(O = occ|O^-\big), \tag{3.11}$$

$$\alpha(emp, v_k) = \sum_{A,O^-} \mathrm{P}(A)\mathrm{P}(v_k|A)\mathrm{P}(C|V,A)\mathrm{P}\big(O^-|A\big)\mathrm{P}\big(O = emp|O^-\big), \tag{3.12}$$

and then, correcting it using the sensor model $\mathrm{P}(Z|O,V)$ by doing

$$\beta(occ, v_k) = \mathrm{P}(Z|occ, v_k)\alpha(occ, v_k), \tag{3.13}$$
$$\beta(emp, v_k) = \mathrm{P}(Z|emp, v_k)\alpha(emp, v_k). \tag{3.14}$$

Finally, one could marginalize over the occupancy and speed to quantify the denominator of Eq. (3.5) as

$$l = \sum_{v \in \{v, \cdots, v_n\}} (\beta(occ, v_k) + \beta(emp, v_k)), \tag{3.15}$$

and then obtaining the sought probability distribution as

$$\mathrm{P}(occ, v_k|Z, C) = \beta(occ, v_k)/l. \tag{3.16}$$

With such a result, we could as well compute, for every cell, the occupancy and speed probability by marginalizing over V and O, respectively. That is

$$\mathrm{P}(O|Z, C) = \sum_V \mathrm{P}(V, O|Z, C) \qquad \mathrm{P}(V|Z, C) = \sum_O \mathrm{P}(V, O|Z, C). \tag{3.17}$$

3.2.3 Gaps inference

Once the probability $p_c = 1 - \mathrm{P}(O = occ|Z = Z_c, C = c)$ with which every cell c in the grid is estimated to be free has been obtained, we proceed to extract, from the DOG, the set of probably-free gaps the motion planners will base their decisions on.

The process begins by setting a finite set

$$\mathbf{p} = \left\{p_1, \cdots, p_{n_p}\right\} \tag{3.18}$$

of probabilities of interest, indicating that n_p subsets of probably-free gaps (one for every probability p_i of interest) are to be extracted. Then, we can identify the subsets

$$\mathcal{C}_l^{>p} = \{c \in \mathcal{C}_l : p_c \geq p\} \qquad \mathcal{C}_l^{<p} = \{c \in \mathcal{C}_l : p_c < p\} \tag{3.19}$$

of cells in the circulatory lane l whose probability of being free is, respectively, above and below a certain probability p. Then, denoting as

$$c_l^+ \coloneqq \texttt{mod}(c + 1, n_{\mathcal{C}_l}) \qquad c_l^- \coloneqq \texttt{mod}(c - 1, n_{\mathcal{C}_l}) \tag{3.20}$$

the index of the next and previous cell of a certain cell $c \in \mathcal{C}_l$, with

$$\texttt{mod}(c, n_{\mathcal{C}_l}) = c - n_{\mathcal{C}_l} \left\lfloor \frac{c}{n_{\mathcal{C}_l}} \right\rfloor \tag{3.21}$$

representing the modulus operator, we can identify the set of cells

$$\mathbf{c}_1(l, p) = \left\{c \in \mathcal{C}_l^{>p} : c_l^- \in \mathcal{C}_l^{<p}\right\} \tag{3.22}$$

that would mark the beginning of the observed gaps of interest.

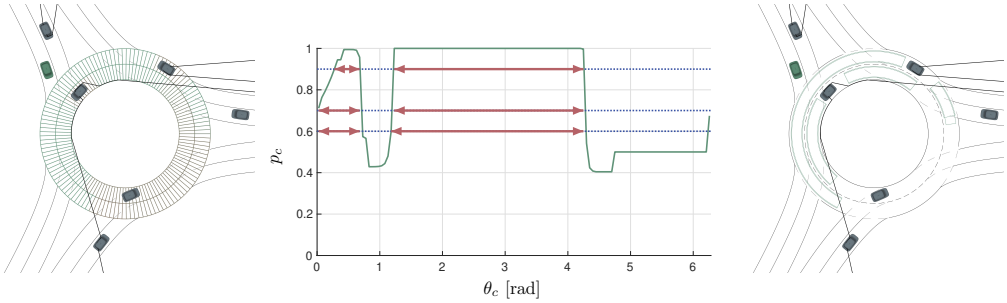

Figure 3.3 – Representation of the probably-free gaps inference process. On the left and right-hand side plots, the considered traffic scene along with the state of the exploited DOG. In the middle, we show the probability p_c with which the cell c is thought to be free w.r.t. its polar position θ_c. Moreover, we show three horizontal arrows representing the probability levels $\mathbf{p} = (0.6, 0.7, 0.9)$, for which gaps are to be extracted. On the right-hand side, representation of the probably-free gaps extracted in the depicted scene (in green).

Furthermore, denoting as

$$\Delta(c, l, p) = \min\left\{k \geq 0 : \texttt{mod}(c + 1 + k, n_{\mathcal{C}_l}) \in \mathcal{C}_l^{<p}\right\} \tag{3.23}$$

the number of subsequent cells to c that belong to the lane l and whose free probability is greater than p, we can construct the subset $\mathcal{G}_{l,p}$ of gaps in l that are free with probability greater than p as

$$\mathcal{G}_{l,p} = \{((\theta_c, \rho_l, \overline{v}_c), (\theta_{c'}, \rho_l, \overline{v}_{c'}), p, l) : c \in \mathbf{c}_1(l, p), c' = c + \Delta(c, l, p)\}, \tag{3.24}$$

where $\overline{v}_c$ is the average speed of cell c, obtained from its distribution $\mathrm{P}(V|Z, C)$.

Therefore, the set of observed gaps that is to be utilized by the decision-makers would be built as

$$\mathcal{G}_{\text{obs}} = \bigcup_{l \in \mathcal{L}_{\text{circ}}, p \in \mathbf{p}} \mathcal{G}_{l,p}. \tag{3.25}$$

The process of identifying the probably-free gaps from a DOG is illustrated in Fig. 3.3 for a two-lane roundabout, where it can be observed that the inferred gaps properly represent the free space that the ego vehicle should use to make driving decisions. It is worth noting that, generally speaking, some positions in the circulatory lanes could simultaneously belong to several gaps, as highly-probable gaps are often included within less probable ones.

3.2.4 Perception models

The perception post-processing approach described in the previous section can lead to several specific perception models by varying the assumptions the process relies on. Specifically, we will consider two types of agents concerning their perception capabilities:

- agents that have a perfect vision, which will be used to emulate: (i) CAVs driving around other CAVs (modeling the fact that such agents can share perception information and might, therefore, *see* through occluded environmental elements), and (ii) the advance perception capabilities of human drivers,
- agents whose perception system is affected by occlusions, aimed to model CAVs and AVs

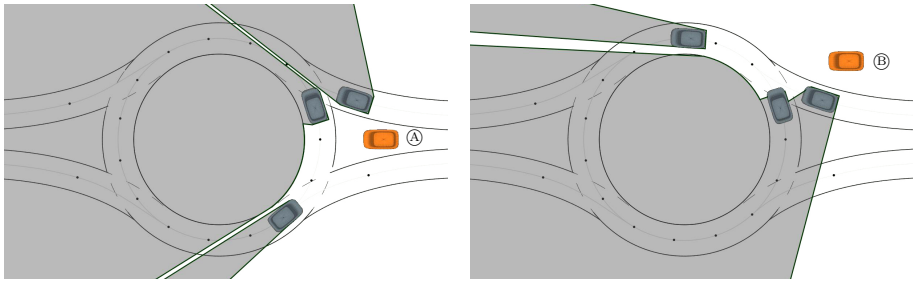

Figure 3.4 – Traffic scenario illustrating the considered static obstacle (orange vehicle) and the position form which it observes the scenario.

surrounded by unconnected vehicles, and with a perception system not capable of performing reliable detections and tracking through occlusions.

3.3 Results

In this section, we show some results illustrating the outcomes that could be expected to be obtained from the methods discussed in this chapter, as well as the effect of the considered design parameters.

Specifically, the results are based on illustrating the evolution of the DOG state, as well as some instances of the inferred probably-free inter-vehicle gaps that would be perceived by a static observer as a set of vehicles driving through the roundabout. The simulated scenario corresponds to a `16R1LR3L1I1O` roundabout, a traffic configuration `20V-1500Q[1 1 1]`, and two positions for the static observer (see Fig 3.3).

3.3.1 Dynamic occupancy grid evolution

In this section, we start by qualitatively analyzing the evolution of the occupancy probability of the DOG, as well as the impact of some of the design parameters.

Let us begin by assessing the case where the fixed observer is positioned at the location Ⓐ, and its perception system is not affected by occlusions of any kind. In such a case, the state of the DOG would evolve as illustrated in Fig. 3.5, where the probability p_c of the cells being free is shown by the shade of gray of every pixel (the brighter the pixel, the higher the probability of the position they represent to be free at the corresponding time), with the vertical axis showing the polar position of every cell, and the horizontal axis representing time. Moreover, every time the observer detects an object in the circulatory lane, its position is represented by a filled red circle (•).

If the vehicle is able to detect the surrounding vehicles perfectly, we would expect to have a perfect knowledge of the cells' occupancy state, i.e. very dark shadows below the detected objects, and very bright areas otherwise, which is what can be observed in Fig. 3.5 for the design parameters of case 2 in Tab. 3.3.

It is worth noting that as a consequence of the accuracy with which the speed of the cells is being estimated, which gets more precise over time, the dark areas caused by the detected objects become more precise the longer the object has been detected.

When the observer is positioned in Ⓐ, and its perception system is affected by occlusions, we obtain the evolutions in Fig. 3.6, where results for the four sets of parameters in Tab. 3.3 are shown.

Let us begin by pointing out that two fundamentally different areas can be observed in such

Table 3.3 – Design parameters

	$\epsilon_{t,occl}$	$\epsilon_{t,noccl}$	$\epsilon_{z,free}$	$\epsilon_{z,occ}$	Enhanced
Case 1	0.13	0.13	0.2	0.2	false
Case 2	0.13	0.13	0.2	0.2	true
Case 3	0.02	0.02	0.2	0.2	false
Case 4	0.02	0.02	0.2	0.2	true

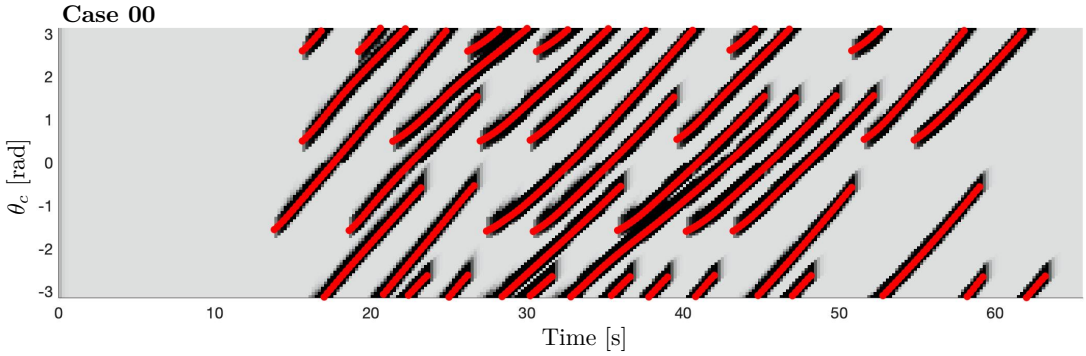

Figure 3.5 – Evolution of the occupancy probability of the circulatory lane when the ego vehicle can detect the surrounding vehicles perfectly. The real position of the vehicles circulating inside the roundabout is represented by (•), and their evolution should be understood as the time-distance diagram of the vehicles moving in the circulatory lane of the roundabout (although we are representing in the vertical axis the polar coordinate instead of distance). The plot's background shows the evolution of the DOG's occupancy probability distribution over time (the brighter the background pixel, the higher the probability of the corresponding location to be free at the corresponding time.

plots: the region of the circulatory lane that is visible despite the roundabout island (represented by the central bright band in the plots) and the area that is occluded by the island (the dark horizontal bands at the bottom and at the top of the plot). Secondly, two different markers are now used to illustrate the position of the vehicles as they drive through the roundabout: filled red circles (•) to represent those positions that are directly visible by the fixed observers, and empty red circles (○) showing the fact that the objects cannot be detected.

The first major aspect that is worth discussing is the change in behavior that the parameters bring to the prediction of the occluded cells' occupancy probability. In essence, the parameters of the transition matrix used to propagate the occupancy probability have control over how much the prior occupancy probability is retained and propagated in the occluded region. In fact, small values of $\epsilon_{t,occl}$ and $\epsilon_{t,noccl}$ would propagate the information further in time than higher values, for which the state of the occluded regions is unknown for most of the time.

The previously discussed effect impacts not only the state of the region occluded by the roundabout island but also the areas that are dynamically occluded by surrounding vehicles. In this case, a more lasting propagation might be beneficial, as, in that way, the grid would be more prone to retain the true state of the dynamically occluded regions, allowing the extraction of more accurate gaps.

The impact of assuming that the surrounding vehicles drive safely can also be perfectly observed in the shown plots. In fact, note in case 2 and case 4 how, when an object appears close to the lower limit of the visible region, a bright band that extends into the occluded region automatically appears. As discussed above, this effect represents the fact that, if such a detected obstacle drives safely, it

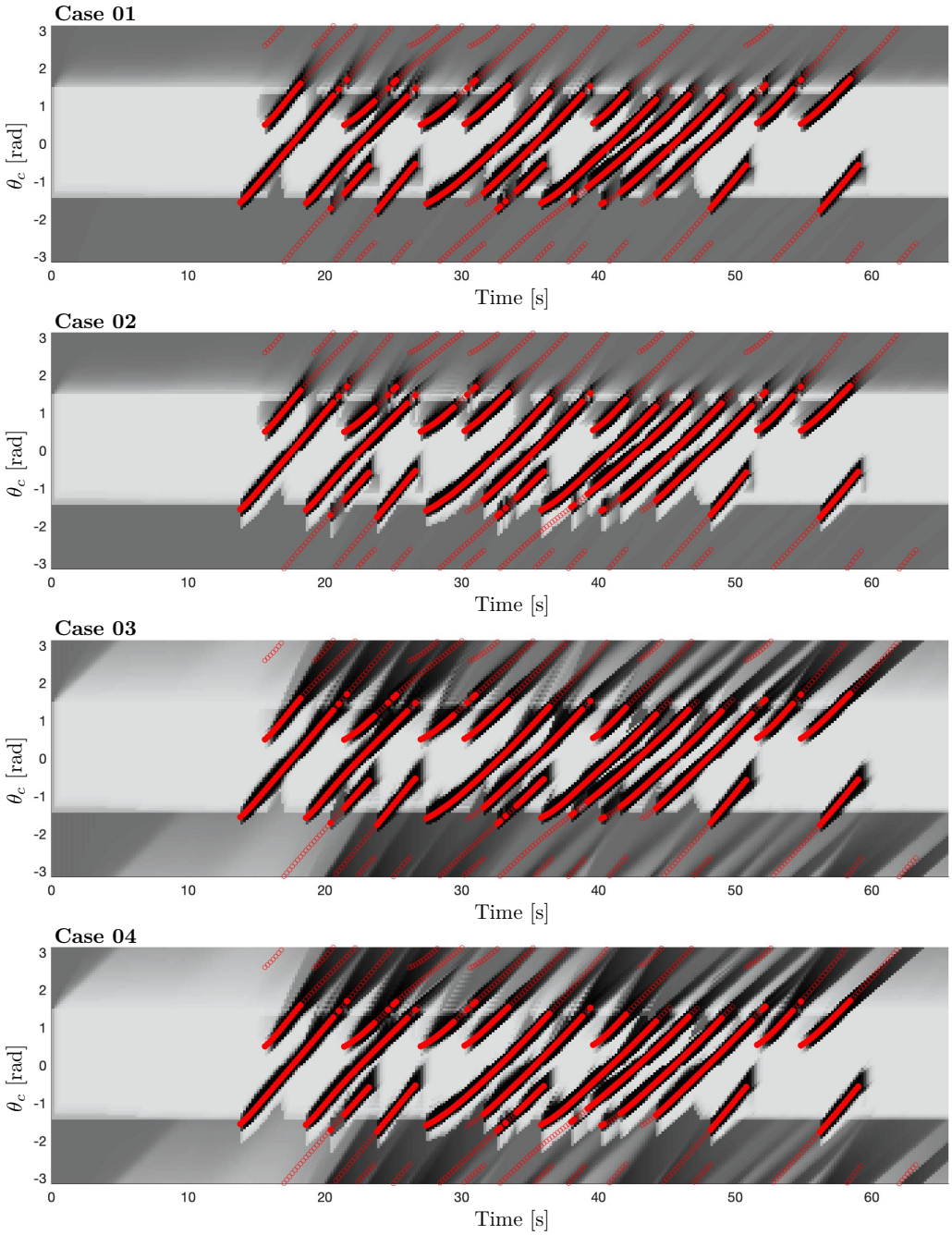

Figure 3.6 – Evolution of the occupancy probability of the circulatory cells when the scene is observed from Ⓐ, surrounding vehicles are assumed to cause occlusions, as does the roundabout island. The position of the vehicles circulating inside the roundabout is represented by (•) when they can be seen by the ego vehicle, and by (○) when they are occluded. The background represents the state of the DOG, in such a way that the brighter the pixel, the higher the probability of the polar position it represents to be free at its corresponding time.

must have a certain safe distance behind, which improves the knowledge of the surrounding state.

When the static observer is positioned at Ⓑ, and for the same combination of parameters used previously, we obtain the evolutions in Fig. 3.7. On this occasion, it can be observed that the occlusions caused by the vehicles merging into the roundabout by the leg on the left-hand side of the static observer significantly deteriorate the estimated state of a crucial part of the intersection. These difficulties resemble the ones incoming vehicles face when merging into multi-lane roundabouts while having some vehicle in parallel to them. In this case, the safety assumption used to enhance the occupancy estimation has a more beneficial effect than in the previous case, as they improve the knowledge of an area whose state has a strong impact on the merging decision-making process.

3.3.2 Probably-free gaps

In this section, we illustrate the effect of the design parameters on the probably-free gaps that can be inferred from the DOG. In particular, for a given time of interest, we represent the probably-free gaps corresponding to: (i) the situation where the ego vehicle has perfect visibility (Fig. 3.8), (ii) the case where the static observer is positioned at Ⓐ (Fig. 3.9), and (iii) the case where the static observer sees the scene from Ⓑ (Fig. 3.10).

As expected, when the observer detects the surrounding vehicles perfectly (Fig. 3.8), the probably-free gaps represent all the inter-vehicle gaps in the circulatory lane. It is worth noting that the set of occupied cells corresponding to every vehicle inside the roundabout, extend slightly beyond the vehicle's area. This difference is caused by an additional safety margin, which is applied at the time of characterizing the occupied cells. Moreover, due to the cell's speed estimation inaccuracy, we observe that the smaller the existence probability of a gap, the closer its rear limit gets to the following vehicles. This feature is a desirable one, as it encourages the motion planner to make decisions using the highly probable and rather conservative observed free gaps while allowing it to use less probable ones if necessary.

In the set of traffic scenes shown in Fig. 3.9, where the static observer is positioned at Ⓐ, evident differences between the first and second pairs of cases can be seen. Specifically, we observe how, when slower transition probabilities are used, the longer the prior knowledge is retained and the better the space that has just being occluded is characterized (see the gaps in the upper part of the circulatory lane).

A similar effect can as well be seen when the vehicle is positioned at Ⓑ (Fig. 3.10). However, the most noticeable change in this case caused by the assumption concerning the circulating vehicles driving safely. Indeed, when such an assumption is integrated (cases 02 and 04), the space around the only vehicle observed in the circulatory lane is better characterized.

3.4 Conclusions

In this chapter, we have discussed aspects concerning the perception capabilities that our motion planning strategies will be built upon. The novel perception feature we require, consists in characterizing the roundabout's circulatory lanes by a set of probably-free inter-vehicle gaps, and not only by a set of detected obstacles. Such a process was shown to provide a suitable representation of the circulatory lanes when the perception system is affected by occlusions.

The strategy was claimed to be suitable for decision-making and was shown to be able to retain previous knowledge to better estimate the state of cells when they are intermittently occluded.

The chapter has been built upon the assumption that objects are first detected by the perception

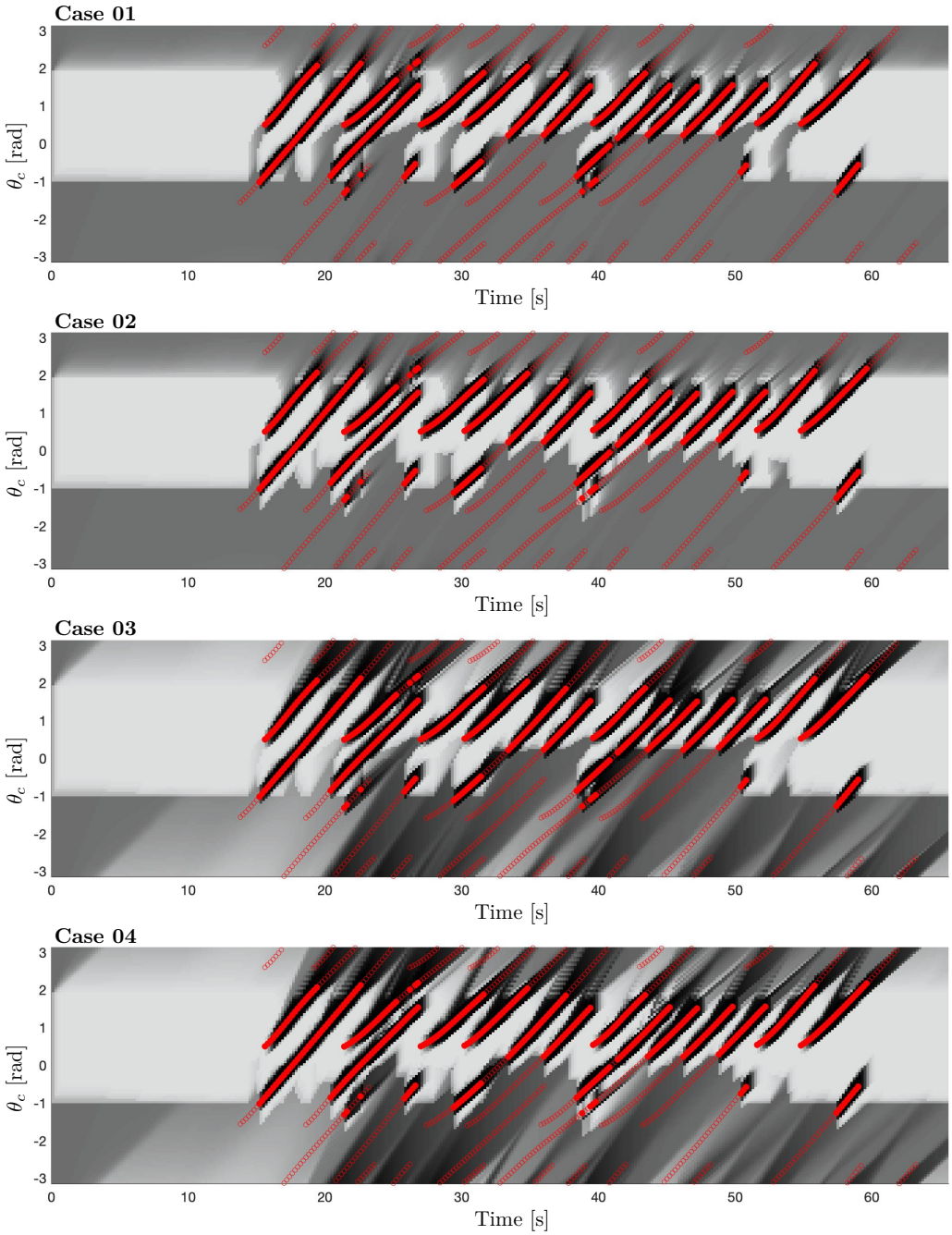

Figure 3.7 – Evolution of the occupancy probability of the circulatory lane when the scene in Fig. 3.4 is observed from Ⓑ, surrounding vehicles are assumed to cause occlusions, as does the roundabout island. The position of the vehicles circulating inside the roundabout is represented by (•) when they can be seen by the ego vehicle, and by (∘) when it is occluded. The background represents the state of the DOG, in such a way that the brighter the pixel, the higher the probability of the polar position it represents to be free at its corresponding time.

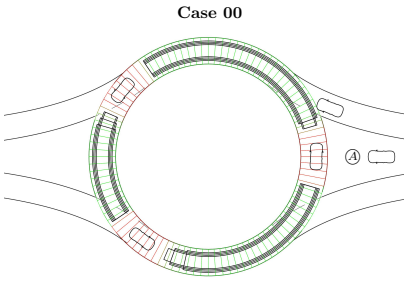

Figure 3.8 – Example of the probably-free gaps extracted in a certain traffic scene, when the static observer has a perfect view of the surroundings. In the circulatory lane, we represent the cells composing the DOG, whose color indicates the occupancy probability of every cell (red for occupied and green for free). Moreover, boxes along the circulatory lane represent the inferred probably-free gaps. The probability assigned to the probably free gaps is represented through the gaps' width, in such a way that the wider the gap, the higher the confidence of it existing.

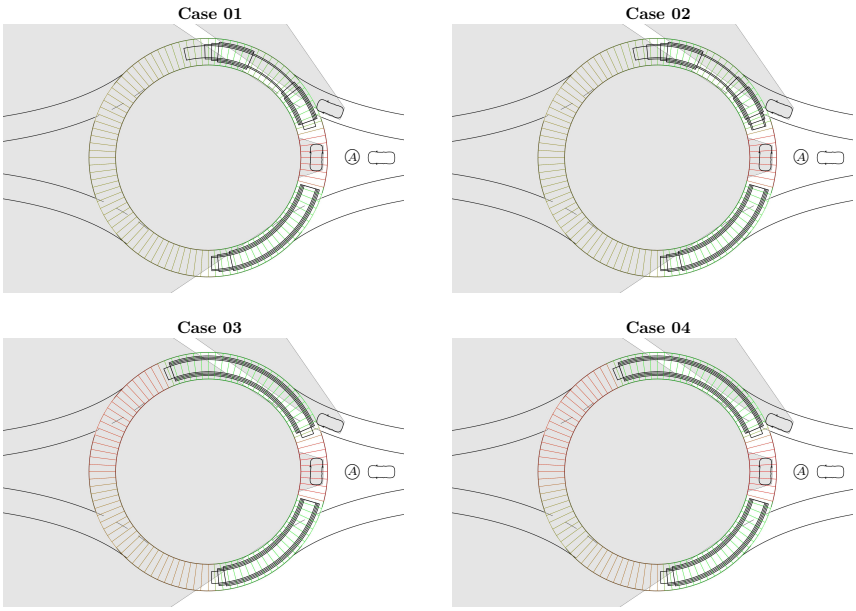

Figure 3.9 – Example of the probably-free gaps (black boxed over the cells) extracted in a certain traffic scene, when the parameters governing the evolution of the DOG take the values in Tab. 3.3 and the static observer is positioned at Ⓐ.

layers and then integrated, along with some additional high-level knowledge, within a DOG. This approach matches the experimental framework where we will further validate some of our motion planning strategies in Chapter 9, according to which we are initially given a set of detected obstacles in the surrounding space that we have to use to maintain the probabilistic representation of the intersection, and from which the available inter-vehicle gaps have to be inferred. Nonetheless, as DOGs are actually used in the literature for object detection and tracking, the probably-free gaps inference method proposed in this chapter could as well be considered as an additional side-product resulting from the grid maintained for object-detection proposes.

A direction in which the content of this chapter could be further explored would be considering

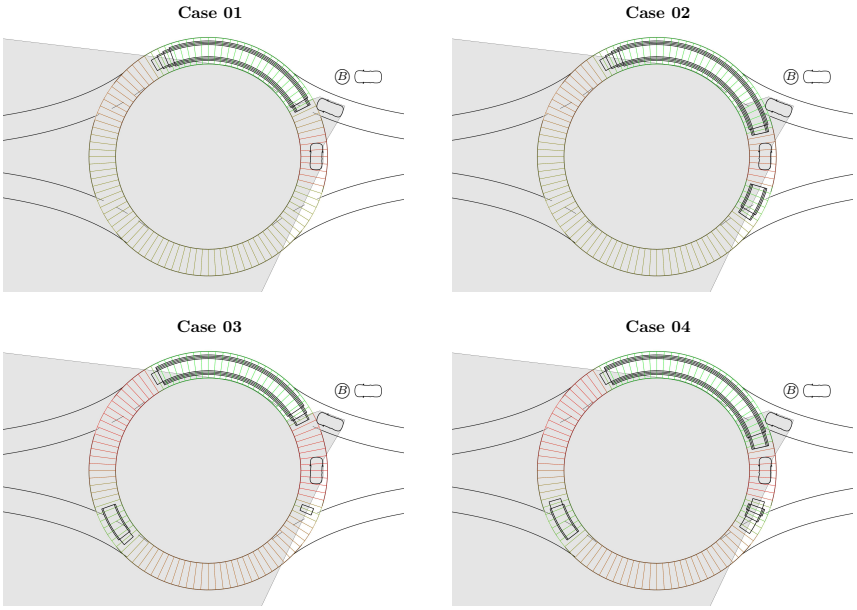

Figure 3.10 – Example of the probably-free gaps (black boxed over the cells) extracted in a certain traffic scene, when the parameters governing the evolution of the DOG take the values in Tab. 3.3 and the static observer is positioned at Ⓑ.

the possibility of CAVs having cooperative perception capabilities. In this setup, CAVs would share their detection information, thereby experiencing a practical reduction of the areas affected by occlusions, as the fleet of CAVs would act as a network of distributed sensing agents. Moreover, we have not taken into account the possibility of having an estimation of the path that vehicles in the circulatory lane might follow. Instead, we always propagate the occupancy probability forward in a polar sense, which implies that if some object becomes occluded, it would be assumed to continue driving in the circulatory lane of the roundabout. In practice, such an extension could be made by correlating the way in which the occupancy probability is increased when a vehicle is detected to the probability with which the vehicle is expected to cross the ego vehicle's path.

Despite its limitations, the presented probably-free gap inference process will be shown in future chapters to enable motion planning strategies to systematically handle uncertain environments, while disregarding the source of uncertainty. In practice, the proposed context representation would allow decision-makers to appropriately handle occluded and/or poorly perceived scenes, by just making safe use of the inferred probably-free gaps.

4 Motion Planning

The term *motion planning* is generally used in the field of mobile robotics to refer to the problem of generating a sequence of states for a robot to move from its current state to a targeted one (illustrated in Fig. 4.1). In other words, it describes the problem of generating a state trajectory

$$x^T(t) = \{x(t), x(t+h), \cdots, x(t+T)\} \tag{4.1}$$

describing a discrete sequence of states that the robot should adopt over a planning horizon T, and sampling time h, given the more or less accurate information provided by the robot's perception system.

Even though a wide variety of motion planning strategies and architectures can be found in the literature, in the field of intelligent vehicles, the problem has been typically addressed by splitting the task into smaller ones covering different abstraction levels. Specifically, all complete solutions in the literature include, either explicitly or implicitly, the following planning levels:

- Route planning is the highest of the planning levels and takes care of finding a way, through a map, to reach a specific location from the current position of the vehicle.
- Tactical planning would specify, at a relatively high-level, the sequence of driving maneuvers that are to be performed to follow the route as efficiently as possible. For instance: change lanes to the left-hand side to overtake as soon as you can, change lanes to the right to take the next exit, merge into the second lane of the upcoming roundabout, etc. Under certain circumstances, path planning could be considered to be included in this task.
- Maneuver planning would subsequently take into account the targeted driving maneuver, along with the environmental information, to determine the fundamental targets and constraints that must be imposed on the trajectory so that it is safe and efficient. For instance, it would set the constraint imposing a safe distance with the vehicle ahead, specify the time window within which a merging spot should be reached, and implicitly decide the specific inter-vehicle gap the vehicle should utilize.
- Trajectory planning would finally generate the explicit sequence of states to pursue so that it meets the requirements set by the maneuver planner while considering a motion model of the vehicle itself.

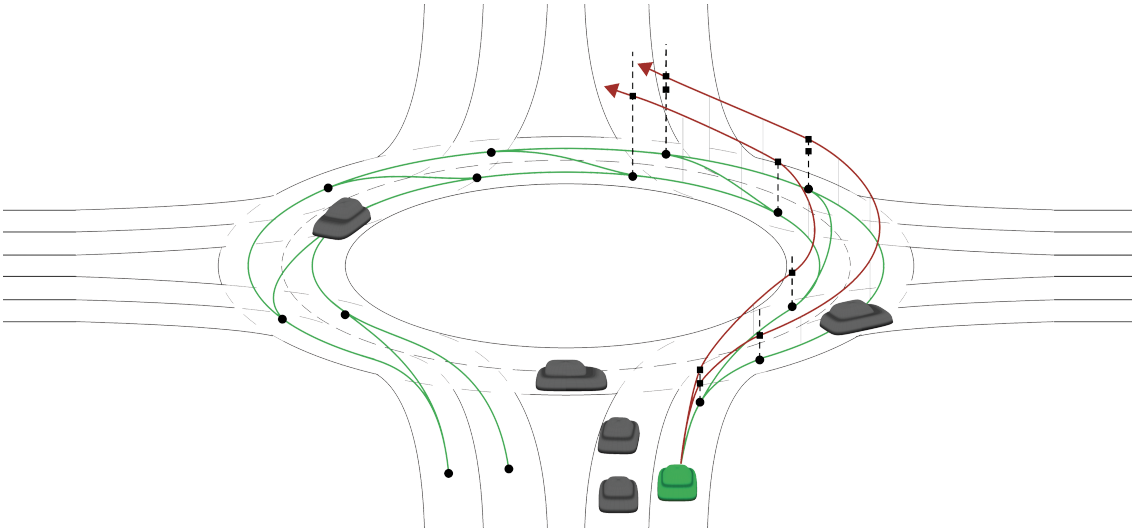

Figure 4.1 – Illustration of the motion planning task. The green vehicle represents the ego vehicle. The two red lines represent two possible trajectories the ego vehicle could follow, whose elevation (vertical displacement) represent time. The set of green lines and dots plotted on the road represent a lane-graph showing some path alternatives that would allow the ego vehicle to drive through the intersection.

It is worth pointing out that the scope of the tasks listed above is not written in stone, and the terms are not always consistently used in the literature. Thus, the above-presented description should be understood as our interpretation of the tasks' scope rather than an absolute and rigid formalization.

Even though the division of tasks mentioned above might seem a reasonable one, the motion planning problem is not always addressed in fully separated modules. Generally speaking, a tendency in the literature can be observed towards approaches aiming to model the motion planning problem as a monolithic one, in such a way that solving such a problem would be equivalent to solving the motion planning problem as a whole. In this context, promising theoretical frameworks such as model predictive control (MPC), Markov decision processes (MDP), or machine learning (ML) have shown great potential to achieve end-to-end solutions to the problem. However, they come at the expense of either an unaffordable rise in complexity and computational time, or making solution's efficiency mostly dependent on the quality and richness of a training set. Furthermore, even if the mentioned drawbacks were not an issue in practice, a fully integrated planning module would make it harder rather than easier for a strategy to address some of the inherent needs of planning motions in mixed traffic.

In partially connected scenarios, where CAVs share the road with other CAVs, AVs, and human drivers, the heterogeneous nature of the surrounding road agents, and therefore of the available interaction mechanisms, provides a rather strong argument to foster modularity in complete motion planning strategies. The heterogeneous technical capabilities of the surrounding road agents are likely to lead to the existence of different interaction mechanisms, each of which should be exploited with a suitable method to address the particular needs and constraints of each of them. For instance, a CAV that is surrounded only by CAVs could be imagined to know their intent and willingness to cooperate perfectly, which could boost solutions oriented to improve the overall traffic performance and not only the ego vehicle's welfare. At the other extreme of the spectrum, a CAV surrounded

only by human drivers would be mainly concerned about the unpredictability of human behavior and how to move safely in such a context. In intermediate scenarios, a CAV that coexists with human drivers and other CAVs should be able to make use, and properly integrate, all the interaction mechanisms available, as well as their corresponding planning methods. Planning motions in the traffic scenario just described is indeed a remarkably complex task, and, even though we do not possess the definite solution to it, it seems extremely unlikely for the planning solution to take a monolithic form.

In this chapter, we propose a novel and complete motion planning architecture designed to tackle the challenges stemming from partially connected scenarios. We start by discussing, in Section 4.1, the planning architecture we propose. Then, the so-called route, tactical, maneuver, and trajectory planning levels are further discussed in Section 4.2, Section 4.3, Section 4.4, and Section 4.5, respectively. Finally, some conclusions and comments are gathered in Section 4.6.

4.1 Planning architecture

The division of tasks and the overall motion planning architecture we propose answers to three general challenges: (i) handling the coexistence of heterogeneous interaction mechanisms in partially connected traffic scenarios, (ii) minimizing the level of redundancy between possibly coexisting modules, (iii) and generating a meaningful and pragmatic architecture that is easy to extend and complement.

Challenges caused by the partially connected nature of the scenario, which were discussed in the introduction to this chapter, are tackled by embracing modularity in the planning architecture. Consider a CAV driving in mixed traffic while trying to merge into a traffic stream. In our view, such a vehicle should be able to evaluate, in parallel, all the options it has to perform the maneuver, and then compare them and choose only one to pursue. If we considered rather monolithic solutions, we would need to have several complete motion planning modules in parallel, which would imply a high degree of redundancy in specific tasks that might remain common. In a way, we foster modularity in our planning architecture so that the aspects of the process that are tailored to the specific interaction mechanisms between vehicles are isolated, and are the only ones duplicated.

Furthermore, the division of planning tasks we explore in this thesis is aligned with our intuition concerning how human drivers seem to make driving decisions and plan their future movements. Indeed, human drivers do not continuously evaluate the explicit sequence of accelerations they could apply in order to make a driving decision. Yet they are arguably good at performing complex driving maneuvers such as merging into traffic streams, changing lanes, or crossing intersections. What human drivers seem to make use of, is a higher level intuition of their driving skills, their car capabilities, and what makes a maneuver safe, to determine the fundamental characteristics of the path and velocity they must follow. Then, according to such an intuition, they pursue a trajectory that fits their objective sufficiently well.

In an attempt to reproduce such a rationale, we consider separated planning modules for each step of the planning process discussed above (illustrated in Fig. 4.2). A so-called tactical module would first identify and weakly characterize the maneuver that should be performed (e.g. a lane change or a merging maneuver). The role of the intuitive decision-maker would then be played by the so-called maneuver planner, which is designed to make rather high-level decisions without explicitly constructing nor exploring the tree of future trajectories that can be followed. Finally, the decisions made by the maneuver planner would be pursued by a trajectory planner.

Regarding the motion planning tasks just described, it is worth stressing that our main interest

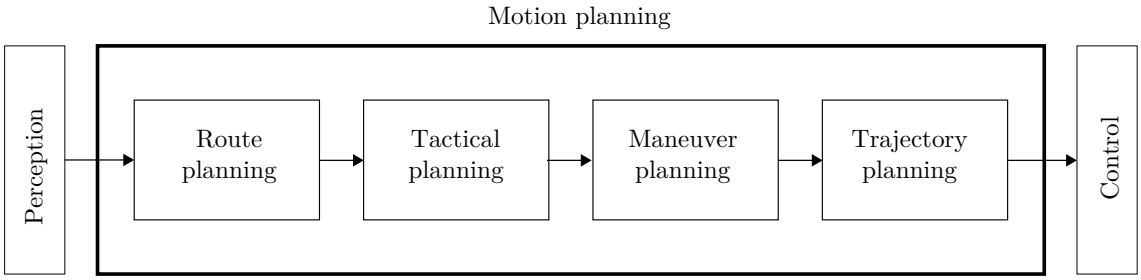

Figure 4.2 – Motion planning architecture. On the left-hand side, the perception module is shown, which feeds information to the motion planning and is further discussed in Chapter 3. On the right-hand side, the motion planning module passing information to the control layer, which is presumed to perfectly follow the plans. In the middle, we represent the motion planning module, which is the one this thesis focuses. Furthermore, the sub-modules the motion planning is composed of are as well shown. Although they are all briefly described in this chapter, the one this thesis focuses the most it the maneuver planner.

lies in the maneuver planning stage, and how different interaction mechanisms and decision-making strategies would impact the overall traffic performance. However, our contribution also includes the specification of the requirements and features that the surrounding modules should have for them to be properly integrated into a complete motion planning module. In this sense, we must define not only the strategies composing the planning submodules themselves but also their interfaces.

4.2 Route planning

Generally speaking, the *route planner* identifies the roads that need to be followed to go from a location A to a location B. However, as we focus on driving through an isolated traffic intersection, we do not address *route planning* strictly speaking. Instead, we directly assume that vehicles in the scenario have a specific origin and destination they target, which is generated in our simulated scenarios as described in Sections 2.3.2-2.3.3.

It must be pointed out that the origin-destination pattern used to test motion planning strategies does have an impact on the complexity of the driving task. Consider, for instance, two extreme cases where, at a certain roundabout scenario, every single vehicle leaves the intersection by: (situation i) the first exit or (situation ii) the last one w.r.t. their origin. Merging into a roundabout in situation i is indeed an effortless task, since, by configuration, the interaction between conflicting traffic streams is inexistent. On the contrary, situation ii is, intuitively, one of the most complex that can materialize in the studied scenario. This aspect is of great importance due to the impact it might have on the measured motion planning performance, which could be expected to be higher when the strategy is exposed to more straightforward scenarios, and vice-versa. In other words, to do a fair assessment of motion planning strategies, they need to be evaluated in a rich set of scenarios.

As described in Section 2.3.3, in our simulations, the origin-destination patterns are created so that u-turns are rather rare events, and the incoming lane that the vehicles use to approach the roundabout is correlated to its most likely destination. Nonetheless, as the destination patterns will be randomly drawn at the time of creating the simulation instances, more extreme traffic configurations will also be considered in our analysis.

4.3 Tactical planning

The role of the *tactical planner* within the proposed planning framework is, generally speaking, to identify the sequence of *driving maneuvers* whose execution should/could be considered by the ego vehicle, and to pass such information to the maneuver planner. Formally, the tactical planner is expected to identify, in a receding horizon fashion, a set $\mathcal{M} = \{\mathcal{M}_1, \cdots, \mathcal{M}_{n_\mathcal{M}}\}$ of driving maneuvers $\mathcal{M}_i$ that might be of interest given the traffic context and the ego vehicle's objective. Such a set of maneuver candidates is to be sent to the maneuver planner for it to come up with the characteristics that should be imposed on the trajectory to successfully execute the maneuver candidates, and pick the most appropriate one. Thus, they should encapsulate enough information to enable the maneuver planner to adequately characterize a safe and efficient way of executing the maneuver candidates. To do so, we first require a rather general and informative way of describing driving maneuvers, and then a strategy to specify the one (or ones) that should be passed to the maneuver planer.

4.3.1 Driving maneuver description

Regarding the driving maneuver description we aim to formalize, it is essential to note that it should allow us to represent two types of driving maneuvers: the so-called *self-serving* and *cooperative* driving maneuvers.

Definition 1 (Driving maneuver)**.** *Driving maneuvers are generally understood as those sets of actions that would require the ego vehicle to abandon the standard lane-keeping and car-following behavior, which are considered an equilibrium state rather than a maneuver in itself.*

Definition 2 (Self-serving driving maneuver)**.** *A self-serving driving maneuver is considered to be one that seeks to improve the way the ego vehicle moves towards its objective, either by increasing the rate at which the goal is approached, or the probability of successfully reaching it.*

Definition 3 (Cooperative driving maneuver)**.** *A cooperative driving maneuver is one that seeks to facilitate the execution of a self-serving maneuver by a surrounding vehicle, at the expense of decreasing the welfare of the ego vehicle.*

Significantly different aspects need to be taken into account to execute the two aforementioned types of driving maneuvers, yet the proposed maneuver description should fit both of them. On the one hand, it should be noted that executing self-serving maneuvers requires occupying—either in a transient or in a more lasting manner—an adjacent lane, thereby either crossing or merging into a different traffic stream. Therefore, the underlying problem that a decision-maker addresses while planning a self-serving motion is determining: (i) the path to follow, and (ii) the best inter-vehicle gap in the conflicting traffic stream that can be used to perform the targeted maneuver—in other words, choosing the homotopy class of the trajectory to be planned. On the other hand, performing cooperative driving maneuvers requires identifying the nearby vehicles seeking to execute a self-serving maneuver that crosses the ego vehicle's path, and deciding how the ego vehicle should behave to facilitate such a maneuver.

Furthermore, aiming to decontextualize, to some extent, the maneuver planning task from the specific traffic scenarios, the maneuver candidates $\mathcal{M}_i \in \mathcal{M}$ should provide a relatively abstract representation of the driving maneuvers. Specifically, for a driving maneuver description to be self-contained and rather general, it must provide information concerning: (i) the path to be pursued,

(ii) the obstacles and gaps that should be taken into account, and (iii) the behavior to be followed in case the maneuver needs to be aborted either because of an inappropriate configuration of the surrounding gaps, or other unexpected events.

A useful realization upon which our maneuver description (and our maneuver planner) is built is that, assuming the ego vehicle starts at a safe state, any path it can follow is composed of two types of segments. On the one hand, segments that the vehicle could follow just by keeping a safe state w.r.t. the obstacle ahead (also denoted as car-following segments). On the other hand, segments that require finding appropriate gaps in a certain set of crossing traffic streams (the so-called gap-acceptance segments). The spot separating these two path portions is denoted as the *decision spot*, and how it is reached has a crucial impact on maneuver safety, execution, and performance.

Definition 4 (Car-following path segments)**.** *A car-following path segment is one that can be followed without making any gap-acceptance decision.*

Definition 5 (Gap-acceptance path segments)**.** *A gap-acceptance path segment is one that can only be traveled once appropriate gaps have been found in the surrounding conflicting traffic streams.*

Based on the above discussion, we introduce the following *decision spot driving maneuver* (DSDM) description.

Definition 6 (Decision Spot Driving Maneuver (DSDM))**.** *A decision spot driving maneuver, here denoted as $\mathcal{M}$, is a maneuver that can be fully described by the tuple $(\pi, \delta, \pi_0, O, \mathfrak{I}_{SS}, \mathfrak{I}_C)$ where*

- *π is the targeted path to perform the maneuver,*
- *δ is the distance along π where the decision spot is located,*
- *π_0 is a path the vehicle can follow without making any gap-acceptance decision and must contain the portion of π that is between the current position and the decision spot,*
- *$O = \{\mathcal{O}_V, \mathcal{O}_R\}$ is a set gathering the subset $\mathcal{O}_V \subseteq \mathcal{O}_{obs}$ of observed objects that are on π and ahead of the ego vehicle, as well as a set $\mathcal{O}_R = \left\{\mathfrak{O}_1^R, \cdots, \mathfrak{O}_{n_{\mathcal{O}_R}}^R\right\}$ of obstacles representing relevant road markings on π,*
- *$\mathfrak{I}_{SS} = \{L, G\}$ is the set of information that would be relevant to execute self-serving driving maneuvers, and is composed of:*
  - *$L = \{l_1, \cdots, l_{n_L}\}$: the set of lanes l_i the path π crosses, and*
  - *$G = \{\mathcal{G}_l : l \in L\}$: a set gathering the sets $\mathcal{G}_l \subseteq \mathcal{G}_{obs}$ of gaps observed on lane l.*
- *$\mathfrak{I}_C = \{\mathfrak{O}_C, \delta_C\}$ is the information set concerning a potential cooperative maneuver, and it contains*
  - *$\mathfrak{O}_C \in \mathcal{O}_{C,obs}$: the obstacle whose maneuver could be facilitated by the ego vehicle, and*
  - *δ_C: the distance along π where the path of obstacle $\mathfrak{O}_C$ is estimated to intersect the ego vehicle's.*

The provided definition implicitly imposes certain constraints on how the driving maneuvers are expected to be planned. Firstly, note that even though the path π may contain portions of different kinds and therefore multiple key locations, the inclusion of a unique decision spot (through the scalar δ) implies that key locations are meant to be addressed one at a time. Moreover, concerning the set O of obstacles, it should be noted that the separation between obstacles representing vehicles and road markings is motivated by the different impacts they have on the decision-making process, which will be further discussed in the following chapters.

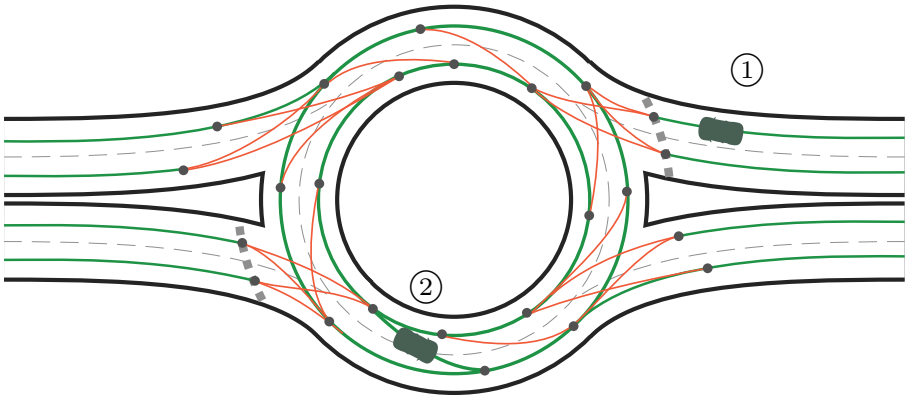

Figure 4.3 – Lane-graph representation of a two-lane roundabout. Segments (—) represent car-following edges, while segments (—) show the gap-acceptance ones.

4.3.2 Set of maneuver candidates

The construction of the set $\mathcal{M}$ of maneuver candidates to be assessed by the maneuver planner depends on whether the vehicle needs to execute a self-serving maneuver, or it is ready to perform a cooperative one. Generally speaking, the set $\mathcal{M}$ could potentially include simultaneously self-serving and cooperative maneuver candidates. However, for the sake of simplicity, we consider that maneuvers of only one type can be included within the set at a given time. Such a simplification is somehow equivalent to presume that performing a cooperative maneuver should only be considered at times when no self-serving maneuver needs to be executed.

Set of self-serving maneuver candidates When a self-serving maneuver needs to be executed (say for instance the ego vehicle seeks to merge into a roundabout or change lanes inside of it to take a specific exit) the construction of the set of maneuver candidates would begin by identifying a set Π of paths that would allow the ego vehicle to execute the targeted maneuver.

For the sake of simplicity, we consider the paths within Π to be generated using a lane-graph representation of the intersection layout. Such a graph would include edges characterizing not only the center of the lanes but also a finite set of lane-changing options. An example of such a lane-graph is shown in Fig. 4.3, where *car-following* edges are depicted in green, while *gap-based* edges are shown in orange.

Once the set Π is built, the set $\mathcal{M}$ will be constructed by including within it a maneuver candidate $\mathcal{M}$ for every path $\pi \in \Pi$.

The decision spot corresponds to the first node along π connecting a car-following edge with a gap-acceptance one.

The path π_0 is obtained by concatenating car-following edges starting from the edge the ego vehicle is at and is common to all the generated maneuver candidates. In this regard, it is important to stress that, as a gap-acceptance decision needs to be made before the vehicle occupies a gap-based edge, once the vehicle is positioned on one of them, they would be considered car-following edges (see vehicle ② in Fig. 4.3).

The set O of objects is composed by gathering: (i) the objects within $\mathcal{O}_{\text{obs}}$ that are on π_0, and (ii) the road markings on π_0 that should be taken into account. In a roundabout scenario, the latter set would only contain the yield marking when the vehicle faces the merging maneuver.

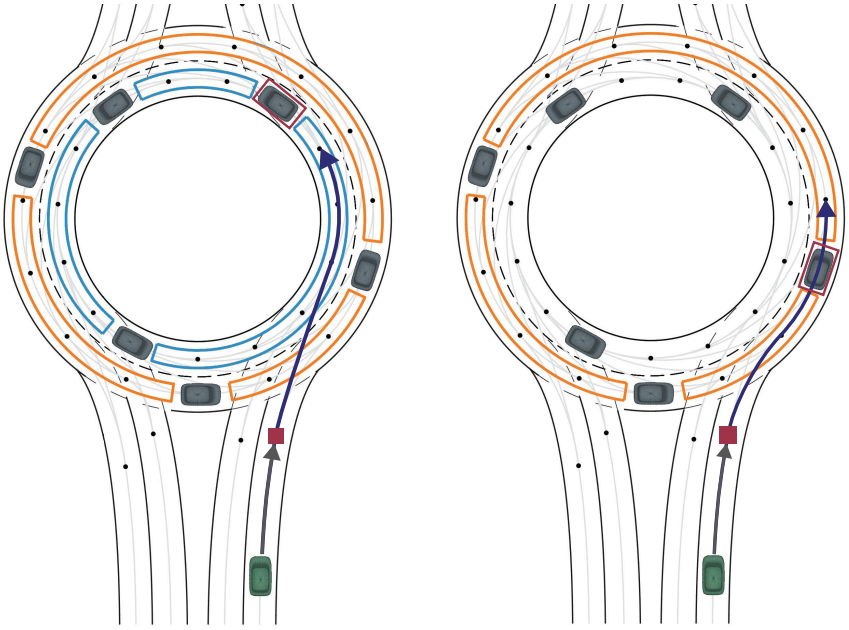

Figure 4.4 – Illustration of two eligible maneuver candidates to perform a merging maneuver into a two-lane roundabout, whose reference path is shown by the blue arrow and its currently safe portion is shown in gray. Inter-vehicle gaps belonging to different subsets are shown in different colors. Filled square represents the decision spot. The vehicles framed in a red box represent the relevant obstacles encoded within the maneuver candidates.

The sets $\mathfrak{I}_{\text{SS}} = \{L, G\}$ gathering, for every maneuver candidate, the information to perform self-serving maneuvers would contain:

- The set L of lanes the path π crosses, which requires having a map available.
- The set G gathering the probably-free gaps corresponding to the lanes that need to be crossed.

Moreover, the set $\mathfrak{I}_{\text{C}}$ meant to provide information to perform cooperative maneuvers would be empty, as only self-serving maneuvers are to be included within the set in this case.

In Fig. 4.4 we illustrate two self-serving maneuver candidates that could be considered when merging into a two-lane roundabout. On the left-hand side, where the vehicle would merge into the innermost circulatory lane, the maneuver candidate would be $\mathcal{M} = (\pi_1, \delta, \pi_0, O_1, \{\mathcal{G}_1 \cup \mathcal{G}_2, \{1, 2\}\}, \varnothing)$ with O_1 gathering the highlighted objects, and $\mathcal{G}_1$ and $\mathcal{G}_2$ gathering, respectively, the set of orange and blue inter-vehicle gaps. On the right-hand side plot in Fig. 4.4 an alternative maneuver candidate to perform the merging maneuver is similarly illustrated, which would be described as $\mathcal{M} = (\pi_2, \delta, \pi_0, O_2, \{\{\mathcal{G}_1\}, \{1\}\}, \varnothing)$.

Before going any further, there are two aspects worth stressing. On the one hand, note that within the tactical planner, we do not tackle path-planning strictly speaking, as we do not select a unique path to be followed, but rather a set of candidate paths. The reason is that, when several paths are available to perform a certain maneuver (for instance in the case of lane-change maneuvers), the one to be followed should be chosen according to not only geometric considerations but also how it can be traversed, which is an aspect evaluated by the maneuver planner. On the other hand, it is important to stress that when composing the set Π, the ego vehicle is implicitly making tactical

decisions. For instance, if the ego vehicle drives inside a roundabout and wants to change lanes before exiting, but wants to do it as late as possible, paths comprising an early lane change would simply be excluded from the set. We, nonetheless, disregard this implicit tactical decision, and consider, for the sake of simplicity, that AVs start seeking to position themselves in the outermost circulatory lane as soon as they merge into the roundabout.

Set of cooperative driving maneuvers Only when the ego vehicle does not have any self-serving maneuver to pursue in the foreseeable future, the tactical planner would include cooperative maneuver candidates within the set $\mathcal{M}$.

On this occasion, the set of maneuver candidates would be created from the set $\mathcal{O}_{\text{obs,C}} \subseteq \mathcal{O}_{\text{obs}}$ of detected surrounding obstacles that are thought to somehow benefit from a cooperative action coming from the ego vehicle. Therefore, the set $\mathcal{M}$ would this time be composed of as many maneuver candidates $\mathcal{M}$ as obstacles within $\mathcal{O}_{\text{obs,C}}$.

The targeted paths π within the maneuver candidates should in this occasion be the result of concatenating only car-following edges and would indeed be identical to π_0. The distance δ to the ego vehicle's decision spot would be empty, as the ego vehicle does not seek to deviate from its current lane. Furthermore, the self-serving maneuver information set $\mathcal{I}_{\text{SS}}$ would be empty, as only information concerning the cooperative maneuver is to be included. On the contrary, the set $\mathcal{I}_{\text{C}} = \{\mathcal{O}_{\text{C}}, \delta_{\text{C}}\}$ would, be composed of the obstacle $\mathcal{O}_{\text{C}} \subseteq \mathcal{O}_{\text{obs,C}}$ subject of the cooperation, as well as the distance δ_{C} along π where its path is expected to intercept the ego vehicle's.

Zero maneuver candidate Among the self-serving and cooperative maneuver candidates identified above, the ego vehicle might as well encounter situations where it only has to follow its traffic stream normally. Such a situation would be described by the so-called zero maneuver candidate $\mathcal{M}_0 = \{\pi_0, O, \pi_0, \varnothing, \varnothing\}$, only expressing the need to keep on circulating on π_0 while staying at a safe distance w.r.t. the observed obstacles within O.

4.4 Maneuver planning

The role of the *maneuver planner* in our motion planning solution consists in selecting one of the maneuver candidates within the set $\mathcal{M}$ built by the tactical planner, as well as calculating the general targets and constraints the trajectories should meet to execute them properly. To do so in a heterogeneous traffic context characterized by the coexistence of road agents with fundamentally different technical capabilities (for which fundamentally different interaction mechanisms may exist), we make the maneuver planner module be composed of several planning submodules as illustrated in Fig. 4.5. Each of such submodules would evaluate the maneuver candidates from the standpoint of a specific interaction mechanism available and would spot their best option. Then, the maneuver chosen by every planning submodule, as well as the fundamental characteristics they impose on the trajectory, would be compared to determine which is the best alternative overall.

It must be noted that two modules labeled as *virtual reality* have been included. These modules represent the communication-based interaction mechanism briefly presented in Section 2.1, whereby CAVs could interact using virtual vehicles. Having a module within the maneuver planner connected to such a *virtual reality* represents the fact that they can take into account the state of the virtual vehicles in the decision-making process.

As for the methods used to perform the maneuver planning task, they depend on the specific maneuver planning submodule being addressed. Nonetheless, all included policies should provide

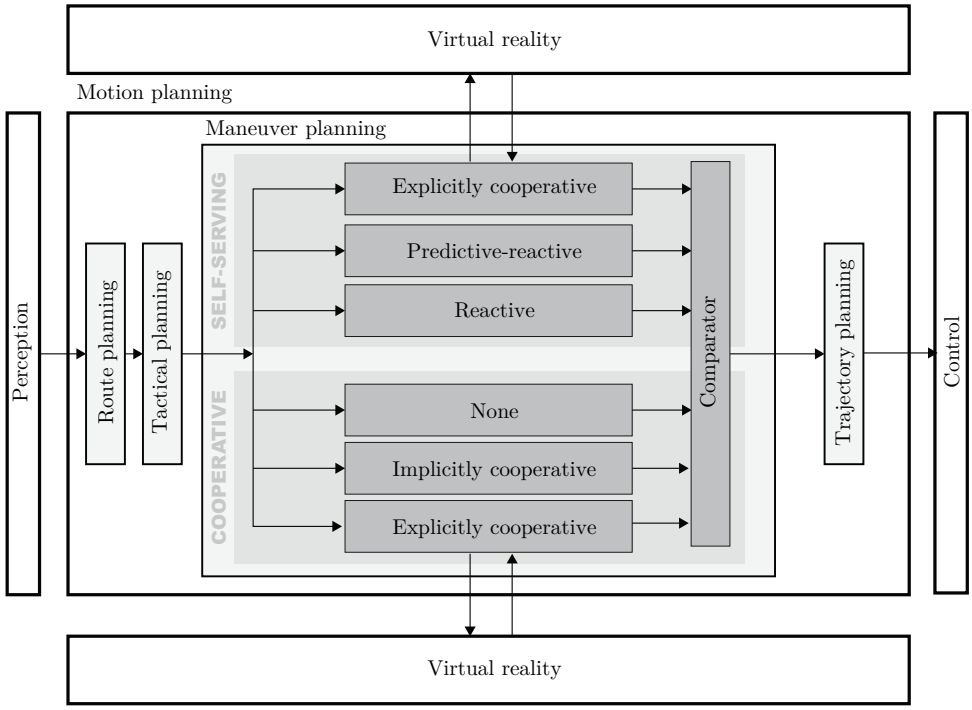

Figure 4.5 – The proposed maneuver planning architecture, where modularity is embraced to address the complexity of planning when heterogeneous interaction mechanisms need to be considered. Modules within the maneuver planning block are divided in two groups regarding whether they are meant to handle cooperative or self-serging maneuvers. Moreover, two blocks labeled as *virtual reality* are included to represent the information that woud be available through V2V, i.e. the state of the virtual vehicles.

enough information to the trajectory planner so that safe trajectories that match the decision made by the maneuver planner can be generated. The output expected from the maneuver planner consists of a chosen maneuver $\mathcal{M}^*$ to target (which implicitly specifies a certain path π to be followed) a set $\mathcal{C} = \{\mathcal{C}_1, \cdots, \mathcal{C}_{n_\mathcal{C}}\}$ of constraints, as well as two sets $\mathcal{V} = \{\mathcal{V}_1, \cdots, \mathcal{V}_{n_\mathcal{V}}\}$, and $\mathcal{D} = \{\mathcal{D}_1, \cdots, \mathcal{D}_{n_\mathcal{D}}\}$ of, respectively, speed and distance targets to be considered by the trajectory planner.

Definition 7 (Trajectory safety constraint)**.** *Given a path of reference π, a* maneuver safety constraint $\mathcal{C}$ *is defined as the tuple $\mathcal{C} = (\tau_\mathcal{C}, x_\mathcal{C}, d_\mathcal{C})$ where*

- *$\tau_\mathcal{C}$ is the time the constraint needs to be taken into account,*
- *$x_\mathcal{C}$ is the state of the obstacle with respect to which a safe behavior must be kept, and*
- *$d_\mathcal{C}$ is the maximum deceleration to be applied to do so.*

Definition 8 (Trajectory velocity target)**.** *A velocity target $\mathcal{V}$ is defined as the tuple $\mathcal{V} = (\tau_\mathcal{V}, v_\mathcal{V})$ representing the objective of having a speed $v_\mathcal{V}$ at time $\tau_\mathcal{V}$.*

Definition 9 (Trajectory distance target)**.** *A distance target $\mathcal{D}$ is defined as the tuple $\mathcal{D} = (\tau_\mathcal{D}, \delta_\mathcal{D})$ representing the objective of traveling a distance $\delta_\mathcal{D}$ in a time $\tau_\mathcal{D}$.*

The distinction between self-serving and cooperative maneuvers encourages us to differentiate to families of maneuver planning submodules, regarding whether they intended to address self-serving or cooperative maneuvers.

4.4.1 Self-serving planning submodule

Given a set of self-serving maneuver candidates, the task of a self-serving maneuver planning submodule would essentially consist in evaluating the maneuver candidates and pick one to pursue. In order to do so, it would identify the probably-free inter-vehicle gap that could be used to execute every maneuver candidate, and define the trajectory targets and constraints that would allow the vehicle to safely follow the path and successfully use the chosen gap.

Selecting a specific inter-vehicle gap to target requires, among other things, characterizing the ways the ego vehicle can move forward, and then analyzing which one of those is the most appropriate. To do so, we generally rely on a low-dimensional representation of the longitudinal motions, which will be shown to be enough to plan efficient yet safe maneuvers. The representation is inspired by the realization that human drivers do not consider the explicit sequences of accelerations that can be applied while planning maneuvers. They seem to use, instead, some intuition concerning how certain key-locations ahead can be reached, and how the traffic around them is likely to evolve. In the described context, such key-locations could be correlated to the decision spots of the DSDMs. Thus, the decision-making can then be addressed by reasoning only about the states the ego vehicle can have while driving through such a spot, rather than how such a state would be reached. Specifically, we introduce the concept of *maneuver target* as a compact way of representing a possible state with which a certain decision spot (or generally speaking a certain location) can be reached.

Definition 10 (Maneuver target)**.** *Given a maneuver* $\mathcal{M} = (\pi, \delta, \pi_0, O, \mathcal{I}_{SS}, \mathcal{I}_C)$*, a* maneuver target $\mathcal{T}_\mathcal{M}$*, is defined as the tuple* $\mathcal{T}_\mathcal{M} = (t_\mathcal{M}, v_\mathcal{M})$ *where*

- $t_\mathcal{M}$ *shows the time at which the decision spot is to be reached, that is,* $s(t_\mathcal{M}) = s(t_0) + \delta$*, and*
- $v_\mathcal{M}$ *is the speed the ego vehicle should have when it reaches the decision spot, that is,* $v(t_\mathcal{M}) = v_\mathcal{M}$*.*

In this thesis, as was depicted in Fig. 4.5, we will formulate and evaluate three different self-serving maneuver planning strategies:

- a purely reactive approach, whereby AVs would make reactive decisions uniquely regarding the traffic state they currently see, or very simple and short predictions at most,
- a communication-based approach enabling CAVs to make efficient decisions by explicitly requesting cooperation to other CAVs through the use of virtual vehicles,
- a predictive-reactive planner, whereby AVs would consider the predicted position of the surrounding traffic in the future, as well as its associated uncertainty, to make safe yet efficient decisions even when their perception system is affected by occlusions.

4.4.2 Cooperative planning submodule

Cooperative planning submodules would essentially reason about how the ego vehicle should adapt its speed profile while following its current path, so that the self-serving maneuver of some nearby vehicle can be facilitated.

Concerning the cooperative maneuver planning submodules, two modules are addressed in this thesis:

- A communication-based cooperative maneuver planner aimed to complement the communication-based self-serving maneuver planner, whereby vehicles would simply react to the relevant virtual vehicles in the surroundings,

- An implicitly cooperative maneuver planner, allowing AVs to cooperate with unconnected vehicles by changing the context rather than using any explicit communication channel.

Note that a possibility that we also consider in our study is having vehicles lacking mechanisms to handle cooperative maneuvers, as expressed by the *none* module in Fig. 4.5. Interestingly, a minimal self-serving maneuver planner would, however, be required, as, without one, the vehicle would not be capable of driving safely through gap-acceptance path segments.

4.5 Trajectory planning

The *trajectory planner* module generates kinetically-feasible state trajectories

$$x^T(t) = \{x(t+0), \cdots, x(t+T)\} \tag{4.2}$$

that comply with the path, constraints, and targets imposed by the maneuver planner. Note that, as the maneuver planner provides the reference path, the task is reduced to obtaining an appropriate speed profile to follow such a path. While doing so, the module needs to take into account the targets within $\mathcal{V}$ and $\mathcal{D}$, and the safety constraints $\mathcal{C}$ set by the maneuver planner.

For the sake of efficiency, we exploit a hybrid architecture that combines a reactive trajectory planning and an optimization-based one. Specifically, the trajectory planner will employ a reactive approach $\mathbb{TR}_{\mathrm{R}}$, based on the Intelligent Driver Model (IDM) [86], when no distance or velocity target is set by the maneuver planner, and would exploit an optimization-based strategy $\mathbb{TR}_{\mathrm{P}}$ otherwise. That is

$$\mathbb{TR} = \begin{cases} \mathbb{TR}_{\mathrm{R}} & \text{if } \mathcal{V} = \varnothing \wedge \mathcal{D} = \varnothing \\ \mathbb{TR}_{\mathrm{P}} & \text{otherwise} \end{cases} . \tag{4.3}$$

In the following sections, both components of the trajectory planner will be described.

4.5.1 Reactive approach

Reactive speed profiles are, in this case, calculated by exploiting a certain car-following model $a_{\mathrm{CF}} = f_{\mathrm{CF}}(x_F, x_L)$ which returns the acceleration to be applied by a following vehicle F, given its state x_F, and the state of its leading vehicle x_L.

The process consists in calculating, at every time t the elements of the speed trajectory

$$v^T = \{v(t), \cdots, v(t+T)\}, \qquad v(t+k) = v(t) + \sum_{i=0}^{k} a(t+i) \tag{4.4}$$

with which the path should be followed, from a certain acceleration profile

$$a^T = \{a_{\mathrm{CF}}(t), \cdots, a_{\mathrm{CF}}(t+T)\} \tag{4.5}$$

whose elements are calculated considering a specific car-following model. In particular, letting x_L denote the state of the closest object within $\mathcal{C}$, the sequence of acceleration would be calculated as

$$a_{\mathrm{CF}}(t+k) = f_{\mathrm{CF}}(\hat{x}_F(t+k), \hat{x}_L(t+k)), \tag{4.6}$$

which relies on a car-following model f_{CF} and assumes constant speed of the leading vehicle. For

simplicity, and considering the longitudinal motion model $x(k+1) = f(x(k), u(k))$ to be

$$x(k+1) = \Phi x(k) + \Gamma u(k), \qquad \Phi = \begin{pmatrix} 1 & h \\ 0 & 1 \end{pmatrix}, \qquad \Gamma = \begin{pmatrix} 0.5h^2 \\ h \end{pmatrix}, \tag{4.7}$$

the predicted states used in Eq. (4.6) are calculated as

$$\hat{x}_L(t+k) = \Phi^k x_L(t) \qquad \hat{x}_F(t+k) = \Phi^k x_F(t) + \Gamma \sum_{i=0}^{k-1} a(t+i). \tag{4.8}$$

That is, assuming (i) constant speed of the leading vehicle and (ii) the perfect application of the reactive acceleration for the following one.

Although the formulation would accept any car-following model, we opt for the IDM [86] due to its simplicity, the realistic acceleration profiles it renders, and the meaningful parameters representing the modeled driving style. In particular, the model calculates the reactive acceleration as

$$f_{\mathrm{CF}}(x_{\mathrm{F}}, x_{\mathrm{L}}) = \psi_1 \left(- \left(\frac{v_F}{\psi_2} \right)^{\psi_3} - \left(\frac{s^*(v_F, v_L)}{s_F} \right)^2 \right), \tag{4.9}$$

$$s^*(v_F, v_L) = \psi_4 + \max \left\{ 0, v\psi_5 + \frac{v_F(v_F - v_L)}{2\sqrt{\psi_1 \psi_6}} \right\}, \tag{4.10}$$

with

- ψ_1 : targeted acceleration,
- ψ_2 : desired speed,
- ψ_3 : acceleration exponent controlling the acceleration decrement as the desired speed is reached (the greater the value, the later such reduction takes place),
- ψ_4 : minimum gap distance (bumper to bumper),
- ψ_5 : time gap, and
- ψ_6 : comfortable braking deceleration.

It is worth noting that although the car-following model has been exploited to plan trajectories within a certain temporary horizon, as only the first acceleration of the planned trajectories are to be executed at every time step, it could have also been applied in a reactive manner.

4.5.2 Optimization-based approach

When the state trajectory needs to be planned while pursuing velocity and/or distance targets, an optimization-based solution is exploited. In particular, we formulate a linearly-constrained quadratic optimization problem, where the targets and safety constraints can be efficiently integrated.

Letting h show the sampling time, and the auxiliary function $\mathtt{K}(\tau) = \lfloor \tau/h \rfloor$ return the time step corresponding to a time interval τ, the speed profile to pursue over a planning horizon T (or equivalently over $N = \lceil T/h \rceil$ time steps) is obtained from

$$\left(u^{T^*}, x^{T^*} \right) = \arg \min_{u^T, x^T} \left\{ \mathcal{J}\left(u^T, x^T, \mathcal{D}, \mathcal{V} \right) : \mathcal{C}_{\mathrm{QP}} \right\}, \tag{4.11}$$

where the decision variables are the state and control input trajectories

$$x^T = \{x(t), x(t+h), \cdots, x(t+Nh)\}, \qquad u^T = \{u(t), u(t+h), \cdots, u(t+Nh)\}. \tag{4.12}$$

The cost function is formulated as

$$\mathcal{J}\left(u^T, x^T, \mathcal{D}, \mathcal{V}\right) = \mathcal{J}_{\mathcal{D}}(s^T, \mathcal{D}) + \mathcal{J}_{\mathcal{V}}(v^T, \mathcal{V}) + \mathcal{J}_u(u^T) + \mathcal{J}_v(v^T), \tag{4.13}$$

where terms

$$\mathcal{J}_{\mathcal{D}}(s^T, \mathcal{D}) = \omega_{\mathcal{D}} \sum_{i=1}^{n_{\mathcal{D}}} \left(s(\mathtt{K}(\tau_{\mathcal{D}_i})) - s_{\mathcal{D}_i}\right)^2, \qquad \mathcal{J}_{\mathcal{V}}(v^T, \mathcal{V}) = \omega_{\mathcal{V}} \sum_{i=1}^{n_{\mathcal{V}}} \left(v(\mathtt{K}(\tau_{\mathcal{V}_i})) - v_{\mathcal{V}_i}\right)^2, \tag{4.14}$$

penalize, respectively, the deviation of the trajectory w.r.t. the targets, whereas the terms

$$\mathcal{J}_u(u^T) = \sum_{k=1}^{N} \omega_{\mathrm{u}} u^2(k), \qquad \mathcal{J}_v(v^T) = \sum_{k=1}^{N} -\omega_{\mathrm{v}} v^2(k), \tag{4.15}$$

account for trajectory smoothness and overall speed.

Moreover, the set $\mathcal{C}_{\mathrm{QP}}$ contains the constraints

$$s(k+1) = s(k) + v(k)h + 0.5u(k)h^2, \ k \in [0, N-1], \tag{4.16}$$

$$v(k+1) = v(k) + u(k)h, \ k \in [0, N-1], \tag{4.17}$$

$$2d_{\mathcal{C}_i}(\delta_{\mathcal{C}_i} + v_{\mathcal{C}_i} k'h - s(k')) + v_{\mathcal{C}_i}^2 \geq v^2(k'), \ i \in [1, n_{\mathcal{C}}], k' \leq \mathtt{K}(\tau_{\mathcal{C}_i}), \tag{4.18}$$

$$v(k) \in [0, v_{\mathrm{M}}], \quad u(k) \in [a_{\mathrm{m}}, a_{\mathrm{M}}], \ k \in [0, N-1], \tag{4.19}$$

$$s(0) = 0, \ v(0) = v_0, \ a(0) = a_0, \tag{4.20}$$

where Eq. (4.16)–(4.17) implement the motion model, Eq. (4.18) imposes the safety constraint, Eq. (4.19) defines the valid range of values of the decision variables, and Eq. (4.20) sets the initial conditions.

Constraint (4.18) is nonlinear but convex. Hence it can be approximated by a set of linear inequalities (Fig. 4.6). In particular, by selecting a set of speed values $\mu = \left\{\mu_1, \cdots, \mu_{n_\mu}\right\}$ distributed within the range $[v_{\mathrm{m}}, v_{\mathrm{M}}]$, Eq. (4.18) can be approximated by the set of inequalities

$$2d_{\mathcal{C}_i}(\delta_{\mathcal{C}_i} + v_{\mathcal{C}_i} kh - s(k)) + v_{\mathcal{C}_i}^2 \geq 2\mu_j v(k) - \mu_j^2, \quad j \in [1, n_\mu]. \tag{4.21}$$

In Fig. 4.7, an example of a speed trajectory generated with this approach is shown. Specifically, we illustrated a case where a speed and a distance target were set (shown by the green filled circles), along with a safety constraint (shown by the set in the plot on the bottom right corner). Concerning the safety constraint, it aims to impose a safe driving behavior w.r.t. a static obstacle at 15m, only during a time interval of 5.5s, which can be translated into the need to keep the distance-speed trajectory within the set depicted in the bottom right corner. Not how, even though the speed target pursues a speed that is equal to the initial one, the generated speed profile is not constant as, in such a case, the safety constraint would not hold true as long as it needs to.

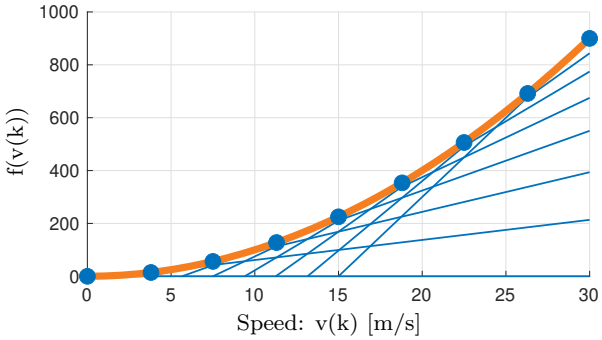

Figure 4.6 – Illustration of the convexification process used to formulate the original non-linear safety constraint as a set of linear inequalities.

Table 4.1 – Parameters used in simulation

	T	h	$\omega_{\mathcal{D}}$	$\omega_{\mathcal{V}}$	ω_{u}	ω_{v}	n_{μ}
Value	25	10^{-1}	10	4000	50	0.1	10
Unit	s	s	m^{-1}	s/m	s^2/m	s/m	-

4.6 Conclusions

In this chapter, we have discussed the motion planning architecture that we exploit in this thesis. Emphasis has been made on its modularity, which was argued to provide a suitable solution to handle the motion planning problem in partially connected scenarios. A self-contained and general driving maneuver description has been proposed, which along with the maneuver-target based low-dimensional trajectory representation, was claimed to compose a general motion planning framework, and to abstract the maneuver planning module from the specific traffic situation. Moreover, a fundamental advantage of this architecture is that it prevents the tactical and trajectory planning tasks from being redundantly executed when different decision-making approaches coexist.

Even though tactical and route planners are not the main focus of this thesis, their implementation and interfaces have been detailed for the sake of completeness. In this sense, their described implementation is a rather simplified one that has been observed to work sufficiently well in simulation. Nonetheless, more advanced and efficient approaches could be easily formulated. For instance, concerning the tactical planner, a more suitable solution would consist in envisioning some strategy to assign weights to the edges of the lane-graph representing the surrounding lanes, which could potentially depend on the surrounding traffic density. Then, the process of building the set of paths from where the set of self-serving maneuver candidates are created could be executed by finding the least costly paths that arrive at the targeted destination. By engineering the weights of the edges, one could somehow control, for instance, the urgency of making lane changes or simply prevent the algorithm from using certain parts of the road. This process implies tactical decisions that could be expected to have a substantial impact on the performance of the solution and that we will study in future work.

The discussed maneuver planner, which is the main focus of this thesis, relies likewise on a modular architecture to meet the needs of efficiently planning motions in mixed-traffic scenarios. Inspired on how human beings seem to make driving decisions, a low-dimensional representation of longitudinal motions was proposed to address the decision-making problem, which will play a

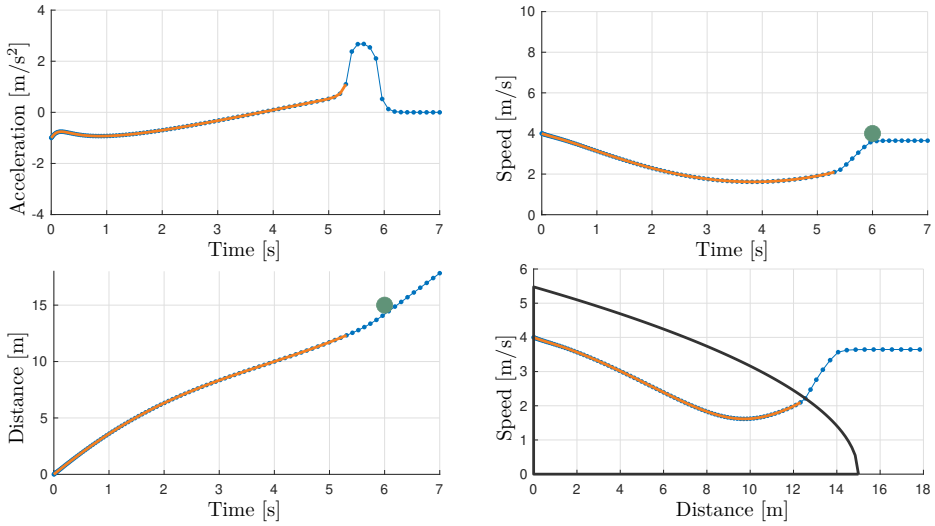

Figure 4.7 – A speed profile generated using the optimization-based approach. On the top-left corner, the resulting acceleration profile. On the top-right corner, the speed profile along with a speed target $\mathcal{V} = (6, 4)$ (shown by (•)). On the bottom-left, the travel distance profile along with a distance target $\mathcal{D} = (6, 15)$ (shown by (•)). On the bottom-right corner, the representation of the resulting distance-speed evolution, along with the representation of a safety constraint corresponding to the constraint $\mathcal{C} = (5.5, 15, 0, 1)$. In all plots, we show in (—), the segment of the profile between times 0s and 5.5s. For the safety constraint shown in the bottom-right plot to be met, the distance-speed trajectory must stay within the shown set during the first 5.5s. That is, the trajectory's orange portion must stay inside the shown set.

pivotal role in the decision-making solutions that will be proposed in future chapters. The modular architecture provides a framework that enables us to easily modify and add new features to the behavior of the vehicle, and facilitates the integration of planning strategies based on fundamentally different interaction mechanisms. Furthermore, the outputs of the maneuver planner have been designed in such a way that generating trajectories is transparent to the decision concerning its homotopy class, which is part of the maneuver planner's output, and the principal advantage of the proposed modular solution.

Finally, a hybrid trajectory planning approach has been shown, which implements (i) a reactive car-following-based strategy when no distance of velocity targets are passed, and (ii) an optimization-based one otherwise.

In general, several aspects of the motion planning architecture could indeed be extended so that more complex cooperative behaviors could be executed, and smarter ways of choosing the path to be pursued applied. However, as will be observed in upcoming chapters, the proposed planning strategy represents a flexible planning framework that enables us to design decision-makers intended to exploit different interaction mechanisms.

5 Reactive Self-Serving Planning

When the challenge of designing a decision-making policy for AVs is tackled, one quickly realizes the vast amount of methods and strategies available in the literature. Among them, the most straightforward approaches are the so-called reactive ones, which determine what to do *now*, based on the current traffic state (or at most the traffic state in the very near future).

Even though addressing the maneuver planning task (described in Section 4.4) in a purely reactive way might not seem a good idea, regarding the big picture, there are numerous advantages for having a robust and reliable reactive decision-making policy available. Firstly, as they represent the simplest family of solutions, they are often used as baseline behaviors, so that the increase in complexity of more advanced and sophisticated techniques should be justified by quantifying the improvement of performance compared to such simple strategies. In this regard, it would not be fair formulating a naive reactive planner, hence we believe its formulation is worth a dedicated chapter. Moreover, reactive strategies are as well the best complement for more advanced decision-makers, as they can act as a backup when other approaches fail to provide an appropriate solution in a reasonable amount of time.

Additionally, regarding the content of this thesis, formulating a simple maneuver planner allows us to discuss concepts and ideas that affect all strategies proposed in the following chapters but in a simpler context. For the reasons above, we start this chapter by tackling the design of a reactive self-serving maneuver planner intended to be used as a baseline for future comparisons, which is an extension of the exploited baseline behavior we used in [16, 17, 19, 18].

This chapter is organized as follows. In Section 5.2, we refine the problem formulation and present the assumptions upon which our reactive planner is built. Then, in Section 5.3, we tackle the design of the reactive planner, whose performance is subsequently assessed in Section 5.4. The chapter concludes in Section 5.5, where we present some conclusions and final remarks.

5.1 Related work

Let us begin in this section by briefly introducing some works that have inspired the baseline reactive behavior we present in this thesis.

Reactive decision-making strategies addressing a similar problem to the one we tackle in this chapter have been extensively used in the transportation community to carry out microscopic

traffic simulations. Such techniques represent an interesting starting point for the development of reactive motion planners for AVs, due to the fundamental similarities of the problems they tackle. Specifically, the content of this chapter has been strongly inspired by lane-change models in the transportation systems literature, as the logic to accept gaps can be extrapolated to any gap-acceptance based maneuver like merging maneuvers.

Several reactive lane-change approaches can be found in the literature (see ,for instance, [24, 85]). Nonetheless, one of the most distinguished approaches is the one presented by Kesting et al. in [41], which consists in *Minimizing the Overall Braking Induced by Lane change*, better known in the literature as the MOBIL model. This model, built upon the *intelligent driving model* [86] (although any other car-following model could be used instead), only triggers the lane change if it finds appropriate the balance between the own vehicle's advantages and the disadvantages imposed on the surrounding vehicles. To include such a fairness balance in the decision-making process, the formulation includes a so-called *politeness* factor as a design parameter, which represents how much the lane-changing vehicle is willing to disturb its surrounding traffic.

One of the earliest practical realizations of reactive gap-acceptance policies on automated vehicles could be attributed to Boss [87], the winner of the urban challenge. This experimental vehicle implemented a gap-acceptance based policy based on a minimum headway distance and time that would be considered feasible. Probably due to the nature of the urban challenge itself, the approach did not take into account any sort of social politeness level in the decision-making.

The approach we present in this chapter is inspired not only on the MOBIL model presented above but also on the concepts Althoff et al. exploited in [3] to formulate their lane-change safety verification method. In essence, they formalize the safety conditions that need to hold for a lane change to be considered safe, which, even though it is proposed as a safety verification method, could also be used to develop planning strategies that impose safety by design.

Although our approach is inspired by the previously mentioned works, it does represent an extension in the sense that it is formulated in terms of the probably-free gaps of Chapter 3, which naturally makes the strategy applicable to occluded scenes. Moreover, its integration within the proposed planning architecture in Chapter 4, makes the proposed method suitable for any gap-acceptance maneuver decision, and not only for lane-changes or merging maneuvers.

5.2 Problem formulation and assumptions

According to the motion planning architecture presented in Chapter 4, the problem the self-serving reactive planner would face can be simply seen as that of finding a specific maneuver candidate $\mathcal{M}^{\mathrm{R}}$ to target, out of the set $\mathcal{M}$ provided by the tactical planner. Additionally, high-level targets and constraints must be set up and passed to the trajectory planner module, so that a trajectory to appropriately execute the chosen maneuver can be generated.

The traffic scenario considered by the herein formulated reactive maneuver planner is a simplification of the general scene described in Chapter 2. In particular, we consider the strategy to be *communication independent*, to have only the capacity of making *instantaneous* decisions, and to take into account only the *current* state of the surrounding vehicles (or a very short term prediction at most). The fact that the strategy does not rely on communication implies that any AV with a sufficient level of autonomy could implement it. Furthermore, for the strategy to be sufficiently versatile and meet our needs, it should be able to make decisions based on the probably-free gaps that the perception layer is assumed to provide (see Chapter 3), so that a reactive but safe behavior can be expected in occluded scenes.

Algorithm 1: Reactive self-serving maneuver planner work-flow

Input: $\mathcal{M} = \{\mathcal{M}_1, \cdots, \mathcal{M}_{n_\mathcal{M}}\}$
Output: $\mathcal{M}^{\mathrm{R}}, \mathcal{C}, \mathcal{V}, \mathcal{D}$

for $\mathcal{M} \in \mathcal{M}$ **do**
  $\mathcal{T}^{\mathrm{R}}_{\mathcal{M}} \leftarrow$ MT resulting from applying the IDM;
  $\mathrm{P}^{S}_{\mathcal{M},\mathcal{T}^{\mathrm{R}}_{\mathcal{M}}} \leftarrow$ probability of the reactive MT being safe w.r.t. the set of relevant gaps G;
end
$(\mathcal{M}^{\mathrm{R}}, \mathcal{T}_{\mathcal{M}^{\mathrm{R}}}) = \arg\max \left\{ \mathcal{Q}(\mathcal{M}, \mathcal{T}^{\mathrm{R}}_{\mathcal{M}}) : \mathcal{M} \in \mathcal{M} \right\}$;
$(\mathcal{C}, \mathcal{V}, \mathcal{D}) \leftarrow$ the constraints and targets to be imposed by the trajectory planner;

In practical terms, making instantaneous decisions translates into the inability of the strategy to use distance and velocity targets that could have been otherwise used to meet future target states. On the other hand, using short-term predictions implies that the strategy is only allowed to make use of constant-velocity traffic predictions, which are typically valid for very short periods of time. Finally, making the strategy able to properly use the observed probably-free gaps entails that it should be aware of the gap it is about to use, and guarantee that the probability of it being free is high enough for the maneuver to be executed.

5.3 Reactive maneuver planner

The features and limitations that we aim to impose on the reactive planner restrict the set of decisions that can be made. For instance, the fact that no velocity or distance target can be set means that the strategy should only rely on the reactive trajectory planning submodule (formulated in Section 4.5.1) to decide which maneuver candidate should be pursued. Thus, the reactive decision that needs to be made can be seen as determining whether such a reactive behavior is safe concerning the state of the surrounding traffic.

In other words, since the planned trajectories are limited to the ones given by the reactive trajectory planner, the maneuver planner is aware of the acceleration the trajectory planner is ready to apply. Therefore, the maneuver planner would only generate a go/no go command showing whether the expected reactive behavior is ready to be executed, or if the ego vehicle should rather stay in its currently safe path option, stopping if necessary.

The proposed reactive maneuver planning strategy, shown in Algorithm 1, tackles the decision-making process in four main steps:

1. calculating, for every maneuver candidate within $\mathcal{M}$, the reactive maneuver target $\mathcal{T}^{\mathrm{R}}_{\mathcal{M}}$ (showing how the decision spot would be reached) resulting from the application of the reactive trajectory planning strategy,
2. quantifying, for every maneuver target, the probability of it being safe w.r.t. the observed probably-free gaps that should be utilized,
3. selecting, according to a specific quality metric, the best maneuver candidate and target to be pursued out of the available ones, and
4. composing the outputs of the maneuver planner.

In the following sections, we will address these steps one at a time.

5.3.1 Reactive maneuver target

Firstly, we will tackle the calculation of the reactive maneuver target $\mathcal{T}^{\mathrm{R}}_{\mathcal{M}} = (\tau^{\mathrm{R}}_{\mathcal{M}}, v^{\mathrm{R}}_{\mathcal{M}})$ describing how the decision spot is expected to be reached if a certain maneuver template is given.

Formally, given a maneuver candidate $\mathcal{M} = \{\pi, \delta_{\mathcal{M}}, \pi_0, O, \{L, G\}, \varnothing\}$ with a decision spot located at a distance $\delta_{\mathcal{M}}$ and a set of relevant objects $\mathcal{O}_{\mathrm{V}} \in O$, the reactive maneuver target $\mathcal{T}^{\mathrm{R}}_{\mathcal{M}}$ can be calculated by exploiting the reactive trajectory planner $\mathbb{TR}_{\mathrm{R}}$, described in Section 4.5. Specifically, we would first identify the closest obstacle

$$\mathcal{O}^{\mathrm{R}} = \arg\min_{\mathcal{O}\in\mathcal{O}_{\mathrm{V}}} \delta_{\mathcal{O}} \tag{5.1}$$

within $\mathcal{O}_{\mathrm{V}}$ (with $\delta_{\mathcal{O}}$ showing the distance from the ego vehicle's position to the obstacle), and then obtain the reactive state trajectory

$$x^T(t_0) = \{(\delta(t_0+\tau), v(t_0+\tau)) : \tau \in [0, T]\} \tag{5.2}$$

as explained in Section 4.5.1. Then, by analyzing the state trajectory x^T, the time and speed with which the ego vehicle would be expected to arrive at the decision spot could be identified by doing

$$\tau^{\mathrm{R}}_{\mathcal{M}} = \arg\min_{\tau\in[0,T]} (\delta_{\mathcal{M}} - \delta(t_0+\tau))^2, \qquad v^{\mathrm{R}}_{\mathcal{M}} = v(\tau^{\mathrm{R}}_{\mathcal{M}}). \tag{5.3}$$

As a consequence, the reactive maneuver target would simply be

$$\mathcal{T}^{\mathrm{R}}_{\mathcal{M}} = \begin{cases} (\tau^{\mathrm{R}}_{\mathcal{M}}, v^{\mathrm{R}}_{\mathcal{M}}) & \text{if } |\delta_{\mathcal{M}} - \delta(\tau^{\mathrm{R}}_{\mathcal{M}})| \leq \epsilon_\delta \\ (\infty, 0) & \text{otherwise} \end{cases}, \tag{5.4}$$

with $\epsilon_\delta \in \mathbb{R}$ being an arbitrarily small positive quantity. Also, Eq. (5.4) takes into account that the considered planning horizon might be too short for the decision spot to be reached. In this case, the target is arbitrarily set to $(\infty, 0)$. Nonetheless, the temporary horizon T used to generate the state trajectory from which the reactive MT is extracted can be given an arbitrarily large value, since the constraint on the arrival time to enforce reactivity will be imposed in a following step.

5.3.2 Maneuver target safety

Once the reactive maneuver target $\mathcal{T}^{\mathrm{R}}_{\mathcal{M}} = (\tau^{\mathrm{R}}_{\mathcal{M}}, v^{\mathrm{R}}_{\mathcal{M}})$ has been calculated, i.e. the way in which the ego vehicle expects to reach the decision spot has been characterized, determining its suitability would essentially be equivalent to evaluating the probability with which such a maneuver target is expected to be safe w.r.t. the surrounding observed gaps.

For a maneuver target $\mathcal{T}^{\mathrm{R}}_{\mathcal{M}}$ to be safe, the state $\hat{x}_{\mathrm{ego}}(\tau^{\mathrm{R}}_{\mathcal{M}}) = (\delta_{\mathcal{M}}, v^{\mathrm{R}}_{\mathcal{M}})$ the ego vehicle would have when meeting the MT must be safe w.r.t. the surrounding gaps. In particular, denoting as $S \in \{0, 1\}$ a binary r.v. expressing whether a situation is safe or not, the probability with which an MT is considered safe can be calculated as

$$\mathrm{P}^{\mathrm{S}}_{\mathcal{M},\mathcal{T}_{\mathcal{M}}} \coloneqq \mathrm{P}(S = 1|\mathcal{M}, \mathcal{T}_{\mathcal{M}}) = \prod_{\mathcal{G}\in G} \max_{\mathcal{G}\in\mathcal{G}} \{\mathrm{P}(\mathrm{S} = 1|\mathcal{T}_{\mathcal{M}}, \mathcal{G})\} \tag{5.5}$$

that is, as the product of the probability of the MT being safe w.r.t. the set of gaps in every conflicting traffic stream it crosses. Furthermore, the probability $\mathrm{P}(\mathrm{S} = 1|\mathcal{T}_{\mathcal{M}}, \mathcal{G})$ of a maneuver

target $\mathcal{T}_{\mathcal{M}}$ being safe w.r.t. a specific gap $\mathcal{G}$ can be interpreted as

$$\mathrm{P}(\mathrm{S}=1|\mathcal{T}_{\mathcal{M}},\mathcal{G}) = \mathrm{P}\Big(\hat{E}_{\mathcal{G}}(\tau^{\mathrm{R}}_{\mathcal{M}})=1\Big)\mathrm{P}\Big(\hat{S}_{g_{\mathrm{F}}}(\tau^{\mathrm{R}}_{\mathcal{M}})=1\Big)\mathrm{P}\Big(\hat{S}_{g_{\mathrm{R}}}(\tau^{\mathrm{R}}_{\mathcal{M}})=1\Big)\ , \tag{5.6}$$

where $\hat{E}_{\mathcal{G}}(\tau^{\mathrm{R}}_{\mathcal{M}}) \in \{0,1\}$ is a r.v. showing whether the gap $\mathcal{G}$ is empty at the time interval $\tau^{\mathrm{R}}_{\mathcal{M}}$ the ego vehicle reaches the decision spot, and $\hat{S}_{g_{\mathrm{F}}}(\tau^{\mathrm{R}}_{\mathcal{M}}) \in \{0,1\}$ and $\hat{S}_{g_{\mathrm{R}}}(\tau^{\mathrm{R}}_{\mathcal{M}}) \in \{0,1\}$ are r.v. representing the probability of the MT being safe w.r.t. the expected state of the gaps' front and rear limits.

Given the reactive nature of the formulated strategy, we consider the probability of the gap being empty by the time $\tau^{\mathrm{R}}_{\mathcal{M}}$ equal to the probability of it being empty at the current time, i.e.

$$\mathrm{P}\Big(\hat{E}_{\mathcal{G}}(\tau^{\mathrm{R}}_{\mathcal{M}})=1\Big) \approx \mathrm{P}(E_{\mathcal{G}}(0)=1), \tag{5.7}$$

which is indeed the probability provided by the perception layer. On the other hand, letting $\mathcal{X}^{\mathrm{SCF}}(x,\underline{h})$ and $\mathcal{X}^{\mathrm{SCL}}(x,\underline{h})$ denote the sets of states that would be considered car-following and car-leading safe w.r.t. a certain vehicle with state x and a minimum headway distance $\underline{h}$ (constructed as will be explained in the Appendix, Sections A.1.4-A.1.5), the probabilities of the MT being safe w.r.t. the gap's limits can be calculated as

$$\mathrm{P}\Big(\hat{S}_{g_{\mathrm{F}}}(\tau^{\mathrm{R}}_{\mathcal{M}})=1\Big) = \begin{cases} 1 & \text{if } \hat{x}_{\mathrm{ego}}(\tau^{\mathrm{R}}_{\mathcal{M}}) \in \mathcal{X}^{\mathrm{SCF}}(\hat{x}_{g_{\mathrm{F}}}(\tau^{\mathrm{R}}_{\mathcal{M}}),\underline{h}) \\ 0 & \text{otherwise} \end{cases}\ , \tag{5.8}$$

$$\mathrm{P}\Big(\hat{S}_{g_{\mathrm{R}}}(\tau^{\mathrm{R}}_{\mathcal{M}})=1\Big) = \begin{cases} 1 & \text{if } \hat{x}_{\mathrm{ego}}(\tau^{\mathrm{R}}_{\mathcal{M}}) \in \mathcal{X}^{\mathrm{SCL}}(\hat{x}_{g_{\mathrm{R}}}(\tau^{\mathrm{R}}_{\mathcal{M}}),\underline{h}) \\ 0 & \text{otherwise} \end{cases}\ . \tag{5.9}$$

In Eq. (5.8)-(5.9), the future state of the gap's limits $\hat{x}_{g_{\mathrm{F}}}(\tau^{\mathrm{R}}_{\mathcal{M}})$ and $\hat{x}_{g_{\mathrm{R}}}(\tau^{\mathrm{R}}_{\mathcal{M}})$ can be approximated by

$$\hat{x}_g(\tau^{\mathrm{R}}_{\mathcal{M}}) = \big(s_g + v_g\tau^{\mathrm{R}}_{\mathcal{M}}, v_g\big),\ g \in \{g_{\mathrm{F}}, g_{\mathrm{R}}\}\ , \tag{5.10}$$

i.e. considering that they move at a constant speed.

Summarizing, the described method to quantify the probability of an MT being safe is based on approximating: the probability with which the gap is thought to be empty, and the probability of the arrival state to the decision spot (represented by the reactive MT) being safe w.r.t. the future state of the gaps' limit. In particular, due to the reactive nature of the proposed planner, such approximations are relatively straightforward. It must be noted, however, that the approximation's validity only holds for very small values of $\tau_{\mathcal{M}}$, i.e. for very short arrival time intervals.

5.3.3 Gap-acceptance decision map

An alternative representation of the implicit reactive decision-making proposed in this chapter can be achieved by realizing that, if the state in which the ego vehicle is expected to reach the decision spot is known, the set of states that the gap's front and rear limits should have for them be considered safe is known as well.

Formally, let us first introduce the sets

$$\mathcal{X}^{\mathrm{F}}_{\mathrm{SCF}}(\mathcal{T}^{\mathrm{R}}_{\mathcal{M}}, \hat{x}_{\mathrm{ego}}(\tau^{\mathrm{R}}_{\mathcal{M}}), \underline{h}) = \big\{x_{g_{\mathrm{F}}} : \hat{x}_{g_{\mathrm{F}}}(\tau^{\mathrm{R}}_{\mathcal{M}}) \in \mathcal{X}^{\mathrm{SCL}}(\hat{x}_{\mathrm{ego}}(\tau^{\mathrm{R}}_{\mathcal{M}}), \underline{h})\big\}, \tag{5.11}$$

$$\mathcal{X}^{\mathrm{R}}_{\mathrm{SCF}}(\mathcal{T}^{\mathrm{R}}_{\mathcal{M}}, \hat{x}_{\mathrm{ego}}(\tau^{\mathrm{R}}_{\mathcal{M}}), \underline{h}) = \big\{x_{g_{\mathrm{R}}} : \hat{x}_{g_{\mathrm{R}}}(\tau^{\mathrm{R}}_{\mathcal{M}}) \in \mathcal{X}^{\mathrm{SCF}}(\hat{x}_{\mathrm{ego}}(\tau^{\mathrm{R}}_{\mathcal{M}}), \underline{h})\big\} \tag{5.12}$$

to represent the set of states that the gap's front and rear limits must have at the current time for

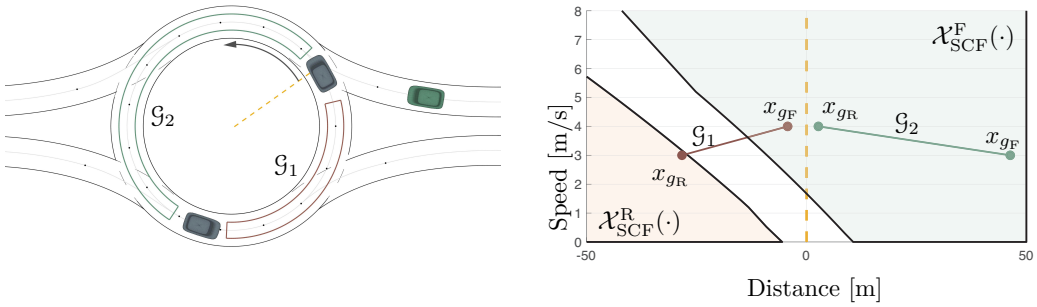

Figure 5.1 – Representation of the so-called gap-acceptance decision map. On the left-hand side, a traffic scene where the ego vehicle (green car) and the gaps it observes are shown. On the right-hand side, we represent the so-called gap-acceptance decision map. In words, the gap-acceptance decision map shows two sets that represent, respectively, the condition that the front and rear limit of a gap need to simultaneously meet, for the gap to be accepted. In practive, only those gaps bridging the two sets would be accepted. Formally, the decision-map is composed of the sets $\mathcal{X}^{\mathrm{F}}_{\mathrm{SCF}}(\mathcal{T}^{\mathrm{R}}_{\mathcal{M}}, \hat{x}_{\mathrm{ego}}(\tau^{\mathrm{R}}_{\mathcal{M}}), \underline{h})$ and $\mathcal{X}^{\mathrm{R}}_{\mathrm{SCF}}(\mathcal{T}^{\mathrm{R}}_{\mathcal{M}}, \hat{x}_{\mathrm{ego}}(\tau^{\mathrm{R}}_{\mathcal{M}}), \underline{h})$ as well as the gaps' state. In the depicted case $\mathcal{T}^{\mathrm{R}}_{\mathcal{M}} = (3\mathrm{s}, 3\mathrm{m/s})$, and $\hat{x}_{\mathrm{ego}}(\tau^{\mathrm{R}}_{\mathcal{M}}) = (0\mathrm{m}, 3\mathrm{m/s})$. The current position of the gaps' limits w.r.t. the decision spot (assumed to be located at 0) are depicted in the right-hand side plots.

their constant-velocity predicted state at $\tau^{\mathrm{R}}_{\mathcal{M}}$ to be considered safe w.r.t. a certain maneuver target $\mathcal{T}^{\mathrm{R}}_{\mathcal{M}}$. Then, the probability of the reactive MT being safe could be calculated as

$$\mathrm{P}\Big(\hat{S}_{g_{\mathrm{F}}}(\tau^{\mathrm{R}}_{\mathcal{M}}) = 1, \hat{S}_{g_{\mathrm{R}}}(\tau^{\mathrm{R}}_{\mathcal{M}}) = 1\Big) = \begin{cases} 1 & \text{if } x_{g_{\mathrm{F}}} \in \mathcal{X}^{\mathrm{F}}_{\mathrm{SCF}}(\cdot) \wedge x_{g_{\mathrm{R}}} \in \mathcal{X}^{\mathrm{R}}_{\mathrm{SCF}}(\cdot) \\ 0 & \text{otherwise} \end{cases} . \tag{5.13}$$

Hence, the safety condition can be graphically represented as shown in Fig. 5.1. There, we represent, on the left-hand side, a traffic scene where the ego vehicle is trying to merge into the roundabout with $\mathcal{T}^{\mathrm{R}}_{\mathcal{M}} = (3\mathrm{s}, 3\mathrm{m/s})$, and, on the right-hand side, a representation of the reactive decision-making. Specifically, the plot on the right-hand contains the sets $\mathcal{X}^{\mathrm{F}}_{\mathrm{SCF}}(\mathcal{T}^{\mathrm{R}}_{\mathcal{M}}, \hat{x}_{\mathrm{ego}}, \underline{h})$ and $\mathcal{X}^{\mathrm{R}}_{\mathrm{SCF}}(\mathcal{T}^{\mathrm{R}}_{\mathcal{M}}, \hat{x}_{\mathrm{ego}}, \underline{h})$, and the current state of the front and rear limits of every gap whose acceptance is considered (represented as segments connecting the states of its limits). In such a plot, a gap would be considered safe if its state *bridges* the two sets. In the provided example, such a constraint would hold for the red gap but not for the green one. The representation on the right-hand side will be, from now on, referred to as the *gap-acceptance decision map*, and will be used in future chapters.

5.3.4 Maneuver selection and scoring

To determine which maneuver should be pursued out of the maneuver candidates within $\mathcal{M}$, we propose the use of the quality metric

$$\mathcal{Q}(\mathcal{M}, \mathcal{T}^{\mathrm{R}}_{\mathcal{M}}) = \begin{cases} \omega_\delta \delta_{\mathcal{M}} + \omega_\tau \tau^{\mathrm{R}}_{\mathcal{M}} + \omega_v v^{\mathrm{R}}_{\mathcal{M}} + \omega_{\mathrm{P}} \mathrm{P}^{\mathrm{S}}_{\mathcal{M}, \mathcal{T}_{\mathcal{M}}} & \text{if } \mathrm{P}^{\mathrm{S}}_{\mathcal{M}, \mathcal{T}_{\mathcal{M}}} > \underline{\mathrm{P}} \wedge \tau^{\mathrm{R}}_{\mathcal{M}} < \underline{\tau} \\ -\infty \end{cases} \tag{5.14}$$

to score every pair $(\mathcal{M}, \mathcal{T}^{\mathrm{R}}_{\mathcal{M}})$. The proposed metric weights the distance to the decision spot, the arrival time and speed the corresponding MT represents, as well as the probability of the MT being safe. It also imposes a minimum safe probability to be accepted, as well as an upper bound to the arrival time that should be considered *reactive*.

Once the maneuver candidates are scored, the only step remaining is to choose the maneuver candidate to be pursued, as well as its corresponding maneuver target as

$$(\mathcal{M}^{\mathrm{R}}, \mathcal{T}^{\mathrm{R}}_{\mathcal{M}}) = \arg \max_{\mathcal{M}\in\mathcal{M}, \mathcal{T}_{\mathcal{M}}=\mathcal{T}^{\mathrm{R}}_{\mathcal{M}}} \mathcal{Q}(\mathcal{M}, \mathcal{T}_{\mathcal{M}}). \tag{5.15}$$

The typical value for the weights within the cost function are included in Tab. 5.1. In practice, however, as only very short arrival time intervals are considered, the variations concerning the distance to the decision spot, the arrival speed, and the arrival time itself of valid maneuver candidates should be expected to be small. Thus, when several maneuver candidates are compared, the term that affects the decision the most is the safety-related one.

5.3.5 Planner outputs

At the time of composing the planner outputs, we aim to make the vehicle: (i) behave normally considering the vehicles that it observes on the path π if the expected reactive behavior was deemed to be safe, and (ii) act safely w.r.t. the relevant road markings and adopt a searching behavior otherwise. This behavior, as explained below, will be achieved by the manipulation of the safety constraints passed to the trajectory planner.

Given the chosen maneuver $\mathcal{M}^{\mathrm{R}} = (\pi, \delta_{\mathcal{M}^{\mathrm{R}}}, \pi_0, O, \{L, G\}, \varnothing)$, the maneuver planner needs to specify the value of the targets $\mathcal{D}$ and $\mathcal{V}$ and the safety constraints $\mathcal{C}$.

On the one hand, as imposed by design, the sets of targets are set to be empty sets, i.e.

$$\mathcal{D} = \varnothing, \qquad\qquad \mathcal{V} = \varnothing, \tag{5.16}$$

as the strategy is reactive by design, and future targets cannot be pursued as it would entail planning with a certain anticipation.

On the other hand, a set of safety constraints have to be included in the output to keep a safe distance w.r.t. observed vehicles, and making the vehicle adopt a searching behavior if the merging maneuver is considered to be infeasible. Specifically, we do so by first defining the states

$$x_{\mathrm{S}} = (\delta_{\mathrm{S}}, v_{\mathrm{S}}), \qquad\qquad x_{\pi_0} = (\delta_{\pi_0}, v_{\pi_0}) \tag{5.17}$$

representing two ancillary virtual obstacles, $\mathcal{O}_{\mathrm{S}}$ and $\mathcal{O}_{\pi_0}$, which are designed to make the vehicle adopt, respectively, a searching behavior and a safe behavior w.r.t. the end of the path π_0. Such obstacles would then be added to the set $\mathcal{O}_{\mathrm{V}}$ of observed obstacles on π_0, only if no valid maneuver was found within $\mathcal{M}$, resulting in an extended set

$$\mathcal{O}' = \begin{cases} \mathcal{O}_{\mathrm{V}} \cup \{\mathcal{O}_{\mathrm{S}}\} \cup \{\mathcal{O}_{\pi_0}\} & \text{if } \mathcal{Q}(\mathcal{M}^{\mathrm{R}}, \mathcal{T}^{\mathrm{R}}_{\mathcal{M}}) = -\infty \\ \mathcal{O}_{\mathrm{V}} & \text{otherwise} \end{cases} \tag{5.18}$$

of obstacles to be considered. Then, the set of safety constraints would be composed as

$$\mathcal{C} = \{(\infty, x_{\mathcal{O}}, d_{\mathrm{M}}) : \mathcal{O} \in \mathcal{O}'\}, \tag{5.19}$$

with $d_{\mathrm{M}} \geq 0$ representing the maximum deceleration the ego vehicle would consider when calculating the minimum safe distance from the obstacle.

This construction achieves the desired effects and enables us to tune the searching behavior throughout the parameters δ_{S} and v_{S} (whose typical values are shown in Tab. 5.1).

5.4 Results

In this section, we present a simulation-based analysis of the proposed reactive behavioral policy. Specifically, results at three different levels of abstraction will be provided. Firstly, in Section 5.4.1, we show qualitative results concerning the decision that would result from the application of the strategy on a set of example traffic scenes. Then, the evolution of three traffic scenarios with different traffic densities will be analyzed in Section 5.4.2, showing not only the vehicles' trajectory but also the distribution of some higher-level performance metrics. Finally, in Section 5.4.3, we will quantify the average impact that the strategy could be expected to have on the overall traffic performance, obtained from a broad set of simulated traffic scenarios and configurations.

Table 5.1 – Design parameters

	ω_δ	ω_τ	ω_v	ω_P	$\underline{h}$	$\underline{\mathrm{P}}$	$\underline{\tau}$	δ_S	v_S	d_M
Value	1	2	0.2	20	2	0.8	1	20	4	1
Unit	1/m	1/s	s/m	-	m	-	s	m	m/s	$\mathrm{m/s^2}$

5.4.1 Decision-making

In this section, we illustrate the decision-making resulting from the application of the formulated reactive planner in several merging scenarios. The results are shown in Fig. 5.2, where a set of five merging scenes are represented along with the corresponding gap-acceptance decision map the merging vehicles would base their decisions on.

In all cases, the gap-acceptance decision map is calculated for a maneuver target $\mathcal{T}_\mathcal{M} = (3\mathrm{s}, 3\mathrm{m/s})$ and the minimum desired headway distance in Tab. 5.1. As can be observed, the algorithm finds it feasible to perform the merging maneuver in all of the shown scenarios except the last one.

Generally speaking, it can be seen that the decision map does illustrate relatively well the intuition humans could have in each of the merging situations shown. In the first three cases, the gap the merging vehicle sees is sufficiently large for it to merge comfortably. Indeed, the further the extremes of the gap bridging the two safe sets are from the boundary of the sets, the more comfortable and safe the merging maneuver would be.

In case 04, the inter-vehicle gap is significantly tighter than in the other cases. Nonetheless, given the specific value of the parameters used, the merging maneuver would be considered safe. It should be emphasized that in this case, the vehicle defining the rear limit of the gap drives 1m/s slower than the leading vehicle. Thus, the merging gap could be expected to grow in the instants following, which would explain the algorithm accepting it.

Finally, case 05 represents a scenario where vehicles in the circulatory lane drive too close to each other for the incoming vehicle to find a feasible merging gap. Therefore, the vehicle would have to stop at the yield line and wait for an appropriate gap to appear.

5.4.2 Single traffic scenario

In this section, we assess the trajectories that a set of vehicles driving through a single-lane roundabout would follow if their behavior resulted from the application of the proposed reactive strategy. In particular, we will consider a roundabout of 16m radius, 1 circulatory lane, 3 legs with 1 incoming, and 1 outgoing lane (i.e. a `16R1LR3L1I1O` roundabout). Moreover, we generate scenarios of 100 vehicles (i.e. `100V`), and three different incoming traffic configurations corresponding

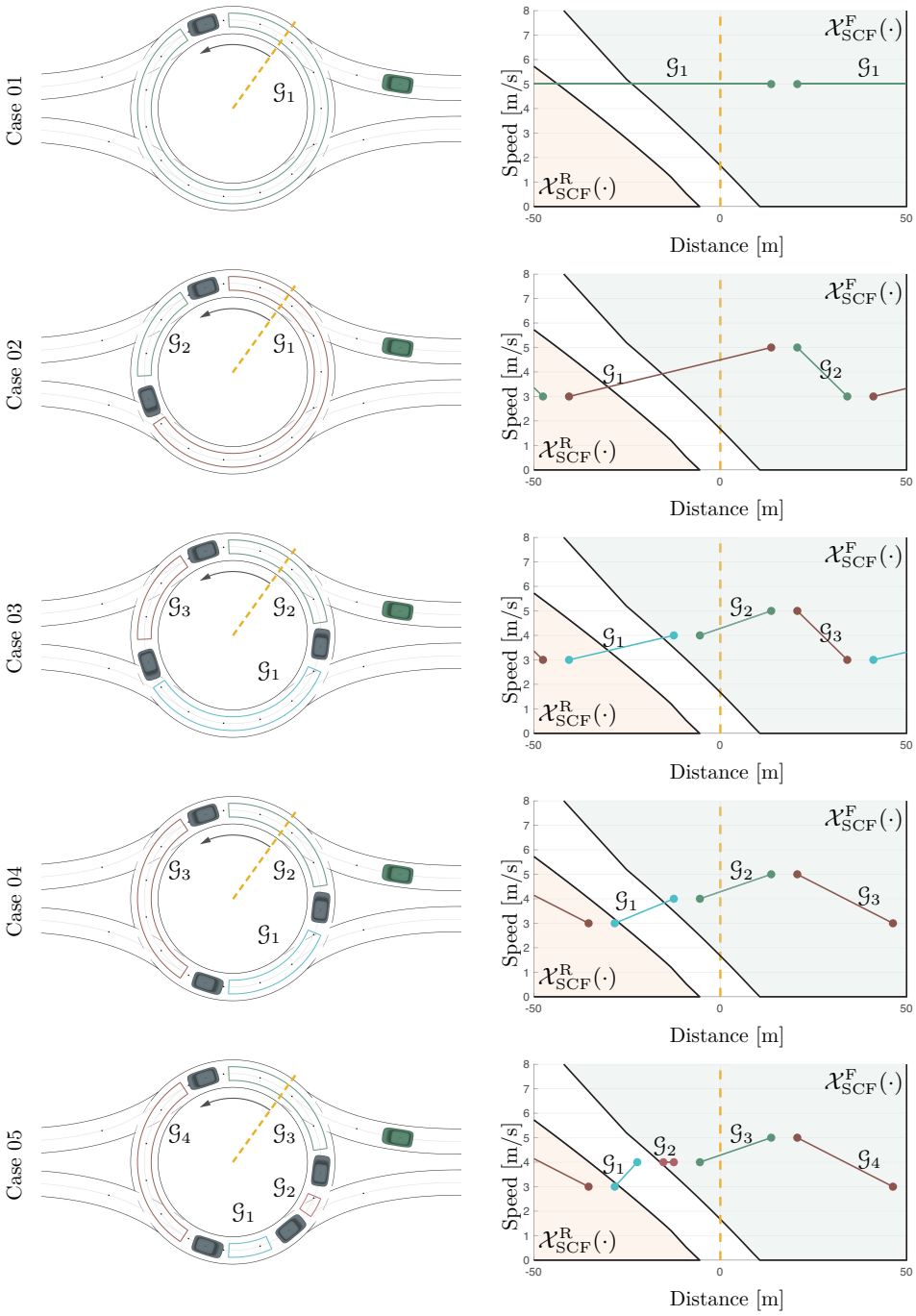

Figure 5.2 – Examples of the decision resulting from the application of the proposed self-serving reactive maneuver planner in a set of five traffic scenes (one case per row). The representation follows the same structure than 5.1.

to an incoming traffic volume of 500vehs/h, 1500vehs/h, and 2500vehs/h evenly distributed among the incoming legs. In other words, we consider the incoming traffic configurations `500Q[1 1 1]`, `1500Q[1 1 1]`, and `2500Q[1 1 1]` (see Section 2.3.4 for details concerning our labeling strategy).

The results are shown in Fig. 5.3-5.11. For every simulated scenario, we represent: (i) the evolution of the traffic in the circulatory lane, (ii) the traffic evolution along the roundabout's three incoming lanes, as well as (iii) a set of histograms showing the travel speed, travel time, arrival delay, and jerk of the vehicles in the scene. Moreover, in Tab. 5.2 we gather the resulting intersection throughput, as well as some fairness metrics of every performance indicator of interest.

Table 5.2 – Intersection throughput and fairness metrics

	Throughput [vehs/h]	TT. fairness [%]	TS. fairness [%]	J. fairness [%]	D. fairness [%]
16R1LR3L1I1O-100V-500Q[1 1 1]	486	98	99	86	96
16R1LR3L1I1O-100V-1500Q[1 1 1]	1340	96	98	82	60
16R1LR3L1I1O-100V-2500Q[1 1 1]	1475	85	93	88	55

In general, we can observe that the reactive approach manages to avoid collisions in the shown cases, and the overall traffic behaves as could be expected, given the simulated traffic densities.

In very-low-density traffic (Fig. 5.3-5.5), circulating vehicles drive almost at a constant speed, as they are not disturbed by merging vehicles. Incoming vehicles do as well merge without difficulties since, by the time they arrive at the intersection, the roundabout is nearly empty. Additionally, the registered travel speed is relatively high, the jerk low, and the fairness metrics in Tab. 5.2 indicate that the vehicles' trajectory are practically identical.

In medium-density traffic (Fig. 5.6-5.8), we still observe a smooth traffic evolution in the circulatory lane, although some disturbances start appearing in the incoming traffic flows since vehicles sometimes need to stop entirely at the yield line to wait until an appropriate gap appears. Although the travel speed and travel time stay relatively high, vehicles need to apply a higher jerk to navigate through the scenario safely, and some arrival delays start appearing due to the slow pace at which traffic moves at some instants along some of the incoming lanes. Moreover, the overall fairness of the traffic scene decreases, as only a few vehicles have to stop at the yield line, whereas everybody else drives smoothly around the roundabout.

In high-density traffic (Fig. 5.9-5.11), the strategy also results in a smooth evolution of the traffic inside the roundabout. The incoming traffic, however, gets highly congested, and the majority of the vehicles need to stop at the yield line. Moreover, as can be seen in the histograms, vehicles require more time to drive through the scenario and experience significant delays in these circumstances. Furthermore, even though nearly the same number of vehicles approach the roundabout by each leg at approximately the same rate, vehicles driving towards the roundabout by incoming lane 2 evolve much more smoothly than the traffic in the other legs.

It must be noted that, regardless of the traffic density, the proposed reactive approach avoids disturbing vehicles in the circulatory lane, as they wait until an inter-vehicle gap that can be utilized without the cooperation of the circulating vehicles emerges. Moreover, even though the incoming traffic configuration is relatively homogeneous (i.e. the same number of vehicles approach the intersection by each incoming lane, with the same average arrival time interval) the randomly drawn origin-destination patterns and the resulting sequence of vehicles merging into the intersection might lead to a somewhat uneven incoming traffic flow evolution. Especially in highly congested

scenarios.

5.4.3 Traffic coordination performance

In this section, we address the evaluation of the described baseline reactive strategy from the point of view of the overall traffic coordination performance. In this occasion, the assessment approach differs from the one followed in Section 5.4.2, in which we are interested in quantifying the distribution of travel speed, travel time, and jerk that the vehicles would be expected to experience, considering a broad set of traffic scenarios. In the coming sections, we first discuss the creation of the simulation batch, and then show and assess the simulation results.

In this chapter, only one type of agent driving the behavior of the vehicles is considered (whose main characteristics are summarized in Tab. 5.3), which will be exploited through this thesis as a baseline behavior.

Table 5.3 – Driver agent used in our simulation study

	Perception	Communication	Self-serving planner	Cooperative planner
R-Agent	Perfect perception	None	Reactive	None

Simulation batch setup

The set of simulation instances used to carry out the analysis is generated according to the traffic configurations in Tab. 5.4, and the tree structure illustrated in Fig. 5.12. A total of 18 different traffic inflow configurations are tested where not only the total volume of incoming vehicles (`QI`), but also the way they are distributed among the legs (`DI`) is varied. For every traffic scenario $\texttt{G} - \texttt{QIDI}$, ten different instances ($\texttt{I1}, \cdots, \texttt{I10}$) are created in such a way that the specific arrival time and origin-destination of every vehicle are randomly drawn.

Table 5.4 – Simulation batch scenario configuration

	Value
G	16R1LR3L1I1O-100V
QI1	1000Q
QI2	1500Q
QI3	2000Q
QI4	2500Q
QI5	3000Q
QI6	3500Q
DI1	[1.0 1.0 1.0]
DI2	[1.0 0.5 1.0]
DI3	[0.5 1.0 0.5]

Simulation batch results

Three aspects of the simulation results are assessed in this section. On the one hand, in Fig. 5.13, we show, for every scenario, the distribution of the overall travel speed the vehicles experience in the simulated instances. Then, in Fig. 5.14, the vehicles' arrival delay is shown. Finally, in Fig. 5.15, the total throughput, as well as the distributions of 15min segments throughput, are represented.

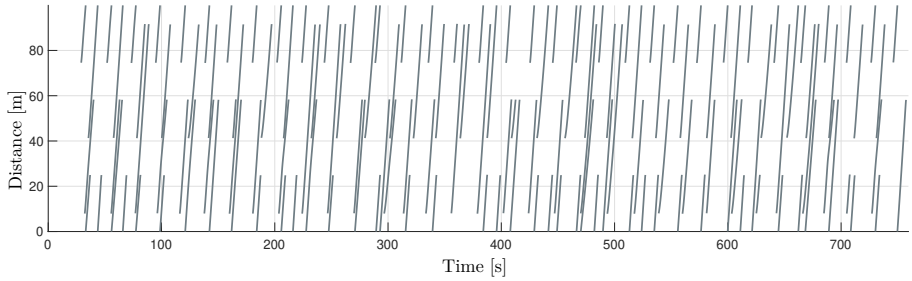

Figure 5.3 – Time-distance diagram representing the evolution over time of the vehicles in the circulatory lane, in the simulated scenario `16R1LR3L1I1O-100V-500Q[1 1 1]`.

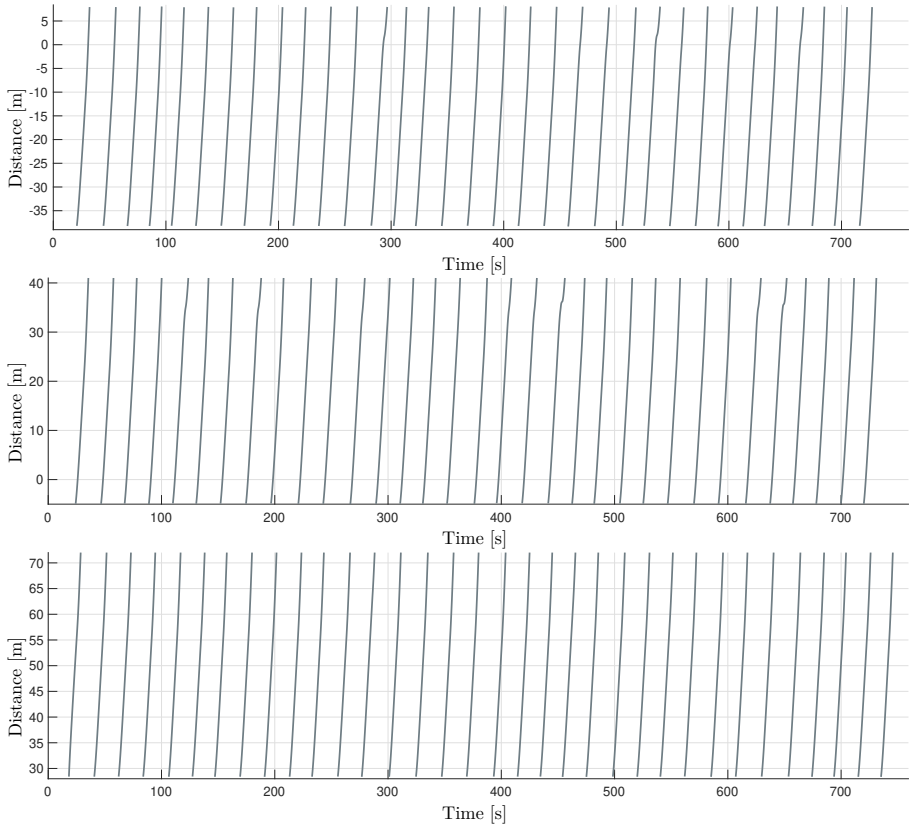

Figure 5.4 – Time-distance diagrams representing the evolution of the incoming traffic in every incoming lane in the simulated scenario `16R1LR3L1I1O-100V-500Q[1 1 1]`.

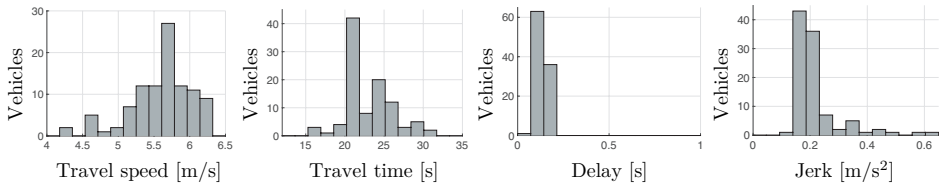

Figure 5.5 – Histogram of the registered travel speed, travel time, arrival delay, and jerk of the vehicles in the simulated scenario `16R1LR3L1I1O-100V-500Q[1 1 1]`.

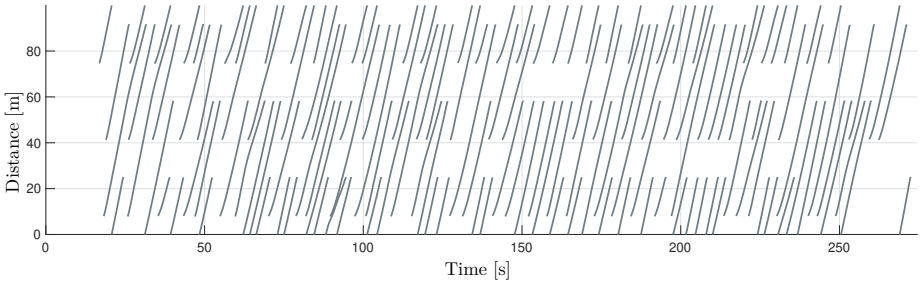

Figure 5.6 – Time-distance diagram representing the evolution over time of the vehicles in the circulatory lane, in the simulated scenario `16R1LR3L1I1O-100V-1500Q[1 1 1]`.

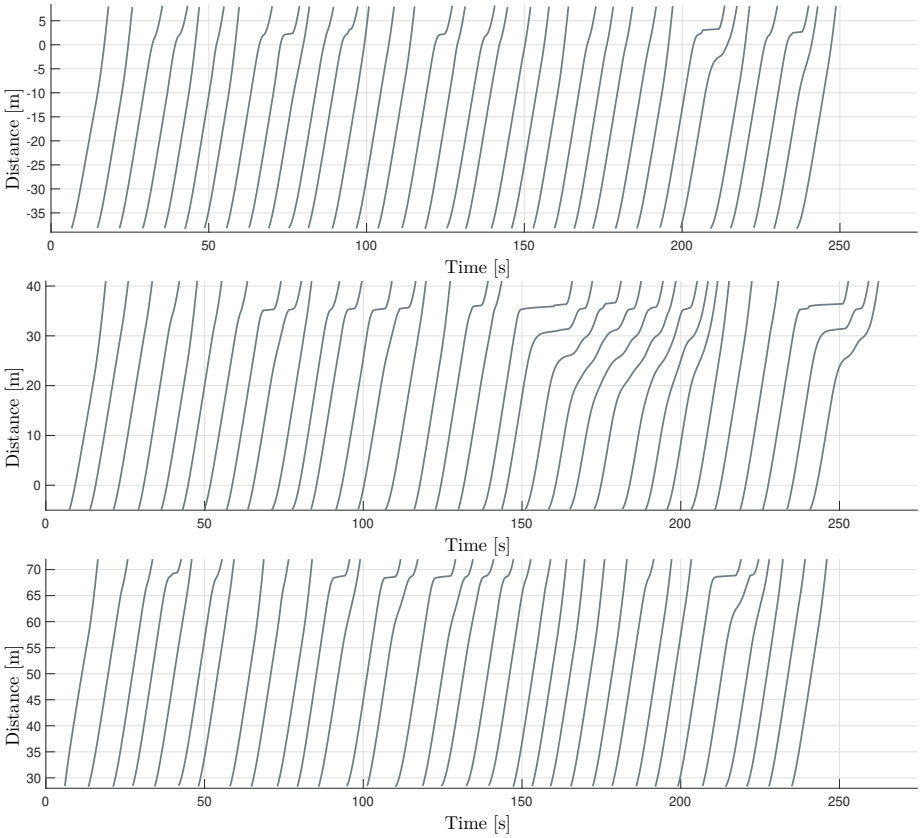

Figure 5.7 – Time-distance diagrams representing the evolution of the incoming traffic in every incoming lane in the simulated scenario `16R1LR3L1I1O-100V-1500Q[1 1 1]`.

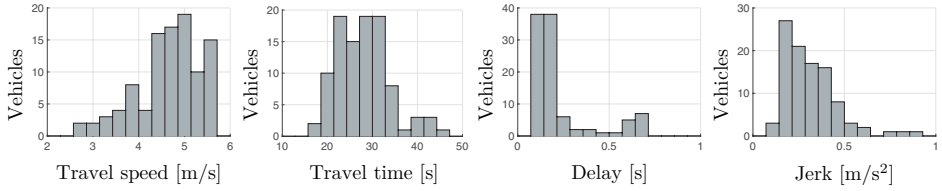

Figure 5.8 – Histogram of the registered travel speed, travel time, arrival delay, and jerk of the vehicles in the simulated scenario `16R1LR3L1I1O-100V-1500Q[1 1 1]`.

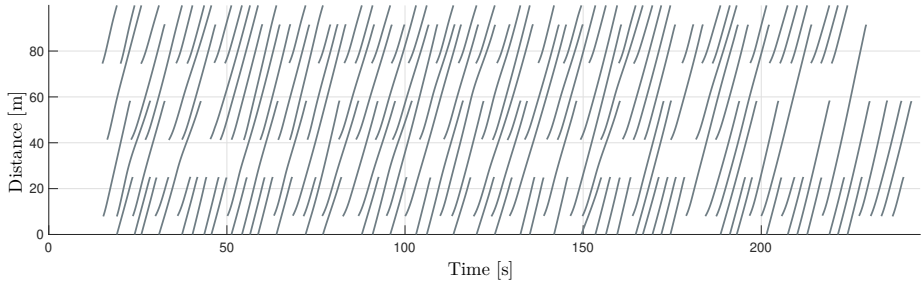

Figure 5.9 – Time-distance diagrams representing the evolution of the incoming traffic in every incoming lane in the simulated scenario `16R1LR3L1I1O-100V-2500Q[1 1 1]`.

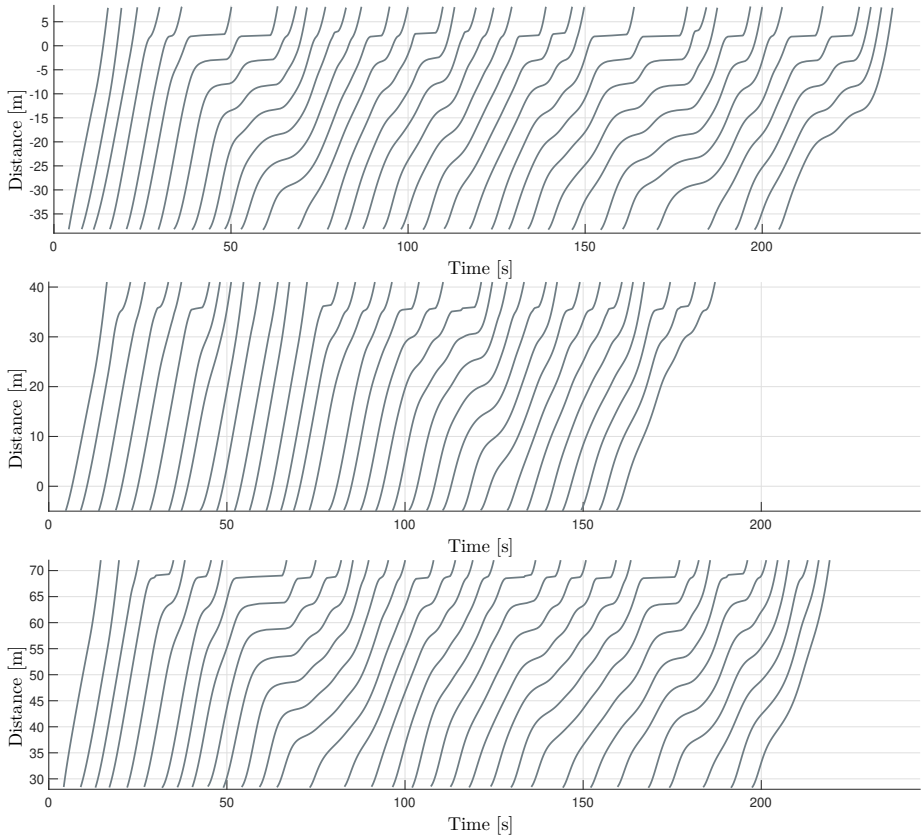

Figure 5.10 – Time-distance diagrams representing the evolution of the incoming traffic in every incoming lane in the simulated scenario `16R1LR3L1I1O-100V-2500Q[1 1 1]`.

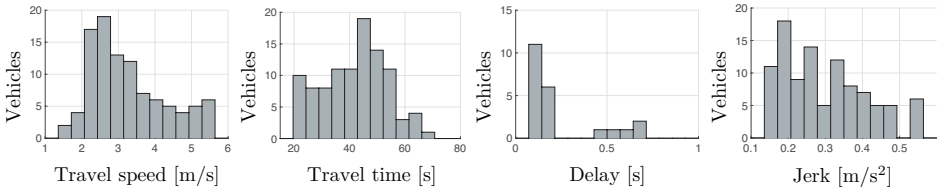

Figure 5.11 – Histograms characterizing the vehicles' trajectory resulting from the proposed reactive planning strategy in the scenario `16R1LR3L1I1O-100V-2500Q[1 1 1]`.

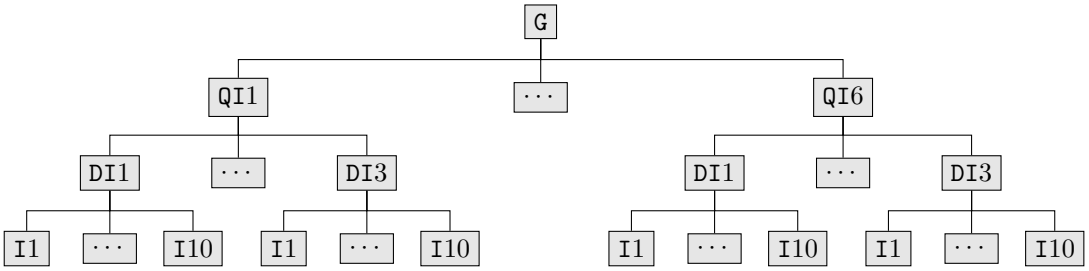

Figure 5.12 – Generation of the batch of simulated traffic scenarios.

Let us point out that the boxplots in Fig. 5.13–5.15 are first grouped w.r.t. the total traffic inflow (`QI1`, $\cdots$, `QI6`). Furthermore, within each of those groups, three boxplots representing the three different ways the traffic inflow is distributed (`DI1, DI2, DI3`) are included.

It is worth remembering that, in this case, all vehicles follow the same reactive behavioral policy. Thus, the discussion of the simulation results will focus on the impact that the distribution of the traffic inflow might have on the performance metrics of interest.

In terms of overall travel speed (i.e. the one taking into account the vehicles' arrival delay), whose distribution for every traffic scenario is represented in Fig. 5.13, we can observe that the incoming traffic distribution `DI2` presents, on average, a higher travel speed, which, by looking at Fig. 5.14, seems to be the result of the vehicles arriving at the scenario closer to their theoretical arrival time.

When the vehicles' arrival delay (shown in Fig. 5.14) is analyzed, we observe that the average arrival delays are systematically smaller in case `DI2`, although the highest fairness with which the delay is distributed among the agents corresponds to the case `DI3`. The fact that the highest average arrival delay takes place in case `DI3` was somehow to be expected since, in order to reach the same amount of total traffic inflow, such a configuration is the one resulting in the highest observed congested incoming lane. Interestingly, despite this, it turns out that the most imbalanced situation in terms of delays corresponds to the case where the incoming traffic is evenly distributed among the incoming lanes (case `DI1`).

In terms of throughput, we can observe in Fig. 5.15 that cases `DI1` are the ones reporting the highest 15min-throughput and total throughput values, while cases `DI2` and `DI3` report similar values despite the differences in terms of overall travel speed. We can further observe that the intersection throughput saturates for the reactive behavior evaluated herein, at around 1400 veh/h.

In general, it is interesting to observe that the traffic coordination performance at the roundabout is strongly affected by the fairness with which the merging maneuvers are performed, and the fact that balanced incoming traffic configurations are not necessarily correlated with a balanced evolution of the vehicles in the scenario.

5.5 Conclusions

In this chapter, we have described a reactive self-serving maneuver planning policy, which is to be used as a baseline in future comparisons. The approach was nonetheless exploited to introduce some concepts used in more advanced strategies, as well as the assessment approach followed in the remaining chapters of this thesis. The approach in itself was formulated so that vehicles would only merge when they found a sufficiently-large inter-vehicle gap in the circulatory lanes of the

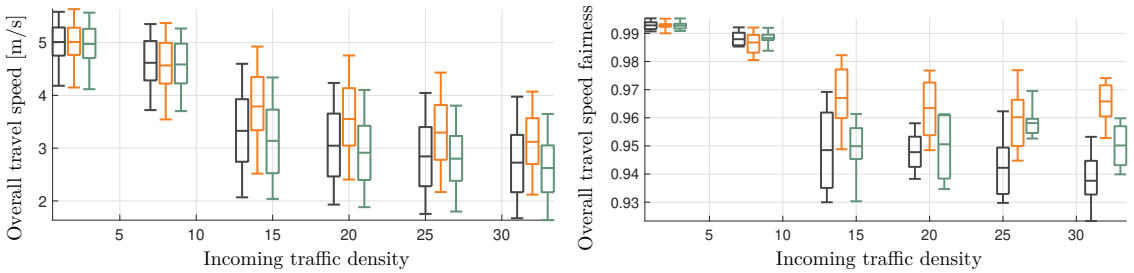

Figure 5.13 – On the left-hand side, boxplots representing the distribution of overall travel speed for different incoming traffic inflow volumes and configurations. On the right-hand side, the fairness with which the overall travel speed is distributed among the vehicles in the scenarios.

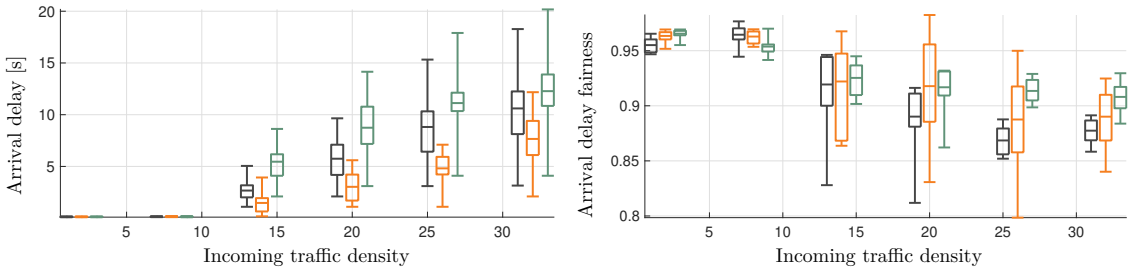

Figure 5.14 – On the left-hand side, boxplots representing the distribution of arrival delay for different incoming traffic inflow volumes and configurations. On the right-hand side, the fairness with which the arrival delay is distributed among the vehicles in the scenarios.

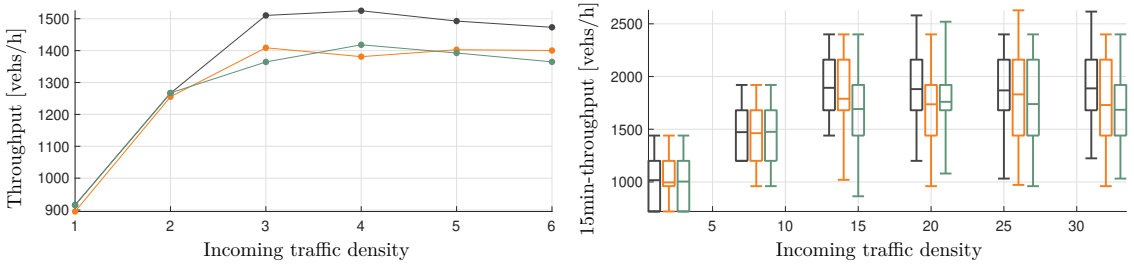

Figure 5.15 – On the left-hand side, total intersection's throughput measured for different traffic inflow configurations. On the right-hand side, the distribution of 15min-throughput.

roundabout, which could be utilized without requiring the cooperation of any circulating vehicle. Furthermore, we introduced the so-called gap-acceptance decision map, which provides a very intuitive way of representing and understanding the decisions made by the algorithm.

The approach was shown to be collision-free, and to keep a relatively clean and smooth traffic evolution in the circulatory lane regardless of the traffic volume heading towards the intersection.

In the batch of simulations carried out, we compared the overall traffic performance for different incoming traffic densities and distributions among the incoming lanes. From the study shown, we can conclude that situations where the incoming traffic is evenly distributed among the incoming legs result in higher intersection throughputs, but represent, as well, the most unfair scenarios.

The strategy could be extended by changing the number of trajectory templates it takes into account. Specifically, we have assumed that the ego vehicle has only one trajectory template to approach the decision spot (which results in a single reactive maneuver target). However, the same approach could as well be applied to a scenario where a finite set of trajectory templates are available, which might improve the performance, as it would represent a better approximation of the solution space.

Furthermore, it must be noted that the reactive nature of the approach is only explicitly considered when calculating the quality metric of the reactive maneuver target, where we forced the arrival time to be below a certain threshold. It would indeed be tempting to ignore such a temporary constraint and make use of the approach without constraining the arrival time of the maneuver target. However, the assumptions considered when the safety of the MT was approximated only hold for very short-term plans and should be revisited and extended if a more predictive behavior was pursued. This is, in fact, an extension that will be addressed in Chapter 8.

Finally, although this strategy is to be used as a baseline and more advanced strategies will be shown in the following chapters, its performance is relatively good, especially taking into consideration its simplicity.

6 Communication-Based Planning

Reactive driving strategies, as the one studied in the previous chapter, can indeed make AVs drive through roundabouts safely and relatively efficiently. However, even though simplistic reactive behavioral policies may perform well in standard driving situations, there are, unfortunately, frequent traffic conditions where such strategies perform poorly, at least from the ego vehicle's standpoint. A familiar example could be the scenario of trying to merge into a primary traffic stream from a secondary road, at peak hour, when the inter-vehicle distances in the targeted traffic stream are too small to perform a comfortable merging maneuver. In such a situation, a reactive strategy would be prone to make the ego vehicle wait until a gap that is large enough appears, which might only happen after a rather long wait. This scenario not only reflects the fact that reactivity is often insufficient to achieve an effective driving policy in dense traffic, but also that traffic priority rules must sometimes be bent for the sake of reaching a fairer situation for all road participants.

One could claim that one of the things that reactive driving strategies lack for them to perform well in dense traffic is the ability to profit from traffic predictions, as well as to account for potential cooperative actions performed by surrounding vehicles. The cooperative dimension of the driving task has indeed become a hot topic in the intelligent vehicles (IV) community over the last decade, as it is considered to be a fundamental aspect of driving that has not yet been adequately integrated into behavioral policies for AVs.

In this context, many authors in the literature assume inter-vehicle communication in an attempt to better understand what makes the coordination of the vehicles optimal and to evaluate the adequacy of different communication-based interaction methods. Rather than focusing on the limitations of V2V communication, such studies use V2V communication as a mere justification to focus on the cooperation problem and disregard the limitations stemming from perception uncertainty. This philosophy is, in a way, the one we apply in this chapter.

In this chapter, we propose a so-called explicitly cooperative maneuver planner for CAVs, built on the VV-based interaction mechanism described in Section 2.1. The main objective is to investigate the coordination problem of AVs at roundabouts in its purer form, i.e. without the constraints and limitations imposed by the uncertainty concerning the surrounding vehicles' intent or perception inaccuracies. Specifically, considering a CAV aiming to perform a merging maneuver into a conflicting traffic stream and it being able to target any inter-vehicle gap it wanted, we address the question: how should it decide which one to pursue?

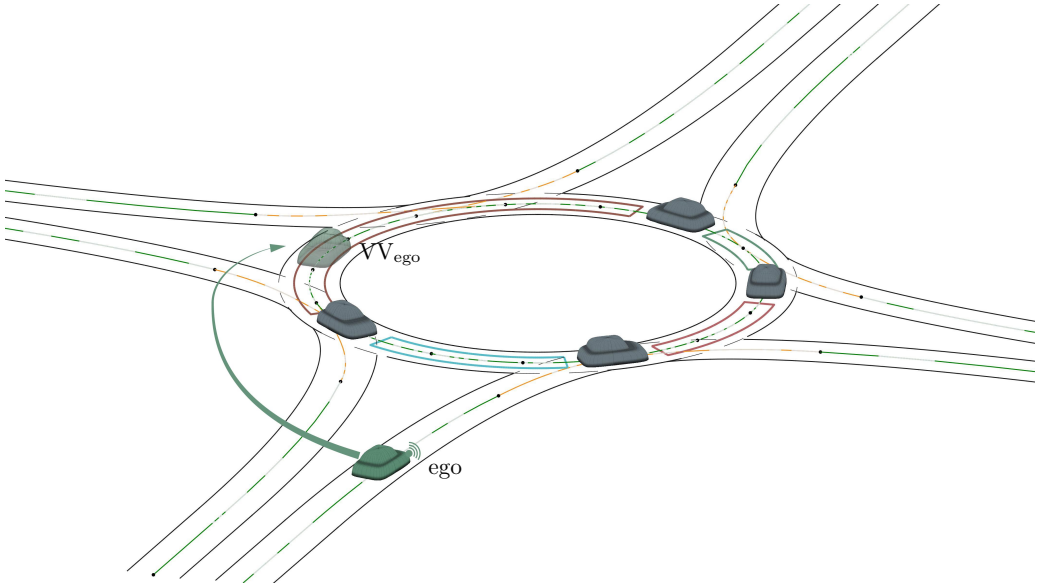

Figure 6.1 – Illustration of the problem tackled by the communication-based maneuver planner. The ego vehicle is represented by the merging green vehicle. In the circulatory lane, the translucent vehicle represents the virtual vehicle the ego vehicle projects in the circulatory lane, so that such location is reserve for it to perform its merging maneuver.

The policy we formulate in this chapter is decentralized and is said to be cooperative, as self-serving maneuver requests are assumed to be accepted by the surrounding vehicles. Self-serving decisions are made by accounting for their impact on the overall traffic performance. Furthermore, we denote the strategy as explicitly cooperative to refer to the fact that communication is used to request and grant cooperation explicitly, and to highlight the fundamental differences compared to the implicitly cooperative driving strategy discussed later in Chapter 7.

The content of this chapter is built upon [15], where we first presented the V2V-based interaction mechanism the proposed method is built upon, and [17], where we presented a version of the planning strategy discussed herein. In summary, the interaction mechanism we envision is based on the idea of CAVs being able to project virtual vehicles (VVs) within the surrounding traffic streams they intend to either merge into or cross. VVs are to be taken into account by those surrounding CAVs that are willing to cooperate with the ego vehicle. Furthermore, the state of the VVs should evolve in such a way that CAVs in the targeted traffic stream would only need to treat the VV as a real vehicle to effectively cooperate with the ego vehicle.

Given such a communication-based interaction framework, we propose a self-serving maneuver planner whereby the ego vehicle would explore the conflicting traffic streams seeking a location to position its ancillary VVs. The ego vehicle does so while considering the impact on the overall traffic of such a VV insertion, which is quantified by exploiting a simplified microscopic traffic-model.

This chapter is organized as follows. In Section 6.1, we gather some works related to the proposed strategy. Then, in Section 6.2, we detail the specific problem and assumptions we address, as well as discuss the interaction mechanism we envision to make CAVs cooperate. The description of the explicitly cooperative maneuver planning approach is addressed in Section 6.3, and the strategy is assessed in simulation in Section 6.4. Finally, Section 6.5 gathers our conclusions and further considerations.

6.1 Related work

The problem of communication-based planning for AVs has been studied in the ITS and the IV community from two slightly different standpoints. In the field of ITS, the problem is typically denoted as the *coordination problem* and regarded from a centralized point of view. In contrast, in the field of IVs, the problem is referred to as *cooperative motion planning* and usually addressed in a decentralized manner.

In essence, the so-called coordination problem consists of optimizing the aggregated value of a specific cost function for every vehicle in the scenario, subject to safety and comfort constraints. Formulating the problem turns out to be a much simpler task than solving it, and the combinatorial nature of the problem demands the application of heuristics and approximations to find feasible near-optimal solutions [34]. The need for heuristics is indeed what leads to the broad set of solutions that can be found in the literature, some of which are gathered in this section.

The main difference between the approaches found in the IV and the ITS community concerns the architecture of the solution. In the intelligent vehicles field, communication is considered a means to gather further information and broadcast the vehicle's intent, whereas in the ITS, it allows researchers to consider a so-called *intersection manager* in charge of gathering information and decide how the vehicles should drive through the intersection. Thus, even though the research topics investigated in the transportation community serve as a source of inspiration, because of the fundamentally different architecture of the solutions, we will mostly discuss research on decentralized and communication-based motion planning strategies. The reader is nonetheless referred to [8] and [74] for in-depth reviews on intersection management and communication-based motion planning strategies, especially concerning centralized planning architectures.

Concerning decentralized communication-based motion planning, a broad range of methods can be found in the literature. These can be roughly divided considering whether they use heuristics or optimization-based methods to determine the crossing order of the vehicles through the intersections, or the sequence of accelerations they need to apply to drive forward while safely respecting the assigned priorities. Connectivity is crucial in this sense, as it allows us to assume that vehicles have access to a very accurate estimation of the state of the surrounding vehicles (and in some cases even their currently planned motion). As a result, we can engineer behavioral policies while disregarding certain sources of uncertainty, which, in a way, reduces the overall complexity of the task.

Hafner et al. proposed in [28] a communication-based collision avoidance supervisor using a promising method from the decision-making standpoint. Their approach is based on characterizing, given a pair of vehicles, the so-called bad set (gathering the configurations that would represent a collision), as well as the capture set (composed of the states that would inevitably result in the pair of vehicles crossing the bad set). A supervisor collision avoidance algorithm is therein proposed, whereby drivers can freely control their vehicle unless they hit the boundary of the capture set, in which case the controller would take control and use V2V communication to determine how to stay out of the capture set while moving forward.

The method proposed in [28] could also be used in communication-based motion planning in such a way that a pair of vehicles would continuously plan the best joint evolution that avoids the bad set. In fact, this approach resembles the priority-based planning framework Gregoire et al. presented in [27], whereby vehicles are assumed to know their relative priority w.r.t. the surrounding vehicles, characterize then the bad set, and plan collision-free maneuvers accordingly. Such a coordination framework represents the foundation of the approach proposed by Xiangjun Qian et al. in [73], where legacy vehicles are taken into account, and [72] where Model Predictive Control (MPC) is

incorporated to generate optimal trajectories. However, these studies formalize the framework and the control side of the problem but do not pay much attention to how the vehicles' relative priority is assigned, which is usually assumed given or calculated with a simple heuristic.

Similarly, Gabriel Rodrigues et al. present in [13] a strategy whereby the coordination problem is tackled in two steps. Firstly, the order in which the vehicles in the scenarios are to make a decision is determined using a heuristic built on their previous work [14]. Secondly, an optimization-based trajectory planning is used for the vehicles to generate, in their turn, the explicit sequence of accelerations.

Yet another family of methods relies on scheduling theory to approximate the optimal crossing sequence. For instance, Li Li et al. in [47] use a cooperative-scheduling-based strategy to determine the crossing order, which is then used by the vehicles to plan their trajectories across the intersection sequentially.

Even though several heuristics have been proposed to assign the crossing order between vehicles, very few approaches consider the impact that the maneuver could have on the surrounding traffic at the time the decision is triggered (see [89] for a more in-depth discussion of this aspect). The lack of research efforts in such a direction might be caused by the overuse of highways and crossings scenarios to validate planning strategies. However, the need for considering the decision's impact on traffic does emerge naturally at roundabouts due to their circular geometry, which motivates our exploration of such an idea in the strategy we propose. It is interesting to stress that studies in the IV community addressing the problem of interaction-aware planning do often account for the impact of the maneuver being planned [86], but, usually, only on the vehicles directly affected by the maneuver and not on the overall traffic.

Moreover, as inter-vehicle communication is commonly regarded as the means that allows assuming perfect knowledge transfer between vehicles, most studies consider that vehicles simply share their state or intent for the surrounding vehicles to take such information into account. Nonetheless, not many variations of the interaction mechanisms can be found. An exception would be the body of research exploiting the concepts of virtual vehicles (VV) and virtual platooning (VP), which provide a very comprehensive representation of the coordination problem and mechanism. Interestingly, such concepts are compatible with reactive trajectory planners as for the coordination to materialize, vehicles would no longer be required to drive through the intersection within a specific time window, but only to keep a safe distance with the surrounding VVs.

The concept of using VVs and VPs to coordinate vehicles was first introduced by Atsuya Uno et al. in [76], where it was applied to a merging scenario. In essence, the strategy is based on making the ego vehicle react to VVs resulting from mapping the position of vehicles on another lane (and driving towards the intersection area) on the ego vehicle's lane. Vehicles would then avoid collisions and safely drive through the intersection if, by the time they reach it, the real and VVs formed a so-called VP. The VP idea has also been exploited by other authors [30, 46, 48, 49, 55, 56, 57] to coordinate vehicles in different intersection scenarios. In this chapter, we also use the VV ideas to coordinate connected vehicles. Still, as will be explained in the following sections, we further extend the concept by considering that vehicles have the freedom to position their corresponding VV wherever they find an inter-vehicle gap they want to reserve.

6.2 Problem formulation and assumptions

In this chapter, we address the design of a self-serving maneuver planner that analyzes the maneuver candidates within the set $\mathcal{M}$ and decides which one would be the best one to pursue. In particular,

given the strategy being designed for CAVs to interact with other CAVs, the maneuver candidates within such a set are to be evaluated w.r.t. a communication-based interaction mechanism.

Vehicles are presumed to interact according to the VV-based coordination framework presented in [15], whereby a CAV can reserve a position in a traffic stream it intends to use by inserting VVs at the location of interest. Once the virtual vehicles are created, the surrounding connected vehicles would react to them as if they were real ones, which implies that cooperation requests cannot be denied. Therefore, only the creation of virtual vehicles that can be appropriately integrated into the conflicting traffic flows is allowed.

As we intend to focus on the interaction mechanism and the decision-making itself, issues emerging from inter-vehicle communication [22, 93], such as packages lost or channel saturation, are disregarded. Nevertheless, in terms of a real implementation, the proposed planning strategy should be complemented with additional modules to deal with communication delays and errors, which is out of our scope here.

Furthermore, CAVs are to share their intended destination in such a way that, at the time of identifying inter-vehicle gaps, positions occupied by vehicles that are not likely to pass by the ego vehicle's decision spot are considered to be free. Similarly, the ego vehicle would ignore a virtual vehicle if the path followed by the corresponding CAV does not cross the ego vehicle's.

Even though in the remainder of the chapter we focus on the communication-based self-serving maneuver planner strategy, the existence of a communication-based cooperative maneuver planner is as well implicit. However, as cooperation requests are imposed to be always accepted by surrounding vehicles, such cooperative behavior would simply consist in considering the virtual vehicles ahead of the ego vehicle while circulating inside the roundabout.

6.3 Planning approach

The strategy we present in this chapter is based on the idea of the ego vehicle assessing the traffic in the roundabout's circulatory lanes, choosing an inter-vehicle gap to merge into, and then creating a VV in such location acting as reservation token. In summary, the strategy consists of: (i) characterizing how the ego vehicle can arrive at the decision spot, (ii) identifying which of those arrival states could be reached by making use of a virtual vehicle, and (iii) selecting one arrival state to pursue.

The planning policy proposed in this chapter is summarized in Alg. 2. Specifically, it starts by constructing the set $\mathcal{T}_{\mathcal{M}}^{\mathrm{R}}$ of reachable maneuver targets (MTs) representing all the ways the ego vehicle can physically reach the decision spot. Then, for every reachable MT, the state that should be assigned to the VV for it to be able to meet its corresponding MT (the so-called virtual insertion state (VIS)) is calculated. Then, the traffic scene is analyzed to isolate the VISs that are safe w.r.t. the current traffic situation. Subsequently, a simplified microscopic traffic model is used to score the MTs, which is done by approximately quantifying the impact the corresponding maneuver execution would have on the overall traffic evolution. Then, such approximated effects would be used, along with other metrics, to score the maneuver candidates within $\mathcal{M}$ and identify the best one to pursue.

In the upcoming sections, every step of the process will be addressed in detail and, for the sake of clarity, illustrated considering the traffic scene in Fig. 6.2.

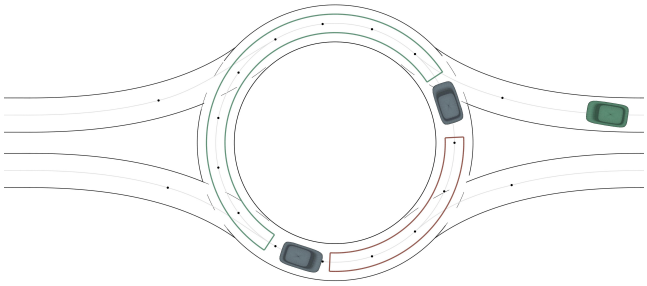

Figure 6.2 – Representation of the traffic scene used along this chapter to illustrate some steps of the planning process. The ego vehicle is represented by the green vehicle.

Algorithm 2: Explicitly cooperative decision-making workflow

Input: $\mathcal{M} = \{\mathcal{M}_1, \cdots, \mathcal{M}_{n_\mathcal{M}}\}$
Output: $\mathcal{M}^{\mathrm{EC}}, x^{\mathrm{V}}_{\mathcal{T}_{\mathcal{M}^{\mathrm{EC}}}}, \mathcal{D}, \mathcal{V}, \mathcal{C}$

for $\mathcal{M} \in \mathcal{M}$ **do**
  $\mathcal{T}^{\mathrm{R}}_{\mathcal{M}} \leftarrow$ set of reachable maneuver targets;
  $\mathcal{X}^{\mathrm{RV}}_{\mathcal{M}} \leftarrow$ set of reachable virtual insertion states (VISs);
  $\mathcal{X}^{\mathrm{SRV}}_{\mathcal{M}} \leftarrow$ set of safe and reachable VIS;
  $\mathcal{T}^{\mathrm{SR}}_{\mathcal{M}} \leftarrow$ subset of MTs whose VIS is safe and reachable;
  $r^{T_T}_{\varnothing} \leftarrow$ predicted traffic evolution if maneuver was not performed;
  for $\mathcal{T}_{\mathcal{M}} \in \mathcal{T}^{SR}_{\mathcal{M}}$ **do**
    $x^{\mathrm{V}}_{\mathcal{T}_{\mathcal{M}}} \leftarrow$ corresponding VIS;
    $r^{T_T}_{\mathcal{T}_{\mathcal{M}}} \leftarrow$ traffic prediction for such a VIS;
    $q_{\mathcal{T}_{\mathcal{M}}} = f(r^{T_T}_{\mathcal{T}_{\mathcal{M}}}, r^{T_T}_{\varnothing})$ maneuver target score
  end
end
$(\mathcal{M}^{\mathrm{EC}}, \mathcal{T}_{\mathcal{M}^{\mathrm{EC}}}) = \arg\max_{\mathcal{M}\in\mathcal{M}, \mathcal{T}_{\mathcal{M}} \in \mathcal{T}^{\mathrm{SR}}_{\mathcal{M}}} \{q_{\mathcal{T}_{\mathcal{M}}}\}$;
$x^{\mathrm{V}}_{\mathcal{T}_{\mathcal{M}^{\mathrm{EC}}}} \leftarrow$ chosen VIS;
$(\mathcal{D}, \mathcal{V}, \mathcal{C}) \leftarrow$ targets and constraints to impose on the trajectory.

6.3.1 Reachable maneuver target candidates

Consistent with the workflow we followed in Chapter 5, we begin by characterizing how the ego vehicle can reach the decision spot. However, on this occasion, we aim to take into account the whole solution space instead of a single maneuver target stemming from a predefined maneuver template, as was the case in Chapter 5. Given a self-serving maneuver candidate $\mathcal{M} = \{\pi, \delta_{\mathcal{M}}, \pi_0, O, \{L, G\}, \varnothing\}$, such a solution space is here referred to as the set of *reachable maneuver targets* and is denoted as

$$\mathcal{T}^{\mathrm{R}}_{\mathcal{M}} \coloneqq \mathcal{T}^{\mathrm{dR}}(x_0, \delta_{\mathcal{M}}). \tag{6.1}$$

Definition 11 (Reachable maneuver target)**.** *Given a maneuver candidate $\mathcal{M} = (\pi, \delta_{\mathcal{M}}, \pi_0, O, \mathcal{I}_{SS}, \varnothing)$, the current state x_0 of the ego vehicle, and the min/max accelerations $a_1 < 0$ and $a_2 > 0$ that the ego vehicle is allowed to apply, a maneuver target $\mathcal{T}_{\mathcal{M}} = (\tau_{\mathcal{M}}, v_{\mathcal{M}})$ is said to be reachable if the ego vehicle is capable of traveling the distance $\delta_{\mathcal{M}}$ in a time interval $\tau_{\mathcal{M}}$ and arriving with a speed $v_{\mathcal{M}}$.*

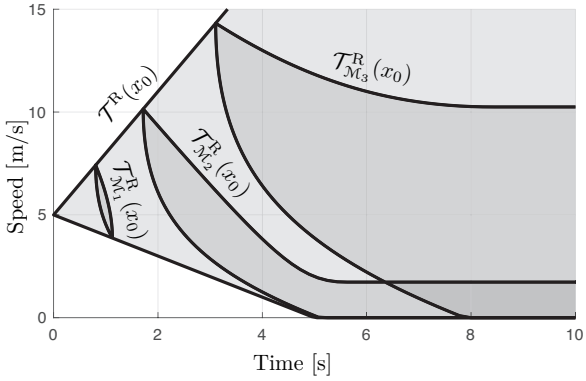

Figure 6.3 – Illustration of three sets of reachable maneuver targets, given an initial state $x_0 = (0, 5)$, and for three maneuvers $\mathcal{M}_1$, $\mathcal{M}_2$, and $\mathcal{M}_3$, whose decision spot is located at a distance 1m, 3m, and 5m, respectively; along with its envelope set.

Assuming a simplified longitudinal motion model, the set we seek to construct accepts an analytical formulation, which is expressed in Eq. (6.1) by the constructor $\mathcal{T}^{\mathrm{dR}}(\cdot)$. For the sake of clarity, we do not formulate herein the construction process that $\mathcal{T}^{\mathrm{dR}}(\cdot)$ represents, but in the Appendix (Section A.3). Nonetheless, some example sets that can be obtained through the process are illustrated in Fig. 6.3.

Specifically, three sets of reachable maneuver targets (for three hypothetical decision spots located at different distances) are illustrated in Fig. 6.3, along with their envelope set. Generally speaking, the further the decision spot is located, the bigger and the more to the right the set is positioned, as the vehicle could execute a wider set of trajectories to reach the spot. Moreover, the fact that the lower boundary of the set passes by $v = 0$ represents that the ego vehicle has time to brake before the decision spot and, thus, can reach it with null velocity. On the contrary, a set of reachable maneuver targets that appears to be floating (e.g. $\mathcal{T}^{\mathrm{R}}_{\mathcal{M}_1}$ in Fig. 6.3) corresponds to a situation where the ego vehicle cannot stop before the decision spot even if it applied its maximum allowed deceleration.

It is worth noting at this point that the set $\mathcal{T}^{\mathrm{R}}_{\mathcal{M}}$ represents the full solution space of the decision-making problem. Hence, the task of deciding how a maneuver candidate should be executed would be equivalent to the task of choosing the best MT $\mathcal{T}_{\mathcal{M}} = (\tau_{\mathcal{M}}, v_{\mathcal{M}})$ from $\mathcal{T}^{\mathrm{R}}_{\mathcal{M}}$.

6.3.2 Feasible virtual vehicle state

The communication-based interaction mechanism we aim to exploit in this chapter requires the ego vehicle to *insert* a VV on each conflicting traffic stream for any MT $\mathcal{T}_{\mathcal{M}} \in \mathcal{T}^{\mathrm{R}}_{\mathcal{M}}$ it intends to use; so that it guarantees that the MT can be safely pursued. Indeed, the state assigned to the VV would serve as a reservation of the inter-vehicle gap the ego vehicle plans to utilize in the future, and the ancillary VV should, therefore, be able to meet the targeted MT.

If we considered the VVs able to change their speed freely, a set $\mathcal{X}^{\mathrm{V}}(\mathcal{T}_{\mathcal{M}})$ composed of several VISs that could be assigned to the ego vehicle's virtual counterpart would exist for every MT $\mathcal{T}_{\mathcal{M}}$. However, the behavior the VV would need to apply to meet the chosen MT from some of those feasible states might require the application of an unnatural acceleration profile and have an unwanted impact on the traffic stream.

For this reason, and for the sake of simplicity, we impose that the insertion state assigned to the

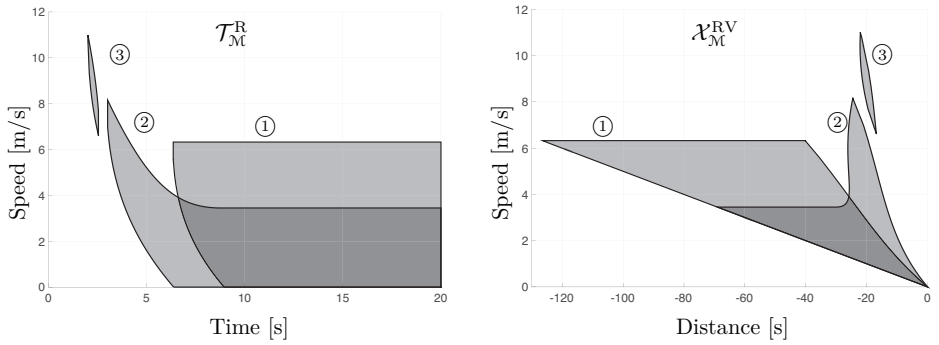

Figure 6.4 – On the left-hand side, three sets of reachable maneuver targets. On the right-hand side, three sets of VISs (one for every set of reachable MTs on the left-hand side). The three sets result from considering that the ego vehicle is at 20m from its decision spot, and approaching it with speeds $v_{①} = 0$, $v_{②} = 5.3$, and $v_{③} = 9$. On the left-hand side, the distance is referred to as the merging spot, hence the negative values represent position before such a location.

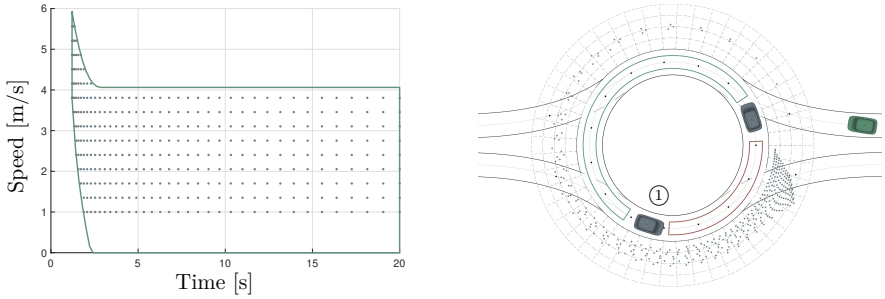

Figure 6.5 – On the left-hand side, the set of reachable maneuver targets, and a particular set of MTs within it shown by (•). On the right-hand side, the VISs corresponding to the finite set of MTs shown on the left-hand side. The VISs are plotted in a polar grid where the angular position is the one corresponding to its distance to the decision spot, and the radial displacement with respect to the outermost boundary of the intersection, represents its speed.

VVs must allow them to meet the MT by moving forward at a constant speed. Such an assumption has some desirable implications.

- The set $\mathcal{X}^{\mathrm{V}}(\mathcal{T}_{\mathcal{M}})$ of VISs corresponding to an MT $\mathcal{T}_{\mathcal{M}} = (\tau_{\mathcal{M}}, v_{\mathcal{M}})$ would consequently be a singleton containing only the state

$$x_{\mathcal{T}_{\mathcal{M}}}^{\mathrm{V}} := \texttt{MT2VS}(\mathcal{T}_{\mathcal{M}}) = (-\tau_{\mathcal{M}} v_{\mathcal{M}}, v_{\mathcal{M}}). \tag{6.2}$$

  Note that the position assigned to the VV is referred to the decision spot and is positive in the sense of traffic. Thus its negative value represents that the VV is located before such a spot.

- The communication burden could be expected to be low since, once a VIS is successfully communicated at time t_1, surrounding vehicles could easily estimate the state of such a VV at a future time $t_2 > t_1$. Thus, the ego vehicle would not need to continuously broadcast its VV state (unless it wants to reposition the VV somewhere else due to changes in the traffic scene).

In practice, the rules concerning the behavior of the virtual vehicles enable us to calculate, given

the distance $\delta_{\mathcal{M}}$ to the decision spot of a certain targeted maneuver $\mathcal{M}$, the set

$$\mathcal{X}_{\mathcal{M}}^{\mathrm{RV}} = \{x_{\mathcal{T}_{\mathcal{M}}}^{\mathrm{V}} : \mathcal{T}_{\mathcal{M}} \in \mathcal{T}_{\mathcal{M}}^{\mathrm{R}}\} \tag{6.3}$$

gathering the VISs corresponding to the reachable MTs, given the VV driving at a constant speed (see Fig 6.4 for some examples of such a pair of sets).

This step is illustrated in Fig. 6.5. On the left-hand side, we show the set $\mathcal{T}_{\mathcal{M}}^{\mathrm{R}}$ along with a finite set of MT candidates within it (gray dots), whereas, on the right-hand side, the insertion points corresponding to the finite set of MTs candidates are represented, with the radial distance representing the insertion speed.

6.3.3 Safe Virtual Vehicle insertion

As VVs are expected to be treated by the surrounding CAVs as real cars, the VIS they can be assigned should be limited to those that are safe, in a car-following sense, w.r.t. the surrounding vehicles. Thus, some of the virtual insertion states represented in Fig. 6.5 should indeed not be allowed due to the reaction they would induce on, for instance, vehicle ①. In fact, some of the shown insertion states represent *virtual* collisions with such a vehicle, which should be avoided.

Definition 12 (Safe VV insertion)**.** *A VV insertion is said to be safe if the virtual insertion state x^V leaves the virtual vehicle in a safe car-following and car-leading situation w.r.t. its leading and following vehicle, respectively.*

In this section, we tackle the identification of the subset of VISs that are reachable and safe concerning the surrounding gaps. We begin by letting $\mathcal{X}^{\mathrm{SCFL}}(x_L, x_F, \underline{h})$ (where SCFL stands for *safe car-following-leading*) denote the set of states that are, simultaneously, car-following safe w.r.t. a leading vehicle L with state x_L, and car-leading safe w.r.t. a following vehicle F with state x_F (whose definition is presented in the Appendix, Section A.1.6). Then, we can proceed to compute the set

$$\mathcal{X}_{\mathcal{M}}^{\mathrm{SV}} = \bigcap_{\mathcal{G}\in G} \left\{ \bigcup_{\mathcal{G}\in\mathcal{G}} \mathcal{X}^{\mathrm{SCFL}}(x_{g_{\mathrm{F}}}, x_{g_{\mathrm{R}}}, \underline{h}) \right\} \tag{6.4}$$

gathering all those VISs that are safe with respect to all the relevant observed gaps in all the conflicting traffic streams. Consequently, the set of virtual insertion states that are safe and reachable would be simply given by

$$\mathcal{X}_{\mathcal{M}}^{\mathrm{SRV}} = \mathcal{X}_{\mathcal{M}}^{\mathrm{RV}} \cap \mathcal{X}_{\mathcal{M}}^{\mathrm{SV}}. \tag{6.5}$$

Moreover, letting the operator

$$\texttt{VIS2MT}((\delta, v)) = (\delta/v, v) \tag{6.6}$$

represent the transformation from a virtual insertion state to its corresponding MT, we can as well construct the set $\mathcal{T}_{\mathcal{M}}^{\mathrm{SR}}$ of those MTs whose corresponding virtual insertion state is safe as

$$\mathcal{T}_{\mathcal{M}}^{\mathrm{SR}} = \{\texttt{VIS2MT}(x^{\mathrm{V}}) : x^{\mathrm{V}} \in \mathcal{X}_{\mathcal{M}}^{\mathrm{SRV}}\}. \tag{6.7}$$

The process is illustrated in Fig. 6.6. On the left-hand side, we represent the set $\mathcal{X}_{\mathcal{M}}^{\mathrm{RV}}$ along with

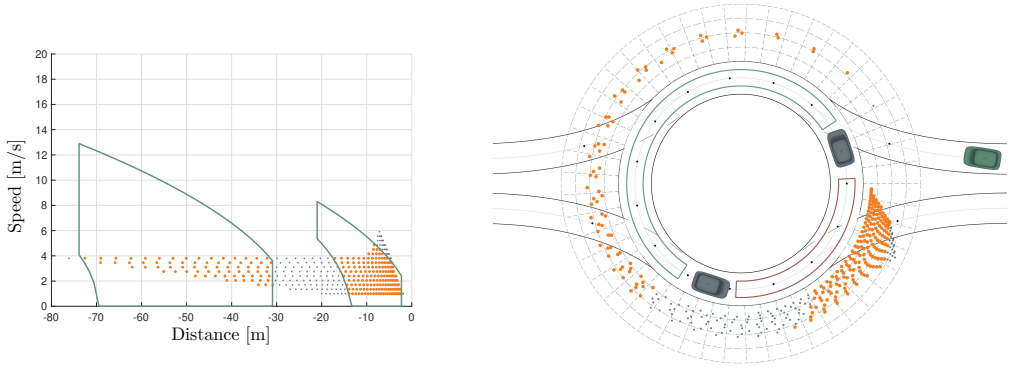

Figure 6.6 – Representation of reachable VISs (●), and the subset of VISs that are as well safe w.r.t. the observed gaps represented by (●). On the-left hand side, we represent the sets of safe VISs (—). Within it, the dots (●) show a finite set of IVs within the sets. Moreover, dots (●) show VISs that happen not to be safe. On the right-hand side, we represent the same finite set of VISs in context. In such a plot, the radial position of the dots shows their corresponding insertion location, and the height w.r.t. the roundabout's outer boundary represents the insertion speed.

the finite set of insertion points in gray, and the subset of them that are considered safe in orange. On the right-hand side, we illustrate the two sets of virtual insertion states in context. As can be observed, we have seemingly achieved our objective, as the safe virtual insertion states (orange dots) do not only avoid overlapping with vehicles in the circulatory lane but also being dangerously close to them.

Furthermore, note that the intersection over the sets in G carried out in Eq. (6.4) represents that for a VIS to be considered safe, it needs to be so w.r.t. all the traffic streams that should be crossed to perform the maneuver, which will be further discussed and illustrated in Section 6.4.1.

6.3.4 Traffic-model-based maneuver target scoring

Once we have isolated those VISs that would result in a safe virtual vehicle insertion, we need a criterion to score them so that the best one can be selected and pursued. To do so, one could simply consider the arrival time to the decision spot or the arrival speed. However, such an approach would completely disregard the impact that the VV creation would have on the surrounding traffic. Instead, we propose to score the virtual insertion states (and therefore their corresponding maneuver targets) by quantifying how the overall traffic performance would be expected to change if the virtual vehicle was created and its corresponding maneuver carried out.

Let us begin by denoting the traffic state as the aggregation of the state of a set $\mathcal{N} = \{1, \cdots, n_{\mathcal{N}}\}$ of vehicles as

$$r(t) = \{x_1(t), \cdots, x_{n_{\mathcal{N}}}(t)\}, \tag{6.8}$$

and representing the predicted traffic evolution over a certain time horizon T_{T}, if the VV corresponding to the maneuver target $\mathcal{T}_{\mathcal{M}}$ was created, as

$$r^{T_{\mathrm{T}}}_{\mathcal{T}_{\mathcal{M}}} \coloneqq \texttt{Pred}(r, x^{\mathrm{V}}_{\mathcal{T}_{\mathcal{M}}}, T_{\mathrm{T}}) = \{r(t+0), r(t+h_{\mathrm{T}}), \cdots, r(t+T_{\mathrm{T}})\}. \tag{6.9}$$

In order to compare traffic evolutions, we propose to consider the set

$$Q = \{\mu_{\text{speed}}, \phi_{\text{speed}}, \phi_{\text{jerk}}\} \tag{6.10}$$

of quality terms to balance, with μ_{speed} representing the overall average vehicles' velocity in the simulation, and terms ϕ_{k} showing the fairness with which the total speed and jerk are distributed among the agents. From the indicators $q \in Q$, we then construct the quality terms:

$$\mathcal{Q}_{\mu_{\text{speed}}}(r) = \texttt{Mean}(\{v_i(k) : i \in \mathcal{N}, k \in [1, N_{\text{T}}]\}), \tag{6.11}$$

$$\mathcal{Q}_{\phi_{\text{vel}}}(r) = \texttt{Fairness}(\{v_i(k) : i \in \mathcal{N}, k \in [1, N_{\text{T}}]\}), \tag{6.12}$$

$$\mathcal{Q}_{\phi_{\text{jerk}}}(r) = \texttt{Fairness}(\{a_i(k)^2 : i \in \mathcal{N}, k \in [1, N_{\text{T}}]\}), \tag{6.13}$$

where $N_{\text{T}} = \lceil H_{\text{T}}/h_{\text{T}} \rceil$ shows the resulting number of time steps in the predictions. The quality score assigned to every virtual insertion state, i.e. to every maneuver target, would be then calculated as

$$\mathcal{Q}(\mathcal{T}_{\mathcal{M}}) = \begin{cases} \sum_{q \in \mathcal{Q}} \omega_q \Big(\mathcal{Q}_q(r_{\mathcal{T}_{\mathcal{M}}}^{T_{\text{T}}}) - \mathcal{Q}_q(r_{\varnothing}^{T_{\text{T}}}) \Big) & \text{if } x_{\mathcal{T}_{\mathcal{M}}}^{\text{V}} \in \mathcal{X}_{\mathcal{M}}^{\text{SRI}} \\ -\infty & \text{otherwise} \end{cases}, \tag{6.14}$$

where $r_{\varnothing}^{T_{\text{T}}}$ represents the traffic evolution if no VV was inserted. The quality metric shown in Eq. (6.14) is defined as the weighted sum of the indicators' increment between the two compared scenarios. As a consequence, the traffic situation would be considered to improve, in overall terms, if $\mathcal{Q}(\mathcal{T}_{\mathcal{M}}) > 0$.

The proposed scoring process is illustrated in Fig. 6.7, where a set of points representing the quality score assigned to every VIS were depicted. Then, the best and worst points are highlighted, and the corresponding traffic predictions are shown. In this case, the specific weights used in the cost function (gathered in Tab. 6.2) prevents the algorithm from picking a state that is too close to its leading vehicle, as those would need to have a low speed for them to be safe. In the presented scene, the quality score of the best maneuver candidate turned out to be $\mathcal{Q}(\mathcal{T}_{\mathcal{M}}) = 2.2$.

Prediction model

In the scoring process presented above, we exploited the operator $\texttt{Pred}(r, x^{\text{V}}, T)$ to represent the process of predicting the traffic evolution over a temporary horizon T, with an initial traffic state r, and a VIS x^{V}. Such a prediction will be carried out by the recurrent application, for every vehicle $i \in \mathcal{N} \cup \{\text{VV}\}$, of the simplistic behavioral model Eq. (6.15)-(6.19).

$$s_i(k) = s_i(k-1) + h v_i(k-1) + 0.5 h^2 a_i(k-1), \tag{6.15}$$

$$v_i(k) = v_i(k) + h a_i(k-1), \tag{6.16}$$

$$a_i(k) = \begin{cases} 0 & \text{if } i = \text{VV} \\ a_{\text{IDM}}(x_i(k-1), \texttt{Lead}(i, r(k-1))) & \text{otherwise} \end{cases}, \tag{6.17}$$

$$x_i(k) = (s_i(k), v_i(k)), \tag{6.18}$$

$$r(k) = (x_1(k), \cdots, x_{n_{\mathcal{N}}+1}(k)). \tag{6.19}$$

A simplified longitudinal motion model is represented by Eq. (6.15)-(6.16). The acceleration applied by every vehicle over the prediction is given by Eq. (6.17), where the term $\texttt{Lead}(i, r(k-1))$ represents the closest vehicle ahead of vehicle i given the traffic state $r(k-1)$. In summary, the acceleration

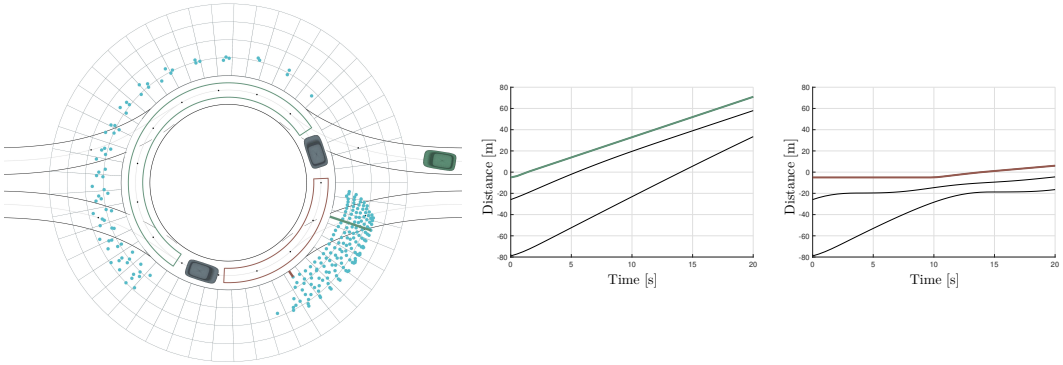

Figure 6.7 – Representation of the quality score assigned to every safe and reachable virtual insertion states shown in Fig. 6.6. On the left-hand side, we show radial points (•) showing the quality score (points' radial displacement w.r.t. to the roundabout's outer boundary) for every location where a insertion is considered (angular position of the dots). Moreover, radial lines (—) and (—) point to the best and worst insertion score, respectively. In the middle and on the right-hand side, we show the results of the simplified traffic-model-based prediction, for the highlighted best and worst insertions. Furthermore, colored trajectory in such a plots, represent the evolution of the ego vehicle.

of the inserted VV is considered null, and the acceleration of the remaining vehicles is given by the IDM. Then, Eq. (6.18)-(6.19) show the construction of the overall traffic state to use in the following iteration.

6.3.5 Maneuver selection

Once the impact on the overall traffic of every maneuver target has been quantified, the maneuver to be pursued, and its corresponding maneuver target, would be obtained as

$$(\mathcal{M}^{\mathrm{EC}}, \mathcal{T}_{\mathcal{M}}^{\mathrm{EC}}) = \arg \max_{\mathcal{M}\in\mathcal{M}, \mathcal{T}_{\mathcal{M}}\in\mathcal{T}_{\mathcal{M}}^{\mathrm{SR}}} \{\mathcal{Q}(\mathcal{T}_{\mathcal{M}})\}, \tag{6.20}$$

that is, by identifying the one with the highest score. Note that due to the cooperative character of the proposed strategy, the MT candidates are only scored w.r.t. their impact on the traffic stream.

6.3.6 Planner outputs

The outputs set by the proposed maneuver planner should simply make the ego vehicle reach its decision spot at the time and with the speed that the chosen maneuver target represents. Such behavior is imposed through the pair of targets

$$\mathcal{D} = \begin{cases} (\tau_{\mathcal{M}}^{\mathrm{EC}}, \delta_{\mathcal{M}^{\mathrm{EC}}}) & \text{if } \mathcal{Q}(\mathcal{T}_{\mathcal{M}}^{\mathrm{EC}}) \neq -\infty \\ \varnothing & \text{otherwise} \end{cases}, \quad \mathcal{V} = \begin{cases} (\tau_{\mathcal{M}}^{\mathrm{EC}}, v_{\mathcal{M}}^{\mathrm{EC}}) & \text{if } \mathcal{Q}(\mathcal{T}_{\mathcal{M}}^{\mathrm{EC}}) \neq -\infty \\ \varnothing & \text{otherwise} \end{cases}. \tag{6.21}$$

Moreover, an extra safety constraint

$$\mathcal{C} = \begin{cases} (\tau_{\mathcal{M}^{\mathrm{EC}}} - \epsilon, \delta_{\pi_0}, 0) & \text{if } \mathcal{Q}(\mathcal{T}^*_{\mathcal{M}}) > 0 \\ (\infty, \delta_{\pi_0}, 0) & \text{otherwise} \end{cases} \tag{6.22}$$

is set, representing the fact that a safe state w.r.t. the yield line should be kept at least for a time interval $\tau_{\mathcal{M}} - \epsilon$ if a VV was successfully inserted, or indefinitely otherwise.

Furthermore, safety w.r.t. the vehicles ahead is achieved through the set of constraints

$$\mathcal{C}' = \cup_{\mathcal{O} \in \mathcal{O}_{\mathrm{V}}} (\infty, x_{\mathcal{O}}, -a_{\mathrm{m}}), \tag{6.23}$$

leading to the final set of constraints $\mathcal{C} = \mathcal{C}' \cup \{\mathcal{C}\}$ that should be passed to the trajectory planner.

6.3.7 Maneuver safety

Before moving on to the evaluation of the strategy, let us briefly discuss some safety considerations. In Chapter 5, we explicitly addressed the calculation of the probability $\mathrm{P}^{\mathrm{S}}_{\mathcal{M},\mathcal{T}_{\mathcal{M}}}$ with which the reactive maneuver targets were considered to be safe, and took that into account at the time of scoring them. In this chapter, however, we do not have the need to quantify such a safety probability, as the proposed strategy imposes safety by design.

In Chapter 5 the safety probability $\mathrm{P}^{\mathrm{S}}_{\mathcal{M},\mathcal{T}_{\mathcal{M}}}$ was claimed to ultimately depend on the probability

$$\mathrm{P}(\mathrm{S} = 1 | \mathcal{T}_{\mathcal{M}}, \mathcal{G}) = \mathrm{P}\Big(\hat{E}_{\mathcal{G}}(\mathcal{T}_{\mathcal{M}}) = 1\Big) \mathrm{P}\Big(\hat{S}_{g_{\mathrm{F}}}(\mathcal{T}_{\mathcal{M}}) = 1\Big) \mathrm{P}\Big(\hat{S}_{g_{\mathrm{R}}}(\mathcal{T}_{\mathcal{M}}) = 1\Big) \tag{6.24}$$

of the MT $\mathcal{T}_{\mathcal{M}}$ being safe w.r.t. a certain gap $\mathcal{G}$. The overall situation would be considered safe if at least one gap (in every conflicting traffic stream) was sufficiently safe.

A similar process could be applied to the communication-based strategy proposed herein. However, in the context of this chapter, we can always consider having the guarantee that if the VV is successfully created (i.e. an MT chosen), (i) the reserved gap will arrive empty at the decision spot, (ii) the follower vehicle will keep a safe distance, and (iii) a safe distance would be kept with the leading vehicle. As a consequence, and thanks to the presumed communication-based interaction framework, the ego vehicle could consider relatively long planning horizons without considering any further safety considerations.

6.4 Results

In this section, we assess the performance of the proposed strategy at several levels. We begin by showing in Section 6.4.1, additional examples concerning the selection of the VIS in several traffic scenes. Then, in Section 6.4.2, we compare the traffic evolution resulting from the application of the proposed strategy with the one emerging from the baseline formulated in Chapter 5, and in three different traffic density scenarios. Finally, the overall traffic coordination performance is evaluated, in Section 6.4.3, for the proposed strategy and a broader set of scenarios.

The simulation study carried out in this section account for two driver agents, whose main features are described in Tab. 6.1. On the one hand, we consider that the agents' perception system is not affected by occlusions. Concerning the vehicles' behavior, R-Agents implement the baseline maneuver planner in Chapter 5 and are aware of the existence of VVs in such a way that they can properly react to them, while the EC-Agents implement the strategy formulated in this chapter.

Table 6.1 – Driver agents used in our simulation study

	Perception	Communication	Self-serving maneuver planner	Cooperative maneuver planner
R-Agent	Perfect	Passive	Reactive	Communication-based
EC-Agent	Perfect	Active	Reactive + Communication-based	Communication-based

Regarding the design parameters, they take the values in Tab. 6.2, that are the same ones used to illustrate the approach throughout the chapter.

Table 6.2 – Design parameters

	a_1	a_2	h_T	T_T	$\omega_{\mu_\mathrm{speed}}$	$\omega_{\phi_\mathrm{speed}}$	$\omega_{\phi_\mathrm{jerk}}$	ϵ	a_m
Value	-2	3	0.2	15	0.14	5	-4	2	3
Unit	$\mathrm{m/s^2}$	$\mathrm{m/s^2}$	s	s	s/m	s/m	$\mathrm{s^2/m}$	s	$\mathrm{m/s^2}$

Furthermore, even though the formulated strategy can be applied to perform merging maneuvers into multi-lane roundabouts and lane changes, the analysis will be limited, for the sake of simplicity, to single-lane roundabout scenarios; thereby focusing on the merging maneuver itself.

6.4.1 Decision-making examples

In this section, we illustrate the decision-making concerning the VIS that would be attributed to the VV in a set of traffic scenes where the ego vehicle has to perform a merging maneuver. The results are shown in Fig. 6.8, where the cost of the evaluated virtual insertion states is shown along with the best and worst cases and their corresponding predicted traffic evolution. Then, the impact the best maneuver targets are expected to have in the traffic stream is gathered in Tab. 6.3.

Qualitatively speaking, we can observe that the approach properly identifies those virtual insertion states that would be safe with respect to the surrounding vehicles. Moreover, the highlighted best virtual insertion states, which are a result of the proposed quality function, also seem appropriate and somehow match the intuition we might have concerning which inter-vehicle gap should and could be pursued.

Furthermore, it is interesting to see, in example 5, that the algorithm identifies very few safe virtual insertion states. On the one hand, such a small set of safe insertions is caused by the specific position and speed assigned to the vehicles in the circulatory lane, which makes executing the insertion of a VV between them unsafe. On the other hand, the temporary horizon the vehicle considers when calculating the set of its reachable maneuver targets and traffic predictions (set to $T = 20$ as shown in Tab. 6.2) prevents the set $\mathcal{X}_\mathcal{M}^\mathrm{SRV}$ from considering virtual insertion states belonging to the furthest inter-vehicle gap.

Moreover, it is important to stress that the traffic predictions the algorithm is built upon, do not explicitly take into account the exiting maneuver of the vehicles in the circulatory lane. However, as was commented above, vehicles share their destination. Thus the ego vehicle is aware of the vehicles in the circulatory lane that are following conflicting paths. In the examples shown, the fact that all vehicles in the scenarios are included in the traffic predictions implies that all vehicles in the circulatory lane are known to pass by the ego vehicle's decision spot.

Furthermore, in the cases illustrated, all the insertion states correspond to a merging maneuver into the innermost circulatory lane of the roundabout. If the ego vehicle wanted to consider merging into the outermost circulatory lane, in practical terms, the vehicles in the innermost circulatory lane should be disregarded. Consequently, merging into the outermost circulatory lane in example 5

would be equivalent to the analysis shown in example 4.

Table 6.3 – Example traffic scores

	Ex. 1	Ex. 2	Ex. 3	Ex. 4	Ex. 5
[%]	2.68	2.84	2.99	2.29	2.86

6.4.2 Single traffic scenario

The algorithm's outcome was illustrated in the previous section for a set of static traffic scenes. In this section, we aim to evaluate the impact the strategy would have once it is applied by a set of vehicles driving through a roundabout.

In particular, we will consider a roundabout of 16m radius, 1 circulatory lane, 3 legs with 1 incoming and 1 outgoing lane (i.e. a `16R1LR3L1I1O` roundabout). Moreover, we generate scenarios of 100 vehicles (i.e. `100V`), and three different incoming traffic configurations corresponding to an incoming traffic volume of 500vehs/h, 1500vehs/h, and 2500vehs/h evenly distributed among the incoming legs. In other words, we consider the incoming traffic configurations `500Q[1 1 1]`, `1500Q[1 1 1]`, and `2500Q[1 1 1]` (see Section 2.3.4 for details concerning our labeling strategy). Each traffic scenario is simulated twice, with the vehicles being driven by: (case-1) R-Agents and (case-2) EC-Agents.

The results are shown in Fig. 6.9-6.17, where we compare, for every pair of simulations:

- the time-distance evolution of the traffic in the circulatory lane,
- the evolution of the incoming traffic for every incoming leg of the roundabout, and
- the distribution of some additional performance metrics concerning the travel time, travel speed, average jerk, and delay that the vehicles in the scenario experience.

Furthermore, we gather in Tab. 6.4 the registered values for the intersection throughput and the fairness value associated with the different performance metrics concerning the vehicles' trajectory.

Table 6.4 – Intersection throughput and fairness metrics

	Throughput [vehs/h]	TT. fairness [%]	TS. fairness [%]	J. fairness [%]	D. fairness [%]
`16R1LR3L1I1O-100V-500Q[1 1 1]-RAgent`	495	97	99	83	96
`16R1LR3L1I1O-100V-500Q[1 1 1]-ECAgent`	497	97	99	85	96
`16R1LR3L1I1O-100V-1500Q[1 1 1]-RAgent`	1310	98	99	84	63
`16R1LR3L1I1O-100V-1500Q[1 1 1]-ECAgent`	1336	98	99	89	96
`16R1LR3L1I1O-100V-2500Q[1 1 1]-RAgent`	1433	80	92	87	35
`16R1LR3L1I1O-100V-2500Q[1 1 1]-ECAgent`	1636	83	94	89	27

In general, we can observe that, even though all vehicles are set up to target exactly the same arrival time, EC-Agents manage to drive through the roundabout quicker and more smoothly than R-Agents in all cases.

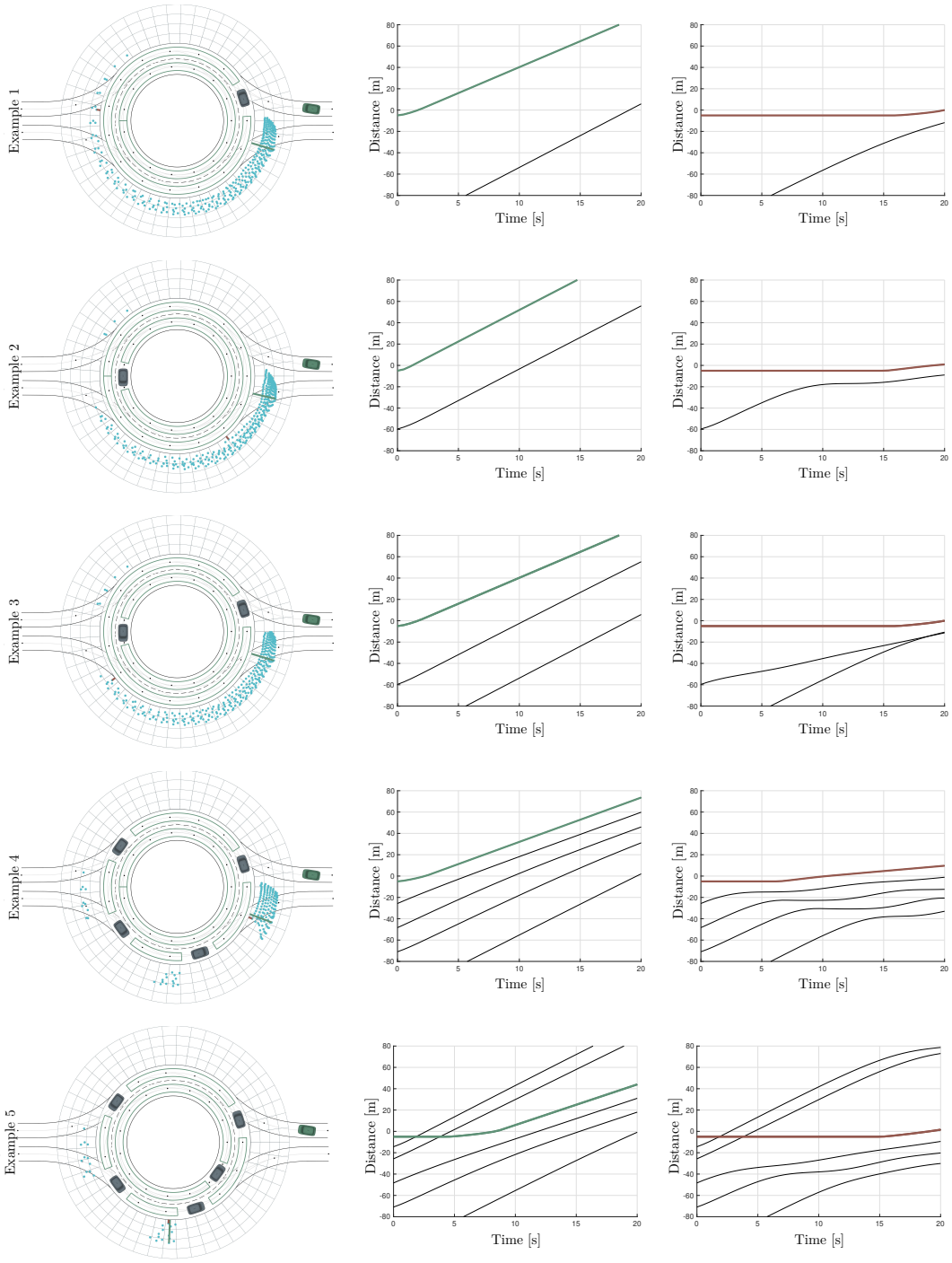

Figure 6.8 – Examples of the decision made by the explicitly cooperative maneuver planner in different scenarios. The representation follows the same format used in Fig. 6.7. On the left-hand side, we show the quality score of a finite set of safe VISs, along with the best and worst VISs. In the middle and on the right-hand side, the traffic prediction corresponding to the best and worst VIS are shown.

In very light traffic conditions (Fig. 6.9-6.11), both agents drive in a virtually identical manner, as is to be expected due to the lack of interaction between vehicles. The small differences that can be observed are a consequence of the approaching behavior being the result of an optimization in the case of EC-agents, and a reactive policy in the case of R-agents. According to the metrics in Tab. 6.4, both agents behave in a very similar way, and the scenario is highly fair in both cases.

In medium-density traffic conditions (Fig. 6.12-6.15), trajectories are as well very similar, but some differences start to be noticeable. Firstly, the traffic in the circulatory lane of the roundabout evolves smoothly in both cases. Concerning the evolution of the incoming traffic, we can observe how the proposed communication-based planning strategy enables all the merging vehicles to merge without stopping at the yield line, which results in a smoother traffic evolution. Typically, this effect is the result of the circulating vehicles braking the right amount to accommodate the merging maneuvers (which is achieved through the use of virtual vehicles) and the incoming vehicles speeding up while approaching. As a consequence, vehicles manage to drive through the intersection in less time and require a smaller amount of jerk. Concerning the metrics in Tab. 6.4, we observe that the overall throughput is roughly the same in both cases, but the EC-agents render a fairer scenario in terms of jerk and delays.

In high-density traffic (Fig. 6.12-6.15), bigger differences between the two compared agents start to arise. Firstly, we can observe that the trajectories of the traffic stream inside the roundabout become slightly wavier when the proposed strategy is applied, which is a consequence of the created virtual vehicles forcing the circulating vehicles to cooperate by slightly decelerating. Additionally, a higher traffic density is achieved in the circulatory lane as a result of the vehicles merging without uncertainty, which results in smaller inter-vehicle gaps. Concerning the dynamics of the incoming traffic, we observe that EC-agents improve the evolution of the incoming traffic significantly. Indeed, vehicles are observed to move towards the roundabout more smoothly and appear more capable of merging into the roundabout without stopping, despite the heavy traffic conditions. Finally, all higher-level quality metrics in Tab. 6.4 are as well improved when the explicitly cooperative strategy is applied. The intersection throughput is observed to increase in 200veh/h, and the fairness metrics slightly improve as well in such harsh traffic conditions.

In general, the approach outperforms the reactive baseline planning policy in all the cases shown. Such an improvement is a consequence of three main aspects:

1. Higher planning horizons improve the approaching behavior of the vehicles and increase the speed with which vehicles merge into the roundabout. This effect is the result of the certainty that V2V communication provides concerning the cooperation willingness of the surrounding vehicles.

2. The appropriate insertion of VV allows the incoming vehicles to find gaps to merge more easily and reduces the inter-vehicle gaps required to merge into the intersection.

3. The use of VVs allows circulating vehicles to adapt their behavior more smoothly to accommodate the merging maneuver of surrounding vehicles.

Furthermore, even though the vehicles are observed to slightly decelerate while they drive inside the roundabout in high traffic density conditions, no significant disturbances are experienced. Such an effect shows that the proposed traffic-model-based approach used to place virtual vehicles in the circulating traffic stream is suitable for the task at hand.

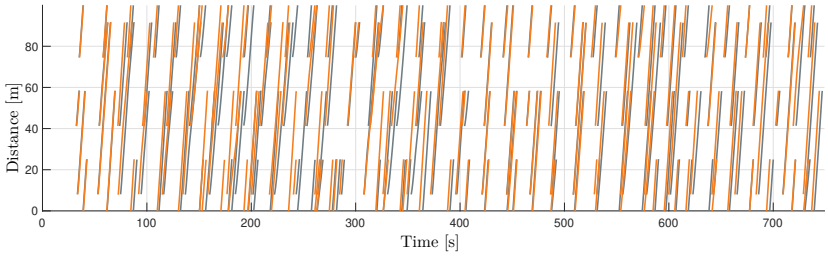

Figure 6.9 – Time-distance diagram representing the evolution over time of the vehicles in the circulatory lane, in the simulated scenario `16R1LR3L1I1O-100V-500Q[1 1 1]`. The trajectories of R-Agents and EC-Agents are represented by (—) and (—), respectively.

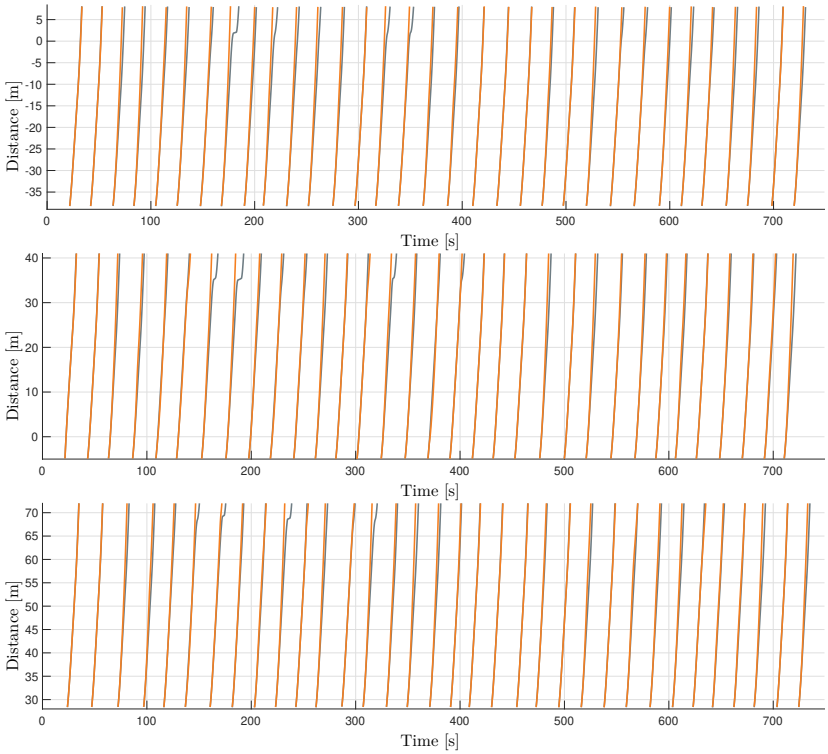

Figure 6.10 – Time-distance diagrams representing the evolution of the incoming traffic in every incoming lane in the simulated scenario `16R1LR3L1I1O-100V-500Q[1 1 1]`. The trajectories of R-Agents and EC-Agents are represented by (—) and (—), respectively.

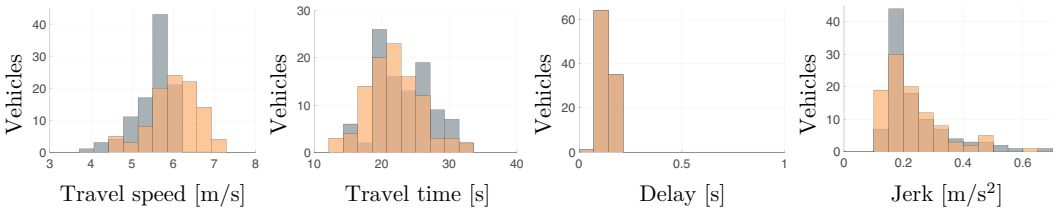

Figure 6.11 – Comparison of the histogram of the registered travel speed, travel time, arrival delay, and jerk of the vehicles in the scenario `16R1LR3L1I1O-100V-500Q[1 1 1]`, when driven by R-agents (gray) and EC-agents (orange).

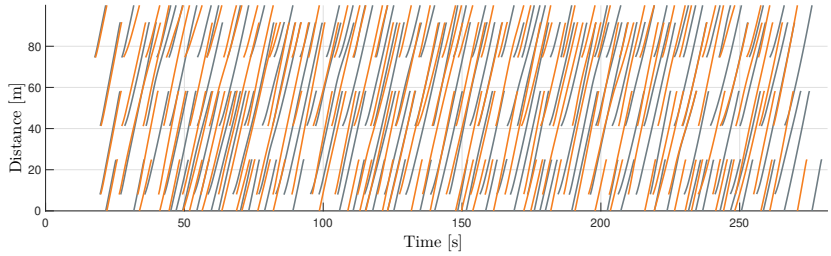

Figure 6.12 – Time-distance diagram representing the evolution over time of the vehicles in the circulatory lane, in the simulated scenario `16R1LR3L1I1O-100V-1500Q[1 1 1]`. The trajectories of R-Agents and EC-Agents are represented by (—) and (—), respectively.

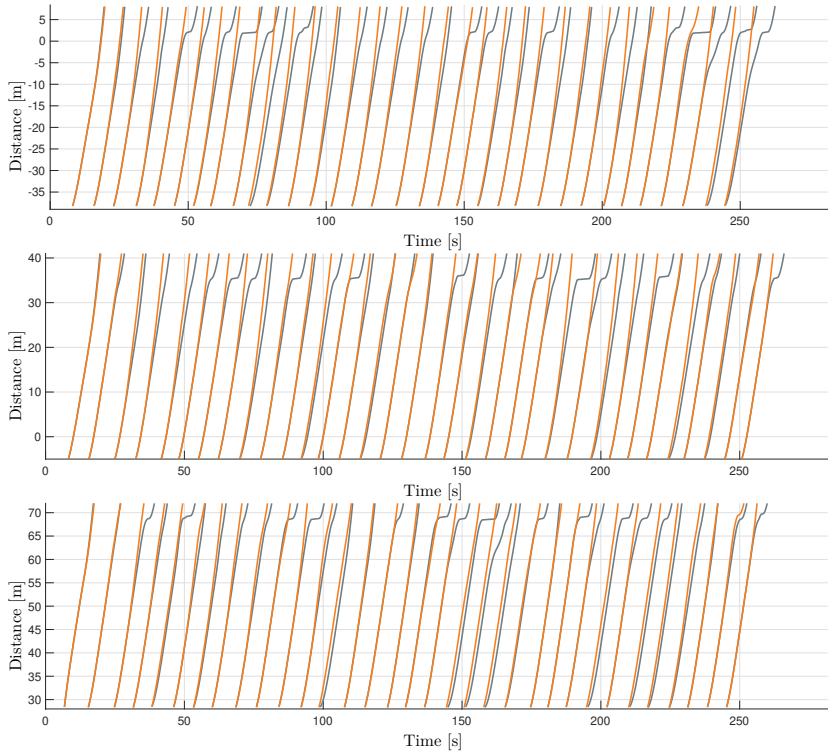

Figure 6.13 – Time-distance diagrams representing the evolution of the incoming traffic in every incoming lane in the simulated scenario `16R1LR3L1I1O-100V-1500Q[1 1 1]`. The trajectories of R-Agents and EC-Agents are represented by (—) and (—), respectively.

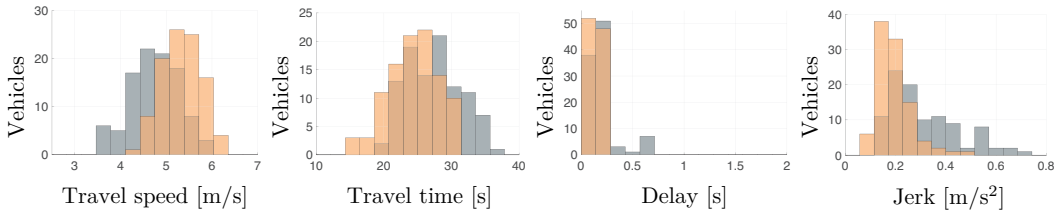

Figure 6.14 – Comparison of the histogram of the registered travel speed, travel time, arrival delay, and jerk of the vehicles in the simulated scenario `16R1LR3L1I1O-100V-1500Q[1 1 1]`, when driven by R-agents (gray) and EC-agents (orange).

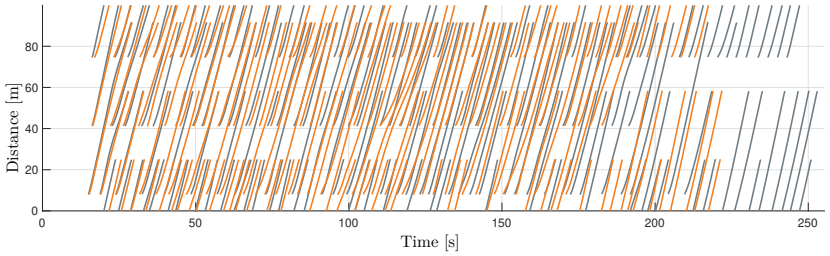

Figure 6.15 – Time-distance diagram representing the evolution over time of the vehicles in the circulatory lane, in the simulated scenario `16R1LR3L1I1O-100V-2500Q[1 1 1]`. The trajectories of R-Agents and EC-Agents are represented by (—) and (—), respectively.

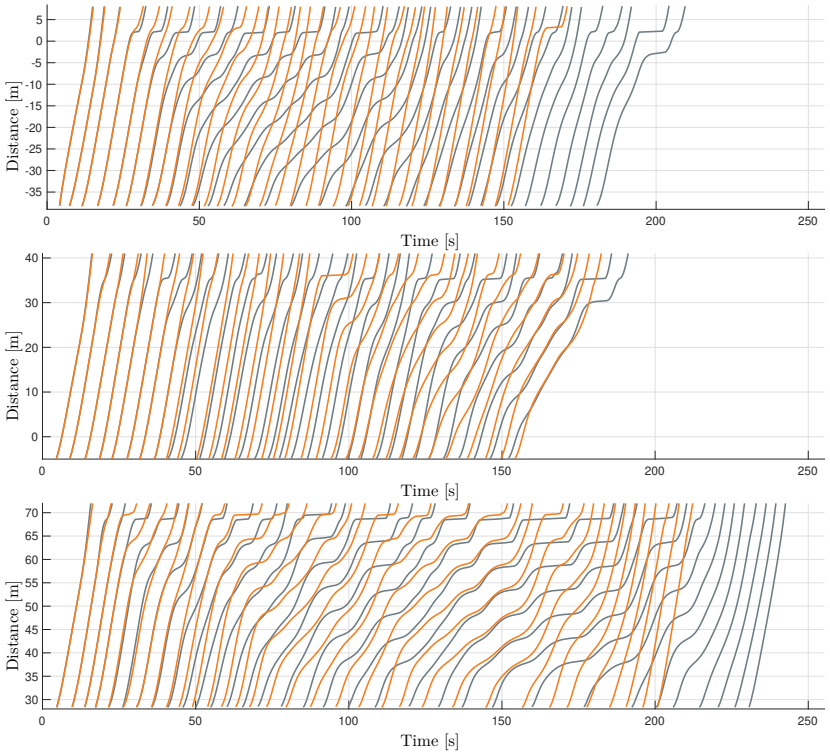

Figure 6.16 – Time-distance diagrams representing the evolution of the incoming traffic in every incoming lane in the simulated scenario `16R1LR3L1I1O-100V-2500Q[1 1 1]`. The trajectories of R-Agents and EC-Agents are represented by (—) and (—), respectively.

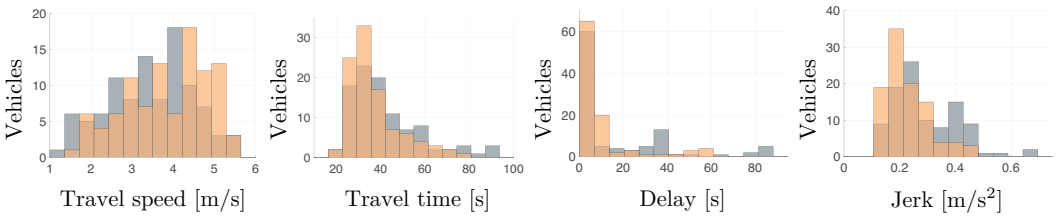

Figure 6.17 – Comparison of the histogram of the registered travel speed, travel time, arrival delay, and jerk of the vehicles in the scenario `16R1LR3L1I1O-100V-2500Q[1 1 1]`, when driven by R-agents (gray) and EC-agents (orange).

6.4.3 Traffic coordination performance

In this section, we address the evaluation of the proposed strategy at the overall traffic coordination level, so that the macroscopic benefits that could be expected from the application of the strategy are quantified. The process is somehow related to the analysis of the single roundabout scenario in the previous traffic scenes. However, here we aim to obtain the average improvement over a relatively large set of randomly-generated traffic scenarios. The main idea is to quantify the benefits of the approach independently from the specific origin-destination pattern, and rather its dependency on the incoming traffic density.

Simulation batch setup

The set of simulation instances used to carry out the analysis was generated according to the parameters in Tab. 6.5 and the tree structure illustrated in Fig. 6.18. A total of 18 different incoming traffic configurations are used, where the total flow of incoming vehicles (`QI`), as well as the way in which it is distributed among the legs (`DI`) is varied. For every traffic scenario, ten different instances ($\texttt{I1}, \cdots, \texttt{I10}$) are randomly created in such a way that different origin-destination patterns and arrival times are tested. Furthermore, every instance is simulated for five different penetration rates (`P`) of EC-Agents driving among R-Agents.

Table 6.5 – Simulation batch scenario configuration

	Value
G	16R1LR3L1I1O-100V
QI1	1000Q
QI2	1500Q
QI3	2000Q
QI4	2500Q
QI5	3000Q
QI6	3500Q
DI1	[1.0 1.0 1.0]
DI2	[1.0 0.5 1.0]
DI3	[0.5 1.0 0.5]
P1	0
P2	0.25
P3	0.5
P4	0.75
P5	1

Simulation batch results

The evaluation of the overall traffic coordination performance is done by analyzing the distribution of average overall travel speed (Fig. 6.19), jerk (Fig. 6.20), and intersection throughput (Fig. 6.21) w.r.t. the incoming traffic volume, and the penetration rate. In each of the shown plots, six different groups of boxplots are shown, which correspond to the six simulated traffic inflows ($\texttt{QI1}, \cdots, \texttt{QI6}$). Moreover, within each group, five different boxplots are represented, corresponding to the five considered penetration levels ($\texttt{P1}, \cdots, \texttt{P5}$). Note that, unlike the analysis carried out in Section 5.4.3, where different distributions were characterized for the three different incoming traffic distributions,

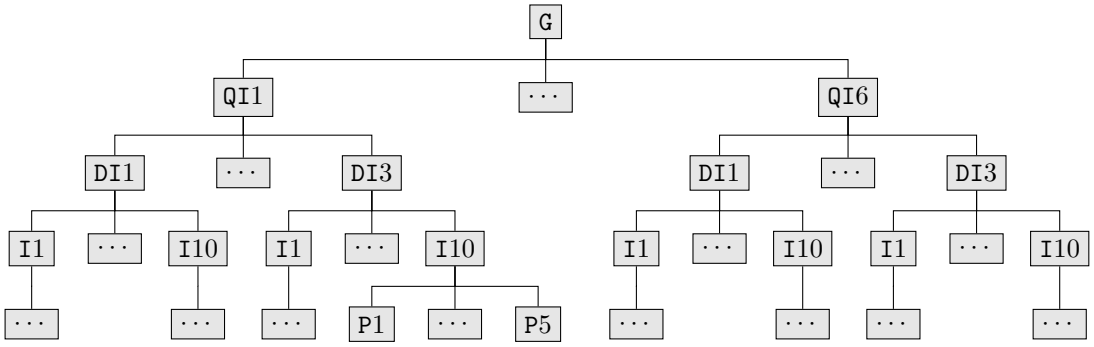

Figure 6.18 – Generation of the batch of simulated traffic scenarios.

we opt here for aggregating such a variable.

Consistent with the results obtained in the previous section, the proposed explicitly cooperative planning strategy outperforms the reactive one in all of the tested traffic configurations.

Regarding the distributions of overall travel speeds, we can observe how not only the overall travel speed but also the fairness with which it is distributed among the agents improves in all cases. This effect was somehow to be expected, as the proposed interaction mechanism allows vehicles to reserve inter-vehicle gaps in an approximately first-come-first-served fashion, thereby leading to a fair scenario by design. Note as well that, whereas the bigger improvement in travel speed is registered at low traffic densities, it is in highly congested situations where the strategies have a stronger impact in terms of fairness.

A similar conclusion can be drawn regarding the distributions of the average jerk applied by the vehicles while driving through the intersection. With the strategy proposed in this chapter, vehicles need to apply less jerk (i.e. drive more comfortably and consuming less energy) and the acceleration/deceleration effort is more fairly distributed among the agents.

Finally, a similar discussion applies to the overall intersection throughput and the distribution of 15min-throughput values. The proposed strategy is observed to improve the overall intersection throughput in up to 200vehs/h for 100% penetration rate of EC-agents, i.e. up to 15% w.r.t. the baseline reactive approach.

6.5 Conclusions

In this chapter, we have tackled the design and evaluation of a communication-based interaction mechanism for CAVs. Cooperation between vehicles is achieved through the use of virtual vehicles that are created by those vehicles in need of cooperation and respected by surrounding cooperative vehicles. The characterization of the whole solution space has also been presented, making the ego vehicle aware of the set of merging trajectories it could apply to merge into the intersection. Furthermore, a traffic-model-based decision-making workflow has been proposed, which was observed to be flexible enough to address different traffic scenes, and significantly beneficial, not only from the individual vehicles' standpoint but also for the overall traffic dynamics.

The benefits stemming from the vehicles being aware of surrounding vehicles' destinations, along with the control power that the VV-based interaction mechanism provides them are evident, and the shown results are somehow what could have been expected.

The exploited traffic-model based decision-making approach has been shown to be very versatile

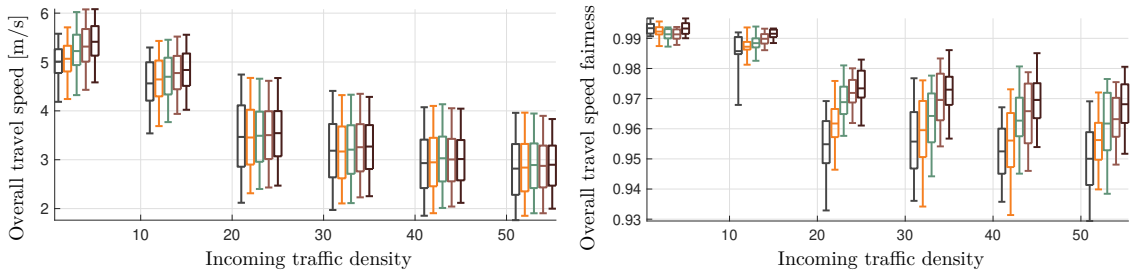

Figure 6.19 – On the left-hand side, boxplots representing the distribution of overall travel speed applied by the vehicles for different incoming traffic inflow configurations and penetration rates. On the right-hand side, the fairness with which the metric is distributed among the vehicles in the scenarios.

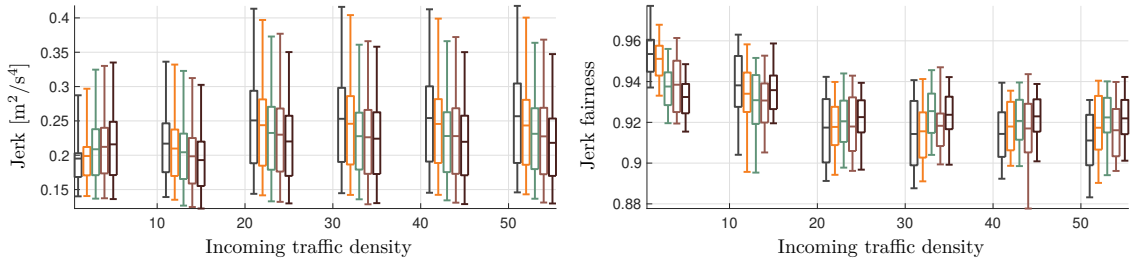

Figure 6.20 – On the left-hand side, boxplots representing the distribution of jerk applied by the vehicles for different incoming traffic inflow configurations and penetration rates. On the right-hand side, the fairness with which the metric is distributed among the vehicles in the scenarios.

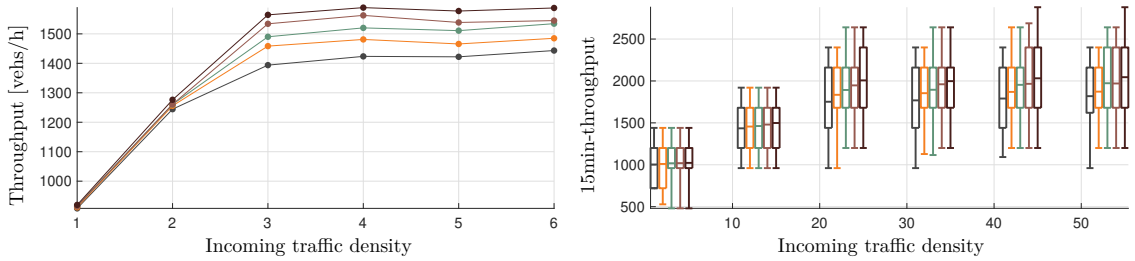

Figure 6.21 – On the left-hand side, the total intersection throughput registered for different incoming traffic density, and values of the penetration rate of EC-agents. On the right-hand side, boxplots representing the distribution of 15min-throughput for different incoming traffic inflow configurations and penetration rates.

and convenient, despite the differences between the exploited traffic model and the actual behavior of the vehicles in our simulations. However, this feature is, at the same time, one of the strongest weaknesses of the algorithm, as running one traffic simulation for each feasible virtual vehicle state is time-consuming. Luckily, such an evaluation only needs to be done sporadically, when the traffic scene undergoes a change that might allow projecting the virtual vehicle in a more suitable spot. Moreover, the computational burden could be further controlled by acting on the number of MT

candidates that are selected to approximate the solution space, or implementing heuristics to identify a near-optimal insertion state with fewer evaluations.

The strategy could be further enhanced in several ways. Firstly, in what concerns the application of the strategy in mixed traffic scenarios, some further aspects should be taken into account. A priori, the proposed planning solution would only be applicable to request gaps whose rear limit is defined by a CAV, as they are the only ones receiving the state of the virtual vehicle. However, one should additionally consider the possibility of some unconnected vehicles merging into the *reserved* gap, or the cooperative CAV the maneuver relies on leaving the roundabout before the maneuver is actually executed. In this sense, the situations would indeed be even less favorable in multi-lane roundabouts, where potential lane changes would compromise the existence of the reserved gaps.

An additional limitation of the approach is related to maneuvers that require crossing several conflicting traffic streams. In those cases, due to the constant-velocity assumption shaping the virtual vehicle's trajectory, the strategy would only find a solution when feasible inter-vehicle gaps are found in every conflicting traffic stream at the same distance from the merging spot. A more flexible alternative would indeed be considering constant acceleration trajectories for the VVs, which would allow us to insert VVs at different distances from the decision spot and making them meet the chosen MT by applying different accelerations.

In summary, even though there are several ways in which the strategy could be improved, the proposed communication-based planning solution represents a pragmatic and promising mechanism to reach effective coordination between CAVs, while keeping the communication-burden arguably low.

7 Implicitly Cooperative Planning

Cooperativeness is a very desirable driving feature in complex traffic scenarios. That is especially the case in situations of high-density traffic where strictly respecting traffic signs and priority rules could potentially result in unbalanced and unfair situations. In this context, the cooperative behavior we studied in Chapter 6 was shown to allow CAVs to drive cooperatively and safely through roundabouts, and to have a significant positive impact on the overall traffic performance and intersection throughput. However, from a practical standpoint, such a strategy has a significant limitation: it can only be deployed once V2V communication technology reaches a sufficient level of maturity, as the cooperation intent is to be made explicit through direct communication channels.

The deployment of explicitly cooperative mechanisms (generally understood as those where the cooperation intent is made explicit through any type of communication channel, whether sound, lights, or explicit wireless communication) is, in general, a remarkably challenging task. Among other reasons, such a complexity stems from the need to correctly read the intentions of the surrounding vehicles (which is an arduous task in itself) and the subtle signs of cooperation willingness. To the best of our knowledge, performing reliable and robust vehicle detection and tracking in partially and/or dynamically occluded scenarios is still a tough challenge for state-of-the-art perception systems. Thus, the perception capabilities that would be required to perform explicitly cooperative maneuvers with human drivers (for instance detecting surrounding drivers' hand gestures, headlight patterns, or recognizing honk patterns communicating a cooperative intent) are yet unsolved problems. In short, making AVs able to cooperate with surrounding human drivers explicitly is a very challenging task that requires perception capabilities that are not available to date.

As an alternative to the explicitly cooperative mechanism described above, implicit cooperation could be considered. In this type of cooperation, an AV that seeks to cooperate with a nearby vehicle would not need to broadcast its cooperation intent explicitly. Instead, it should act on the context so that the other vehicle can naturally take advantage of the cooperative action.

In this chapter, we study a strategy to let AVs cooperate with surrounding vehicles at roundabouts and without the need for explicit V2V communication. The idea, first presented in [16], is based on the type of trajectories resulting from the application of the explicitly cooperative strategy in the previous chapter. There, we considered cooperation to emerge from explicit requests made by the merging vehicles, to which the ones circulating inside the roundabout would react by decelerating in such a way that the demanded inter-vehicle gap was sufficiently enlarged. V2V communication was

required for the vehicles in the roundabout to be aware of the merging vehicles' intent, as it could not have been efficiently transmitted or understood otherwise.

Alternatively, in the cooperative scene just described, the vehicles inside the roundabout could have been given the role of triggering the cooperative maneuvers. That is, a vehicle driving inside the roundabout could determine the suitability of executing a cooperative merging maneuver and then transmitting such information to an incoming vehicle. It is interesting to note that, from this point of view, the vehicle inside the roundabout could also deliberately decelerate to enlarge the inter-vehicle gap ahead of it, so that it could be accepted by some merging vehicle. In this sense, cooperation would be reached without the use of V2V communication. This type of cooperation is herein referred to as *implicit* since it is the transformation of the context, and not the explicit communication of the intent to cooperate, what enables it.

In this chapter, we formulate an implicitly cooperative maneuver planning strategy that aims to allow AVs to reach cooperation through the cooperation mechanism mentioned above. That is, we investigate a cooperative maneuver planner to make AVs inside a roundabout facilitate the merging maneuver of approaching vehicles. The proposed method is based on the gap-acceptance decision map of Section 5.3.3, and a simplistic yet effective method to approximate the benefit that could be expected from the cooperative maneuver.

The chapter is organized as follows. We begin by providing an overview of existing related work in Section 7.1. Then, in Section 7.2, we refine the definition of the scenario as well as the set of assumptions considered in the following sections. In Section 7.3, we briefly review the gap-acceptance decision map and exploit it to provide some insight regarding how a yielding maneuver should be successfully executed. The yielding maneuver planner is subsequently detailed in Section 7.4, and its performance is assessed in Section 7.5. Finally, further conclusions and considerations are presented in Section 7.6.

7.1 Related work

The methods used to address cooperative driving [79] for AVs without communication-capabilities are tightly related to the problem of interaction-aware motion planning; as an interaction model of the surrounding vehicle is needed in both cases to reach the planning objectives. However, both approaches differ in the planning objective. Interaction-aware planning strategies are typically used to execute self-serving maneuvers that need to take into account the expected reaction of the surrounding vehicles. Contrary, cooperative driving strategies (from a decentralized point of view) aim to facilitate the maneuver of a nearby vehicle by exploiting an approximate model of how such a vehicle makes decisions. In the literature, the latter research topic has not been extensively studied. Thus, even though we study in this chapter the effect of the ego vehicle altruistically yielding to some merging vehicles while circulating inside the roundabout, we start in this section by gathering some relevant research in the tightly-related topic of interaction-aware motion planning.

In essence, the interaction-aware planning problem requires, as does the cooperative planning one, planning strategies that take into account how the surrounding vehicles are likely to react. Existing studies typically differ in the way in which the trajectory candidates are generated, and the surrounding vehicles' interaction is modeled.

Firstly, it must be stressed that, as shown by Graf et al. in [26], reactivity and interaction-awareness are not incompatible concepts. In [26], the authors present a lane-change algorithm whereby a lane-change maneuver is only triggered if the reaction expected from the surrounding traffic improves the overall situation.

Another popular type of approach in this direction consists in generating a finite set of trajectory candidates, scoring them, and select one to pursue. The main advantage of such approaches is its computational efficiency, which makes them good candidates for real-time applications. However, such approaches typically make use of a coarse set of maneuver candidates, thereby oversimplifying the solution space and making the approach suboptimal by design. As a consequence, it would be possible to mistakenly consider a certain maneuver infeasible due to the low resolution of the pool of maneuver candidates.

Jin et al. propose in [37] a motion planning solution to perform lane-changes by first generating a set of lane-change trajectory candidates, and then scoring them accounting for the reaction they might induce on the surrounding vehicles. In particular, the behavior of the surrounding vehicles is on this occasion modeled using a Markov model, and the ego vehicle's decision is formulated as a Markov decision tree problem.

David Lenz et al. in [45] proposed a so-called cooperative combinatorial motion planning algorithm whose solution is based on performing a Monte Carlo tree search. The proposed approach first creates a graph representing different combinations of driving maneuvers that can be performed by the surrounding vehicles. Then, for every combination, traffic simulations are run with a simplified car model, which changes according to the necessities of the simulation.

Ward et al. present in [90] a motion planning strategy, for merging scenarios, that begins with the ego vehicle generating a broad set of possible trajectories (as they did in their previous work [91]). Afterward, such a set of candidates are scored by accounting for an approximated prediction of the traffic evolution, based on an extended stochastic version of the IDM [86]. Finally, a decision is made according to the calculated score.

A third family of methods would gather those studies relying on probabilistic decision-making frameworks (such as Markov Decision Processes) to directly infer the sequence of accelerations that would optimize a reward function accounting for the stochastic interaction of the surrounding vehicles. This type of methods presents the advantage of not requiring, a priori, a finite discretization of the solution space. However, even though such planning frameworks represent a very powerful option to model the decision-making problem, finding an optimal solution is typically infeasible. Thus, the solvers used to obtain a solution to the problem require the application of heuristics that typically simplify the solution space.

The latter family of methods has become a popular alternative in recent years, and one of the most relevant solutions is based on modeling the problem as a partially observable Markov decision process (PDMDP). For instance, Constantin Hubmann et al. in [33] address the problem of merging into a highly-dense traffic stream by modeling the decision-making process as a PDMDP. The surrounding vehicles' behavior is modeled by a probabilistic longitudinal motion model, which determines the yielding probability of the surrounding vehicles. As stated by the authors, the approach allows a vehicle to behave so that it can profit from the yielding maneuver of other vehicles. The solution of the POMDP is approximated using the so-called adaptive belief tree algorithm [42], combined with an A* roll-out heuristic.

Yet another family of approaches is based on learning how to react to the surrounding vehicles using naturalistic driving data sets in the hope of learning suitable driving strategies (see, for instance, [11]). Such an approach has the potential of generating suitable interaction-aware behaviors but is limited concerning its scalability and the fact that it would not allow the execution of cooperative maneuvers on demand.

In summary, the existing body of work on interaction-aware motion planning focuses on profiting from the expected reaction of the surrounding vehicles to execute self-serving maneuvers, and very

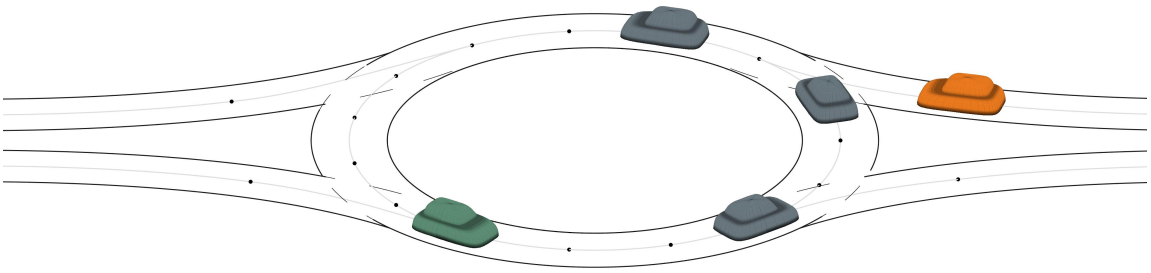

Figure 7.1 – Illustration of the addressed traffic scenario. The green car represents an AV that is evaluating its options regarding behaving cooperatively with the orange vehicle, which is the subject of the cooperation.

few studies exist where the objective is to facilitate surrounding vehicles' maneuvers. Indeed, even when existing studies consider the possibility of the ego vehicle yielding to a surrounding vehicle, it stems from the collision avoidance objective and is not explicitly oriented to cooperate with a surrounding vehicle. In other words, to the best of our knowledge, and as it occurs in [66, 82], yielding maneuvers are only regarded in the literature as a collision avoidance resource, but not a cooperative one. The cooperative planning strategy presented in this chapter investigates the exploitation of altruistic yielding maneuvers to reach cooperation with surrounding vehicles and potentially improve the overall traffic performance in roundabouts.

7.2 Problem formulation, assumptions, and preliminaries

The scenario we address in this chapter is illustrated in Fig. 7.1, where an AV (green car inside the roundabout) considers whether to perform a yielding maneuver to facilitate the merging maneuver of an approaching vehicle (orange car). The planner will be referred to as the *implicitly cooperative yielding maneuver planner*, and, in this chapter, we seek not only to detail its formulation but also assess the impact it has on the overall traffic performance.

The specific traffic scenario addressed herein is, once again, similar to the more general scene described in Chapter 2. However, we consider on this occasion that the ego vehicle does not have communication capabilities.

Furthermore, the planner we aim to propose in this chapter is a cooperative maneuver planner, i.e. it focuses on how to make the ego vehicle cooperate with surrounding vehicles, and not on the execution of self-serving driving maneuvers. In that sense, every maneuver candidate within $\mathcal{M}$ would represent a different vehicle that could benefit from the cooperation of the ego vehicle.

Furthermore, for the sake of simplicity, we only consider here single-lane roundabouts. Although the extension of the strategy to multi-lane roundabouts and the new challenges that might arise in the process will be discussed in Section 7.6.

7.3 Gap-acceptance criterion

Let us begin by briefly discussing, from the standpoint of an isolated inter-vehicle gap, the gap-acceptance criterion, so that the essential features of a successful yield maneuver can be well understood.

Consider the scenario depicted in Fig. 7.2, where the ego vehicle (green car) is evaluating the

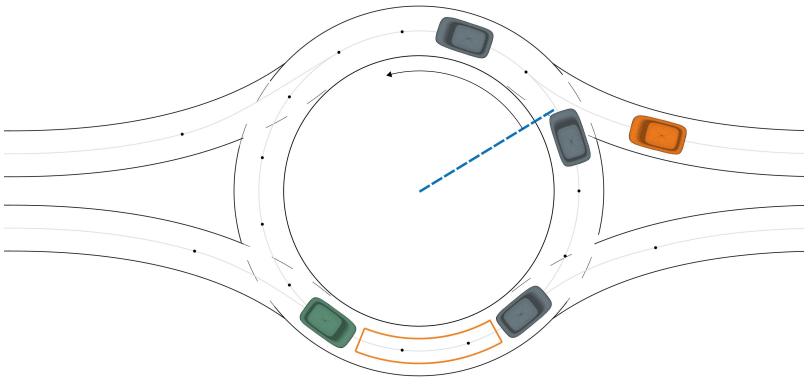

Figure 7.2 – Illustration of the example scenario. The green vehicle represents the ego vehicle, who intends to facilitate the merging maneuver of the orange vehicle. The inter-vehicle gap highlighted in orange, represents the gap the ego vehicle has control over, hence the one it would try to modify so that the orange vehicle merges into it.

possibility of behaving cooperatively with respect to the merging vehicle (orange car). Moreover, the highlighted inter-vehicle gap in Fig. 7.2 represents the one the ego vehicle has control over.

As was discussed in Chapter 5, the merging decision of an approaching vehicle could be represented through the so-called *gap-acceptance decision map* if the merging trajectory it is pursuing was known. In the setup herein considered, such a merging trajectory cannot be exactly known due to the presumed lack of communication between vehicles. However, we could tackle the design of a cooperative yielding planner by assuming a certain merging trajectory, which would then represent the minimum level of reactivity that the agent subject of the cooperation should exhibit for the cooperation to materialize successfully. Specifically, considering a merging vehicle $\mathcal{O}_{\mathrm{C}} \in \mathcal{O}_{\mathrm{obs,C}}$, the distance $\delta_{\mathcal{O}_{\mathrm{C}}}$ between the vehicle's current position and its merging spot (i.e. its decision spot), and its observed current state $x_{\mathcal{O}_{\mathrm{C}}}(t_0)$, we design a cooperative yielding maneuver able to accommodate constantly accelerating merging maneuvers with acceleration $\underline{a}_m > 0$. Thus, such acceleration would represent the minimum acceleration the incoming vehicle should be willing to apply for it to be able to use the emerging gap. Such an assumption allows us to calculate the corresponding maneuver target

$$\mathcal{T}_{\mathcal{O}_{\mathrm{C}}} = (\tau_{\mathcal{O}_{\mathrm{C}}}, v_{\mathcal{O}_{\mathrm{C}}}) \tag{7.1}$$

$$\tau_{\mathcal{O}_{\mathrm{C}}} = \underline{a}_m{}^{-1}(-v_{\mathcal{O}_{\mathrm{C}}}(t_0) + \sqrt{v_{\mathcal{O}_{\mathrm{C}}}(t_0)^2 + 2\underline{a}_m\delta}) \tag{7.2}$$

$$v_{\mathcal{O}_{\mathrm{C}}} = v_{\mathcal{O}_{\mathrm{C}}}(t_0) + \underline{a}_m\tau_{\mathcal{O}_{\mathrm{C}}}, \tag{7.3}$$

and therefore construct its associated gap-acceptance decision map.

In other words, we could then calculate the sets $\mathcal{X}^{\mathrm{F}}_{\mathrm{SCF}}$ and $\mathcal{X}^{\mathrm{R}}_{\mathrm{SCF}}$, composing the *gap-acceptance decision map* for such a presumed MT, which are represented in Fig. 7.3. As discussed in Section 5.3.3, the gap-acceptance decision map is composed of the regions where the front and rear limits of the gap need to be for the gap to be considered safe by the corresponding merging vehicle. As an example, note how the state of the highlighted inter-vehicle gap in Fig. 7.2, is shown in Fig. 7.3 by an orange segment whose extremes represent the state of the gap's limits. From the decision map, one could easily infer that the rear limit of the gap would be considered safe. Nonetheless, the gap's front limit would not meet the safety constraint and, therefore, the gap would not be accepted.

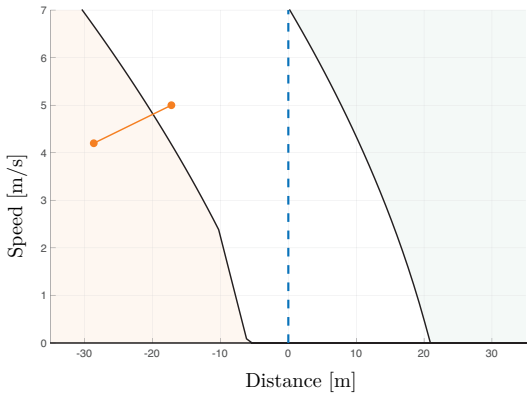

Figure 7.3 – Illustration of the *gap-acceptance decision map* corresponding to the merging trajectory the circulatory vehicle in Fig. 7.2 would presume approaching vehicles apply (see Section 5.3.3 for details on the gap-acceptance decision map). Moreover, the state of the gap ahead of the ego vehicle in Fig. 7.2 is represented by the orange segment. As the gap does not bridge the two sets of the gap-acceptance map, the current state of the gap would not be accepted.

The decision map can also be used to determine whether a certain behavior of the vehicles delimiting the gap would make the merging vehicle accept it. For instance, if the vehicles that are delimiting the highlighted gap in Fig. 7.2 drove at a constant speed, the state of the gap would evolve over time as shown in Fig. 7.4. The color code used there indicates whether a merging vehicle (using the presumed decision map) would consider safe: (—) only the rear limit, (—) only the front limit, or (—) none of them. In particular, as no future time is observed at which both gaps' limits would be considered safe, the merging vehicle would not be expected to accept the gap.

Changing the evolution of the gap so that it can safely accommodate a merging maneuver is possible. Indeed, it could be done by making the vehicle delimiting the front limit of the gap accelerate, or the one defining the gap's rear limit decelerate. However, vehicles could typically be assumed to be driving at the maximum speed they consider safe. Hence, trying to make the vehicle delimiting the gap's front limit cooperate by increasing its speed would produce discomfort and, potentially, an unsafe situation. For this reason, we assume throughout this chapter that the ego vehicle can only cooperate by acting on the state of the gap it has ahead, and not the one behind.

7.4 Yielding maneuver planner

The examples illustrated in the previous section provide a relatively straightforward framework to evaluate the feasibility of performing a deliberate yielding maneuver, as well as to quantify the cooperation effort that would potentially be necessary to cooperate successfully.

A summary of the strategy is provided in Alg. 3. The approach consists in checking, for every cooperative maneuver candidate $\mathcal{M} \in \mathcal{M}$, whether a yielding maneuver could be performing and, if so, calculating the minimum feasible cooperative deceleration and its impact on traffic. Subsequently, the cooperation possibilities are compared and the most beneficial one is chosen.

In the following sections, we address the steps of the process one at a time.

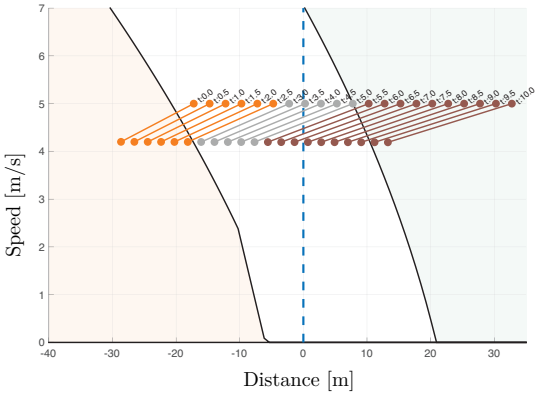

Figure 7.4 – Decision map of the presumed merging trajectory, and the evolution of a gap whose limits move at constant speed. The color code used represents whether: (—) only the gap's rear limit, (—) neither of the gap's limits, and (—) only the gap's front limit would be considered safe by the merging vehicle.

Algorithm 3: Implicitly cooperative maneuver planner workflow.

Input: $\mathcal{M}$
Output: $\mathcal{M}^{\text{IC}}, \mathcal{D}, \mathcal{V}, \mathcal{C}$
for $\mathcal{M} \in \mathcal{M}$ **do**
  $\mathcal{X}^{\text{F}}_{\text{SCF}}, \mathcal{X}^{\text{R}}_{\text{SCF}} \leftarrow$ the states characterizing the gap-acceptance decision map of vehicle $\mathcal{O}_{\text{C}}$;
  $\tau^{\text{tc}}_{\mathcal{M}} \leftarrow$ time window to behave cooperatively;
  $\underline{d}^{\text{c}}_{\mathcal{M}} \leftarrow \infty$ initialize the value of the cooperative deceleration;
  $q_{\text{Y},\mathcal{M}} \leftarrow \infty$ initialize the value of the maneuver impact on traffic;
  if *ValidYield*$(x_0, d^c, \tau^c_{\mathcal{M}}, \mathcal{O}_C)$ **then**
    $\underline{d}^{\text{c}}_{\mathcal{M}} \leftarrow$ minimum deceleration that would allow the cooperation;
    $q_{\text{Y},\mathcal{M}} \leftarrow$ impact the maneuver is expected to have on the overall traffic;
  end
end
$\mathcal{M}^{\text{IC}} = \arg\max_{\mathcal{M}\in\mathcal{M}} \{q_{\text{Y},\mathcal{M}}\}$;
$(\mathcal{D}, \mathcal{V}, \mathcal{C}) \leftarrow$ targets and constraints to impose on the trajectory.

7.4.1 Yielding trajectory

We start here by characterizing the yielding trajectory template the ego vehicle would consider in order to cooperate with an incoming vehicle. Specifically, we consider the yielding trajectory to be a constantly decelerating one, as long as the speed stays above a certain threshold $\underline{v}^{\text{c}}$. That is, we assume a deceleration profile

$$d(\tau) = \begin{cases} d' & \text{if } v(\tau) \geq \underline{v}^{\text{c}} \\ 0 & \text{otherwise} \end{cases} , \tag{7.4}$$

with d' showing a certain targeted deceleration value, and $\underline{v}^{\text{c}}$ being a design parameter showing the minimum cooperative speed the ego vehicle would be willing to drive at for the sake of cooperating.

Consequently, given the initial state x_0 of the ego vehicle, its expected state in a time interval τ

if the deceleration profile was applied would be calculated as:

$$x(t_0+\tau) = (\delta(t_0+\tau), v(t_0+\tau)), \tag{7.5}$$

$$v(t_0+\tau) = \begin{cases} v_0 - d'\tau & \text{if } \tau \leq \overline{\tau}_0^{\mathrm{c}} \\ \underline{v}^{\mathrm{c}} & \text{otherwise} \end{cases}, \tag{7.6}$$

$$\delta(t_0+\tau) = \begin{cases} v_0\tau - 0.5d'\tau^2 & \text{if } \tau \leq \overline{\tau}_0^{\mathrm{c}} \\ \delta(\overline{\tau}_0^{\mathrm{c}}) + \underline{v}^{\mathrm{c}}(\tau - \overline{\tau}_0^{\mathrm{c}}) & \text{otherwise} \end{cases}, \tag{7.7}$$

with

$$\overline{\tau}_0^{\mathrm{c}} \coloneqq d^{-1}(v_0 - \underline{v}^{\mathrm{c}}) \tag{7.8}$$

being the time interval during which the ego vehicle could be decelerating while its speed stays above the minimum cooperative one.

For the sake of notation, let us encapsulate the process above within the auxiliary function $\texttt{Yield}(x_0, d', \tau)$, which would return the state $x(t_0+\tau)$, given the initial state x_0, a deceleration d', and a certain time interval τ.

7.4.2 Expected evolution of the front limit of the gap

As was briefly commented in Section 7.3, the cooperative effort required from the ego vehicle to bring the gap to a state that could be accepted by a merging vehicle depends on the behavior of the vehicle delimiting the front limit of the gap itself. For the sake of simplicity, we will consider the gap's front limit to evolve at its current speed. Note, however, that relaxing this assumption to account for accelerating trajectories would also be possible and relatively straightforward.

The state of the front limit of the gap in a time interval τ would then be calculated as

$$x_{g_{\mathrm{F}}}(t_0+\tau) = (\delta_{g_{\mathrm{F}}}(t_0+\tau), v_{g_{\mathrm{F}}}(t_0+\tau)), \tag{7.9}$$

$$s_{g_{\mathrm{F}}}(t_0+\tau) = \delta_{g_{\mathrm{F}}}(t_0) + v(t_0)\tau, \tag{7.10}$$

$$v_{g_{\mathrm{F}}}(t_0+\tau) = v_{g_{\mathrm{F}}}(t_0)). \tag{7.11}$$

An important piece of information we can infer from such an assumption is the time at which the state of the gap's front limit would first be considered safe by the subject of the cooperation. In other words, the time at which the *cooperation window* begins.

Definition 13 (Cooperation window)**.** *A cooperation window $\tau^c = \{\tau : \tau \in [\tau_m^c, \tau_M^c]\}$, defined through its bounds τ_m^c and τ_M^c, represents the set of time intervals at which the decision the cooperative behavior aims to facilitate only depends on the ego vehicle's state.*

Specifically, given the formulation of $\mathcal{X}_{\mathrm{SCF}}^{\mathrm{F}}$, the maneuver candidate $\mathcal{M} = \{\pi, \varnothing, \pi_0, O, \varnothing, \{\mathcal{O}_{\mathrm{C}}, \delta_{\mathrm{C}}\}\}$ representing the cooperative maneuver, and the state $\hat{x}_{\mathcal{O}_{\mathrm{C}}} = (0, v_{\mathcal{O}_{\mathrm{C}}})$ the vehicle subject of the cooperation is expected to have at the time of merging (using its decision spot as the distance reference), the time $\tau_{\mathcal{M}}^{\mathrm{c}}$ at which the cooperation window begins can be simply calculated as

$$\tau_{\mathcal{M}}^{\mathrm{c}} \coloneqq \min\left\{\tau : x_{g_{\mathrm{F}}}(t_0+\tau) \in \mathcal{X}_{\mathrm{SCF}}^{\mathrm{F}}(\mathcal{T}_{\mathcal{O}_{\mathrm{C}}}, \hat{x}_{\mathcal{O}_{\mathrm{C}}})\right\}. \tag{7.12}$$

Once we have identified the beginning of the cooperation window, and letting the design parameter τ^{c} denote the minimum targeted time window size, we can further define the *minimum cooperation*

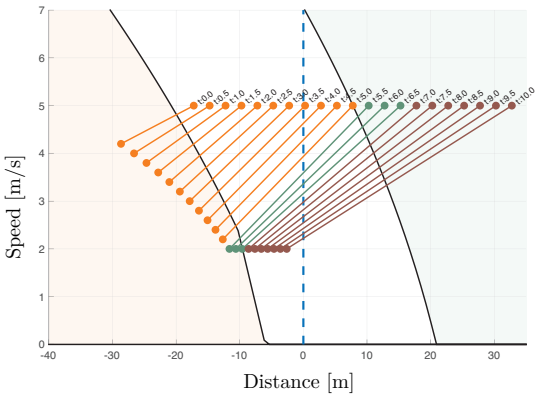

Figure 7.5 – Evolution of the gap in the example scenario when the maximum cooperative deceleration is applied. Colors represent whether: (—) only the gap's rear limit, (—) both of the gap's limits, and (—) only the gap's front limit would be considered safe by the merging vehicle.

window as

$$\tau_{\mathcal{M}}^{\mathrm{tc}} \coloneqq [\tau_{\mathcal{M}}^{\mathrm{c}}, \tau_{\mathcal{M}}^{\mathrm{c}} + \tau^{\mathrm{c}}], \tag{7.13}$$

such that for a yielding maneuver to be considered feasible, it should produce a safe gap to merge, for all time intervals $\tau \in \tau_{\mathcal{M}}^{\mathrm{tc}}$. This condition is further imposed to accommodate a certain reaction time that the merging vehicle might need to recognize the situation as safe and be aware of the cooperation.

7.4.3 Feasibility of the yielding maneuver

Once we have identified the minimum cooperation window, we continue by evaluating whether a feasible cooperative yielding maneuver exists. In order to do that, we introduce an additional design parameter $\overline{d}^{\mathrm{c}}$ representing the maximum deceleration the ego vehicle could apply to cooperate. Hence, determining whether a yielding maneuver exists would be equivalent to checking whether the constraint

$$\exists \tau \in \tau_{\mathcal{M}}^{\mathrm{tc}} | \texttt{Yield}(x_0, \overline{d}^{\mathrm{c}}, \tau) \in \mathcal{X}_{\mathrm{SCF}}^{\mathrm{R}}(\mathcal{T}_{\mathcal{O}_{\mathrm{C}}}, \hat{x}_{\mathcal{O}_{\mathrm{C}}}) \tag{7.14}$$

holds, with $\texttt{Yield}(\cdot)$ representing the state the ego vehicle would have at τ if it triggered a yielding maneuver applying the maximum cooperative deceleration $\overline{d}^{\mathrm{c}}$.

For the example scenario shown in Fig. 7.2, the expected progression of the gap when applying a deceleration $\overline{d}^{\mathrm{c}} = 0.4\mathrm{m/s}^2$ is illustrated in Fig. 7.5. Note how, in the described situation, there is a time window of approximately 1s during which the gap could be accepted by the merging vehicle of interest. Thus, a feasible yielding maneuver would exist in this case, iff $\tau^{\mathrm{c}} \leq 1$.

Furthermore, let us encapsulate the process of checking whether a deceleration d would result in a feasible yielding maneuver for a certain cooperative window $\tau_{\mathcal{M}}^{\mathrm{tc}}$ within the auxiliary operator

$$\texttt{ValidYield}(x_0, d, \tau_{\mathcal{M}}^{\mathrm{tc}}, \mathcal{O}_{\mathrm{C}}) = \begin{cases} 1 & \text{if } \exists \tau \in \tau_{\mathcal{M}}^{\mathrm{tc}} | \texttt{Yield}(x_0, d^{\mathrm{c}}, \tau) \in \mathcal{X}_{\mathrm{SCF}}^{\mathrm{R}}(\mathcal{T}_{\mathcal{O}_{\mathrm{C}}}, \hat{x}_{\mathcal{O}_{\mathrm{C}}}) \\ 0 & \text{otherwise} \end{cases}. \tag{7.15}$$

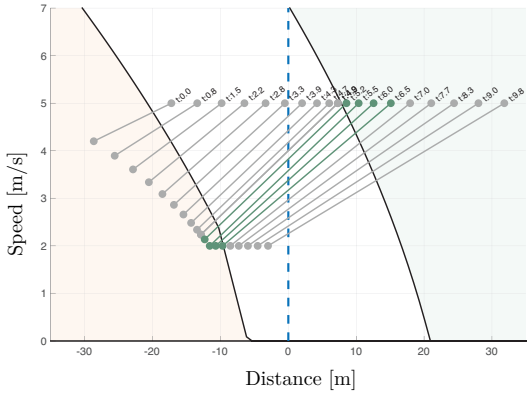

Figure 7.6 – Example of the evolution of the gap in the example scenario, when the minimum cooperative deceleration feasible is applied. The color code used represents in (—) the gap's states that would not be accepted, and in (—) the ones that would.

7.4.4 Minimum effort yielding maneuver

Once the feasibility of the cooperative yielding maneuver has been checked, we continue by calculating the minimum deceleration $\underline{d}^{\mathrm{c}}_{\mathcal{M}}$ that could be expected to render a successful cooperative yielding maneuver. That is

$$\underline{d}^{\mathrm{c}}_{\mathcal{M}} = \min \left\{ d \in [0, \overline{d}^{\mathrm{c}}] : \texttt{ValidYield}(x_0, d, \tau^{\mathrm{c}}_{\mathcal{M}}, \mathcal{O}_{\mathrm{C}}) \right\}. \tag{7.16}$$

Given the numerical efficiency with which the validity of a yielding maneuver can be checked, such a deceleration value can be calculated by checking the condition for a finite set of deceleration values, and then selecting the minimum one for which the constraint holds.

When such a process is applied to the example scenario, we obtain the result in Fig. 7.6 for the parameters in Tab. 7.1. There, the progression of the gap for the minimum cooperative deceleration $\underline{d}^{\mathrm{c}}_{\mathcal{M}} = 0.4$ is shown, along with the time instants at which the gap would be considered safe.

Table 7.1 – Design parameters

	$\overline{d}^{\mathrm{c}}$	$\underline{v}^{\mathrm{c}}$	$\underline{a}_m$	τ^{c}
Value	1.5	4	1.5	2
Unit	$\mathrm{m/s^2}$	m/s	$\mathrm{m/s^2}$	s

7.4.5 Yielding maneuver scoring

Once the minimum cooperative deceleration has been found, and before triggering the yielding maneuver itself, we need to evaluate whether performing the yielding maneuver is thought to be beneficial for the overall traffic coordination. Specifically, we will base the decision on the impact the yielding maneuver is expected to have on the fairness of the incoming traffic state across incoming lanes. Such a proposed decision-making strategy is built on the idea that, in the traffic scenario of interest, decelerating inside the traffic stream enlarges the gap ahead of the vehicle, but at the same time reduces the gap behind. Thus, yielding to a vehicle merging into the roundabout by a certain incoming lane would potentially result in delaying an approaching vehicle at the previous one, and

also facilitating the maneuver of a vehicle in the next incoming lane. This new configuration would only be desirable if the overall fairness of the scenario increases.

We will address this step by first calculating a fairness index related to the currently observed approaching velocities across incoming lanes, and then comparing it with an approximated quantification of the impact the yielding maneuver could have on them.

Let us begin by denoting as $\mathcal{O}_o^{\mathrm{I}} \subseteq \mathcal{O}_{\mathrm{obs}}$ the subset

$$\mathcal{O}_o^{\mathrm{I}} = \{o \in \mathcal{O}_{\mathrm{obs}} : p_o \in \mathcal{L}_o\} \tag{7.17}$$

of observed obstacles that are positioned in the incoming lane $\mathcal{L}_o$, and by introducing

$$\gamma_o = \begin{cases} 1 & \text{if } \mathcal{O}_o^{\mathrm{I}} \neq \varnothing \\ 0 & \text{otherwise} \end{cases} \tag{7.18}$$

to show whether a certain incoming lane o is observed to be empty or not. Then, the vector

$$\mathbf{v}_{\mathrm{in}} = \left(v_1^{\mathrm{t}}, \cdots, v_{n_{\mathcal{L}_{\mathrm{in}}}}^{\mathrm{t}}\right) \tag{7.19}$$

would contain the total speed observed in every incoming lane o, calculated as

$$v_o^{\mathrm{t}} = \begin{cases} \sum_{i \in \mathcal{O}_o^{\mathrm{I}}} v_i & \text{if } \gamma_o = 1 \\ v_{\mathrm{M}} & \text{otherwise} \end{cases} . \tag{7.20}$$

The effect that the yielding maneuver could potentially have on the total speed of the incoming lanes would be approximated as

$$\hat{\mathbf{v}}_{\mathrm{in}}(o) = \mathbf{v}_{\mathrm{in}} + \left(\gamma_1\beta_1, \cdots, \gamma_{n_{\mathcal{L}_{\mathrm{in}}}}\beta_{n_{\mathcal{L}_{\mathrm{in}}}}\right) \tag{7.21}$$

with

$$\beta_i = \begin{cases} 1 & \text{if } i = o \\ -0.9 & \text{if } i = o^- \\ 0.9 & \text{if } i = o^+ \\ 0 & \text{otherwise} \end{cases} , \tag{7.22}$$

where o^- and o^+ represent, respectively, the incoming lanes on the left and on the right of the incoming lane o.

Then the suitability of yielding to a vehicle approaching by the lane $o \in \mathcal{L}_{\mathrm{in}}$ is quantified as

$$\phi_o = \texttt{Fairness}(\hat{\mathbf{v}}_{\mathrm{in}}(o)) - \texttt{Fairness}(\mathbf{v}_{\mathrm{in}}) , \tag{7.23}$$

enabling us to simply score the yielding maneuver candidates as

$$\mathcal{Q}_{\mathrm{Y}}(\mathcal{M}) = \begin{cases} \phi_{\texttt{orig}(\mathcal{O}_{\mathrm{C}})} & \text{if } \phi_{\texttt{orig}(\mathcal{O}_{\mathrm{C}})} > 0 \wedge \texttt{ValidYield}(x_0, d, \tau_{\mathcal{M}}^{\mathrm{c}}, \mathcal{O}_{\mathrm{C}}) \\ 0 & \text{otherwise} \end{cases} , \tag{7.24}$$

with $\mathcal{O}_{\mathrm{C}}$ being the object identified as the possible subject of cooperation (included within $\mathcal{M}$), and $\texttt{orig}(\mathcal{O}_{\mathrm{C}})$ showing the incoming lane it is observed at.

7.4.6 Maneuver selection and planner output

The process described in the preceding subsections of this chapter allows the evaluation of the feasibility of a yielding maneuver w.r.t. a single merging vehicle $\mathcal{O}_{\mathrm{C}}$ that is identified as a possible target for cooperation, and included within the definition of a maneuver candidate $\mathcal{M} \in \mathcal{M}$. However, several cooperative maneuver candidates might be passed by the tactical planner. Therefore it is required that we chose only one to pursue. In particular, the process will simply consist of identifying the cooperative maneuver candidate that would be expected to bring the highest benefit to the overall traffic situation. That is

$$\mathcal{M}^{\mathrm{IC}} = \arg \max_{\mathcal{M} \in \mathcal{M}} \mathcal{Q}_{\mathrm{Y}}(\mathcal{M}). \tag{7.25}$$

The output that this maneuver planner returns should make the trajectory planner generate a constantly decelerating trajectory, corresponding to the pursued cooperative yielding maneuver. Such behavior will be achieved by setting the speed target as

$$\mathcal{V} = \begin{cases} (\epsilon, v_0 + -\underline{d}^{\mathrm{c}}_{\mathcal{M}^{\mathrm{IC}}} \epsilon) & \text{if } \mathcal{Q}_{\mathrm{Y}}(\mathcal{M}^{\mathrm{IC}}) > 0 \\ \varnothing & \text{otherwise} \end{cases}, \tag{7.26}$$

with ϵ representing an arbitrarily small time interval.

The safe car-following behavior with respect to the observed vehicles ahead would then be achieved by setting the safety constraint to

$$\mathcal{C} = \cup_{\mathcal{O} \in \mathcal{O}_{\mathrm{V}}} (\infty, x_{\mathcal{O}}, -a_{\mathrm{m}}). \tag{7.27}$$

Finally, distance targets are set as $\mathcal{D} = \varnothing$ as they are not required to execute this behavior.

7.5 Results

In this section, we assess the proposed implicitly cooperative yielding strategy at different levels. We start by presenting in Section 7.5.1 additional examples concerning the calculation of the minimum effort yielding maneuver. In doing so, we aim to gain a better intuition concerning the kind of traffic scene where the approach would deem feasible yielding to an incoming vehicle. Then, we continue by analyzing, in Section 7.5.2, the aggregated effect that the proposed cooperative planner would have when applied by a set of vehicles while driving in three different levels of traffic density. Furthermore, we conclude by analyzing, in Section 7.5.3, the change in the overall traffic coordination performance that the strategy could bring, averaged across a wide set of traffic configurations.

In subsequent sections, we will make use of several types of driver agents to quantify the benefit of the approach, whose behavior is summarized in Tab. 7.2. Specifically, we consider the perception layer not to be affected by occlusions at this stage, and agents not to be connected. Furthermore, agents adhere to different behavioral policies: R-agents follow a purely reactive behavior, and IC-agents perform self-serving driving maneuvers in a reactive manner and implement the implicitly cooperative maneuver planner proposed herein.

Furthermore, the value of the parameters considered throughout the chapter are those in Tab. 7.1.

Table 7.2 – Driver agents used in the experiments

	Perception	Communication	Self-serving maneuver planner	Cooperative maneuver planner
R-Agent	Perfect perception	None	Reactive	none
IC-Agent	Perfect perception	None	Reactive	Implicitly cooperative

7.5.1 Decision-making

Aiming at gaining a better intuition concerning traffic conditions our strategy would find it feasible to perform an implicitly cooperative yielding maneuver, we analyze, in this section, the decision-making aspect in a total of five traffic scenes. The results are represented in Fig. 7.7, where the traffic scene and the minimum-effort cooperative yielding maneuver are shown. Furthermore, the characteristics of the resulting least-effort yielding maneuver are shown in Tab. 7.3.

Table 7.3 – Example yielding scores

	Ex. 1	Ex. 2	Ex. 3	Ex. 4	Ex. 5
$\underline{d}^{\mathrm{c}}_{\mathrm{M}}$	-1.96	-0.58	0.23	0.23	0.40
τ^{w}	[0, 1]	[0.94, 1.94]	[4.2, 5.2]	[4.2, 5.2]	[6.66, 7.66]

According to the proposed analysis, a yielding maneuver could be successfully performed in all the scenarios shown, as indicated by the fact that green states can be seen in the expected gap evolution in all scenes.

In general, the algorithm seems appropriate and relatively flexible to determine the suitability of the yielding maneuver. In some cases, as in examples 1 and 2, the required minimum cooperative deceleration turns out to be negative, which means that the merging vehicle being studied could merge, even if the ego vehicle accelerates. These cases can be easily identified in Fig. 7.7 by observing that the evolution of the gap's rear limit when the minimum cooperative deceleration is applied increases its speed over time instead of decreasing it.

7.5.2 Single traffic scenario

The proposed strategy makes a decision based on a rather simplistic heuristic intended to approximate how the yielding maneuver would be expected to affect the fairness of the incoming traffic configuration. Presuming the real traffic evolution would differ from the one implicitly predicted by the proposed heuristic, it is therefore of interest to assess how the strategy would change the traffic dynamics in the long term if all vehicles in the scenario implemented it.

In this section, we aim to evaluate the impact the strategy would have if it was applied by a set of vehicles driving through a roundabout. In particular, we will consider a roundabout of 16m radius, 1 circulatory lane, and 3 legs with 1 incoming and 1 outgoing lane (i.e. a `16R1LR3L1I1O` roundabout). Moreover, we generate scenarios of 100 vehicles (i.e. `100V`), and three different incoming traffic configurations corresponding to an incoming traffic volume of 500vehs/h, 1500vehs/h, and 2500vehs/h evenly distributed among the incoming legs. In other words, we consider the incoming traffic configurations `500Q[1 1 1]`, `1500Q[1 1 1]`, and `2500Q[1 1 1]` (see Section 2.3.4 for details concerning our labeling strategy). Each of the three traffic scenarios considered is then simulated twice, considering all the vehicles in the scene to be driven by (case-1) R-Agents and (case-2) IC-Agents.

The results are shown in Fig. 7.8-7.16, where, for every pair of simulations, we compare:

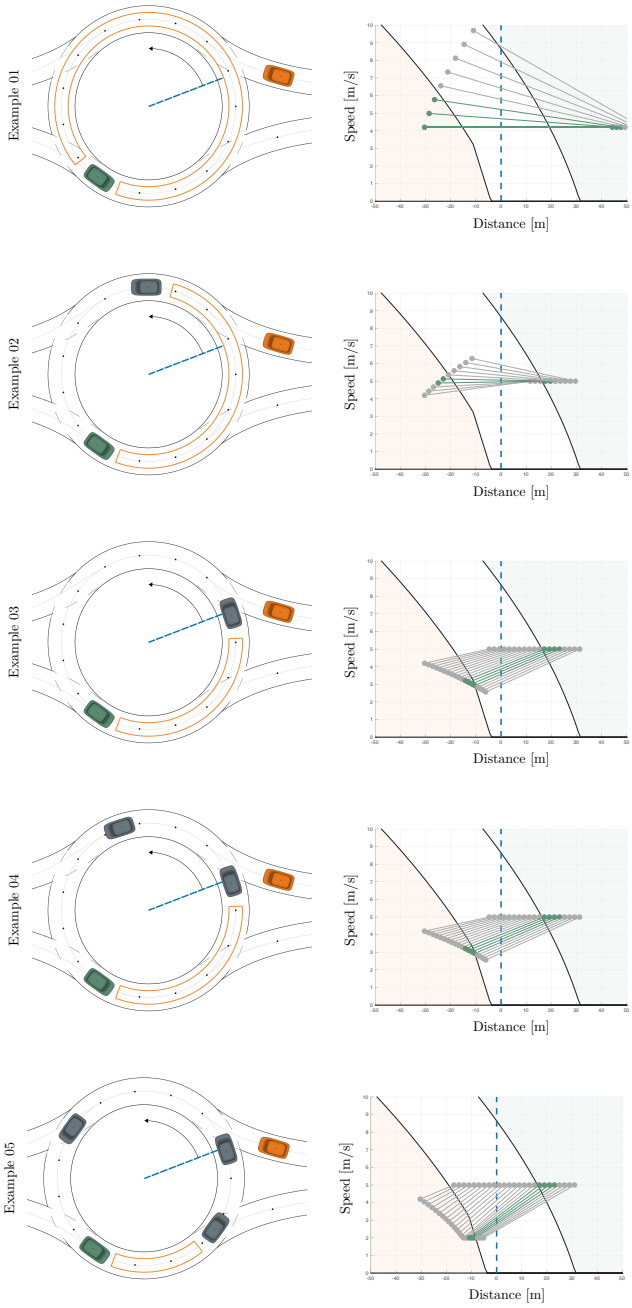

Figure 7.7 – Representation of the yielding decision-making mechanism in five different scenarios. Every row corresponds to a different example. On the left hand side, we represent the yielding scenario being considered. The ego vehicle is shown by the green vehicle, and it attempts to facilitate the merging maneuver of the orange vehicle. The dashed belue line show the reference from which distances are measured. On the right-hand side, we show the gap-accaptence decision map the ego vehicle expects the merging vehicle to use. Moreover, we show the gap's progression over time, if the ego vehicle applied the calculated minimum-effort deceleration in each case (as we did in Fig. 7.6). Segments in green, show the state of the gaps that would be expected to be accepted.

- the time-distance evolution of the traffic in the circulatory lane,
- the evolution of the incoming traffic in every incoming leg of the roundabout, and
- the distribution of some additional performance metrics concerning the travel time, travel speed, average jerk, and delay that the vehicles in the scenario experience.

Furthermore, we gather in Tab. 7.4 the registered values for the intersection throughput and the fairness with which the different performance metrics concerning the vehicles' trajectory are distributed among the vehicles.

Table 7.4 – Intersection throughput and fairness metrics

	Throughput [vehs/h]	15minTh. Firness [%]	TT. fairness [%]	TS. fairness [%]	J. fairness [%]	D. fairness [%]
16R1LR3L1I1O-100V-500Q[1 1 1]-RAgent	490	84	98	100	87	96
16R1LR3L1I1O-100V-500Q[1 1 1]-ICAgent	490	84	98	100	87	96
16R1LR3L1I1O-100V-1500Q[1 1 1]-RAgent	1338	95	98	99	82	85
16R1LR3L1I1O-100V-1500Q[1 1 1]-ICAgent	1360	97	98	99	87	84
16R1LR3L1I1O-100V-2500Q[1 1 1]-RAgent	1712	97	92	95	82	48
16R1LR3L1I1O-100V-2500Q[1 1 1]-ICAgent	1804	99	92	96	84	43

In low-density traffic (Fig. 7.8-7.10), the approach does not have any noticeable impact. Such a result was to be expected as the simulated traffic is so light, that circulating vehicles do not get a chance to coexist in the scenario with another vehicle that could benefit from their cooperation. Then, since the underlying self-serving behavior is reactive for both agents, the trajectories they follow are identical in both cases; to the point that Fig. 7.8-7.10 give the impression that we are representing only the behavior of one type of agents, when what is really happening is that the traces of both agents overlap perfectly.

In medium-density traffic (Fig. 7.11-7.13), some differences start to appear in the resulting trajectories. Firstly, we can notice that the cooperative behavior of the circulating vehicles changes the order in which vehicles merge into the roundabout. Interestingly, such changes in the crossing order cause significant differences in the long-term evolution of the traffic circulating inside the roundabout. The differences regarding the incoming traffic dynamics are as well subtle, yet we can clearly observe that the vehicles that need to stop before merging are different in both cases. In addition, the total number of vehicles that need to fully stop before merging decreases when the proposed cooperative behavior is applied. An interesting aspect concerning the high-level traffic indicators is that the fairness of the 15min-throughput increases, which indicates that the ratio at which vehicles drive through the roundabout is slightly more consistent.

In high-density traffic (Fig. 7.14-7.16), we start noticing bigger differences between the two compared agents. Concerning the circulating traffic, we can again observe the change in crossing order, which starts being noticeable as early as 30s after the simulation is triggered. Concerning the incoming traffic, the discussion presented in the previous case also applies. Nonetheless, a further interesting difference can be noticed. Indeed, it can be seen that the performed cooperative

maneuvers benefit the traffic approaching by the third incoming lane, while slightly delaying the traffic merging by the second incoming lane. The resulting situation is, therefore, a fairer one, as vehicles approaching by the different roundabout's leg merge into the intersection at a more similar rate. This behavior is to be expected as, in highly populated scenarios, decelerating to yield to some vehicle could be expected to reduce a gap that could otherwise be used by some other vehicle, which is aligned with the criterion used in the decision-making process. As in the previous case, a decrement of the variability of the 15min-throughput distribution can also be observed, not only in Tab. 7.4 but also in the corresponding throughput histogram in Fig. 7.16. Furthermore, in this case, the total intersection throughput was observed to increase in 100veh/h.

In general, we can observe that as IC-Agents are to behave reactively while merging, their merging maneuvers look very similar to those generated by R-Agents. However, due to the application of the proposed cooperative planner, their merging sequence, i.e. their crossing order, changes. The fact that the approach outperforms the baseline reactive planning policy in all the shown cases further suggests that the new resulting crossing order is more appropriate from the overall traffic point of view. The impact the strategy has on the overall through is positive yet moderate. Nonetheless, such a weak influence was also to be expected as we are proposing a strategy that makes vehicles decelerate inside a roundabout, an action that, given the circular geometry of the intersections, benefits some vehicles while negatively affecting other ones. The main virtue of the approach, however, is its capacity to render a fairer traffic scenario, whereby the waiting times of the vehicles and the frequency of merging maneuvers by the roundabout's legs are more evenly distributed.

7.5.3 Traffic coordination performance

In this section, we tackle an analysis of the strategy consisting of evaluating its average impact on a broader set of scenarios. The study is intended to analyze how the traffic density and the percentage of vehicles implementing the strategy affects the overall traffic performance. By reporting the distribution of the quality metrics over several sample scenarios, we aim to provide a measurement of the average improvement that could be expected, regardless of the specific origin-destination pattern and incoming traffic configuration.

Simulation batch setup

The set of simulation instances used to carry out the analysis was generated according to the parameters in Tab. 7.5 and the tree structure illustrated in Fig. 7.17. A total of 18 traffic scenarios are randomly created by combining different traffic inflow volume (`QI`) and distribution (`DI`). Furthermore, ten instances (`I`) of every final scenario are randomly created and simulated five times, where the penetration rate (`P`) of vehicles being driven by IC-Agents among R-Agents is varied.

Simulation batch results

The evaluation of the overall traffic coordination performance is done by analyzing the overall travel speed (Fig. 7.18), jerk (Fig. 7.19), and intersection throughput (Fig. 7.20) with respect to the incoming traffic configuration, and the penetration rate. In each of the shown plots, six different groups of boxplots are shown, which correspond to the six configurations of traffic inflow. Moreover, within each group, five different boxplots are represented, corresponding to the five considered penetration levels.

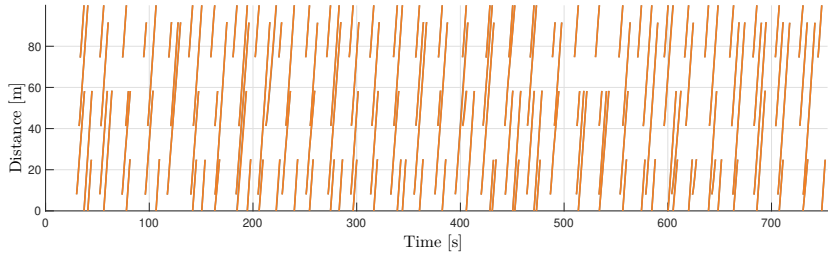

Figure 7.8 – Time-distance diagram representing the evolution over time of the vehicles in the circulatory lane, in the simulated scenario `16R1LR3L1I1O-100V-500Q[1 1 1]`. The trajectories of R-Agents and IC-Agents are represented by (—) and (—), respectively.

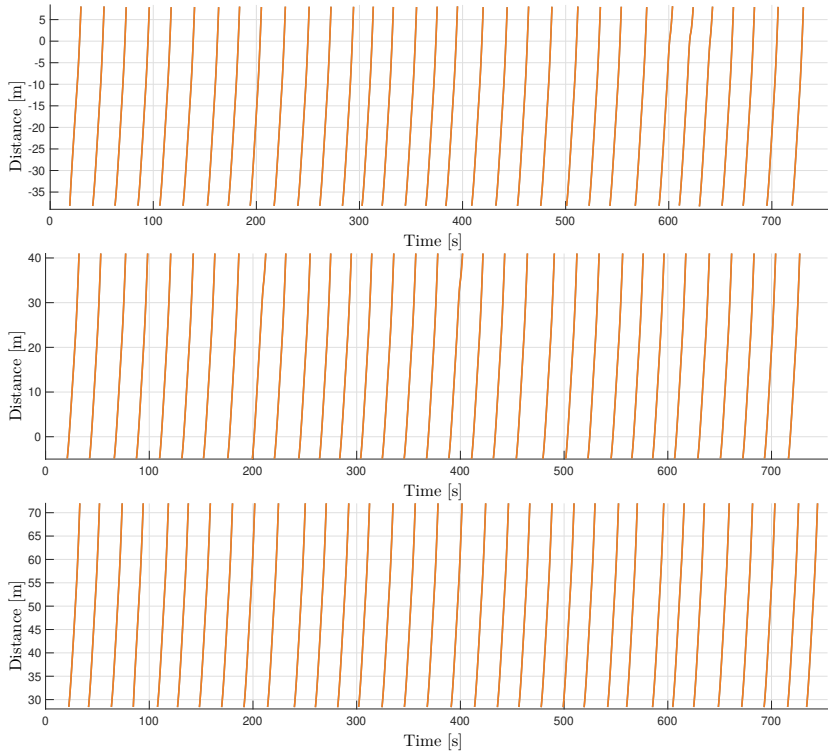

Figure 7.9 – Time-distance diagrams representing the evolution of the incoming traffic in every incoming lane in the simulated scenario `16R1LR3L1I1O-100V-500Q[1 1 1]`. The trajectories of R-Agents and IC-Agents are represented by (—) and (—), respectively.

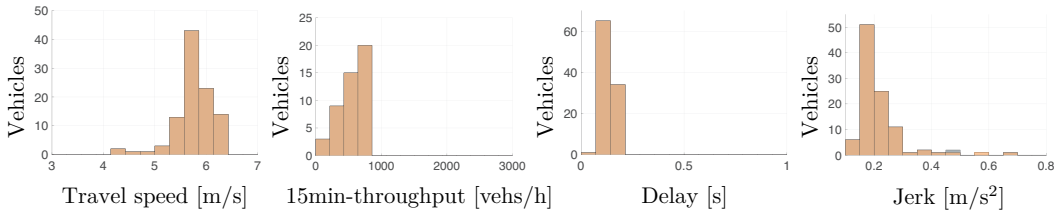

Figure 7.10 – Comparison of the histogram of the registered travel speed, 15-min throughput, arrival delay, and jerk of the vehicles in the scenario `16R1LR3L1I1O-100V-500Q[1 1 1]`, when driven by R-agents (gray) and IC-agents (orange).

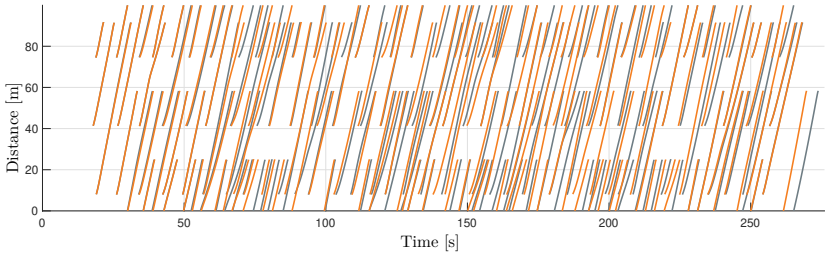

Figure 7.11 – Time-distance diagram representing the evolution over time of the vehicles in the circulatory lane, in the simulated scenario `16R1LR3L1I1O-100V-1500Q[1 1 1]`. The trajectories of R-Agents and IC-Agents are represented by (—) and (—), respectively.

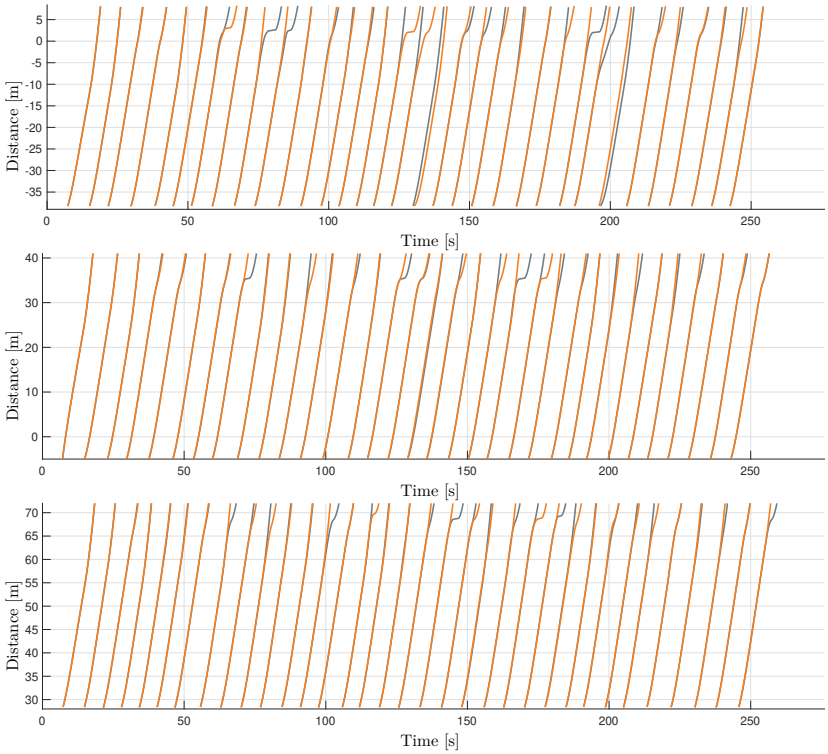

Figure 7.12 – Time-distance diagrams representing the evolution of the incoming traffic in every incoming lane in the simulated scenario `16R1LR3L1I1O-100V-1500Q[1 1 1]`. The trajectories of R-Agents and IC-Agents are represented by (—) and (—), respectively.

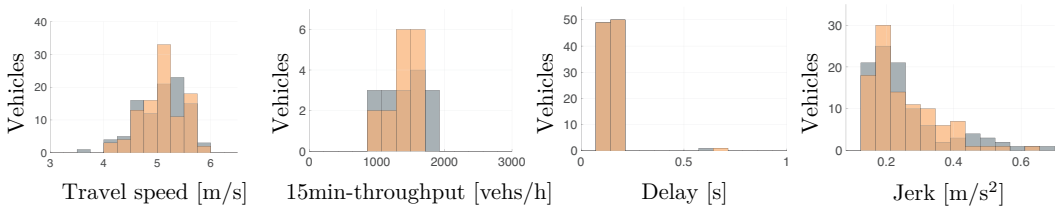

Figure 7.13 – Comparison of the histogram of the registered travel speed, 15-min throughput, arrival delay, and jerk of the vehicles in the simulated scenario `16R1LR3L1I1O-100V-1500Q[1 1 1]`, when driven by R-agents (gray) and IC-agents (orange).

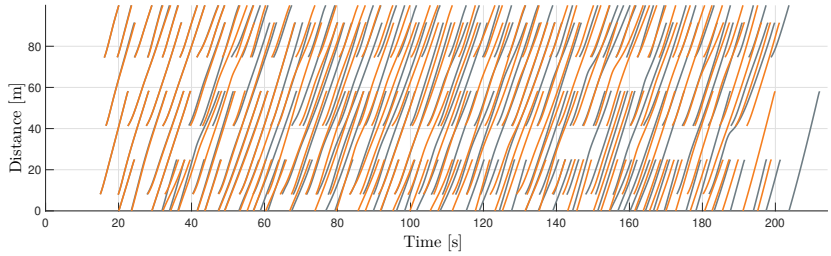

Figure 7.14 – Time-distance diagram representing the evolution over time of the vehicles in the circulatory lane, in the simulated scenario `16R1LR3L1I1O-100V-2500Q[1 1 1]`. The trajectories of R-Agents and IC-Agents are represented by (—) and (—), respectively.

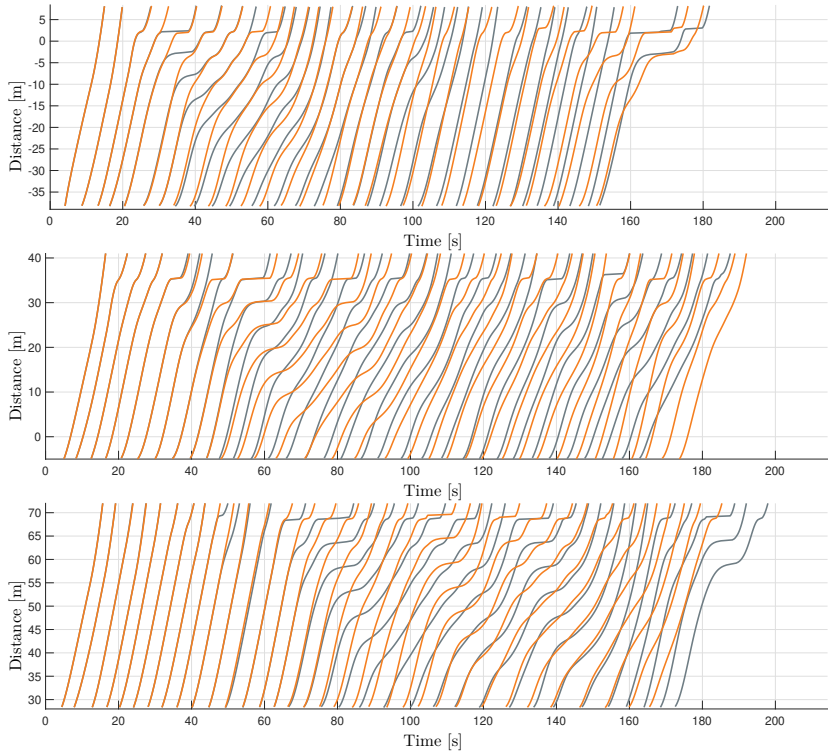

Figure 7.15 – Time-distance diagrams representing the evolution of the incoming traffic in every incoming lane in the simulated scenario `16R1LR3L1I1O-100V-2500Q[1 1 1]`. The trajectories of R-Agents and IC-Agents are represented by (—) and (—), respectively.

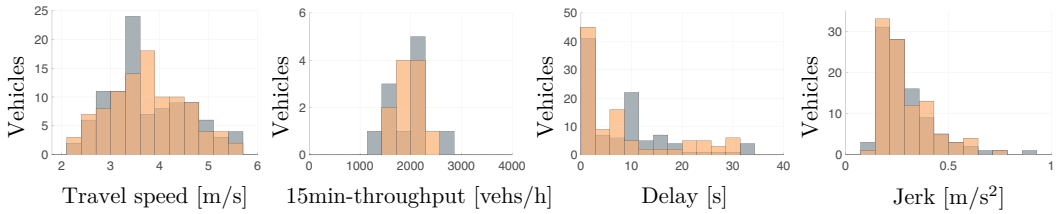

Figure 7.16 – Comparison of the histogram of the registered travel speed, 15-min throughput, arrival delay, and jerk of the vehicles in the scenario `16R1LR3L1I1O-100V-2500Q[1 1 1]`, when driven by R-agents (gray) and IC-agents (orange).

Table 7.5 – Simulation batch scenario configuration

	Value
G	16R1LR3L1I1O-100V
QI1	1000Q
QI2	1500Q
QI3	2000Q
QI4	2500Q
QI5	3000Q
QI6	3500Q
DI1	[1.0 1.0 1.0]
DI2	[1.0 0.5 1.0]
DI3	[0.5 1.0 0.5]
P1	0
P2	0.25
P3	0.5
P4	0.75
P5	1

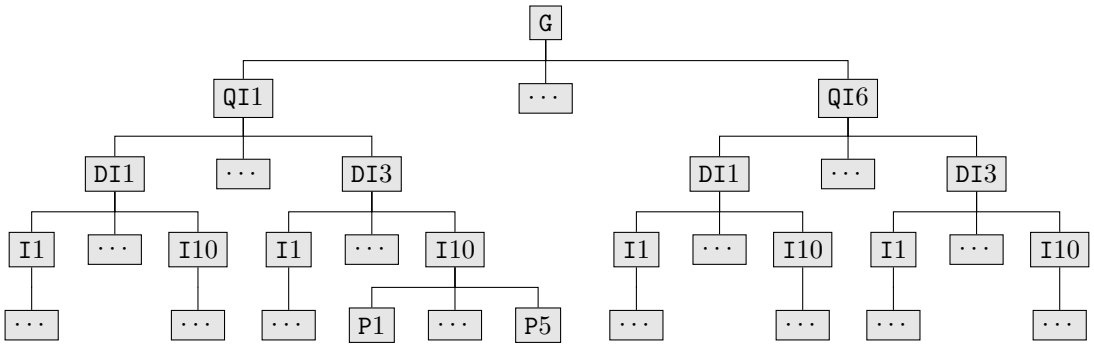

Figure 7.17 – Generation of the batch of simulated traffic scenarios.

Consistently with the results obtained in the previous section, the proposed implicitly cooperative planning strategy outperforms the reactive one for all the tested traffic configurations.

Regarding the distributions of overall travel speeds, we observe that the strategy does not have a strong impact on the resulting overall values, but it does have one on the fairness with which the speed is distributed among the agents. This effect was somehow to be expected, as the strategy was formulated while taking into consideration the total speed fairness across incoming lanes.

Considering the distribution of the average jerk applied by the vehicles, we observe that the average jerk slightly increases with our strategy, but such an increment comes along an increment in the fairness with which it is distributed. Once again, as we are proposing a strategy that encourages circulating vehicles to decelerate altruistically, the increase in average jerk was to be expected.

Finally, regarding the total intersection throughput and the distribution of 15min-throughput values, we can conclude that the proposed cooperative maneuver improves the intersection throughput compared to the baseline reactive strategy presented in Chapter 5. The results showed an increment of up to 100veh/s for 100% penetration rate of IC-agents (i.e. up to 7% improvement w.r.t. the baseline reactive approach), which is consistent with the results obtained in the previous Section. Such an increment is indeed a very subtle one, but still reasonable taking into consideration that the strategy is solely based on inducing decelerations on the circulating vehicles.

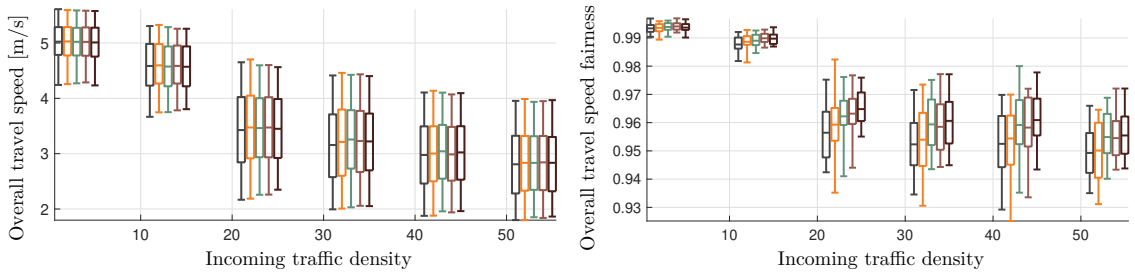

Figure 7.18 – On the left-hand side, boxplots representing the distribution of overall travel speed for different incoming traffic inflow volumes and configurations. On the right-hand side, the fairness with which the overall travel speed is distributed among the vehicles in the scenarios.

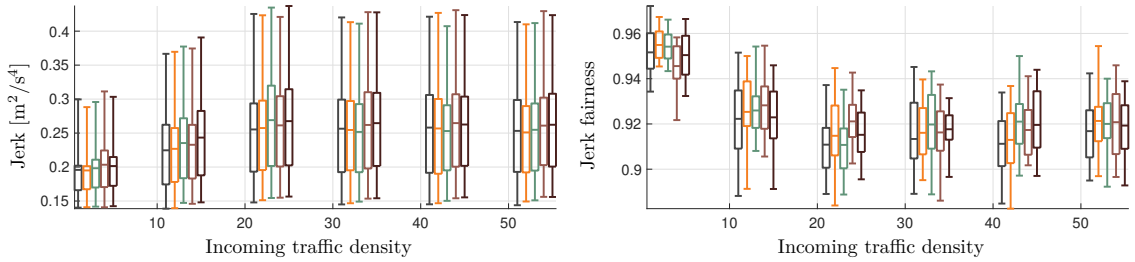

Figure 7.19 – On the left-hand side, boxplots representing the distribution of jerk for different incoming traffic inflow volumes and configurations. On the right-hand side, the fairness with which the jerk is distributed among the vehicles in the scenarios.

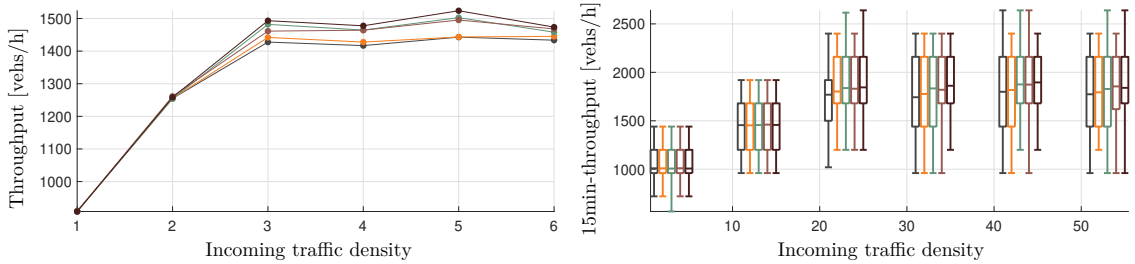

Figure 7.20 – On the left-hand side, the total intersection throughput registered for different incoming traffic density, and values of the penetration rate of IC-agents. On the right-hand side, boxplots representing the distribution of 15min-throughput for different incoming traffic inflow configurations and penetration rates.

7.6 Conclusions

In this chapter, we studied a method that allows AVs to execute altruistic yielding maneuvers with the objective of cooperating with surrounding unconnected vehicles that follow a conflicting path and do not have the right of way. The proposed approach consists of assessing whether the evolution of the gap the ego vehicle has control over (i.e. the one right ahead of it) could be accepted by the vehicle that is the subject of the cooperation if the ego vehicle followed a constantly decelerating

trajectory. The strategy is tackled by defining the merging trajectory the cooperation is expected to accommodate, and then analyzing the expected progression of the gap w.r.t. the gap-acceptance decision map presented in Section 5.3.3. Moreover, the decision concerning the execution of a feasible yielding maneuver is made by approximately quantifying the impact that the yielding maneuver would have on the fairness with which the speed of the vehicles approaching the intersection is distributed among the incoming lanes.

The results shown stress that the method allows the successful execution of deliberate yielding maneuvers and that the proposed simplistic decision-making heuristic does have a positive impact on the scenario. Concerning the traffic coordination performance, the impact in terms of intersection throughput is subtle but positive, although the more noteworthy effect concerns the fairness of the overall traffic evolution.

Moreover, the effectiveness of the approach indicates that assuming a constant speed of the vehicle delimiting the front limit of the gap, as well as the simplistic decision-making heuristic used to trigger the yielding maneuvers are valid to address the problem at hand. Note indeed that, even though those assumptions were made, the vehicles included in the simulations were not encouraged in any way to follow such behavior.

Furthermore, one could claim that the improvement of the overall traffic performance is too modest. However, it is worth stressing that such an improvement is being caused by a strategy that makes vehicles decelerate while driving inside roundabouts, a cause-effect that might, a priori, appear counterintuitive.

The proposed approach does, however, have several limitations that might require further exploration. On the one hand, the approach is built on the assumption that vehicles in need of cooperation (the vehicles approaching the roundabout in our case) are correctly detected by the ego vehicle. Although that would be a fair assumption in scenarios like highways, it is possible that at roundabouts, occlusions caused by the central island prevent the ego vehicle from having an accurate estimation of the speed with which the approaching vehicles drive towards the intersection. On the other hand, even though the proposed method could be easily extended to multi-lane roundabouts, one would face some additional challenges in the process. Specifically, one should take into account that, in those cases, the merging maneuver of approaching vehicles would as well depend on the behavior of the vehicles on the other circulatory lanes, which might make the efficacy of the method, as well as its positive impacts, even more modest. The method would, however, be expected to be still useful as is, in situations where the ego vehicle drives in the outermost circulatory lane of multi-lane roundabouts, and at single-lane roundabouts in general. In those situations, the ego vehicle would have direct control of the merging decision of those vehicles aiming to merge into the outermost lane.

Despite the discussed limitations, the proposed method allows AVs to perform yielding maneuver selectively and effectively, as well as to increase the overall fairness of the traffic scenario while having a subtle but positive impact on the total intersection throughput.

8 Predictive-Reactive Self-Serving Planning

In Chapter 6, we addressed a communication-based planning strategy able to perform self-serving and cooperative driving maneuvers. Following that, a method to perform altruistic driving maneuvers without the need to communicate was studied in Chapter 7. A self-serving reactive planner was also presented in Chapter 5, which was intended to serve as a simplistic baseline behavior with respect to which other planning strategies could be compared. It was, however, discussed that the reactive self-serving planning method could be extended for it to profit from longer traffic predictions, which is precisely the task that we address in this chapter.

The reactivity and simplicity of the self-serving reactive planner in Chapter 5 are its greater strengths, and at the same time, its most significant limitations. On the one hand, it turned out to be a reasonable and easy to compute strategy. On the other hand, however, it required the use of very short-term traffic predictions and motion plans, which prevents the strategy from taking full advantage of the trajectory planning mechanism described in Section 4.5. In addition, by only considering short planning horizons, the level of anticipation that the planner can achieve is strongly constrained. Furthermore, as the strategy only accounts for the possibility of moving forward in the way dictated by the IDM, the solution space considered there for decision-making is very restricted. These limitations will be addressed in this chapter.

Our main objective is designing a strategy that is effective and safe by design, despite the uncertainty stemming from considering longer predictions and the uncertainty of the perception output. Two main extensions are presented w.r.t. the approach in Section 4.5. Specifically, we aim to use a more general and accurate approximation of the solution space available, as well as to formulate a method to quantify the probability of the maneuver targets being safe for longer predictions.

In this chapter, whose content is based on our previous publication [18], we investigate a self-serving maneuver planning strategy capable of planning safe motions in traffic scenes like the one in Fig. 8.1. That is, where the ego vehicle's perception system is affected by occlusions and other perception inaccuracies. The strategy is said to be predictive-reactive, as it makes use of longer traffic predictions while remaining ready to safely react to environmental changes if necessary.

At the core of the proposed method lies the realization that uncertainty constrains the number of trajectories that can be pursued without jeopardizing the availability of reacting safely if the context does not evolve as it is expected. However, at the same time, uncertainty about the future traffic state enables us to consider as well that traffic situations might mistakenly appear inappropriate.

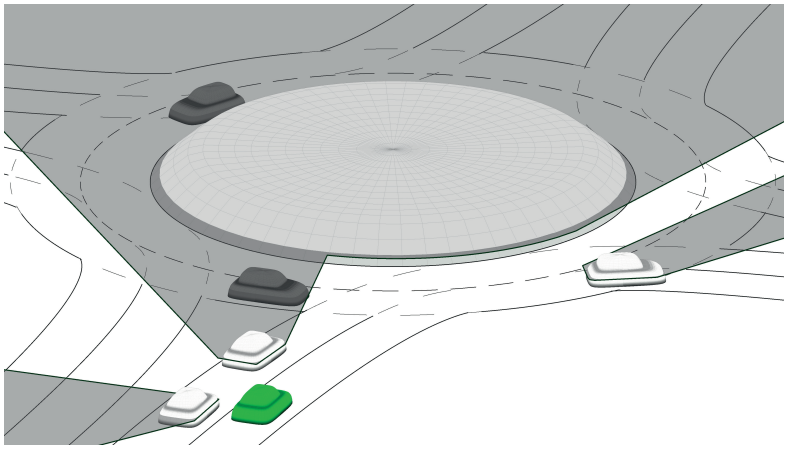

Figure 8.1 – The ego vehicle, in green, approaching a two-lane roundabout, which is partially occluded by the surrounding vehicles and the roundabout island.

In fact, when considering long planning horizons, one could justify targeting maneuvers that rely on currently-infeasible gaps, in the hope that they become feasible in the future. Hence, long-term uncertainty not only forces us to be cautious concerning the execution of maneuvers that depend on a future traffic state but also enables us to be optimistic concerning the possibility that the traffic might evolve to a more appropriate configuration.

The chapter is organized as follows. We start by gathering some related work in Section 8.1. The problem and the assumptions herein considered are detailed in Section 8.2. The planning approach itself is then described in Section 8.3, and its performance studied in Section 8.4. Finally, our conclusions and further comments are included in Section 8.5.

8.1 Related work

In this chapter, we present an extension of the reactive maneuver planner in Chapter 5, whereby the inferred probably-free gaps (see Chapter 3) can be safely used while considering longer planning horizons. In essence, we seek to formulate an uncertainty-aware motion planning strategy adapted to our planning architecture.

Uncertainty-aware motion planning is a popular research topic in the IV community due to its crucial role in real applications. As could be expected, such a line of research is tightly related to the problems of interaction-aware and occlusion-aware motion planning, since interactions and occlusions are two specific sources of uncertainty. Thus, a parallelism can be observed concerning the methods exploited by the existing solutions for both interaction-aware and uncertainty-aware motion planning.

A first broad category of solutions would include strategies based on optimizing the sequence of accelerations over a planning horizon, w.r.t. a cost that somehow includes the risk associated with the uncertainty of the future traffic state.

In [96], Xu et al. propose a planning strategy based on generating a set of trajectory candidates through the exploitation of a sampling-based method. Such candidates are then scored w.r.t. a cost function that includes the trajectory's safety probability (whose formulation is not explicitly provided). In their approach, the surrounding vehicles are expected to follow their optimal trajectories, and

the predicted state uncertainty is modeled as a Gaussian distribution.

Mouhagir et al. proposed in [61] a planning strategy consisting in generating a set of trajectory candidates using clothoid-based trajectories, which are then scored using an evidential occupancy grid representing the surrounding space.

Hubmann et al. present in [31] an approach based on modeling the decision-making problem as a partially observable Markov decision process (POMDP). In their formulation, the path the surrounding vehicles are going to follow is considered uncertain and contained within a precomputed finite set of path alternatives. The strategy also considers an uncertain and interactive (yet simple) motion model to predict the future state of the surrounding vehicles.

An alternative and efficient way of planning under uncertainty consists in accounting for uncertainty through the manipulation of the trajectory constraints. In particular, one could impose safety constraints on the trajectory planning so that the existence of a fail-safe maneuver (i.e., one that can be safely executed in case the surrounding vehicles do not evolve as expected) is guaranteed. In this way, one could potentially disregard the risk stemming from uncertainty at the time of scoring the trajectory candidates.

In this direction, Wei Zhan et al. propose in [99] a unified planning framework under uncertainty that renders *non-conservatively defensive* trajectories. The idea consists in using an optimization-based trajectory planner to generate two trajectories that share the initial portion: one corresponding to driving normally, and a second one meant to perform an emergency maneuver if a nearby car does something unexpected.

Similarly, Pek et al. propose in [71] a solution based on reachability-analysis and the fail-safe planning framework presented in [51]. In their approach, safety is guaranteed by verifying that a fail-safe maneuver exists for any legal action of the surrounding vehicles. The authors consider not only braking maneuvers as fail-safe reactions, but also lane-changes.

De Campos et al. in [12] address the design of a supervisor collision avoidance system that would override human drivers if they dangerously approach the point of no return, represented by the so-called attraction set. In the process, they consider a probabilistic predicted state of the surrounding vehicles, which is composed by exploiting an Unscented Kalman Filter [39].

The approach we formulate in this chapter is based on the concepts presented in [51] and resembles the one in [90] in which we aim to evaluate a given set of maneuver candidates by taking into account the probability of them being safe. An evident difference between our approaches is the method we exploit to represent the trajectory candidates, the way in which we propagate the prediction uncertainty, and the fact that we do not seek to count on the reactive deceleration of circulating vehicles to merge into the roundabout.

8.2 Assumptions and problem formulation

In this chapter, we formulate a self-serving maneuver planner that does not rely on V2V communication and is able to profit from longer traffic predictions. Generally speaking, we address the problem formulated in Chapter 2, but considering that the AVs do not communicate and their perception layer is affected by occlusions and other perception uncertainties. As mentioned above, the proposed maneuver planner is built upon the perception model formulated in Chapter 3, and, in practical terms, decision-making under occlusion does naturally arise if the observed probably-free inter-vehicle gaps are properly used.

8.3 Planning approach

The maneuver planner studied in this chapter, like the other self-serving planners studied in this thesis, selects one maneuver candidate $\mathcal{M}^{\text{PR}}$ to be targeted out of the set $\mathcal{M}$ provided by the tactical planner. Moreover, decisions are similarly tackled by analyzing the MTs describing how the decision spots of the maneuver candidates can be reached.

Intuitively, executing a decision-spot driving maneuver (defined in Section 4.3.1) generally involves adapting the vehicle's longitudinal motion in an attempt to drive through the decision spot in an efficient and safe way w.r.t. the relevant surrounding gaps and objects. To do so, one needs to consider that (i) the perception and understanding of the traffic scene around the decision spot improve as the latter is approached, and that (ii) the ego vehicle should be able to safely drive on π_0 as long as the surrounding traffic is not sufficiently trusted.

The strategy we propose is strongly inspired by the logic described above. Specifically, it consists of three fundamental steps. Firstly, we aim to identify the subset of reachable MTs that are indeed safely reachable w.r.t. the vehicles ahead, and existing road markings where the ego vehicle might need to stop if no feasible gap is found. Secondly, the probability of the MTs being safe w.r.t. the surrounding relevant gaps is quantified. Finally, a decision is made according to such a safety score.

Definition 14 (Safely reachable maneuver target)**.** *Given a maneuver $\mathcal{M} = (\pi, \delta, \pi_0, O, \mathcal{I}_{SS}, \mathcal{I}_C)$, a maneuver target is said to be safely reachable w.r.t. a set of obstacles $\mathcal{O}$, if it is reachable while keeping a safe state w.r.t. the obstacles considered.*

Algorithm 4: Predictive-reactive decision-making workflow

Input: $\mathcal{M} = \{\mathcal{M}_1, \cdots, \mathcal{M}_{n_\mathcal{M}}\}$
Output: $\mathcal{M}^{\text{PR}}, \mathcal{D}, \mathcal{V}, \mathcal{C}$

for $\mathcal{M} \in \mathcal{M}$ **do**
  $\mathcal{T}_\mathcal{M}^{\text{SR}} \leftarrow$ set of safely reachable maneuver targets;
end
$(\mathcal{M}^{\text{PR}}, \mathcal{T}_{\mathcal{M}^{\text{PR}}}) = \arg\max_{\mathcal{M}\in\mathcal{M}, \mathcal{T}_\mathcal{M}\in\mathcal{T}_\mathcal{M}^{\text{SR}}} \mathcal{Q}(\mathcal{M}, \mathcal{T}_\mathcal{M})$, i.e. the best maneuver;
$(\mathcal{D}, \mathcal{V}, \mathcal{C}) \leftarrow$ targets and constraints to impose on the trajectory.

The decision-making workflow is shown in Alg. 4. In summary, it consists in calculating the best maneuver candidate $\mathcal{M}^{\text{PR}} \in \mathcal{M}$ w.r.t. a quality metric $\mathcal{Q}$. To do so, we first construct, for every maneuver $\mathcal{M} = \{\pi, \delta_\mathcal{M}, \pi_0, O, \{L, G\}, \varnothing\} \in \mathcal{M}$, the set $\mathcal{T}_\mathcal{M}^{\text{SR}}$ gathering the safely reachable MTs w.r.t. the set of obstacles O. We then formulate a quality function $\mathcal{Q}$ to score the MTs within $\mathcal{T}_\mathcal{M}^{\text{SR}}$ by weighting, among other factors, the probability $\text{P}(S = 1|\mathcal{M}, \mathcal{T}_\mathcal{M})$ of the MT being safe w.r.t. the set G of surrounding probably-free gaps. Such a score is then used to identify the best maneuver candidate $\mathcal{M}^{\text{PR}}$ and its corresponding maneuver target $\mathcal{T}_{\mathcal{M}^{\text{PR}}}$, from which the output of the maneuver planner will be composed.

It must be noted that the criterion used to identify the optimal MT does not necessarily match the one locally applied by the trajectory planner. The former could favor decisions with a positive impact not only on the ego vehicle but also on the surrounding traffic, whereas the latter would typically focus on the smoothness of the trajectory itself.

Note that if no maneuver within $\mathcal{M}$ is found to be feasible, the planner's output should allow the ego vehicle to drive on π_0 safely.

8.3.1 Safely reachable maneuver targets

In this section, we seek to construct the set $\mathcal{T}_{\mathcal{M}}^{\mathrm{SR}}$ of safely reachable maneuver targets w.r.t. the set $O = \{\mathcal{O}_{\mathrm{V}}, \mathcal{O}_{\mathrm{R}}\}$ of a self-serving maneuver candidate $\mathcal{M}$. The process can simply be formulated as

$$\mathcal{T}_{\mathcal{M}}^{\mathrm{SR}} = \mathcal{T}_{\mathcal{M}}^{\mathrm{SR},\mathcal{O}_{\mathrm{V}}} \cap \mathcal{T}_{\mathcal{M}}^{\mathrm{SR},\mathcal{O}_{\mathrm{R}}}, \tag{8.1}$$

that is, as finding the intersection between the set of MTs that are safely reachable w.r.t. the obstacles within $\mathcal{O}_{\mathrm{V}}$ and $\mathcal{O}_{\mathrm{R}}$, respectively.

Definition 15 (Safely reachable maneuver target w.r.t. $\mathcal{O}_{\mathrm{V}}$)**.** *Given a maneuver candidate $\mathcal{M}$, a maneuver target $\mathcal{T}_{\mathcal{M}} = (\tau_{\mathcal{M}}, v_{\mathcal{M}})$ is said to be safely reachable w.r.t. the set of obstacles $\mathcal{O}_V \in O$ if it is reachable while driving safely behind the set of obstacles in $\mathcal{O}_V$ during the whole maneuver execution.*

Definition 16 (Safely reachable maneuver targets w.r.t. $\mathcal{O}_{\mathrm{R}}$)**.** *Given a maneuver candidate $\mathcal{M}$, a maneuver target is said to be safely reachable w.r.t. the set of obstacles $\mathcal{O}_R \in O$ if it is reachable and allows the ego vehicle to safely stop before the road markings in $\mathcal{O}_R$ up to a time interval ϵ before the decision spot is reached.*

The proposed formulation explicitly differentiates between the two subsets of obstacles within O due to the fundamentally different safety constraints they impose, which will be further discussed in the upcoming sections. In the following subsections, we start by revisiting the set $\mathcal{T}_{\mathcal{M}}^{\mathrm{R}}$ of reachable maneuver targets and continue discussing the procedure to build the sets $\mathcal{T}_{\mathcal{M}}^{\mathrm{SR},\mathcal{O}_{\mathrm{V}}}$ and $\mathcal{T}_{\mathcal{M}}^{\mathrm{SR},\mathcal{O}_{\mathrm{R}}}$.

Reachable maneuver targets

The first step of the process consists in characterizing the ways in which the decision spot (located at a distance $\delta_{\mathcal{M}}$), can be reached given the kinematic constraints and the current state x_0 of the ego vehicle. This process was previously addressed in Section 6.3.1, through the exploitation of the constructor $\mathcal{T}^{\mathrm{dR}}(x_0, \delta_{\mathcal{M}})$ (described in Section A.3). The set of reachable MTs was there denoted as $\mathcal{T}_{\mathcal{M}}^{\mathrm{R}}$, and it was claimed to represent the whole solution space of the decision-making problem at hand.

Aside from such a set, the envelope set $\mathcal{T}^{\mathrm{R}}(x_0)$ containing all sets $\mathcal{T}_{\mathcal{M}}^{\mathrm{R}}$ of reachable MTs can also be analytically constructed, as explained in Section A.3.4.

In addition, the analytical formulation of the sets presented above can be exploited to construct as well the set

$$\mathcal{X}^{\mathrm{R},\tau} \coloneqq \mathcal{X}^{\mathrm{tR}}(x_0, \tau) \tag{8.2}$$

of states that are reachable in a specific time interval τ, as well as its envelope set $\mathcal{X}^{\mathrm{R}}$ (whose construction is fully detailed in Section A.2.10 and Section A.2.7, respectively).

As an example, we have illustrated in Fig. 8.2 several instances of the sets mentioned in this Section. On the left-hand side plot, we show three sets of reachable MTs resulting form considering a common initial state and three hypothetical decision spots. Similarly, on the right-hand side, we represented three sets of reachable states for a common initial state and three different time intervals. In both cases, the envelope sets are as well represented.

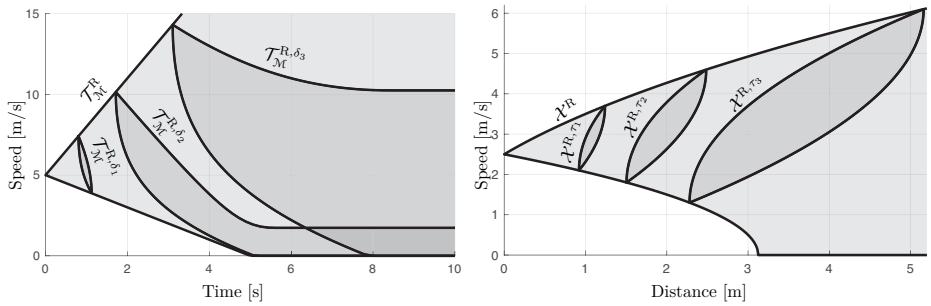

Figure 8.2 – On the left-hand side, illustration of three sets of reachable maneuver targets, given an initial state $x_0 = (0, 5)$, and for distances $\delta = \{1, 3, 5\}$ to three hypothetical decision spots; along with their envelope set. On the right-hand side, illustration of three sets of reachable states for three different time intervals and initial state $x_0 = (0, 2.5)$.

Safely reachable maneuver targets w.r.t. vehicles ahead

The set $\mathcal{T}_{\mathcal{M}}^{\mathrm{R}}$ of reachable maneuver targets represents all the ways a location at a certain distance $\delta_{\mathcal{M}}$ can be reached. However, it does not take into account the possibility of having a vehicle driving ahead of the ego vehicle, with respect to which a safe car-following behavior must be kept during the whole maneuver. Such an aspect is the one we aim to include in the construction of the set $\mathcal{T}_{\mathcal{M}}^{\mathrm{SR},\mathcal{O}_{\mathrm{V}}} \subseteq \mathcal{T}_{\mathcal{M}}^{\mathrm{R}}$, which is meant to contain the MTs that are reachable and allow the ego vehicle to keep a safe distance from the obstacles within $\mathcal{O}_{\mathrm{V}}$.

As might be evident, the set $\mathcal{T}_{\mathcal{M}}^{\mathrm{SR},\mathcal{O}_{\mathrm{V}}}$ depends on the evolution that the vehicles in $\mathcal{O}_{\mathrm{V}}$ are expected to follow, which we consider to be a constant-speed trajectory for the sake of simplicity.

We address the construction of such a set by relying, once again, on an intermediary result detailed in the Appendix. Specifically, we will make use of the constructor $\mathcal{T}^{\mathrm{SdR}}(x_0, x_{\mathcal{O}}, \delta_{\mathcal{M}})$ (detailed in Section A.3.3) representing the set of reachable MTs that are expected to be car-following safe w.r.t. the future state of an obstacle $\mathcal{O}$. Thanks to such an intermediary result, the set of safely reachable MTs would be constructed as

$$\mathcal{T}_{\mathcal{M}}^{\mathrm{SR},\mathcal{O}_{\mathrm{V}}} \coloneqq \bigcap_{\mathcal{O} \in \mathcal{O}_{\mathrm{V}}} \mathcal{T}^{\mathrm{SdR}}(x_0, x_{\mathcal{O}}, \delta_{\mathcal{M}}). \tag{8.3}$$

Although the derivation is fully documented in Section A.3.3, let us stress here that the sets $\mathcal{T}^{\mathrm{SdR}}(x_0, x_{\mathcal{O}}, \delta_{\mathcal{M}})$ are built as

$$\mathcal{T}^{\mathrm{SdR}}(x_0, x_{\mathcal{O}}, \delta_{\mathcal{M}}) = \mathcal{T}_{\mathcal{M}}^{\mathrm{R}}(x_0) \cap \mathcal{T}^{\mathrm{SCF}}(x_{\mathcal{O}}, \delta_{\mathcal{M}}). \tag{8.4}$$

That is, as the intersection of the set $\mathcal{T}_{\mathcal{M}}^{\mathrm{R}}(x_0)$ of reachable MTs and the set $\mathcal{T}^{\mathrm{SCF}}(x_{\mathcal{O}}, \delta_{\mathcal{M}})$ of MTs that are car-following safe w.r.t. the predicted state of the obstacle at the arrival time.

The construction process is illustrated on the left-hand side plot of Fig. 8.3. There, we illustrate how the set of reachable states gets constrained over time due to the presence of a vehicle ahead. In particular, we represent the progression of the sets $\mathcal{X}^{\mathrm{SCF}}(\hat{x}_{\mathcal{O}}(\tau), \underline{h})$ and $\mathcal{X}^{\mathrm{tR}}(x_0, \tau)$ at three different time instants. Furthermore, the intersection between the two sets at every time interval has been highlighted as well. On the right-hand side of Fig. 8.3 we illustrate the set $\mathcal{T}_{\mathcal{M}}^{\mathrm{R},\mathcal{O}_{\mathrm{V}}}$ of MTs that are reachable and car-following safe w.r.t. a vehicle ahead, as well as the intermediary sets $\mathcal{T}_{\mathcal{M}}^{\mathrm{R}}(x_0)$ and $\mathcal{T}^{\mathrm{SCF}}(x_{\mathcal{O}}, \delta)$ involved in its construction.

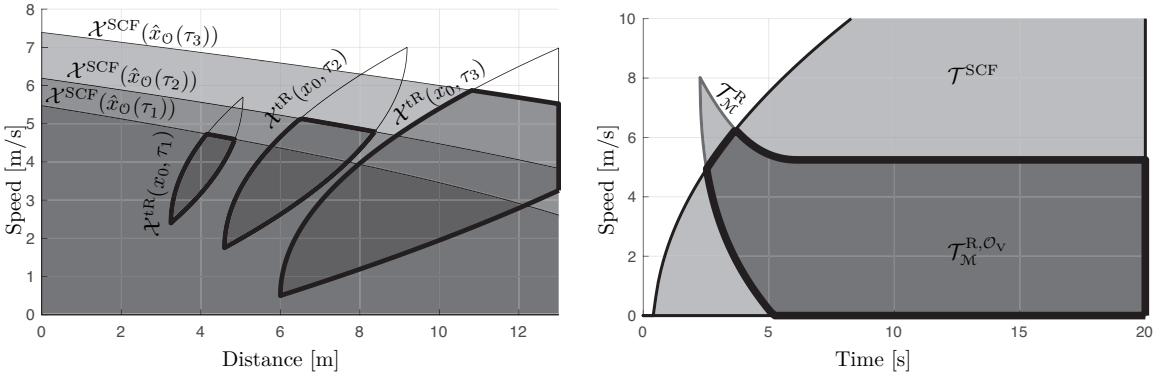

Figure 8.3 – On the left, a group of $\mathcal{X}^{\mathrm{tR}}(x_0,\tau)$ and $\mathcal{X}^{\mathrm{SCF}}(\hat{x}_{\mathcal{O}}(\tau))$ showing how a vehicle circulating ahead of the ego vehicle constrains the reachable states for three different time intervals. On the right-hand side, the set $\mathcal{T}^{\mathrm{R}}_{\mathcal{M}}$ of unconstrained reachable maneuver targets, the set $\mathcal{T}^{\mathrm{SCF}}$ of safe car-following MTs, as well as their intersection $\mathcal{T}^{\mathrm{R},\mathcal{O}_{\mathrm{V}}}_{\mathcal{M}}$. The intersection set, represents the reduction in MT candidates caused by the existence of a vehicle between the ego vehicle's position and a certain decision spot.

Safely reachable maneuver targets w.r.t. road markings

In the previous Section, we characterized the subset of MTs that the ego vehicle can reach while keeping a safe state w.r.t. a certain vehicle. However, such a set does not take into account that in order to pursue some of the targets in the resulting set, the ego vehicle might jeopardize the execution of a safe braking maneuver before the yielding line (if one exists) sooner than desired. Such a consideration is the one we address in this section by constructing the set $\mathcal{T}^{\mathrm{SR},\mathcal{O}_{\mathrm{R}}}_{\mathcal{M}}$ of safely reachable MTs w.r.t. the road marking represented within the set $\mathcal{O}_{\mathrm{R}}$.

The introduction of this set is motivated as follows. Consider a situation where, for the ego vehicle to reach a certain decision spot, it needs to drive through a road marking where it should stop if no feasible gap is found. Such a scenario entails that the capacity of safely braking before the road marking is lost at a certain time interval ϵ before the decision spot is actually reached. This, in turn, implies that to drive safely through the road marking, the ego vehicle needs to be confident that the surrounding traffic will stay favorable during the time interval ϵ, as stopping before the road marking is not possible during such a time. Hence, the smaller ϵ, the more certain the traffic prediction the decision needs to be based on, the safer the maneuver.

The set we aim to construct in this section should contain the so-called *safe ϵ reachable* MTs, i.e. those that can be reached by losing the capacity of braking before the closest road marking less than a time interval ϵ before the decision spot is reached. The time interval ϵ would then be a design parameter whose value could be related to the level of confidence concerning the gaps' future state.

Definition 17 (safe ϵ-reachable MT)**.** *A maneuver target $\mathcal{T}_{\mathcal{M}} = (\tau, v)$ is said to be safe ϵ-reachable (SϵR) w.r.t. a decision spot at a location $s_{\mathcal{M}}$ and a road marking $\mathcal{O}$ if there is at least one trajectory that meets the maneuver target while losing the capacity of braking before $\mathcal{O}$ only for a time interval ϵ before the decision spot is reached. The set of SϵR MTs is denoted as $\mathcal{T}^{S\epsilon R}_{\mathcal{M}}$.*

We tackle the construction process by defining the set we seek to construct as

$$\mathcal{T}^{\mathrm{SR},\mathcal{O}_{\mathrm{R}}}_{\mathcal{M}} \coloneqq \bigcap_{\mathcal{O}\in\mathcal{O}_{\mathrm{R}}} \mathcal{T}^{\mathrm{S}\epsilon\mathrm{R}}_{\mathcal{M}}(x_0, x_{\mathcal{O}}), \tag{8.5}$$

Algorithm 5: Set of safely reachable maneuver targets.

$\mathcal{X}^{\mathrm{RS}\epsilon\mathrm{A}} \leftarrow \mathcal{X}^{\mathrm{R}} \cap \mathcal{X}^{\mathrm{SCF}} \cap \mathcal{X}^{\epsilon\mathrm{A}}$;
$\mathcal{T}_{\mathcal{M}}^{\mathrm{S}\epsilon\mathrm{R}} \leftarrow \varnothing$;
for $x \in \mathcal{X}^{RS\epsilon A}$ **do**
  $\mathcal{T}_{\mathcal{M}}^{\epsilon\mathrm{R}}(x) \leftarrow$ the set of ϵ-RMTs from x;
  $\mathcal{T}_{\mathcal{M}}^{\mathrm{S}\epsilon\mathrm{R}} = \mathcal{T}_{\mathcal{M}}^{\mathrm{S}\epsilon\mathrm{R}} \cup \big(\mathcal{T}_{\mathcal{M}}^{\epsilon\mathrm{R}}(x)\big)$;
end

that is, as the intersection of the sets $\mathcal{T}_{\mathcal{M}}^{\mathrm{S}\epsilon\mathrm{R}}(\cdot)$ of MTs that are SϵR w.r.t. every road marking in $\mathcal{O}_{\mathrm{R}}$.

The construction of the set $\mathcal{T}_{\mathcal{M}}^{\mathrm{S}\epsilon\mathrm{R}}(x_0, x_{\mathcal{O}})$ is therefore crucial for the result we seek in this Section, and the procedure is described in Algorithm 5. The process starts by characterizing the states that:

- are reachable by the ego vehicle (reachable state),
- allow the ego vehicle to reach the decision spot in less than a time ϵ (ϵ-approaching state),
- allow the ego vehicle to stop before the road marking of interest (safe state).

The states that meet the three requirements listed above are referred to as *reachable safe ϵ-approaching*.

Definition 18 (ϵ-approaching state)**.** *A state x is said to be an ϵ-approaching (ϵA) state w.r.t. a spot at a location d, if a vehicle with initial state $x = (s, v)$ can reach the location d in less than a time interval ϵ. The set of ϵA states w.r.t. a position d is denoted as $\mathcal{X}^{\epsilon A}(d)$ and constructed as*

$$\mathcal{X}^{\epsilon A}(d) = \big\{(s, v) : s \leq d, v \geq \epsilon^{-1}(d - s) - 0.5\epsilon a_M\big\} \ . \tag{8.6}$$

Definition 19 (safe ϵ-approaching state)**.** *A state x is said to be a safe ϵA ($S\epsilon A$) state w.r.t. a spot at a distance d and a road marking $\mathcal{O}$ with state $x_{\mathcal{O}} = (s_{\mathcal{O}}, 0)$, if x is an ϵA state that allows the vehicle to brake before obstacle $\mathcal{O}$. The set of $S\epsilon A$ states w.r.t. a position d is constructed as*

$$\mathcal{X}^{S\epsilon A}(x_{\mathcal{O}}, d) = \mathcal{X}^{SCF}(x_{\mathcal{O}}) \cap \mathcal{X}^{\epsilon A}(d) \ . \tag{8.7}$$

Definition 20 (reachable safe ϵ-approaching state)**.** *A state x is said to be a reachable $S\epsilon A$ ($RS\epsilon A$) w.r.t. a spot at a distance d and a road marking $\mathcal{O}$ with state $x_{\mathcal{O}} = (s_{\mathcal{O}}, 0)$, if x is an $S\epsilon A$ that is reachable from x_0. The set of $RS\epsilon A$ states can then be constructed as*

$$\mathcal{X}^{RS\epsilon A}(x_0, x_{\mathcal{O}}, d) = \mathcal{X}^{R}(x_0) \cap \mathcal{X}^{SCF}(x_{\mathcal{O}}) \cap \mathcal{X}^{\epsilon A}(d) \ . \tag{8.8}$$

The construction process of the set of RSϵA states is depicted on the right-hand side plot in Fig. 8.4, where all the sets involved in the construction are shown as well.

Considering the Def. 18-20, the set $\mathcal{T}_{\mathcal{M}}^{\mathrm{S}\epsilon\mathrm{R}}(x_0, x_{\mathcal{O}})$ can then alternatively understood as the one gathering the MTs that can be reached by following a trajectory such that at least one of its states belongs to the set $\mathcal{X}^{\mathrm{RS}\epsilon\mathrm{A}}(x_0, x_{\mathcal{O}}, d)$. In other words, all safe approaching trajectories need to first arrive to a state in $\mathcal{X}^{\mathrm{RS}\epsilon\mathrm{A}}$ and reach the decision spot in less than a time interval ϵ.

Taking into account the aspects above discussed, the construction of $\mathcal{T}_{\mathcal{M}}^{\mathrm{S}\epsilon\mathrm{R}}$ can be tackled as follows. Firstly, let us introduce the notion of ϵ-reachable MT to denote those MTs that can be reached, from a certain initial state, in less than a time interval ϵ.

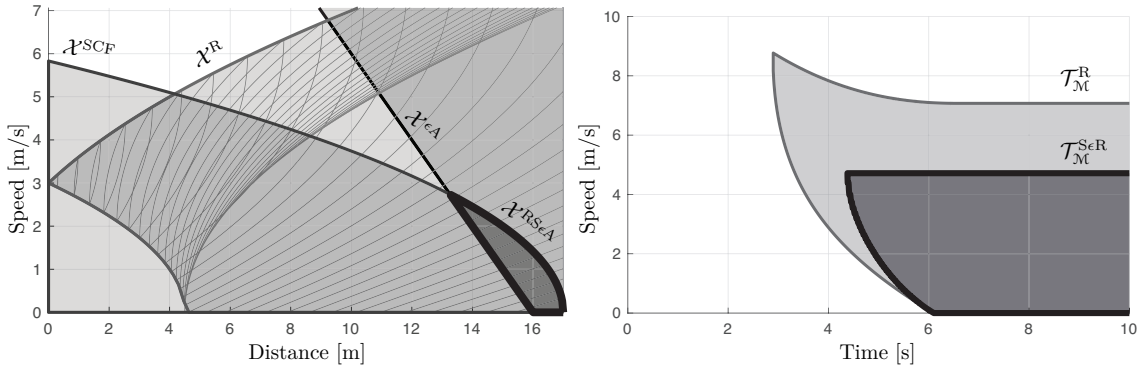

Figure 8.4 – On the left-hand side, illustration of the construction of the set $\mathcal{X}^{\mathrm{RS}\epsilon\mathrm{A}}$ of reachable states that allow to brake before a road marking and reach the decision spot in less than a time interval $\epsilon = 1$. The construction process involves the envelope set $\mathcal{X}^{\mathrm{R}}$ of reachable states (within which several time-constrained $\mathcal{X}^{\mathrm{R},\tau}$ are shown for illustration proposes), the set $\mathcal{X}^{\mathrm{SCF}}$ of states that allow the ego vehicle stop before the yield marking, and the set $\mathcal{X}^{\epsilon\mathrm{A}}$ from which the decision spot can be reached in less than a time interval ϵ. On the right-hand side, the resulting set $\mathcal{T}_{\mathcal{M}}^{\mathrm{S}\epsilon\mathrm{R}}$ of MTs that would be considered safely reachable w.r.t. the yield marking, along with $\mathcal{T}_{\mathcal{M}}^{\mathrm{R}}$ for the sake of comparison.

Definition 21 (ϵ-reachable maneuver target)**.** *A maneuver target $\mathfrak{T}_{\mathcal{M}} = (\tau_{\mathcal{M}}, v_{\mathcal{M}})$ referred to a location d is said to be ϵ-reachable (ϵR) from a state x, if $\tau_{\mathcal{M}} \leq \epsilon$. Thus, the set of MTs that are ϵR can be built as*

$$\mathcal{T}^{\epsilon R}(x, d) = \big\{(\tau, v) \in \mathcal{T}^{dR}(x, d) : \tau \leq \epsilon\big\}. \tag{8.9}$$

An additional aspect we need to take into consideration is that the ego vehicle could reach the states in $\mathcal{X}^{\mathrm{RS}\epsilon\mathrm{A}}$ in a certain set of arrival times, depending on the acceleration profile it used to do so. Hence, even though we can now calculate the ϵR MTs from a certain state $x \in \mathcal{X}^{\mathrm{RS}\epsilon\mathrm{A}}$, the arrival time interval included in the MTs would be referred to the state x and not the initial state x_0 the ego vehicle starts with. Thus, to capture this aspect, let us further construct the set

$$\mathcal{T}_{\mathcal{M}}^{\epsilon\mathrm{R}}(x_0, x) \coloneqq \mathcal{T}'(x_0, x, s_{\mathcal{M}}) = \mathcal{T}^{\epsilon\mathrm{R}}(x, s_{\mathcal{M}}) + \{(\tau, 0) : \tau \in \tau^{\mathrm{a}}(x_0, x)\} \tag{8.10}$$

gathering the MTs that are ϵ-reachable from a certain state x, but accounting for the time required to reach x from x_0. In Eq. (8.10), the term $\tau^{\mathrm{a}}(x_0, x)$ represents the set of time intervals needed to travel from x_0 to x, and its construction is formulated in Section A.2.11.

As a result, the set $\mathcal{T}_{\mathcal{M}}^{\mathrm{S}\epsilon\mathrm{R}}$ we aim to construct in this chapter is calculated as

$$\mathcal{T}_{\mathcal{M}}^{\mathrm{S}\epsilon\mathrm{R}}(x_0, x_{\mathcal{O}}) = \bigcup_{x \in \mathcal{X}^{\mathrm{RS}\epsilon\mathrm{A}}(x_0, x_{\mathcal{O}}, s_{\mathcal{M}})} \mathcal{T}_{\mathcal{M}}^{\epsilon\mathrm{R}}(x_0, x). \tag{8.11}$$

An example of the set $\mathcal{T}_{\mathcal{M}}^{\mathrm{S}\epsilon\mathrm{R}}$ is shown on the right-hand side plot in Fig. 8.4. There, the set $\mathcal{T}_{\mathcal{M}}^{\mathrm{R}}$ of reachable MTs is as well shown for comparison proposes. As expected, safety constraint imposed reduces the set of feasible maneuver candidates, or, in other words, the decision-making solution space.

Note as well that this safety condition needs to be imposed due to the inherent uncertainty of the

predicted state of the context, which typically increases as longer planning horizons are accounted for. Nonetheless, a deeper and more precise understanding of how the surrounding context would evolve, stemming from either better prediction models or explicit communication channels, would allow the use of larger ϵ values, and therefore less constraining $\mathcal{T}_{\mathcal{M}}^{\mathrm{S}\epsilon\mathrm{R}}$ sets.

8.3.2 MT safety w.r.t. observed gaps

Once we have characterized the safely reachable MTs, we tackle the calculation of the probability of those MTs being safe w.r.t. the surrounding observed gaps. Let us stress here that the safety aspects studied in the previous Section are related to the way in which the decision spot is approached. On the contrary, the safety consideration we address herein only relates to the instant at which the ego vehicle meets the decision spot.

In order to fulfill the task while avoiding strong assumptions concerning the future state of the gaps, we propose approximating the probability

$$\mathrm{P}^{\mathrm{S}}_{\mathcal{M},\mathcal{T}_{\mathcal{M}}} \coloneqq \mathrm{P}(S=1|\mathcal{M},\mathcal{T}_{\mathcal{M}}) = \prod_{\mathcal{G}\in G} \max_{\mathcal{G}\in\mathcal{G}} \mathrm{P}(\mathrm{S}=1|\mathcal{T}_{\mathcal{M}},\mathcal{G}) \tag{8.12}$$

of the maneuver $\mathcal{M}$ being safe (condition represented by the r.v. $S=\{0,1\}$) if the MT $\mathcal{T}_{\mathcal{M}}=(\tau,v)$ is pursued. Representing by $E_{\mathcal{G}}=\{0,1\}$ whether a gap $\mathcal{G}$ is empty and by $S_{g_{\mathrm{F}}}=\{0,1\}$ and $S_{g_{\mathrm{R}}}=\{0,1\}$ the fact that safety is achieved w.r.t. the front and rear limits of the gap, the probability we seek to approximate can be expressed as

$$\mathrm{P}(\mathrm{S}=1|\mathcal{T}_{\mathcal{M}},\mathcal{G}) = \mathrm{P}\Big(\hat{E}_{\mathcal{G}}=1\Big)\mathrm{P}\Big(\hat{S}_{g_{\mathrm{F}}}=1\Big)\mathrm{P}\Big(\hat{S}_{g_{\mathrm{R}}}=1\Big), \tag{8.13}$$

which is composed of the terms:

- $\mathrm{P}\Big(\hat{E}_{\mathcal{G}}=1\Big)$ showing the probability with which the gap is expected to be empty at τ, which can be calculated as

$$\mathrm{P}\Big(\hat{E}_{\mathcal{G}}=1\Big) = \mathrm{P}(E_{\mathcal{G}}=1)\mathrm{P}\Big(\hat{E}_{\mathcal{G}}=E_{\mathcal{G}}\Big) + \mathrm{P}(E_{\mathcal{G}}=0)\mathrm{P}\Big(\hat{E}_{\mathcal{G}}{\neq}E_{\mathcal{G}}\Big), \tag{8.14}$$

  with $\mathrm{P}(E_{\mathcal{G}}=1)$ and $\mathrm{P}(E_{\mathcal{G}}=0)$ being, respectively, the likelihood of the gap being currently empty and occupied, and $\mathrm{P}\Big(\hat{E}_{\mathcal{G}}=E_{\mathcal{G}}\Big)$ and $\mathrm{P}\Big(\hat{E}_{\mathcal{G}}{\neq}E_{\mathcal{G}}\Big)$ showing, respectively, the probability of the gap keeping and changing its current state, and

- $\mathrm{P}\Big(\hat{S}_{g_F}=1\Big)$ and $\mathrm{P}\Big(\hat{S}_{g_R}=1\Big)$ showing the probability that the state $\hat{x}_{\mathrm{ego}}$, with which the ego vehicle plans to reach the decision spot, is safe w.r.t. the expected state of the gap' front and rear limit, which can equivalently be expressed as

$$\mathrm{P}\Big(\hat{S}_{g_F}=1\Big) = \mathrm{P}\big(\hat{x}_{\mathrm{ego}}\in\mathcal{X}^{\mathrm{SCF}}(\hat{x}_{g_{\mathrm{F}}})\big), \qquad \mathrm{P}\Big(\hat{S}_{g_R}=1\Big) = \mathrm{P}\big(\hat{x}_{g_{\mathrm{R}}}\in\mathcal{X}^{\mathrm{SCF}}(\hat{x}_{\mathrm{ego}})\big). \tag{8.15}$$

From the listed terms, $\mathrm{P}(E_{\mathcal{G}}=0)$ and $\mathrm{P}(E_{\mathcal{G}}=1)$ are part of the information provided by the perception layer. Thus, we only need to approximate the values of: (i) the occupancy transition probabilities $\mathrm{P}\Big(\hat{E}_{\mathcal{G}}=E_{\mathcal{G}}\Big)$ and $\mathrm{P}\Big(\hat{E}_{\mathcal{G}}{\neq}E_{\mathcal{G}}\Big)$, and (ii) the probabilities $\mathrm{P}\Big(\hat{S}_{g_F}=1\Big)$ and $\mathrm{P}\Big(\hat{S}_{g_R}=1\Big)$, concerning whether the MT is safe w.r.t. the gap's limits.

The occupancy transition probabilities of the gap would generally depend on the estimation the ego vehicle has concerning the driving intent of the surrounding vehicles, and the geometry of the

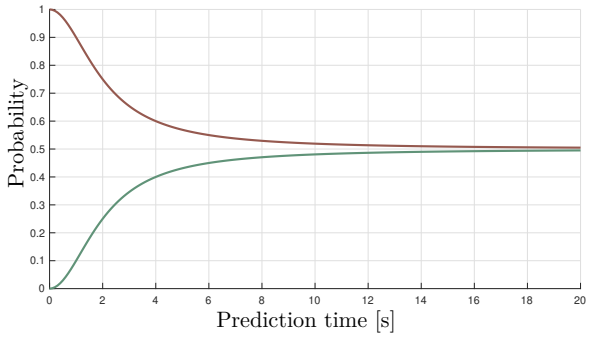

Figure 8.5 – Illustration of the model used to approximate the occupancy transition probability. Line (—) represents the probability $\mathrm{P}\Big(\hat{E}_{\mathcal{G}} \neq E_{\mathcal{G}}\Big)$ whereas (—) shows the probability $\mathrm{P}\Big(\hat{E}_{\mathcal{G}} = E_{\mathcal{G}}\Big)$.

road layout itself. Nonetheless, we will opt for using a much simpler approach. Concerning the safety probabilities w.r.t. the gap's limits, we will approximate those by assuming the future state of the gaps' limits to be a r.v. normally distributed, and exploiting the car-following safety constraint.

Occupancy probability

The occupancy transition probability denoted as $\mathrm{P}\Big(\hat{E}_{\mathcal{G}} \neq E_{\mathcal{G}}\Big)$ is modeled herein as

$$\mathrm{P}\Big(\hat{E}_{\mathcal{G}} \neq E_{\mathcal{G}}\Big) = 0.5 - \left(0.4\tau^2 + 2\right)^{-1}, \qquad \mathrm{P}\Big(\hat{E}_{\mathcal{G}} = E_{\mathcal{G}}\Big) = 1 - \mathrm{P}\Big(\hat{E}_{\mathcal{G}} \neq E_{\mathcal{G}}\Big). \tag{8.16}$$

This simple model, illustrated in Fig. 8.5, reflects the idea that: (i) the state of the gap is expected to remain as is currently observed for a short period of time, and (ii) the longer the prediction horizon, the less certain the future state of the gap becomes.

Car-following safety

In order to quantify the probability with which an MT is expected to be safe w.r.t. the future state of a gap's front and rear limits, we start by assuming that they move forward with an acceleration $a_{g_k} = \overline{a}_{g_k} + \omega_a$. In particular, the term $\overline{a}_{g_k}$ shows the expected acceleration, whereas $\omega_a \sim \mathcal{N}(0, \sigma_a^2)$ is a random variable normally distributed with zero mean and variance σ_a^2. The predicted state $\hat{x}_{g_k} = (\hat{s}_{g_k}, \hat{v}_{g_k})$ of the gap's limits at τ would be calculated considering

$$\hat{v}_{g_k} = v_{g_k} + \overline{a}_{g_k}\tau + \omega_v = \overline{v}_{g_k} + \omega_v, \tag{8.17}$$

$$\hat{s}_{g_k} = s_{g_k} + v_{g_k}\tau + 0.5\overline{a}_{g_k}\tau^2 + \omega_s = \overline{s}_{g_k} + \omega_s, \tag{8.18}$$

with $\omega_v \sim \mathcal{N}(0, \tau^2\sigma_a^2)$, and $\omega_s \sim \mathcal{N}(0, (0.5\tau^2\sigma_a)^2)$.

The car-following conditions can be then calculated, according to Eq. (A.55), as

$$\mathrm{P}\big(\hat{x}_{\mathrm{ego}} \in \mathcal{X}^{\mathrm{SCF}}(\hat{x}_{g_{\mathrm{F}}})\big) = \mathrm{P}(\hat{s}_{g_{\mathrm{F}}} \geq s_{\mathrm{ego}})\mathrm{P}(g_{\mathrm{SCF}}(\hat{x}_{g_{\mathrm{F}}}, \hat{x}_{\mathrm{ego}}) \geq 0)\ , \tag{8.19}$$

$$\mathrm{P}\big(\hat{x}_{g_{\mathrm{R}}} \in \mathcal{X}^{\mathrm{SCF}}(\hat{x}_{\mathrm{ego}})\big) = \mathrm{P}(s_{\mathrm{ego}} \geq \hat{s}_{g_{\mathrm{R}}})\mathrm{P}(g_{\mathrm{SCF}}(\hat{x}_{\mathrm{ego}}, \hat{x}_{g_{\mathrm{R}}}) \geq 0). \tag{8.20}$$

On the one hand,

$$\mathrm{P}(\hat{s}_{g_\mathrm{F}} \geq s_\mathrm{ego}) = 1 - \mathrm{P}(\omega_s \geq s_\mathrm{ego} - \overline{s}_{g_\mathrm{F}}(\tau)) \ , \tag{8.21}$$
$$\mathrm{P}(s_\mathrm{ego} \geq \hat{s}_{g_\mathrm{R}}) = \mathrm{P}(\omega_s \geq s_\mathrm{ego} - \overline{s}_{g_\mathrm{R}}) \tag{8.22}$$

can be obtained directly, as s_ego, $\overline{s}_{g_\mathrm{F}}$ and $\overline{s}_{g_\mathrm{R}}$ are constants, and ω_s is normally distributed. On the other hand, operating with equation Eq. (A.1) we obtain

$$\mathrm{P}(g_\mathrm{SCF}(\hat{x}_{g_\mathrm{F}}, \hat{x}_\mathrm{ego}) \geq 0) = \mathrm{P}(-\beta_L \leq g_\mathrm{SCF}(\overline{x}_{g_\mathrm{F}}, \hat{x}_\mathrm{ego})) \ , \tag{8.23}$$
$$\mathrm{P}(g_\mathrm{SCF}(\hat{x}_\mathrm{ego}, \hat{x}_{g_\mathrm{R}}) \geq 0) = \mathrm{P}(\beta_F \leq g_\mathrm{SCF}(\hat{x}_\mathrm{ego}, \overline{x}_{g_\mathrm{R}})), \tag{8.24}$$

where $\overline{x}_{g_k} = (\overline{s}_{g_k}, \overline{v}_{g_k})$, and

$$\beta_L = \omega_s + 0.5 d^{-1}\omega_v^2 + d^{-1}\overline{v}_{g_\mathrm{F}}\omega_v \ , \tag{8.25}$$
$$\beta_F = \omega_s + \omega_v\Theta_{g_\mathrm{R}} + 0.5 d^{-1}\omega_v^2 + d^{-1}\overline{v}_{g_\mathrm{R}}\omega_v, \tag{8.26}$$

are r.v. normally distributed with zero mean and variance

$$\sigma^2_{\beta_L} = \sigma_s^2 + 0.5^2 d^{-2}\tau^4\sigma_a^4 + d^{-2}\overline{v}^2_{g_\mathrm{F}}(\tau)\tau^2\sigma_a^2 \ , \tag{8.27}$$
$$\sigma^2_{\beta_F} = \sigma_s^2 + \tau^2\sigma_a^2\Theta^2_{g_\mathrm{R}} + d^{-2}\tau^4\sigma_a^4 + d^{-2}\overline{v}^2_{g_\mathrm{R}}\tau^4\sigma_a^4, \tag{8.28}$$

which can be directly quantified as well.

8.3.3 Maneuver selection

The task of choosing a maneuver $\mathcal{M}^\mathrm{PR}$ to be targeted, out of the set $\mathcal{M}$ built by the tactical planner is carried out by comparing the quality score $\mathcal{Q}(\mathcal{M}, \mathcal{T}_\mathcal{M})$ of the valid MTs of all the maneuver candidates. That is

$$(\mathcal{M}^\mathrm{PR}, \mathcal{T}_{\mathcal{M}^\mathrm{PR}}) = \arg \max_{\mathcal{M}\in\mathcal{M}, \mathcal{T}_\mathcal{M}\in\mathcal{T}_\mathcal{M}^{\mathrm{SR},\delta}} \{\mathcal{Q}(\mathcal{M}, \mathcal{T}_\mathcal{M})\}. \tag{8.29}$$

We propose a quality function of the form

$$\mathcal{Q}(\mathcal{M}, \mathcal{T}_\mathcal{M}) = \begin{cases} \omega_\delta\delta + \omega_\tau\tau + \omega_v v + \omega_\mathrm{P}\mathrm{P}^\mathrm{S}_{\mathcal{M},\mathcal{T}_\mathcal{M}} & \text{if } \mathrm{P}^\mathrm{S}_{\mathcal{M},\mathcal{T}_\mathcal{M}} \geq p_\mathrm{m} \\ -\infty & \text{otherwise} \end{cases} \ , \tag{8.30}$$

which is the weighted sum of (i) the distance to the decision spot, (ii) the arrival time and speed, and (iii) the probability $\mathrm{P}^\mathrm{S}_{\mathcal{M},\mathcal{T}_\mathcal{M}}$ of the MT being safe. Such a quality function enables us to balance the objective of performing the maneuver as soon as possible and in the safest possible way.

In Eq. (8.30) we impose a threshold for the minimum success probability an MT should have in order to be a valid candidate, which takes the form

$$p_\mathrm{m} = 1/(0.05\delta_\pi^2 + 1) \tag{8.31}$$

in such a way that its value grows as the decision spot is approached. This is expected to allow the ego vehicle to be optimistic about the future state of the surrounding gaps while there is enough time to react to unexpected changes but forces it to be conservative when the decision spot is close.

8.3.4 Planner output

Given the selected maneuver $\mathcal{M}^{\mathrm{PR}}$ and its corresponding MT $\mathcal{T}_{\mathcal{M}^{\mathrm{PR}}}$, the outputs of the maneuver planner are set as follows.

The path π^{PR} to be followed is directly extracted from $\mathcal{M}^{\mathrm{PR}}$ if $\mathcal{M}^{\mathrm{PR}} \neq \varnothing$, and is set to π_0 otherwise. The set of constraints would be $\mathcal{C} = \{\mathcal{C}_{\mathcal{O}} : \mathcal{O} \in O\}$, with

$$\mathcal{C}_{\mathcal{O}} = \begin{cases} \left(\tau^{\mathrm{PR}} - \epsilon, x_{\mathcal{O}}, d\right) & \text{if } \mathcal{M}^{\mathrm{PR}} \neq \varnothing \wedge \mathcal{O} \in \mathcal{O}_{\mathrm{R}} \\ (\infty, x_{\mathcal{O}}, d) & \text{otherwise} \end{cases}, \tag{8.32}$$

whereas the sets of trajectory targets would be

$$\mathcal{V} = \begin{cases} \left\{\left(\tau^{\mathrm{PR}}, v^{\mathrm{PR}}\right)\right\} & \text{if } \mathcal{M}^{\mathrm{PR}} \neq \varnothing \\ \varnothing & \text{otherwise} \end{cases}, \qquad \mathcal{D} = \begin{cases} \left\{\left(\tau^{\mathrm{PR}}, \delta^{\mathrm{PR}}\right)\right\} & \text{if } \mathcal{M}^{\mathrm{PR}} \neq \varnothing \\ \varnothing & \text{otherwise} \end{cases}, \tag{8.33}$$

which are empty if no maneuver is found to be feasible.

8.4 Results

In this section, we present some results to illustrate the performance of the proposed strategy. We begin by further analyzing in Section 8.4.1 the implications the proposed method has on the vehicle's trajectories to approach roundabouts. Then, in Section 8.4.2, we provide additional examples of safely reachable MTs, the probability of them being safe, as well as the MT the proposed approach would choose. In Section 8.4.3, we continue by comparing the traffic evolution resulting from the proposed planning approach with the one arising from the baseline formulated in Chapter 5, in three different traffic density scenarios. Finally, the overall traffic coordination performance resulting from the application of the strategy is further assessed in Section 8.4.4.

In our study, we make use of two driver agents, whose main features are described in Tab. 8.1. On the one hand, we consider that the perception system of both agents is affected by occlusions. Concerning their behavior, vehicles can be driven by two types of agents: R-Agents that behave in a purely reactive manner, and PR-Agents that implement the strategy formulated in this chapter. Furthermore, the parameters used in our implementation are gathered in Tab. 8.2.

Table 8.1 – Driver agents used in our simulation study

	Perception	Communication	SS Maneuver planner	C Maneuver planner
R-Agent	Perfect perception	None	Reactive	None
PR-Agent	Perfect perception	None	Predictive + Reactive	None

Table 8.2 – Design parameters

	ϵ	$\overline{a}_{g_{\mathrm{F}}}$	$\overline{a}_{g_{\mathrm{R}}}$	σ_a	ω_δ	ω_τ	ω_v	ω_{P}
Value	0.5	-0.2	0.2	0.8	1	2	0.2	20
Unit	s	$\mathrm{m/s^2}$	$\mathrm{m/s^2}$	$\mathrm{m/s^2}$	1/m	1/s	s/m	-

Furthermore, even though the strategy has been formulated so that it can be applied to perform merging maneuvers into multi-lane roundabouts, as well as to perform lane changes, the analysis will be limited, as in the previous chapters, to single-lane roundabout scenarios. Thus, we mainly analyze the merging maneuver itself.

8.4.1 Safe approaching behavior

In this section, we further analyze the implications that the use of the set of SϵR MTs has on the resulting driving behavior. The analysis will simply consist in representing the set of SϵA states and SϵR MTs for several scenarios so that the method's implications can be better understood.

The results are shown in Fig. 8.6, where pairs of plots similar to the ones used in Section 8.3.1 are shown for the initial states and distances to the decision spot gathered in Tab. 8.3.

Table 8.3 – Safe ϵ-reachable MTs scenarios

	δ_0 [m]	v_0 [m/s]	ϵ [s]	a_1 [m/s^2]	a_2 [m/s^2]
Example 1	20	1	1.5	-1	1
Example 2	20	3	1.0	-1	1
Example 3	20	4	0.5	-1	1
Example 4	5	0	1.5	-1	1
Example 5	5	1	1.0	-1	1

First of all, it is important to point out that the smaller the time interval ϵ (time interval before reaching the decision spot during which the ego vehicle is willing to lose the capacity of fully stopping before the decision spot), the smaller the set of safe ϵ-approaching states is. Thus, the smaller the set of trajectories that can be pursued while fulfilling the safety constraint that ϵ explicitly imposes. Such an effect can also be observed by analyzing the difference between the set of reachable MTs and the set of safe ϵ-reachable MTs, which increases as ϵ decreases. This effect is reasonable, and it indicates that the harder the safety constraint imposed on the trajectory (i.e. the smaller the value of ϵ), the smaller the set of maneuvers fulfilling the constraints.

If the ego vehicle is sufficiently close to the decision spot and driving sufficiently slow (examples 4 and 5), it turns out that both the set of reachable MTs and safe ϵ-reachable MTs are identical. Thus, all trajectories the ego vehicle could pursue turn out to be sufficiently safe. This points out the type of situations where the proposed algorithm could be expected to make a difference compared to the reactive strategy. Indeed, the proposed strategy is most useful when the vehicle is in a position to pursue a trajectory that does not pass through the set of safe ϵ-approaching states, i.e. when the vehicle is sufficiently far away. However, there is a point where the ego vehicle is so closed to its decision spot that all the feasible trajectories it has available are safe. Hence the reactive merging decision logic could be applied without the risk of jeopardizing too early the safe braking maneuvers.

8.4.2 Decision-making

In this section, we illustrate the MTs the algorithm would decide to target in a set of six traffic scenes. The results are shown in Fig. 8.7, where we illustrate six merging scenarios along with: (i) the set of safely reachable MTs, (ii) the MT the algorithm would choose, as well as (iii) the safe probability assigned to each of the MTs within the constructed solution space. Moreover, in Tab. 8.4, we show the value of the safe probability assigned to the chosen MT in each scenario.

The first thing to note is that the further the ego vehicle is from the decision spot, the smaller the safety probability assigned to the best MT. Intuitively, when the ego vehicle selects a target that is sufficiently far in time, even if it is considered to be the best option, the future traffic state the decision is built upon would be significantly uncertain.

The safe probability of the SϵR MTs represented by the contour curves in Fig. 8.7, seems to accurately illustrate what could be intuitively said about the merging decision in the shown scenarios.

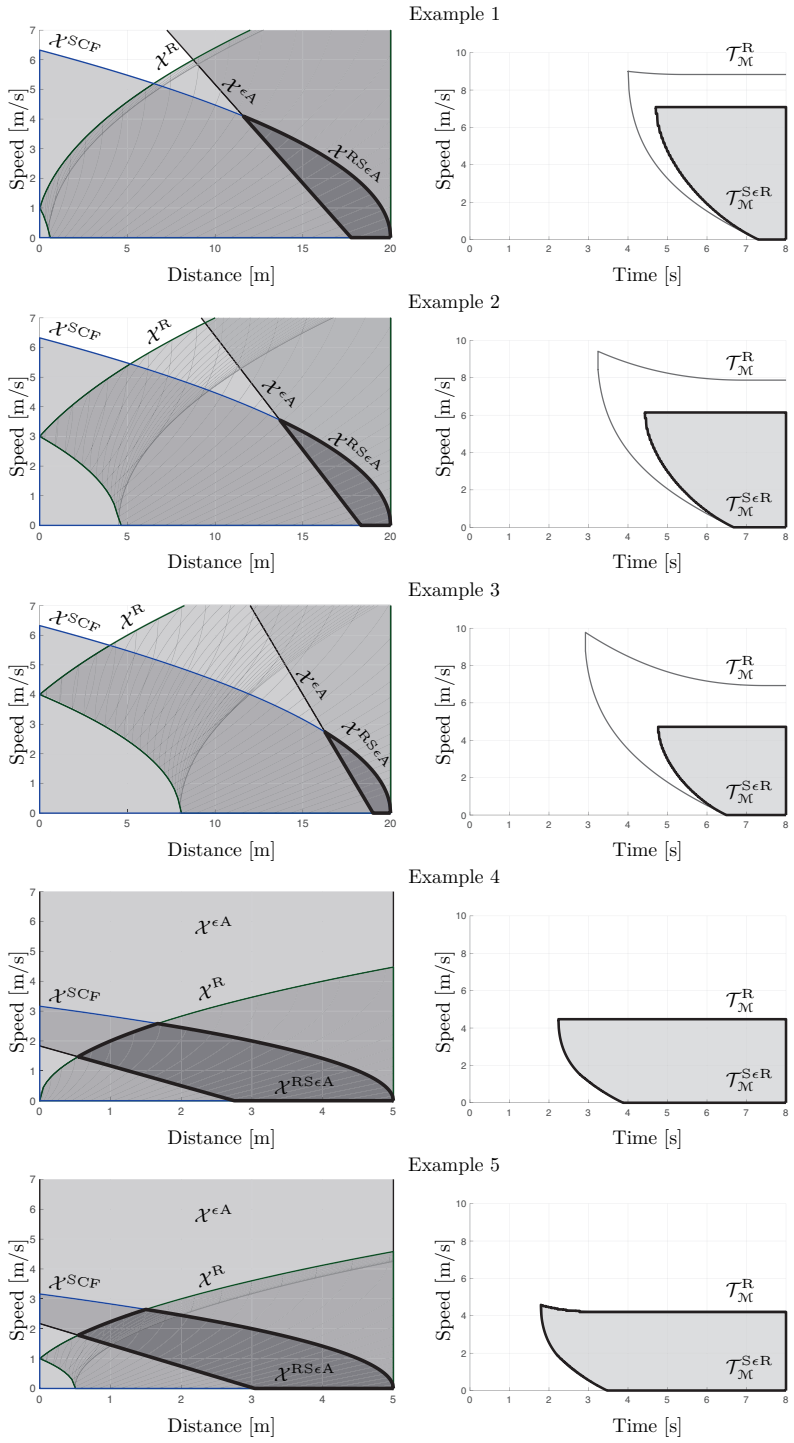

Figure 8.6 – Examples of the set of safe ϵ-approaching states, and safe ϵ-reachable MTs for five different scenarios. Every raw correspond to a different example, and for each of them, the same information than the one provided in Fig. 8.4 is included.

Table 8.4 – Safe ϵ-reachable MTs scenarios

	MT	$P_{\mathcal{M},\mathcal{T}_\mathcal{M}}$
Example 1	(5.11, 4.06)	16
Example 2	(2.60, 3.86)	71
Example 3	(4.62, 4.06)	12
Example 4	(8.54, 4.06)	4
Example 5	(3.86, 4.06)	4
Example 6	(4.21, 4.06)	8

For instance, note how in examples 1, 3, 4, and 6, the earliest merging maneuvers in each case are indeed not very safe as they might be risky when the vehicle just passing by the ego vehicle's merging spot is considered. Moreover, in example 4, where two relatively large inter-vehicle gaps can be seen in the circulatory lane, the contours show two orange regions (i.e. a relatively high probability of being safe), representing MTs that correspond to the two mentioned gaps.

It is worth stressing as well that in cases 1, 3, and 6, the ego vehicle would always try to merge right after the vehicle passing by its merging spot. However, it is worth noting that the closer the following vehicle is to such a vehicle, the earlier the algorithm suggests trying to merge, so that the probability of the maneuver being safe w.r.t. such following vehicle remains sufficiently high.

Furthermore, the safe probabilities assigned to the chosen MTs indeed have a relatively low value in cases 1, 3, 4, 5, 6, and 7 due to the fact that the chosen MTs represent in those cases a relatively late merging maneuver. In example 2, however, the ego vehicle is sufficiently close to the decision spot, and the scenario is sufficiently safe for the chosen MTs to be assigned a high safe probability.

8.4.3 Single traffic scenario

In this section, we assess the trajectories that a set of vehicles driving through a single-lane roundabout would follow if their behavior resulted from the application of the proposed predictive-reactive strategy. In particular, we will consider a roundabout of 16m radius, 1 circulatory lane, 3 legs with 1 incoming and 1 outgoing lane (i.e. a `16R1LR3L1I1O` roundabout). Moreover, we generate scenarios of 100 vehicles (i.e. `100V`), and three different incoming traffic configurations corresponding to an incoming traffic volume of 500vehs/h, 1500vehs/h, and 2500vehs/h evenly distributed among the incoming legs. In other words, we consider the incoming traffic configurations `500Q[1 1 1]`, `1500Q[1 1 1]`, and `2500Q[1 1 1]` (see Section 2.3.4 for details concerning our labeling strategy). Each of the three cases considered leads to a different traffic scenario that is simulated twice, with the vehicles being driven by: (case-1) R-Agents, and (case-2) PR-Agents. The results are shown in Fig. 8.8-8.16, where we compare, for every pair of simulations:

- the time-distance evolution of the traffic in the circulatory lane,
- the evolution of the incoming traffic for every incoming lane of the roundabout, and
- the distribution of some additional performance metrics concerning the travel time, travel speed, average jerk, and delay that the vehicles in the scenario experience.

Furthermore, we gather in Tab. 8.5 the registered values for the intersection throughput and the fairness with which the different performance metrics concerning the vehicles' trajectory are distributed among the vehicles.

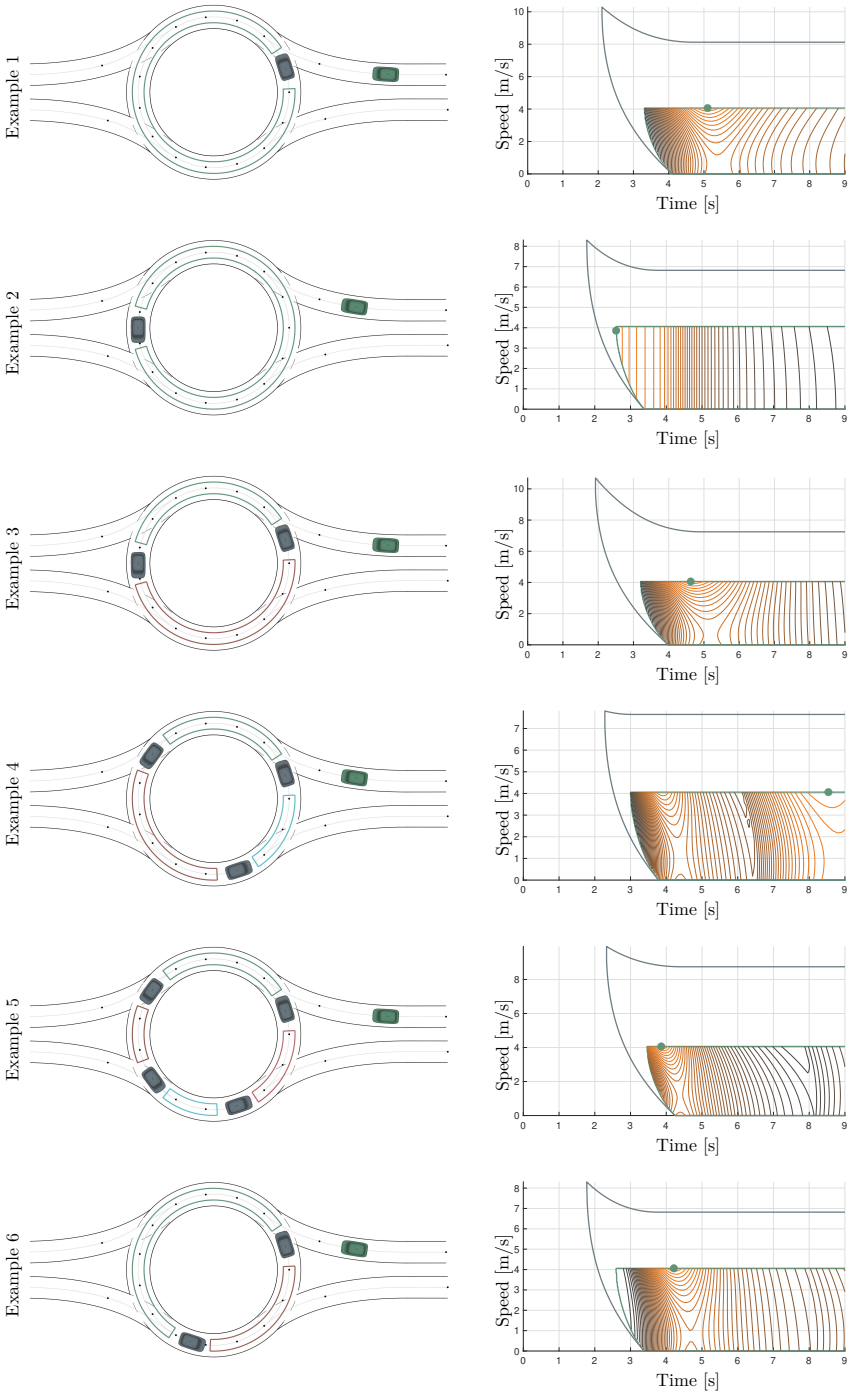

Figure 8.7 – Illustration of the predictive-reactive decision-making process in a set of six different scenarios (one per row). On the left-hand side, a traffic scene with the ego vehicle shown in green. On the right-hand side, the illustration of the decision-making. There, we represent the set $\mathcal{T}_{\mathcal{M}}^{\mathrm{R}}$ of reachable MTs in (—) along with the set $\mathcal{T}^{\mathrm{S}\epsilon\mathrm{R}}$ of safe ϵ-reachable MTs within it. Contours within $\mathcal{T}^{\mathrm{S}\epsilon\mathrm{R}}$ represent the safe probability assigned to every MT (the higher the safe probably the more orange the contour). Finally, the MT that would be chosen by the algorithm is represented by (•).

Table 8.5 – Intersection throughput and fairness metrics

	Throughput [vehs/h]	15min Throughput fairness [%]	TT. fairness [%]	TS. fairness [%]	J. fairness [%]	D. fairness [%]
16R1LR3L1I1O-100V-500Q[1 1 1]-RAgent	488	87	98	99	86	96
16R1LR3L1I1O-100V-500Q[1 1 1]-PRAgent	488	83	98	99	85	96
16R1LR3L1I1O-100V-1500Q[1 1 1]-RAgent	1355	97	97	99	84	60
16R1LR3L1I1O-100V-1500Q[1 1 1]-PRAgent	1374	96	96	99	75	40
16R1LR3L1I1O-100V-2500Q[1 1 1]-RAgent	1460	97	84	92	88	44
16R1LR3L1I1O-100V-2500Q[1 1 1]-PRAgent	1782	96	93	98	85	54

In general, we can observe that even though all vehicles are set up to target exactly the same arrival time to the scenario, PR-Agents manage to drive through the roundabout avoiding collisions, quicker, and more smoothly than R-Agents in all the chosen scenarios.

As expected, in low-density traffic (Fig. 8.8-8.10), both agents drive in a virtually identical manner due to the lack of interaction between vehicles. Note that, for this reason, the trajectory traces resulting from both simulated cases overlap almost perfectly.

In medium-density traffic (Fig. 8.11-8.14), significant differences start appearing in the way the vehicles approach and merge into the roundabout, and, subsequently, in the way the traffic evolves in the circulatory lane. It can be observed that the behavior of the incoming vehicles start deviating from the reactive one when vehicles are far from the decision spot, which was to be expected given the predictive nature of the proposed method. Due to such changes, vehicles are observed to have fewer problems merging into the roundabout, as can be extracted from the fact that the number of vehicles that need to stop at the yield line before merging into the intersection decreases significantly. The benefits of the proposed method can as well be observed by looking at the distribution of travel time, 15min-throughput segments, and jerk, which are also improved.

In high-density traffic (Fig. 8.11-8.14), the benefit of the approach becomes more noticeable. Indeed, aside from the fact that vehicles find a feasible merging gap more easily, it is worth noting that they also manage to drive closer together, to the point that we can observe merging maneuvers where vehicles merge into the roundabout in small platoons of two vehicles. This behavior arises from the fact that, unlike in the reactive baseline driving policy, vehicles can apply the proposed method even when they are not the first vehicle in their queue. In this case, vehicle's travel speed and overall delay improve, but it does so at the expense of slightly increasing the average jerk vehicles require to drive through the roundabout.

In general, the approach outperforms the reactive baseline planning policy in all the cases shown. Such an improvement comes from the fact that vehicles can safely adapt their behavior while approaching the intersection, according to the most probable traffic configuration they believe they might encounter by the time they arrive at their yielding line. The approach turned out to have

a more noticeable effect at higher traffic density scenarios, as they are the scenarios where the vehicles feel a stronger need for adapting their approaching behavior and deviating from a purely reactive behavioral policy. The algorithm was observed to improve the intersection throughput in the high-level traffic scenario by 300vehs/h, or a 22% w.r.t. the reactive baseline policy.

8.4.4 Traffic coordination performance

In this section, we evaluate the impact of the proposed strategy at the traffic coordination level. The process is somehow related to the analysis of the single roundabout scenario in the previous traffic scenes. However, here we aim to obtain the average improvement over a broader set of randomly generated traffic scenarios.

Simulation batch setup

The set of simulation instances used to carry out the analysis was generated according to the parameters in Tab. 8.6 and the tree structure illustrated in Fig. 8.17. A total of 18 different incoming traffic configurations are used, where the total flow (`QI`) and distribution (`DI`) of incoming vehicles are varied. For every traffic scenario, ten different instances (`I1`, $\cdots$, `I10`) are randomly created in such a way that different origin-destination patterns and arrival times are tested. Furthermore, every instance is simulated for five different penetration levels (`P`) of PR-Agents.

Table 8.6 – Simulation batch scenario configuration

	Value
G	16R1LR3L1I1O-100V
QI1	1000Q
QI2	1500Q
QI3	2000Q
QI4	2500Q
QI5	3000Q
QI6	3500Q
DI1	[1.0 1.0 1.0]
DI2	[1.0 0.5 1.0]
DI3	[0.5 1.0 0.5]
P1	0
P2	0.25
P3	0.5
P4	0.75
P5	1

Simulation batch results

The evaluation of the overall traffic coordination performance is done by analyzing the overall travel speed (Fig. 8.18), jerk (Fig. 8.19), and intersection throughput (Fig. 8.20) w.r.t. the incoming traffic configuration, and the penetration rate. In each of the shown plots, six different groups of boxplots are shown, which correspond to the six configurations of traffic inflow. Moreover, within each group, five different boxplots are represented corresponding to the five penetration levels considered.

Consistent with the results obtained in the previous Section, the proposed predictive-reactive

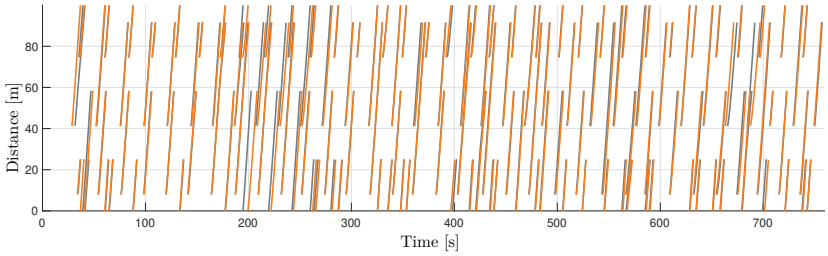

Figure 8.8 – Time-distance diagram representing the evolution over time of the vehicles in the circulatory lane, in the simulated scenario `16R1LR3L1I1O-100V-500Q[1 1 1]`. The trajectories of R-Agents and PR-Agents are represented by (—) and (—), respectively.

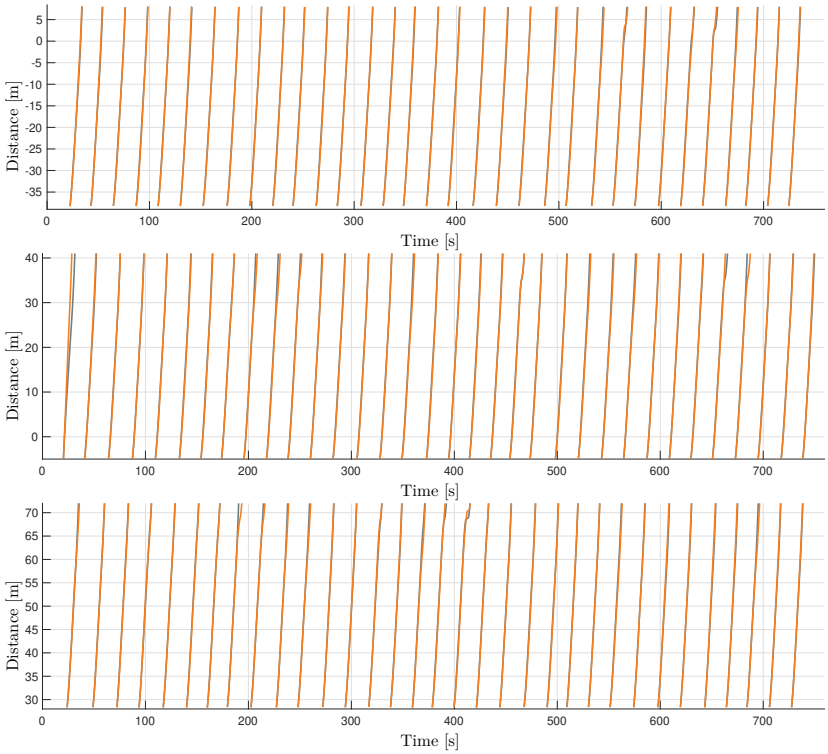

Figure 8.9 – Time-distance diagrams representing the evolution of the incoming traffic in every incoming lane in the simulated scenario `16R1LR3L1I1O-100V-500Q[1 1 1]`. The trajectories of R-Agents and PR-Agents are represented by (—) and (—), respectively.

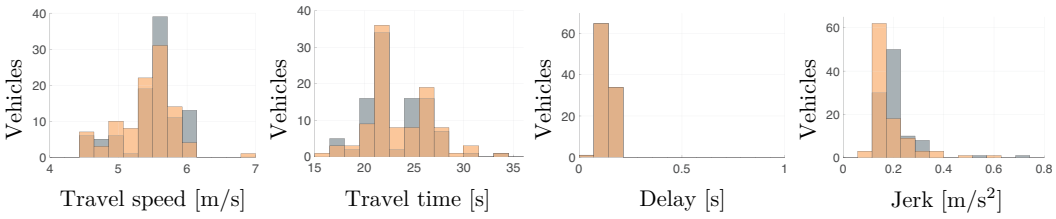

Figure 8.10 – Comparison of the histogram of the registered travel speed, travel time, arrival delay, and jerk of the vehicles in the scenario `16R1LR3L1I1O-100V-500Q[1 1 1]`, when driven by R-agents (gray) and PR-agents (orange).

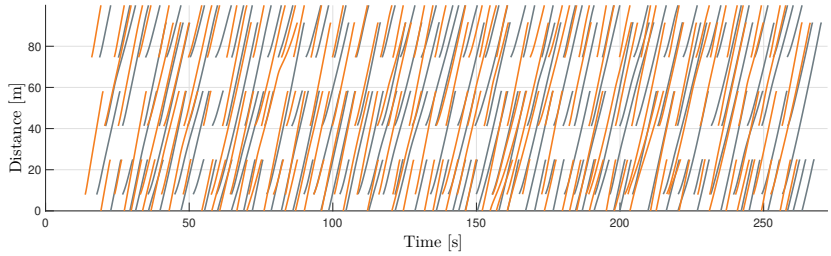

Figure 8.11 – Time-distance diagrams representing the evolution of the incoming traffic in every incoming lane in the simulated scenario `16R1LR3L1I1O-100V-1500Q[1 1 1]`. The trajectories of R-Agents and PR-Agents are represented by (—) and (—), respectively.

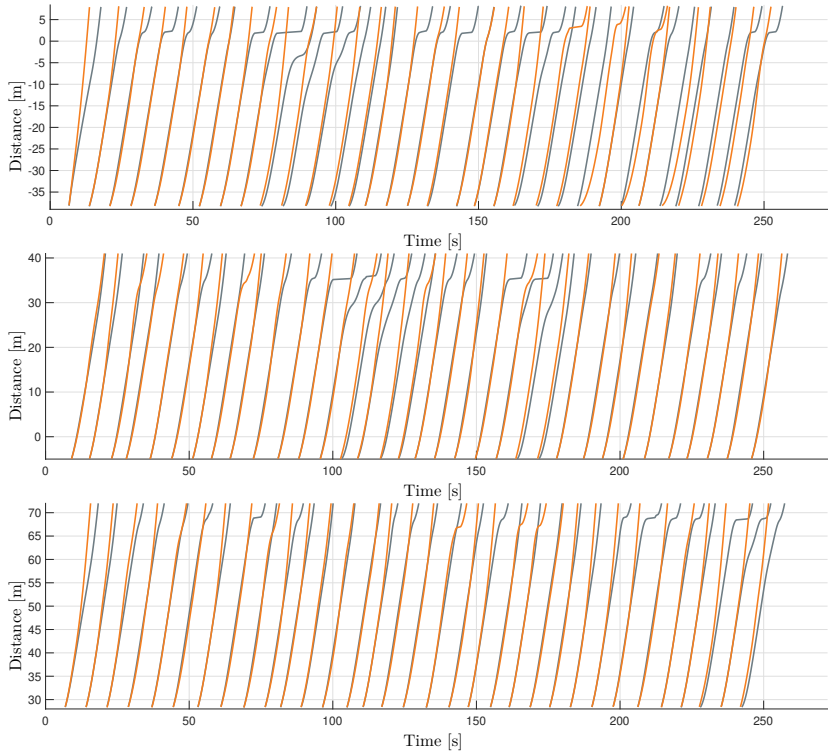

Figure 8.12 – Approaching vehicles' time-distance trajectory resulting from predictive-reactive planning in the scenario. `16R1LR3L1I1O-100V-1500Q[1 1 1]`. The trajectories of R-Agents and PR-Agents are represented by (—) and (—), respectively.

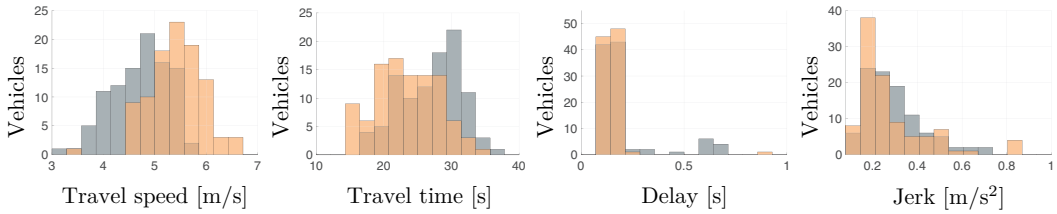

Figure 8.13 – Comparison of the histogram of the registered travel speed, travel time, arrival delay, and jerk of the vehicles in the simulated scenario `16R1LR3L1I1O-100V-1500Q[1 1 1]`, when driven by R-agents (gray) and PR-agents (orange).

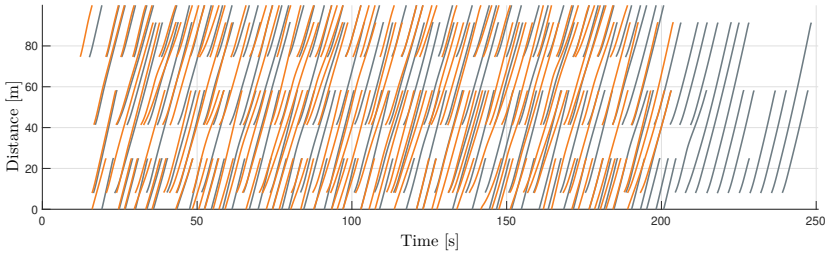

Figure 8.14 – Time-distance diagram representing the evolution over time of the vehicles in the circulatory lane, in the simulated scenario `16R1LR3L1I1O-100V-2500Q[1 1 1]`. The trajectories of R-Agents and PR-Agents are represented by (—) and (—), respectively.

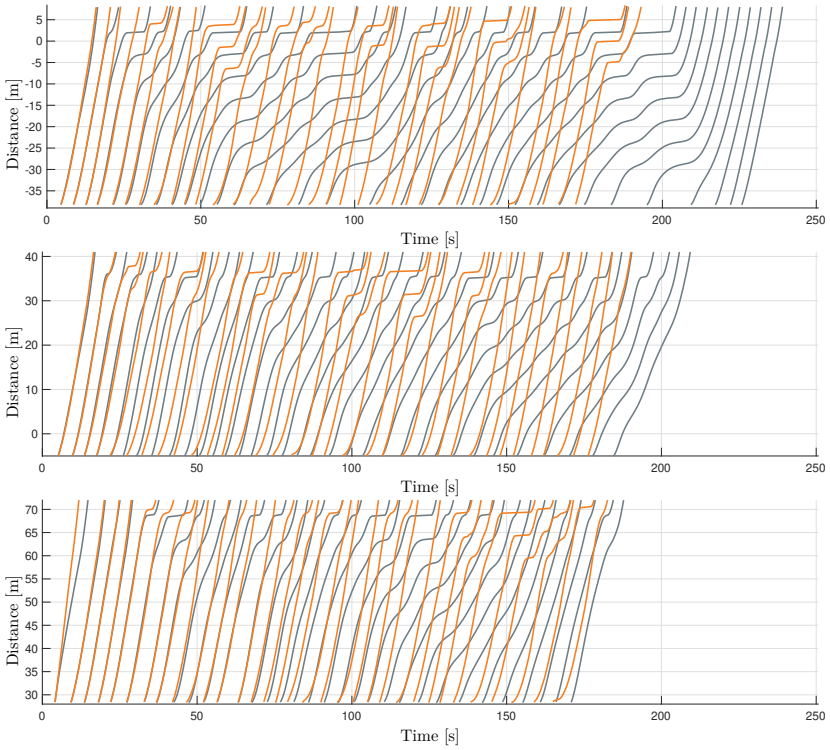

Figure 8.15 – Time-distance diagrams representing the evolution of the incoming traffic in every incoming lane in the simulated scenario `16R1LR3L1I1O-100V-2500Q[1 1 1]`. The trajectories of R-Agents and PR-Agents are represented by (—) and (—), respectively.

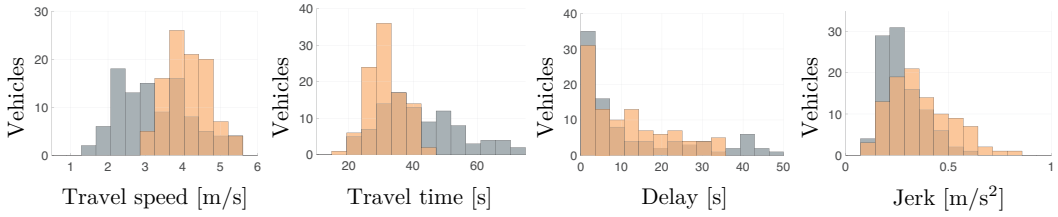

Figure 8.16 – Comparison of the histogram of the registered travel speed, travel time, arrival delay, and jerk of the vehicles in the scenario `16R1LR3L1I1O-100V-2500Q[1 1 1]`, when driven by R-agents (gray) and PR-agents (orange).

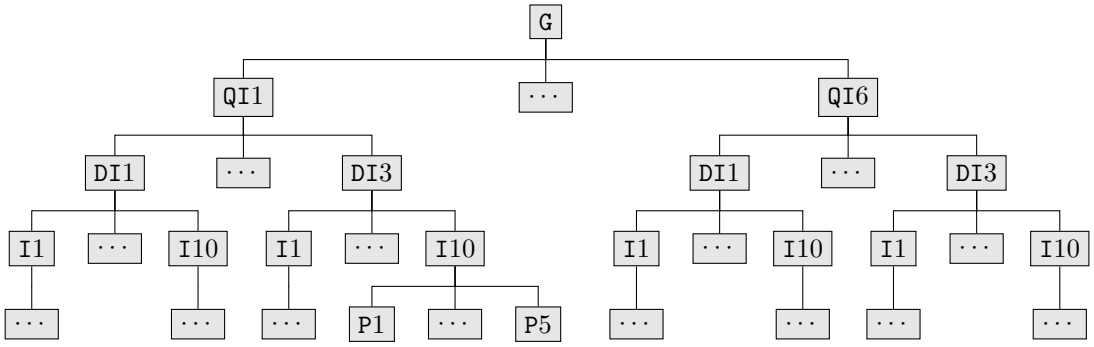

Figure 8.17 – Generation of the batch of simulated traffic scenarios.

planning strategy outperforms the reactive one for all the tested traffic configurations and penetration rates. Regarding the distributions of overall travel speeds, we can observe how not only higher overall travel speeds are achieved, but also that vehicles in the scenario experience a more similar travel speed, i.e. a fairer scenario is generated. Quantitatively, an increment of up to 30% is measured for the highest penetration rate.

Analyzing the distribution of jerk, and consistent with what was observed in the previous Section, the increase in average travel speed comes at the cost of increasing the average jerk vehicles require to drive through the intersection. Part of this effect comes generated by the fact that vehicles sometimes accelerate to pursue maneuver targets that then happen not to be feasible, forcing them to decelerate before the yielding line.

Furthermore, the strategy is observed to have a strong positive impact on the overall intersection throughput, as well as the distribution of 15-min throughput segments. Indeed, we measured a progressive improvement of the intersection throughput with the penetration rate reaching an absolute throughput increase of 250veh/h, i.e. a maximum average relative improvement of 25%.

8.5 Conclusions

In this chapter, an extension of the reactive self-serving maneuver planning strategy proposed in Chapter 5 was formulated, allowing us to consider longer planning horizons and predictions while accounting for uncertainty and guaranteeing safety. This time, the decision-making process considered the whole planning solution space, represented by the set of reachable MTs. For the sake of guaranteeing safety despite the long planning horizons, we further identified the subset of MTs that are safely reachable. That is the subset of MTs that would allow the ego vehicle to comfortably brake and abort the maneuver if the prediction it uses to make an early decision happens not to materialize.

As the formulated maneuver planner is as well based on the probably-free gaps provided by the perception layer, it can be applied to situations where the perception system is affected by occlusions.

The results show that the proposed method brings a significant improvement compared to the baseline reactive self-serving strategy. Indeed, the approach not only renders faster yet safe merging maneuvers despite occlusions but also increases the overall traffic performance at different AV penetration rates.

The proposed strategy could still be extended in several ways. On the one hand, at the time of

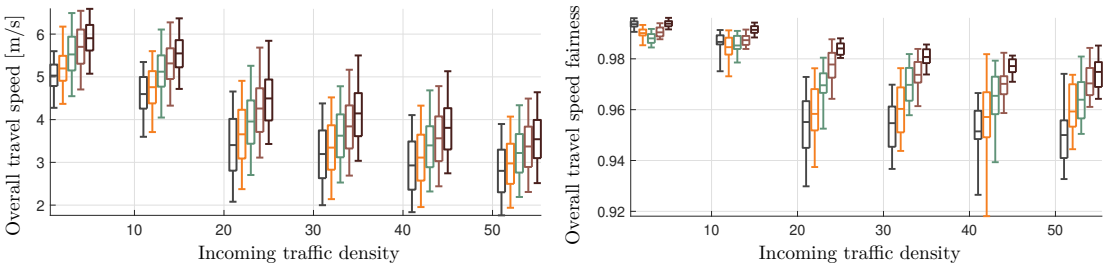

Figure 8.18 – On the left-hand side, boxplots representing the distribution of overall travel speed applied by the vehicles for different incoming traffic inflow configurations and penetration rates. On the right-hand side, the fairness with which the metric is distributed among the vehicles in the scenarios.

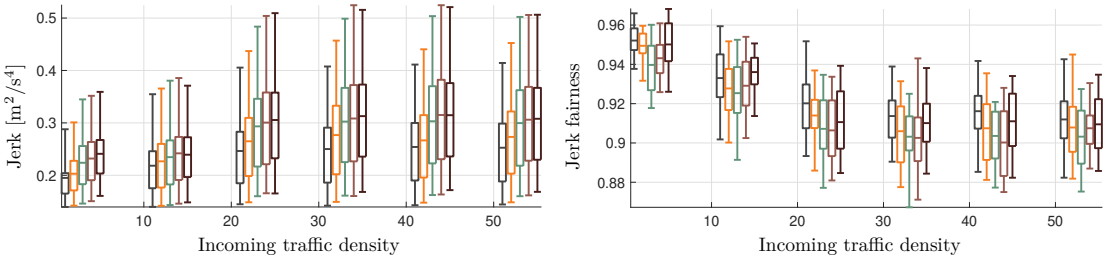

Figure 8.19 – On the left-hand side, boxplots representing the distribution of jerk for different incoming traffic inflow volumes and configurations. On the right-hand side, the fairness with which the jerk is distributed among the vehicles in the scenarios.

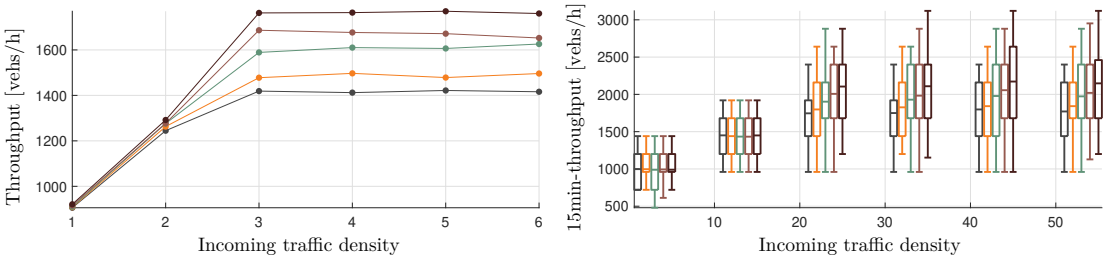

Figure 8.20 – On the left-hand side, the total intersection throughput registered for different incoming traffic density, and values of the penetration rate of PR-agents. On the right-hand side, boxplots representing the distribution of 15min-throughput for different incoming traffic inflow configurations and penetration rates.

evaluating the probability with which the MTs are safe, we have considered uncertainty concerning the future position and velocity of the vehicles in the circulatory lane. However, we still assumed that the vehicles that are currently observed in the circulatory lane would stay in the circulatory lane during the planning horizon. In this direction, the approach could be enhanced by considering that some of the currently observed gaps in the circulatory lane might merge because of the exiting maneuver of some vehicles.

Furthermore, at the time of identifying the MTs that are safely reachable w.r.t. a certain vehicle ahead, we assumed constant velocity of the leading vehicle. This assumption could be indeed relaxed

by adding a term in the MT safety analysis, representing the probability of the MT being safe w.r.t. the position of the currently leading vehicle.

Generally speaking, the proposed strategy has been shown to be a reliable and efficient way of making driving decisions with relatively long planning horizons while guaranteeing safety. Additionally, the proposed method sheds some light on the characteristics that vehicles approaching a roundabout need to take into account to not jeopardize their safety for the sake of arriving at the intersection as soon as possible. Several aspects can still be enhanced and further analyzed, yet the proposed method paves the way towards scalable, efficient, and safe driving decision-making.

9 Application

In this chapter, we apply some of the theoretical results obtained in this dissertation, considering the output of a real experimental detection algorithm. By doing this, we aim to connect the investigations presented so far with the experimental setup of our industrial partners (PSA Group and Safran Tech). The objective of this chapter is twofold. On the one hand, we aim to evaluate the suitability of the perception post-processing strategy presented in Chapter 3 to achieve a meaningful description of the ego vehicle's surroundings in the presence of occlusions. On the other hand, we seek to analyze the decisions made by some of our maneuver planning strategies when applied to the output of a real detection algorithm. Furthermore, we will also discuss the challenges that may arise for the evaluation of the planning strategies not validated in this setup.

A significant challenge we encountered in the process is related to the fact that some of the strategies studied in this thesis are built upon the assumption of highly capable perception modules (for instance, capable of vehicle-to-vehicle communication). Hence, evaluating the impact of the strategies requires having control over the trajectory planner. However, as will be described, we are constrained to perform an off-line evaluation. Thus, we cannot influence the trajectory followed by the vehicles in the data set. Instead, we will perform an off-line validation of our strategies when they are applied to inaccurate detection information and will compare the results of the decision-making approaches with the ones made by the person driving the experimental vehicle during the data collection tests.

To put into perspective and understand the motivation behind the specific task carried out in this chapter, we start in Section 9.1 by describing the context in which the exploited data set was gathered and further defining the scope of our application. We then continue by presenting in Section 9.2 the structure of the application as well as its main components. Results are then provided in Section 9.3, where we show the information that the proposed perception post-processing would provide, as well as the decision made by some of the planning algorithms in this thesis. Finally, the chapter ends in Section 9.4, where our conclusions and further remarks are gathered.

9.1 Experimental setup and data set

The data set this chapter is built upon is the result of a series of experiments performed by our industrial partners, the PSA Group and Safran Tech, near the facilities of Safran Tech in Chateaufort,

France.

The experiments were initially intended to test a series of detection algorithms in an environment populated with objects that cause occlusions. Consequently, the experiments consisted of a person driving a car (equipped with cameras and a LIDAR sensor) several times through a set of two roundabouts connected by a straight road, while the vehicle's perception system detected the surrounding vehicles.

The provided data set contains:

- a pixel-based map (Fig. 9.1) with a color code to identify: (i) the circulatory lanes of the roundabouts, (ii) the lanes within each roads, and (iii) regions of the lanes approaching the roundabout where completely stopped vehicles could be expected to be found,
- the position of the ego vehicle as it moves in the scenario (Fig. 9.2),
- the speed of the ego vehicle over time (Fig. 9.3), from which the acceleration profile can be obtained,
- the estimated position, orientation, and size of the surrounding vehicles detected, and
- the video footage of the whole experiment, captured from two cameras attached to the vehicle's front bumper.

Given the above-described data set, our objective is to evaluate the decision-making output of some of the proposed planning strategies when they are exposed to the real detection information acquired during the experiments. As expected, the information concerning the detection of surrounding vehicles was somewhat inaccurate, since the detection system the experiments were meant to test was in development. Thus, one of the main aspects we are interested in evaluating in this chapter concerns the impact of such inaccuracies and uncertainties in the proposed probably-free gaps extraction process, and the decisions generated by some of the proposed planning approaches.

9.2 Application implementation description

The implementation of our application follows the pseudocode in Alg. 6, where two main stages can be identified. On the one hand, we need to build an approximated geometry model of the roundabouts found in the map so that we can afterward position surrounding obstacles on specific lanes of the intersection and infer if they are merging, exiting, etc. This step does not need to be executed at a high frequency, but rather when roundabouts that have not been previously modeled are detected to appear in the surrounding map. In our setup, this step is performed off-line as the map where the experiment takes place is known beforehand.

On the other hand, the following steps are performed in a high-frequency loop while the ego vehicle evolves through the scene:

- receive information from the perception layer concerning the ego vehicle's position in the map and the surrounding obstacles (i.e. retrieving information from the data set),
- identify the specific roundabout that is being approached by exploiting the localization of the ego vehicle and the simplified roundabout models extracted from the map,
- approximate the field of view of the vehicle given the surrounding detected obstacles and the presumed occluding environmental elements,
- update the dynamic occupancy grid (DOG) representation of the circulatory lanes where the detection and higher-level information is fused,

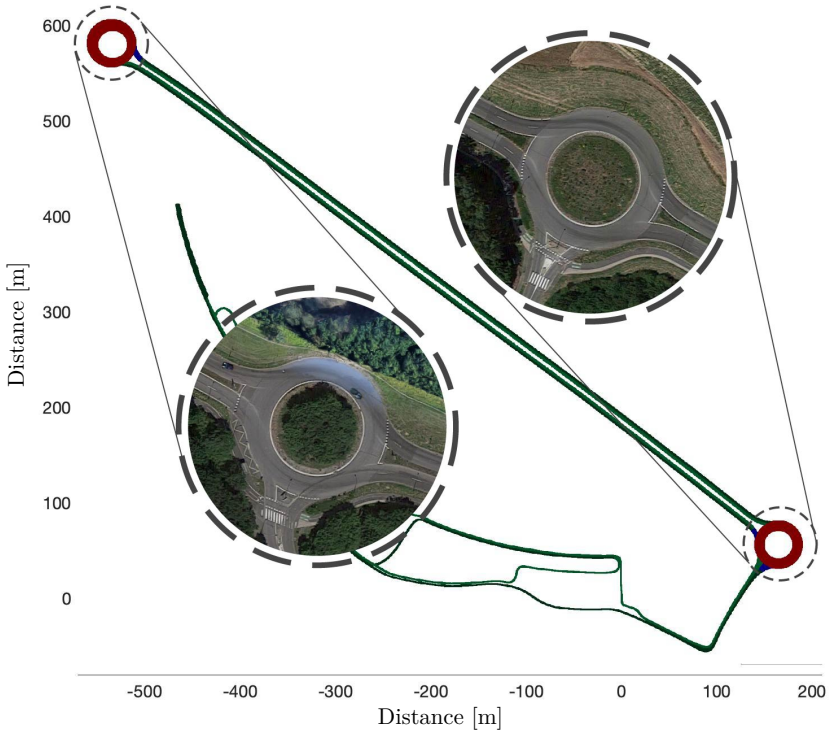

Figure 9.1 – Map of the scenario where the experiments take place. Green pixels represent lanes where the ego vehicle is allowed to drive. Red pixels show positions inside the surrounding roundabouts. Blue pixels, found in the incoming lanes to the roundabout, show the areas where the ego vehicle could expect to find fully stopped vehicles, and would be allowed to fully stop itself.

Algorithm 6: Application pseudocode

Input: Map
Output: go/no go
$\mathcal{R} = \{\mathcal{R}_1, \cdots, \mathcal{R}_{n_\mathcal{R}}\} \leftarrow$ roundabouts detected in the map;
while *1* **do**
    Localize the ego vehicle;
    Detect surrounding obstacles;
    Identify the roundabout the ego vehicle approaches;
    Estimate the field of view given the surrounding objects;
    Update the Bayesian Occupancy Grid;
    Extract probable-free gaps from DOG;
    Trigger maneuver planner for a go/no go decision;
end

- extract the probably-free gaps in the circulatory lane from the DOG, and
- trigger the planning strategies and record the decision made for further comparisons.

In the following sections, further details of the previous steps will be provided.

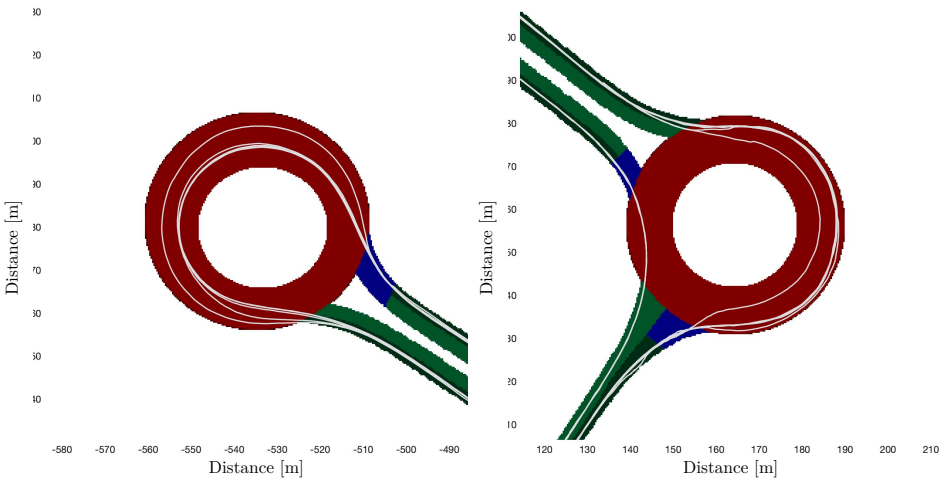

Figure 9.2 – Trajectory traces of the experimental vehicle while crossing the two roundabouts in the scenario. Note that both roundabouts are two-lane roundabouts.

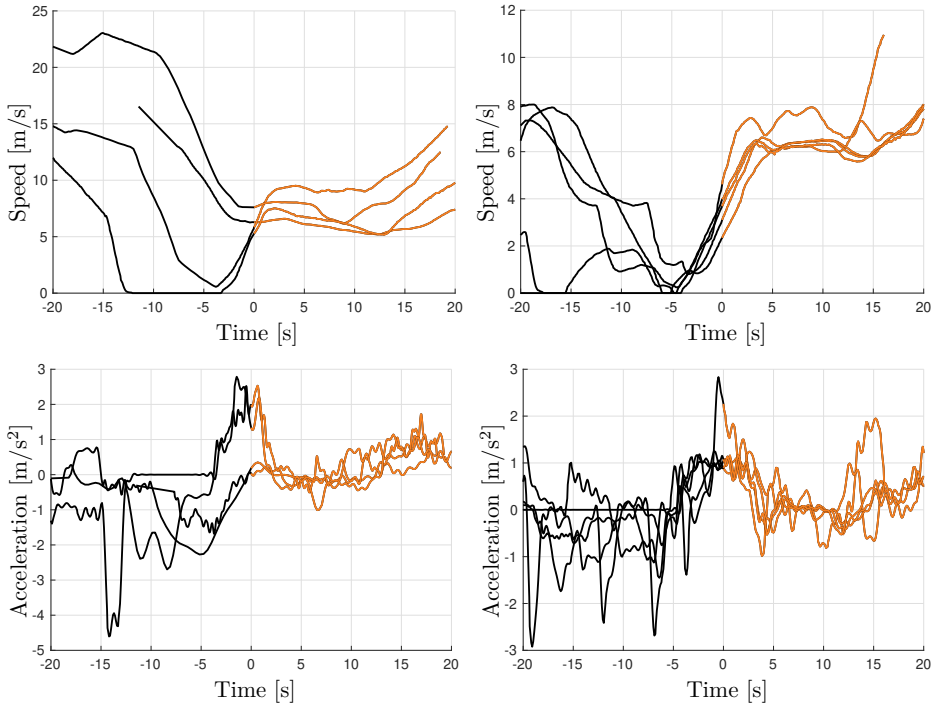

Figure 9.3 – Examples of the speed and acceleration merging profiles registered in each of the roundabouts in the scenario. Segments (—) represent positions out of the roundabout, while (—) correspond to instants where the ego vehicle is inside either of the roundabouts.

9.2.1 Scene processing

The so-called preprocessing step aims to generate a simplified geometric model of the roundabout. Such a model will enable us to extract high-level knowledge from the surrounding vehicles' position

and construct the dynamic occupancy grid representation of the circulatory lanes.

Definition 22 (Simplified roundabout geometric model)**.** *The approximated geometry of a roundabout is here represented by* $\mathcal{R} = (p_{\mathcal{R}}, \mathbf{R})$*, where*

- $p_{\mathcal{R}} = (x_{\mathcal{R}}, y_{\mathcal{R}})$ *shows the position of its center, and*
- $\mathbf{R} = (r_1, r_2, \cdots, r_{n_R})$*, with* $r_k < r_k + 1$*, gathers the radii of the circulatory lane's boundaries.*

In our particular case, the identification process is straightforward given the color code used in the map representing the surrounding roads. The task simply consists in:

1. clustering the red pixels of the map so that the groups of red pixels related to each roundabout are differentiated, and
2. identifying the center of the roundabout by finding the white pixel around which the two smallest concentric circles containing all the red pixels can be built.

In particular, denoting the set of white pixels where the center of the roundabout could be as $\mathcal{P}^{\mathrm{W}}$, and the set of red pixels related to one roundabout as $\mathcal{P}^{\mathrm{R}}$, the pixel representing the center of the roundabout (from which the position $p_{\mathcal{R}}$ is later inferred) can be obtained as

$$j^* = \arg\min_{j \in \mathcal{P}^{\mathrm{W}}} (r_{out}(p_j) - r_{in}(p_j)), \tag{9.1}$$

where

$$r_{in}(p_j) = \min_{i \in \mathcal{P}^{\mathrm{R}}} \|p_j - p_i\|_2, \qquad r_{out}(p_j) = \max_{i \in \mathcal{P}^{\mathrm{R}}} \|p_j - p_i\|_2 \tag{9.2}$$

represent, respectively, the minimum and maximum radii within all red pixels are contained.

Then, we could estimate the number n_l of circulatory lanes as

$$n_l = \left\lceil \frac{r_{out}(p_{\mathcal{R}}) - r_{in}(p_{\mathcal{R}})}{3} \right\rceil \tag{9.3}$$

and construct the vector $\mathbf{R} = (r_1, \cdots, r_{n_l})$ of boundaries radius considering

$$r_i = r_{in}(p_{\mathcal{R}}) + \frac{(i-1)}{(n_l - 1)} (r_{out}(p_{\mathcal{R}}) - r_{in}(p_{\mathcal{R}})). \tag{9.4}$$

Afterward, the DOG is initialized so that we have a placeholder to store the polar discretization of the circulatory lanes and the probability distributions assigned to each cell (see Fig. 9.4). As we are always approximating the roundabouts with perfectly concentric circles, and the ego vehicle approaches one roundabout at a time, only one DOG placeholder is needed.

Additionally, the roundabout models could be further exploited to identify environmental objects that could be expected to cause occlusions and have an impact on the decision-making performance. The worst-case scenario would correspond to considering two types of environmental occlusions. On the one hand, it should be assumed that the roundabout island occludes the opposite side of the roundabout. On the other hand, we will further consider that occluding environmental elements that form a narrow corridor around the incoming lanes. As a result, the region of the roundabout that must be observed to make the merging decision would only be visible when the ego vehicle is sufficiently close to the intersection.

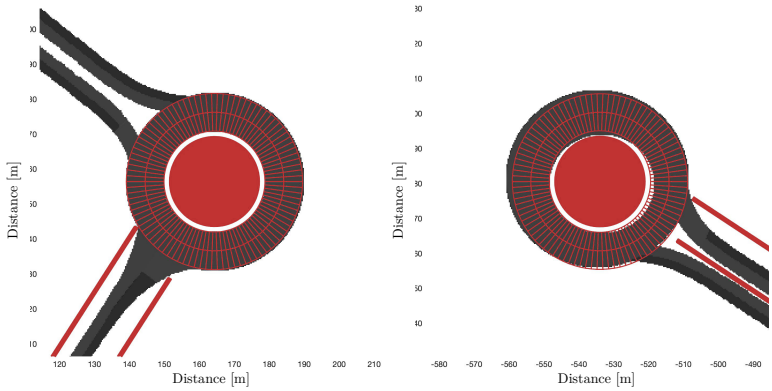

Figure 9.4 – Representation of the two roundabouts in the experimental scenario, along with the fitted occupancy grid, and the considered environmental obstacles.

9.2.2 Approaching roundabout

In cases where several roundabouts surround the ego vehicle, a procedure needs to be envisioned to identify which specific roundabout is the one being approached. We tackle the process by first calculating the vectors $\vec{r}_{\text{ego}}^{\mathcal{R}_i}$ with the ego vehicle's position as the origin and the center of the roundabout i as the destination. Then, denoting as $\vec{\psi} = (\cos(\psi), \sin(\psi))$ a unitary vector aligned with the ego vehicle's orientation, the roundabout r^* being approached can be found as

$$r^* = \arg \min_{i \in [1, n_{\mathcal{R}}]} \left\{ \|\vec{r}_{\text{ego}}^{\mathcal{R}_i}\|_2 : \vec{r}_{\text{ego}}^{\mathcal{R}_i} \cdot \vec{\psi} \geq 0.5 \right\}, \tag{9.5}$$

that is, by identifying the closest roundabout found in the direction in which the ego vehicle is oriented.

9.2.3 Perception information

As explained in Chapter 3, the obstacles detected by the perception layer and the presumed occluding environmental objects are then taken into account to (i) maintain the occupancy probability of the DOG's cells, and (i) infer the probably-free gaps from the DOG.

9.2.4 Decision-making

The information the perception module provides could then be used as the input of the decision-making strategies discussed in this thesis. Nonetheless, we opt, in this chapter for only analyzing the reactive planner used as the baseline (i.e. the one formulated in Chapter 5). Among other reasons, we do so because comparing the baseline strategy to a human driver would enable us to draw conclusions about the performance of the remaining strategies w.r.t. the human driver—as all strategies are compared to the reactive baseline.

In this context, the role of the tactical planner in our motion planning architecture is simplified, as we only aim to study the merging decision. In particular, we run the reactive maneuver planner for a set of two maneuver candidates: one representing the merging maneuver into the outermost circulatory lane, and a second one describing the merging maneuver into the innermost one.

9.3 Results

There are two fundamental results we aim to analyze in this section. On the one hand, we are interested in seeing how the DOG and probably-free gap extraction procedure proposed in Chapter 3 performs given the inaccurate detection of the exploited perception algorithm. On the other hand, we aim to analyze the decision of the reactive self-serving maneuver planner formulated in Chapter 5 and compare it with the decision made by the human driver in the experiments.

9.3.1 Perception post-processing

In this section, we assess the performance of the proposed DOG perception post-processing using the detected object in the dataset. The discussion will be based on Fig. 9.5, where we represent:

- The evolution of the occupancy probability of the DOG over time (shaded background) represented as described in Chapter 3, and by splitting the two circulatory lanes into two separate plots for the sake of clarity.
- The ego vehicle's angular position, w.r.t. the roundabout's center, shown by the bi-color trajectory starting around the middle of the plot. The colors used represent whether the ego vehicle is (—) inside or (—) outside the roundabout at every time step. Since the incoming lane by which the vehicle approaches the roundabout is nearly radial to the roundabout, such a trajectory is roughly horizontal while the vehicle approaches the roundabout.
- The angular position of the detected obstacles over time (—). In particular, only those detections of objects inside the circulatory lanes of the roundabout are shown.

In the representation, there are several features that should be stressed. On the one hand, as the roundabout's island is assumed to occlude the other side of the intersection, only half of the roundabout (at most) should be expected to be observed. As a consequence of this occlusion, the visible area (shown by the bright pixels in the images) is always surrounded by a darker band corresponding to the occluded side of the roundabout. Moreover, the region below the ego vehicle's trajectory corresponds to what it sees on the left-hand side, which corresponds to the most critical area for the merging decision. Thus, when the vehicle merges into the roundabout (where the trajectory transitions from black to orange), the free space (bright pixels) below the trajectory represents the gap size that the driver considered safe to perform the merging maneuver.

Furthermore, at the beginning of the plots, we can observe dark regions roughly shaped as ellipses. Such areas represent the occlusions caused by the environmental element presumed to form a narrow corridor around the lane by which the ego vehicle approaches the intersection.

Every time an obstacle is detected, deep dark areas show appear, representing that such locations are almost certainly occupied.

The advantages that were attributed to the perception post-processing procedure in Chapter 3 are observed to persist when the method is applied to a real perception output.

- the smoothness with which the cells' occupancy probability evolves allows retaining prior knowledge concerning the occupancy of some cells when they are briefly occluded, and
- the instantaneous false-positive detections are observed to be retained by the DOG for a short time, allowing the ego vehicle to make decisions more conservatively by considering that such a quick detection might indeed be caused by a real obstacle that was lost.

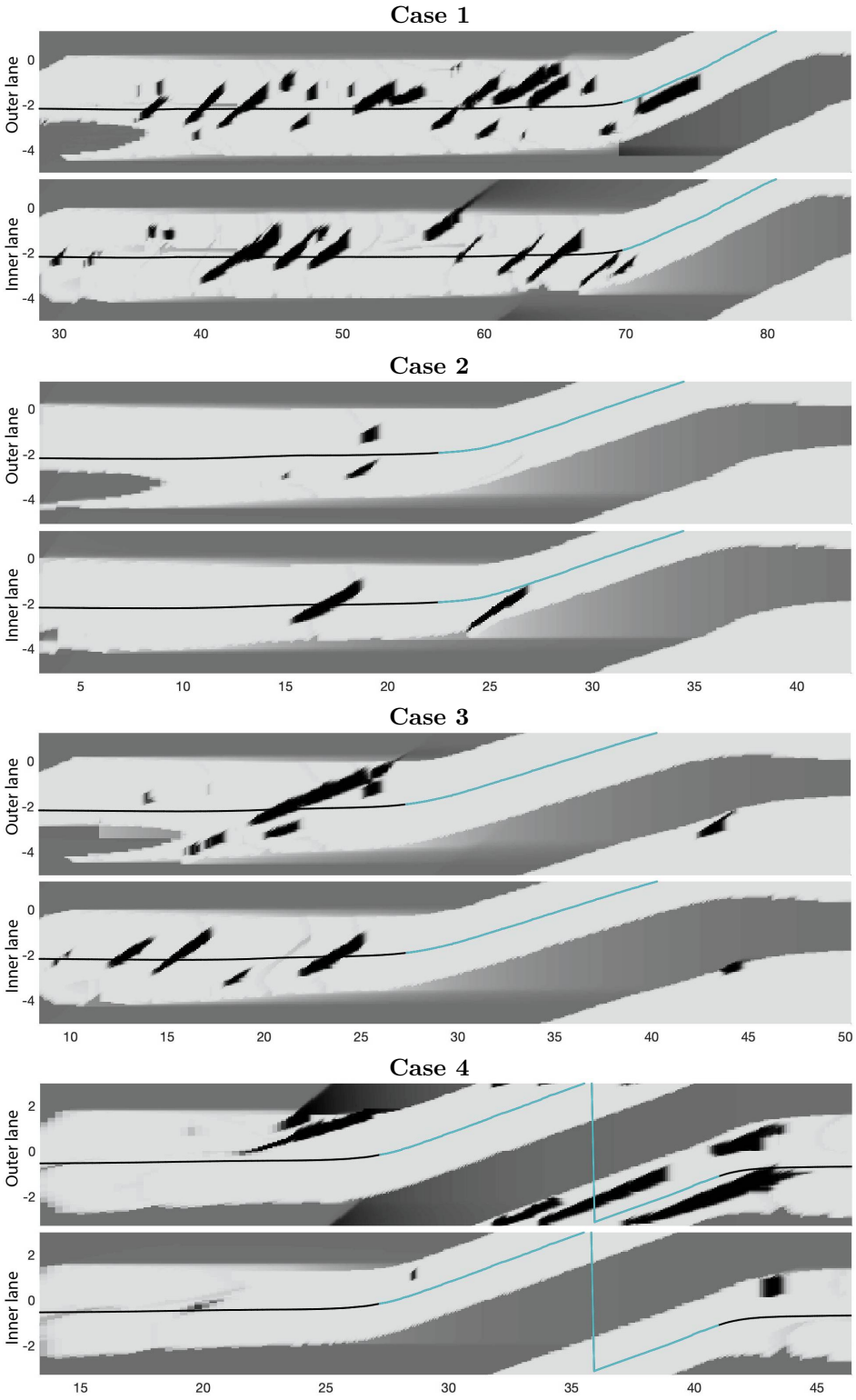

Figure 9.5 – Samples of the evolution of the DOG representing the occupancy state of the circulatory lanes, in four different scenarios registered in the provided data set.

9.3.2 Gap inference

In this section, we represent the state of the DOG and the extracted probably-free gaps in a set of nine different situations, aiming to illustrate that the information derived from the DOG is meaningful for it to be the foundation of any decision-making strategy.

The results are shown in Fig. 9.6-9.8[1], where we show, for every chosen instant: the state of the DOG, the probably-free gaps extracted from it, and the images captured by the two onboard cameras so that the real surrounding space can be visualized.

As observed, the information provided by the DOG, as well as the extracted free gaps, accurately represents the state of the visible area of the roundabout. This shows that the addition of environmental occluding elements forming a corridor around the incoming lanes does provide a more realistic representation of the environment.

Concerning the extracted probably-free gaps, in general, the free inter-vehicle gaps should not be expected to be represented by a single gap, but rather by a set of them corresponding to different certainty levels. In the figures, the probability of the gaps being free is shown by the gap's width. Hence, the wider the represented gap, the more likely the gap is to be free. Especially in areas that are delimited by the boundary of the occluded regions, where the transition to unknown occupancy probability is smooth, it is often possible to guess, with a slightly lower certainty, that the free space does indeed extend beyond the visible region.

Moreover, the suitability of considering the narrow corridor around the incoming lanes can be observed in cases 01, 06, and 08. There, the bushes surrounding the incoming lane occlude the view and prevent the ego vehicle from correctly detecting the obstacles in the circulatory lanes.

Additionally, the smooth transition model that is exploited by the DOG was claimed to retain previous information of certain regions, which allows a better estimation during relatively short occlusions. Such an effect can be observed in cases 04 and 09.

Finally, merging paths are represented in those cases where the reactive maneuver planner would consider the merging maneuver to be safe. In this direction, the algorithm would consider cases 01, 03, 06, 08, and 09 unsafe, either because the ego vehicle is too far from the intersection, or because of the specific configuration of the observed inter-vehicle gaps. In cases 04 and 05, a merging maneuver to the outermost circulatory lane is considered safe. Moreover, in cases 02 and 07, the merging maneuver into any of the two circulatory lanes is considered feasible. Although a more detailed comparison concerning the decision-making result will be tackled in the following section, intuitively, it can be seen that the merging trajectories that are considered safe by the algorithm would also be considered so by a human driver.

9.3.3 Decision-making

In this section, we aim to perform a more thorough comparison of the output of the proposed reactive planner and the merging maneuver performed by the human driver in the experiments. The results are shown in Fig. 9.9-9.11, where the decisions made by the implemented planner will be illustrated by showing:

- a 3D representation of the trajectory followed by the ego vehicle as it drives through the roundabout, with the speed represented in the vertical axis,
- the speed evolution over time,

[1]The video from which such set of frames has been extracted is available in https://youtu.be/mxfsCDIRXUU.

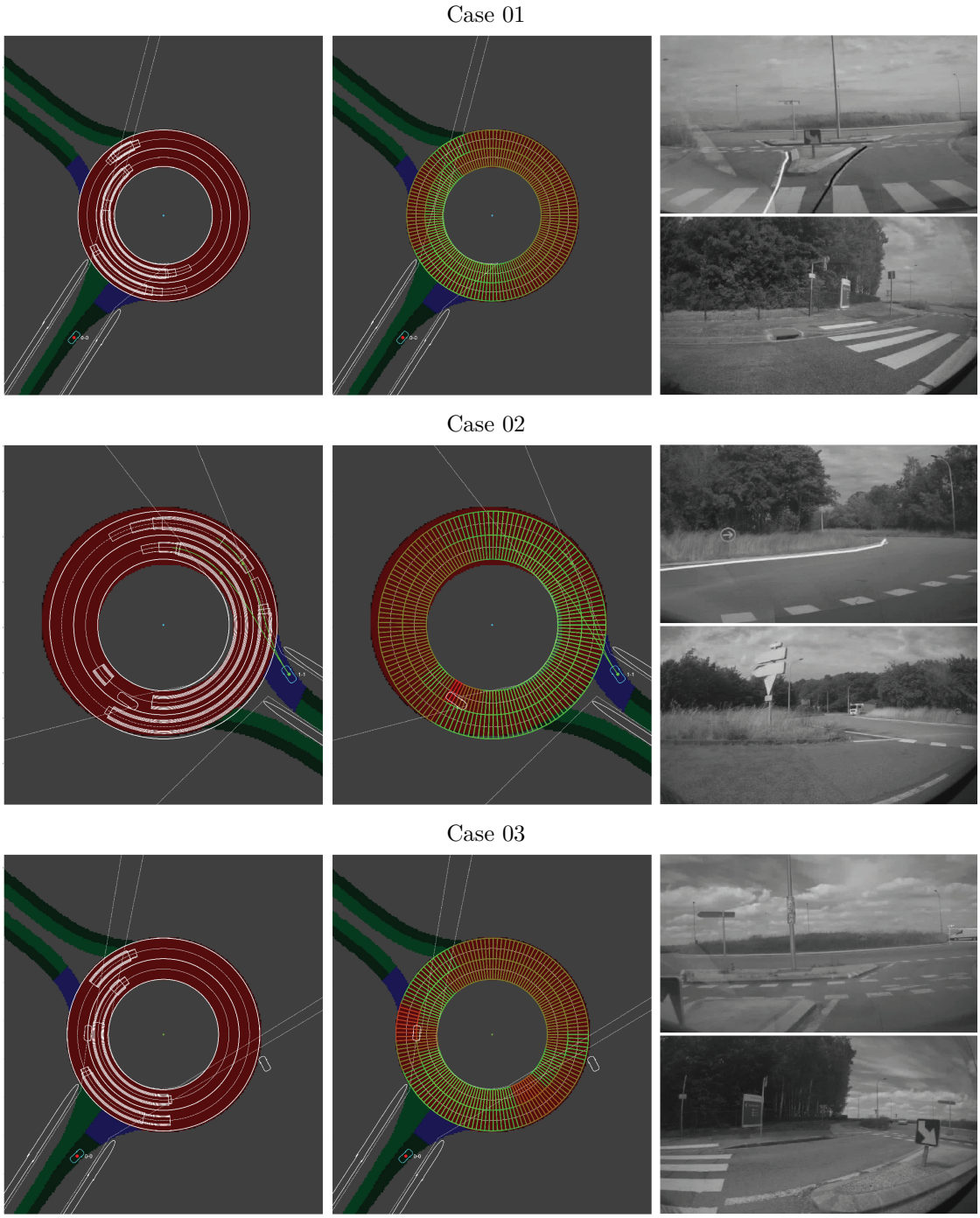

Figure 9.6 – Representation of the probably-free gaps extraction at three different times (one case per row). Cases 1-3. From left to right: state of the DOG representing the occupancy probability distribution of the circulatory lanes, representation of the extracted gaps, footage of two cameras in the vehicle's front bumper.

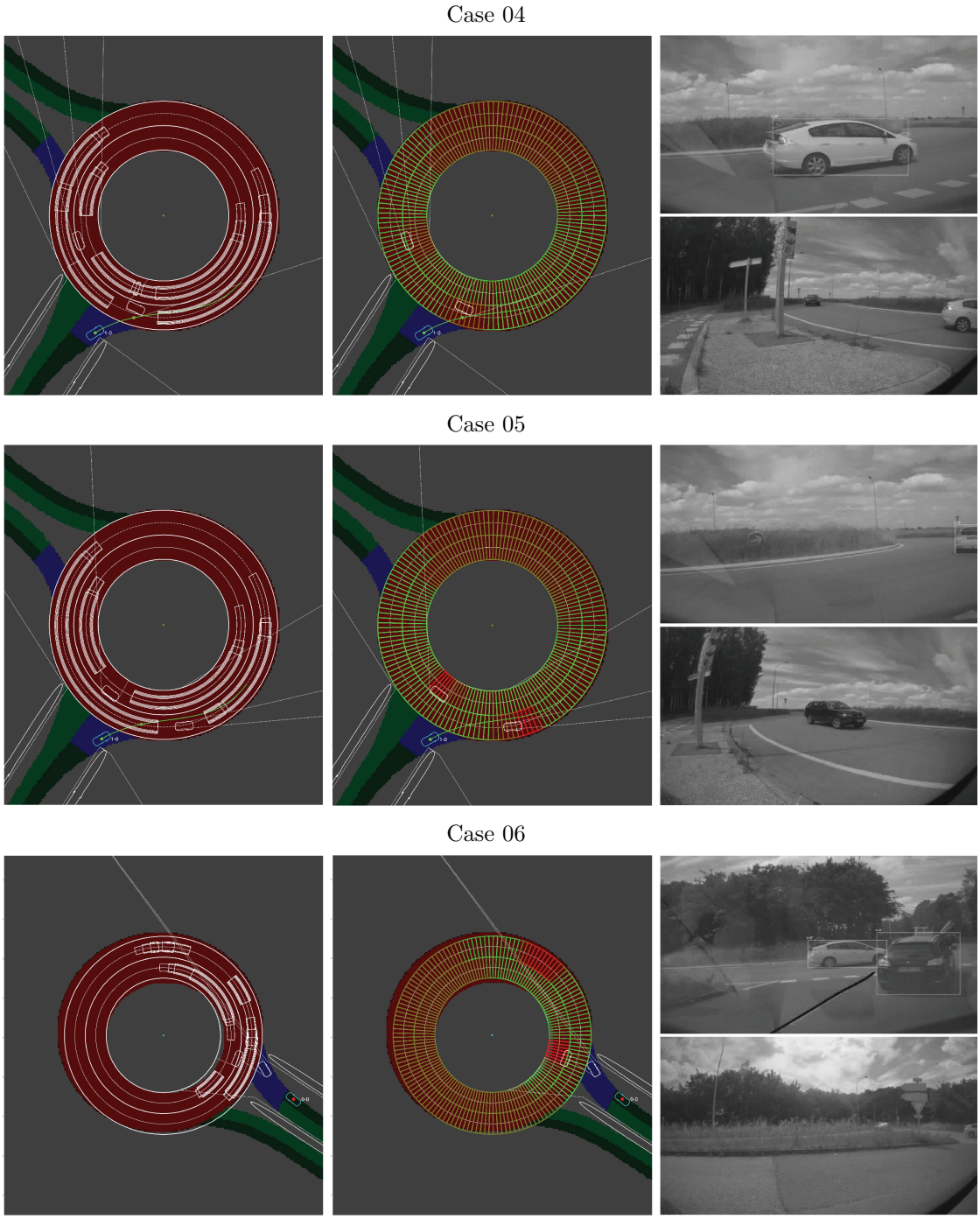

Figure 9.7 – Representation of the probably-free gaps extraction at three different times (one case per row). Cases 4-6. From left to right: state of the DOG representing the occupancy probability distribution of the circulatory lanes, representation of the extracted gaps, footage of two cameras in the vehicle's front bumper.

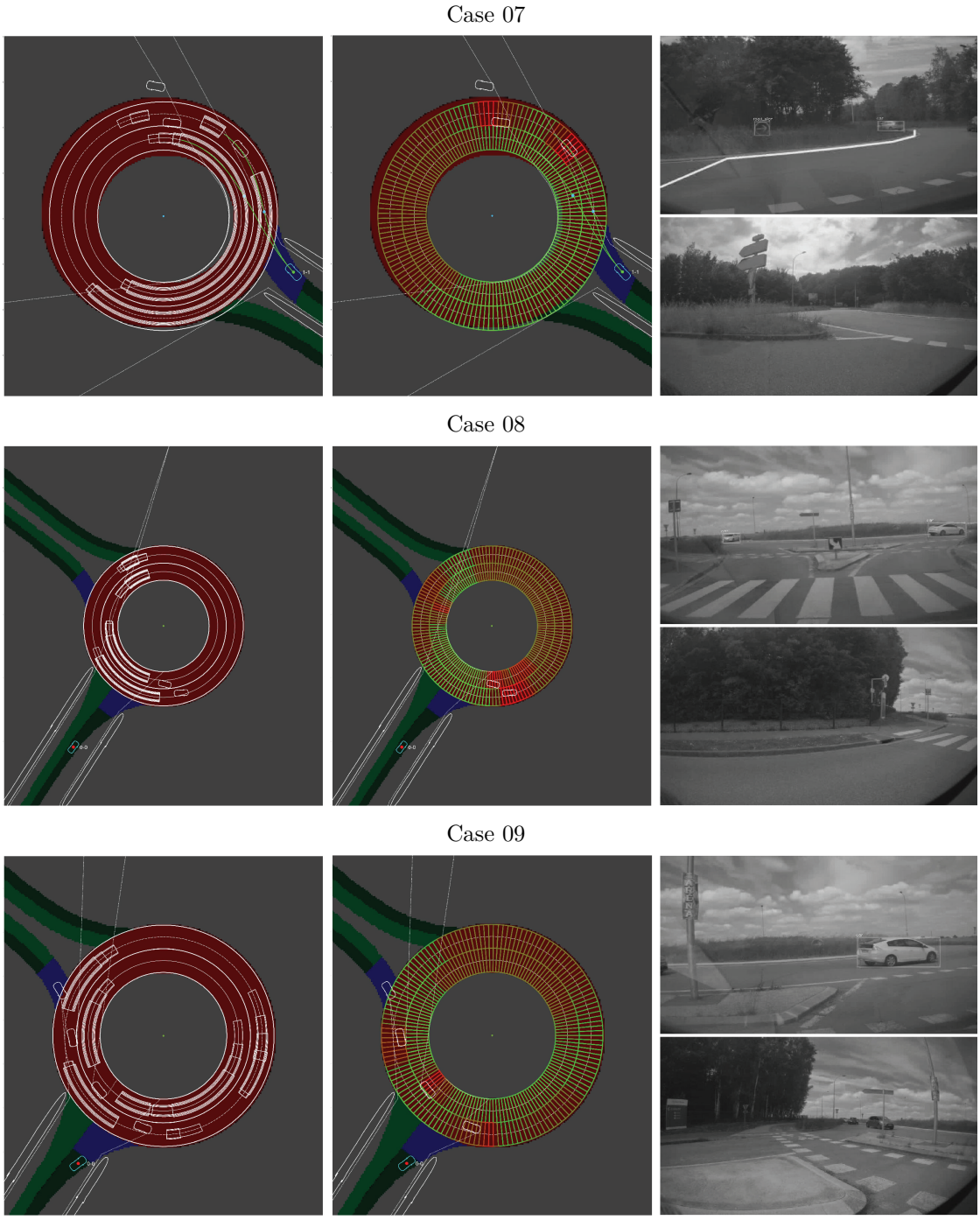

Figure 9.8 – Representation of the probably-free gaps extraction at three different times (one case per row). Cases 7-9. From left to right: state of the DOG representing the occupancy probability distribution of the circulatory lanes, representation of the extracted gaps, footage of two cameras in the vehicle's front bumper.

- the distance to the center of the roundabout over time,
- the angular position of the vehicle over time, superimposed on the evolution of the DOG so that decisions can be observed along with the contextual representation they are based on.

Moreover, the following color code has been used to represent the output of the decision-maker within the representation of the trajectories:

- segments (—) represent the instants when the algorithm considers safe merging into any of the two circulatory lanes,
- segments (—) show the times at which the algorithm finds safe merging only into the outermost circulatory lane,
- segments (—) illustrate the periods during which the ego vehicle is inside the roundabout,
- segments (—) mark the remaining portions of the trajectory.

In general terms, it can be observed that even the simplest of the approaches formulated in this thesis presents a higher-level of reactivity than the human driver involved in the experiment. The algorithm is indeed able to react faster to situations where the merging maneuver is not possible. This effect can be seen at the instants marked with ① when the algorithm does not see a feasible merging maneuver (as shown by the fact that the trajectory becomes (—)) before the human driver starts decelerating.

Similarly, the merging maneuvers are sometimes detected faster by the algorithm, as can be seen in the moments marked with ②, when the algorithm considers the merging maneuver safe instants before the human driver starts accelerating. Also, as the driver in the experiments performed the merging maneuver with different levels of conservativeness, there are occasions where the algorithm recommends performing the merging maneuver even though the driver does not do it.

Furthermore, at times when the algorithm determines that it is only possible to merge into the outermost circulatory lane (③), the human driver shows a somewhat hesitating behavior and seems to approach the intersection more carefully. This behavior might be caused by the human driver not feeling confident enough to merge into the outermost circulatory lane while having another moving vehicle in parallel. Such behavior would indeed be reasonable if the driver predicted that such a vehicle would soon occupy the outermost circulatory lane to exit the roundabout. Although this is a behavior that would result from considering sophisticated traffic predictions, a similar result could be obtained from the tested decision-maker by considering the roundabout as a single-lane roundabout, thereby forcing the algorithm to trigger merging maneuvers only when both circulatory lanes are empty.

9.4 Conclusions

In this chapter, we have applied the baseline reactive planning strategy to real object detection information, and compare the reactive decision-making with the decisions made by a human driver. Emphasis has been made on how the proposed motion planning architecture, and the DOG it is built upon, deal with dynamic occlusions.

The use of a DOG to infer probably-free gaps that would then be used by the decision-makers is a robust and viable strategy to deal with motion planning under occlusions and other sources of uncertainty, such as false-positive detections. In particular, it has been observed that due to the smooth dynamics with which the probabilities of the DOG evolve, it successfully retains the

knowledge concerning the occupancy of specific cells during short and dynamic occlusions. Moreover, due to the use of the DOG, the proposed system should be able to fuse and provide meaningful probabilistic information even if there are other perception inaccuracies.

The reactive planner tested was observed to perform relatively well, especially when compared to the behavior of the human driver in the experiments. Specifically, it was seen to react faster than the human driver in some cases, and render reasonable decisions given the available perception information. Such reactive behavior is the one used as a baseline for our more advanced planning strategies. Thus, as they were shown in our simulation studies to outperform the baseline considerably, better behaviors could also be expected from their application in a more realistic setup.

Even though some of our methods were successfully applied to the data set provided, there is still room for improvement. For instance, while comparing the decision-maker output with the decisions made by the human driver is indeed interesting, determining whether the decisions made by the algorithm are safe would require knowing the actual positions of the vehicles around the ego vehicle. Such information could be obtained by involving an additional driver in the experiments while registering their position with a GPS, or for instance, recording the scene from a zenith perspective and then post-processing the footage to obtain the location of the surrounding vehicles.

Regarding the identification of occlusions, we have implemented our strategies by taking a conservative approach, i.e. assuming that, without exception, the island of the roundabout and elements on the left-hand side and right-hand side of the approaching roads cause occlusions. A better approach would be to make use of the labeled LIDAR point cloud along with the map, to identify which parts of the nearby roads are not visible, and then dynamically generating environmental occluding objects accordingly.

Furthermore, an additional enhancement that could be implemented concerns the simplified geometric model. On the one hand, we have assumed perfectly circular geometry, which does not always fit the real geometry of the roundabouts. Consequently, it might be reasonable to extend the model so that it can better approximate the actual geometry of the observed intersections. Moreover, we have further assumed that there is no information available concerning the position of the legs in the roundabout, which would be of interest to assess the spots in which the detected vehicles are likely to appear and disappear. Adding some basic information about the incoming/outgoing legs of the roundabout, which could be done by using the map itself, or even the trajectory of the observed obstacles, would provide further options to improve the roundabout model, and refine the occupancy probability of the DOG.

In summary, although several aspects of our experiments could be enhanced, our proposed strategy provides a considerable level of robustness concerning the detection of the probably-free gaps in the circulatory lanes. Explicitly, the shown results confirm the suitability of using a gap-based representation of the circulatory lanes to address the merging maneuver into roundabouts and highlight the similarities between the reactive maneuver planner (used as baseline behavior in this thesis) and a human driver.

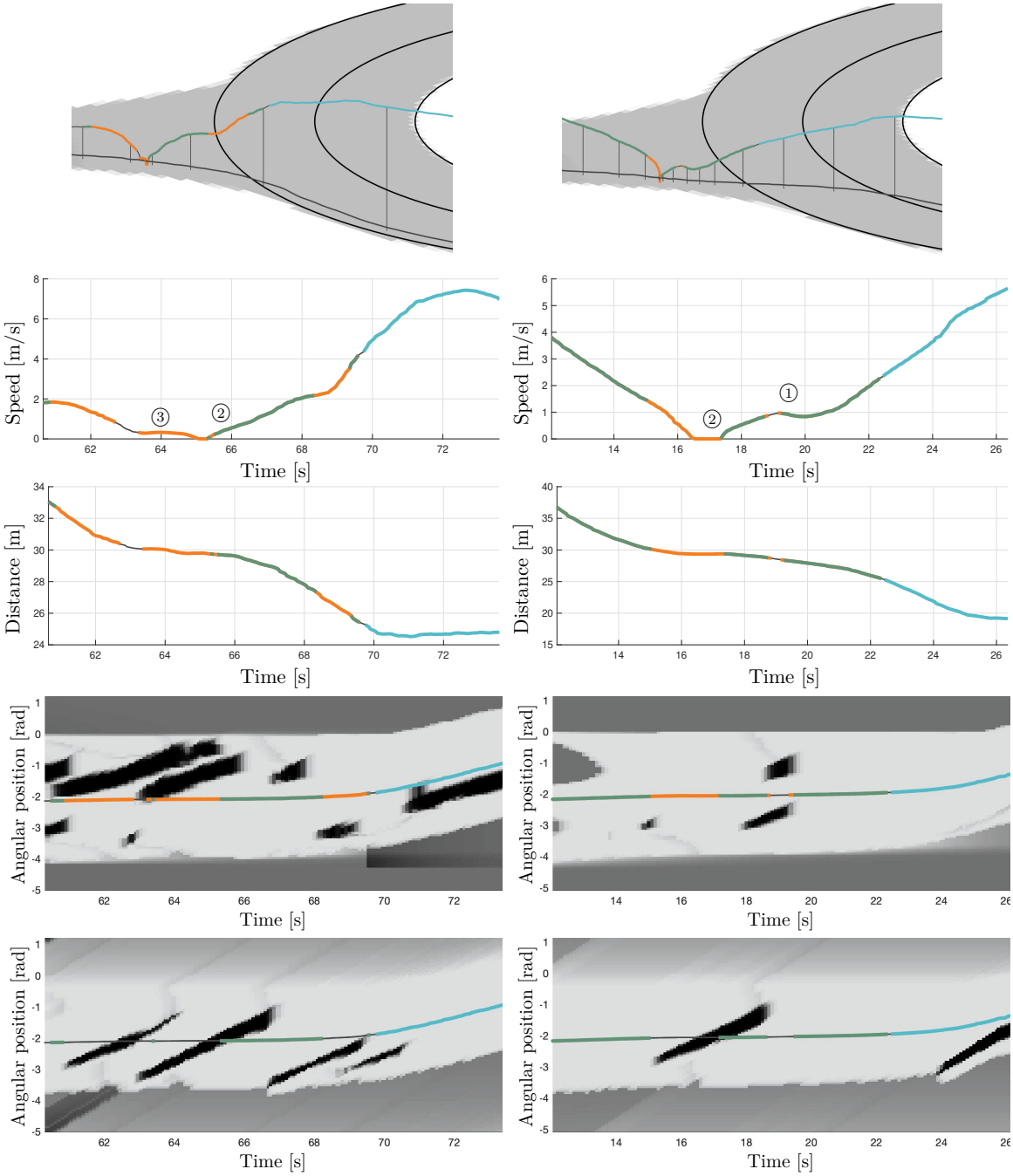

Figure 9.9 – Reactive maneuver planner output for two merging maneuvers registered within the data set. Examples 1-2. From top to bottom: three-dimensional representation of the merging maneuver (with elevation representing speed), speed profile, evolution of the distance to roundabout's center, and the evolution of the DOG for the two circulatory lanes. Trajectories color code: (—) shows that merging into any of the two circulatory lanes is considered safe, (—) shows that only merging into the outermost circulatory lane is safe, (—) illustrates that the ego vehicle is inside the roundabout.

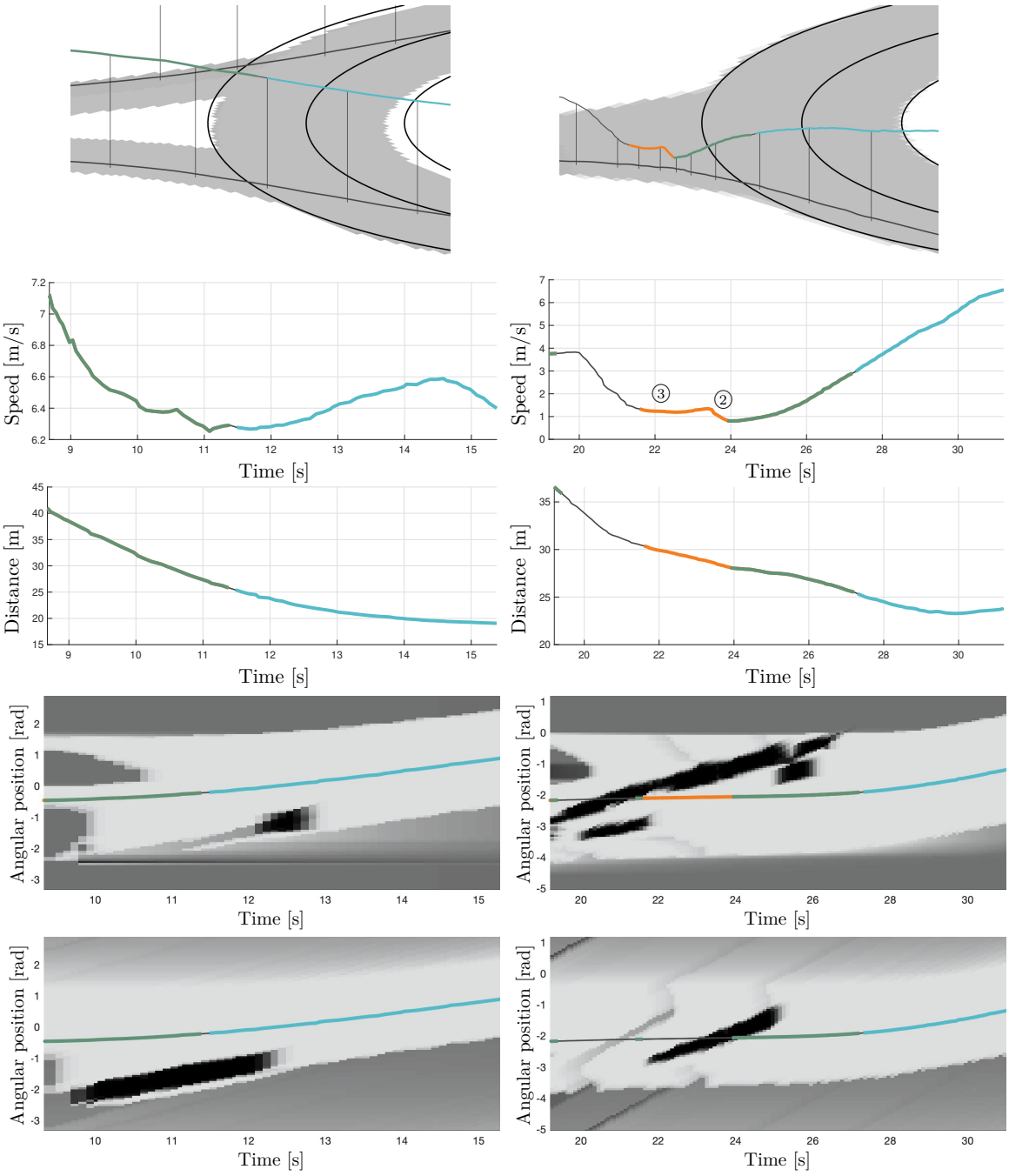

Figure 9.10 – Reactive maneuver planner output for two merging maneuvers registered within the data set. Examples 3-4. From top to bottom: three-dimensional representation of the merging maneuver (with elevation representing speed), speed profile, evolution of the distance to roundabout's center, and the evolution of the DOG for the two circulatory lanes. Trajectories color code: (—) shows that merging into any of the two circulatory lanes is considered safe, (—) shows that only merging into the outermost circulatory lane is safe, (—) illustrates that the ego vehicle is inside the roundabout.

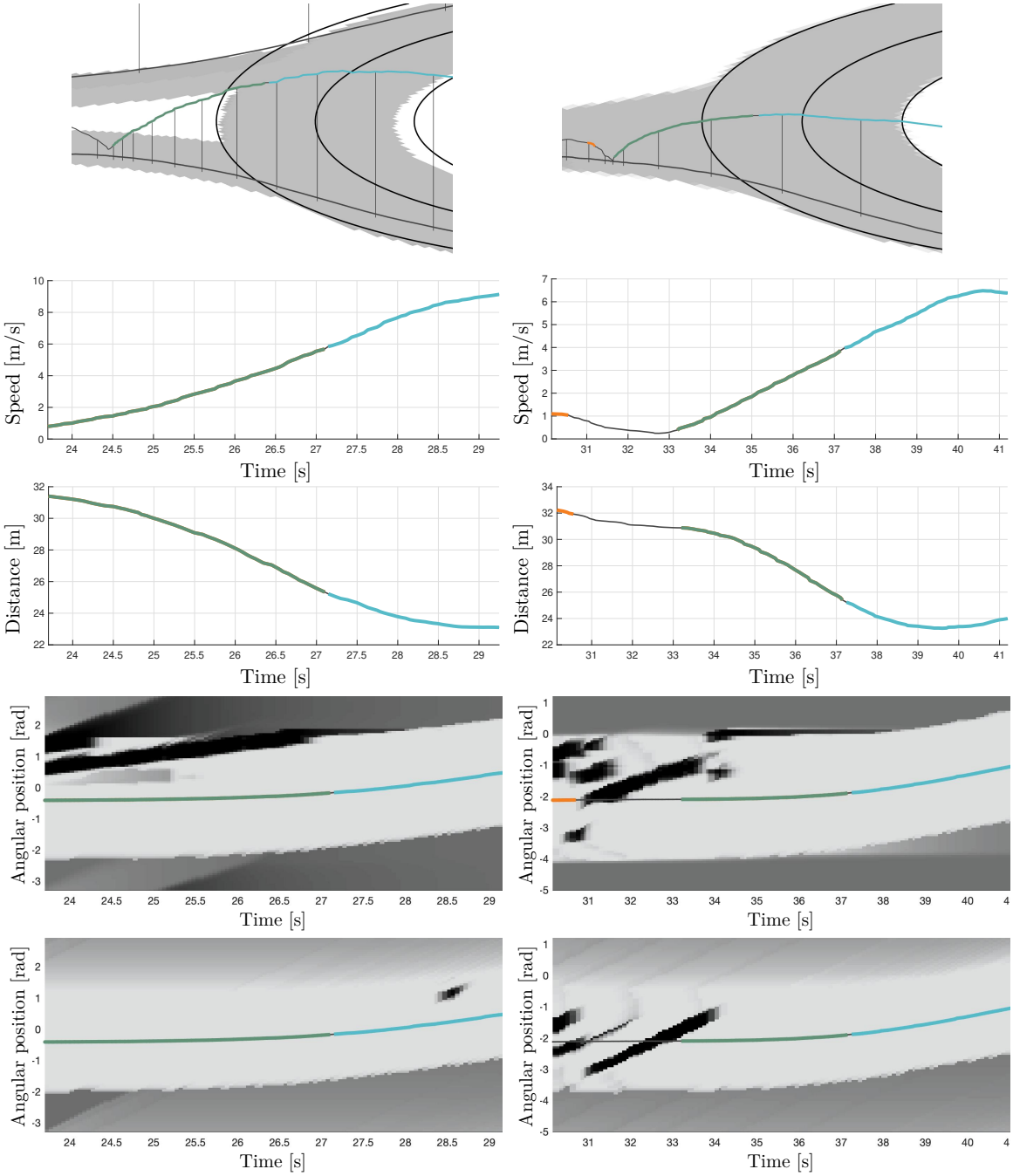

Figure 9.11 – Reactive maneuver planner output for two merging maneuvers registered within the data set. Examples 5-6. From top to bottom: three-dimensional representation of the merging maneuver (with elevation representing speed), speed profile, evolution of the distance to roundabout's center, and the evolution of the DOG for the two circulatory lanes. Trajectories color code: (—) shows that merging into any of the two circulatory lanes is considered safe, (—) shows that only merging into the outermost circulatory lane is safe, (—) illustrates that the ego vehicle is inside the roundabout.

10 Conclusions

This dissertation has addressed the problem of motion planning for CAVs and AVs by tackling some of the specific challenges that stem from the inevitable coexistence of AVs and CAVs with other human drivers. This coexistence calls for new motion planning architectures and methods, to enable automated vehicles to simultaneously evaluate maneuver executions considering the different interaction mechanisms that could coexist. In this chapter, we will first present a summary of the content of this dissertation, making emphasis on how the different methods have been linked. Then, we discuss some options for prospective work.

10.1 Overview

The primary topics addressed in this thesis are represented in Fig. 10.1. Even though our study revolves around motion planning, we started discussing some aspects concerning the type of information that was expected from the perception layer. Then, we tackled the formalization of a motion planning architecture that met our needs and designed several planning approaches, which would account for different interaction mechanisms. We then finalize the thesis, with the validation of the baseline behavior using a data set provided by our industrial partners.

Generally speaking, we have presented a family of intuitive model-based decision-making strategies and assessed their performance in a broad set of simulated scenarios. According to our results, the proposed approaches are valid options not only to act as backup/verification modules complementing other techniques (for instance, data-driven ones) but also to address the decision-making processes by themselves.

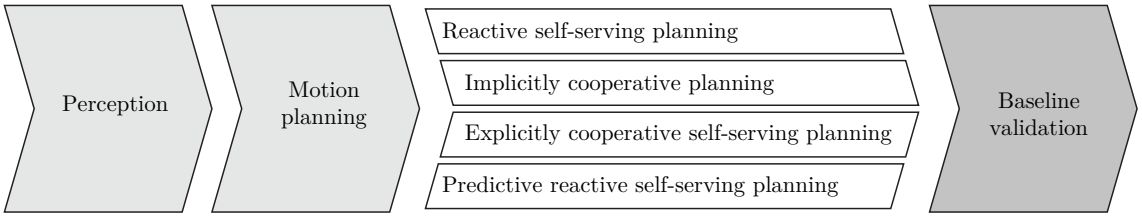

Figure 10.1 – Illustration of the research topics addressed in this thesis.

10.1.1 Perception model

Our discussion concerning the information provided by the perception layer was motivated by the problem of planning safe motion in dynamically occluded scenarios. We observed that existing occlusion-aware motion planning strategies would potentially become rather cumbersome in situations where dynamic occlusions took place. Specifically, we considered the problem to emerge from the *objects-detection and avoidance* approach typically followed in the literature. In response, we proposed a DOG-based strategy to post-process the perception output, which enables the extraction of probably-free gaps, which are to be used by the motion planning modules.

The use of such probably-free gaps turned out to be a very useful tool to understand the space surrounding the ego vehicle both in simulation and in real setups (see Fig. 10.2). Moreover, designing motion planning modules based on such inter-vehicle gaps was also shown to make them suitable to make decisions in partially and dynamically occluded environments.

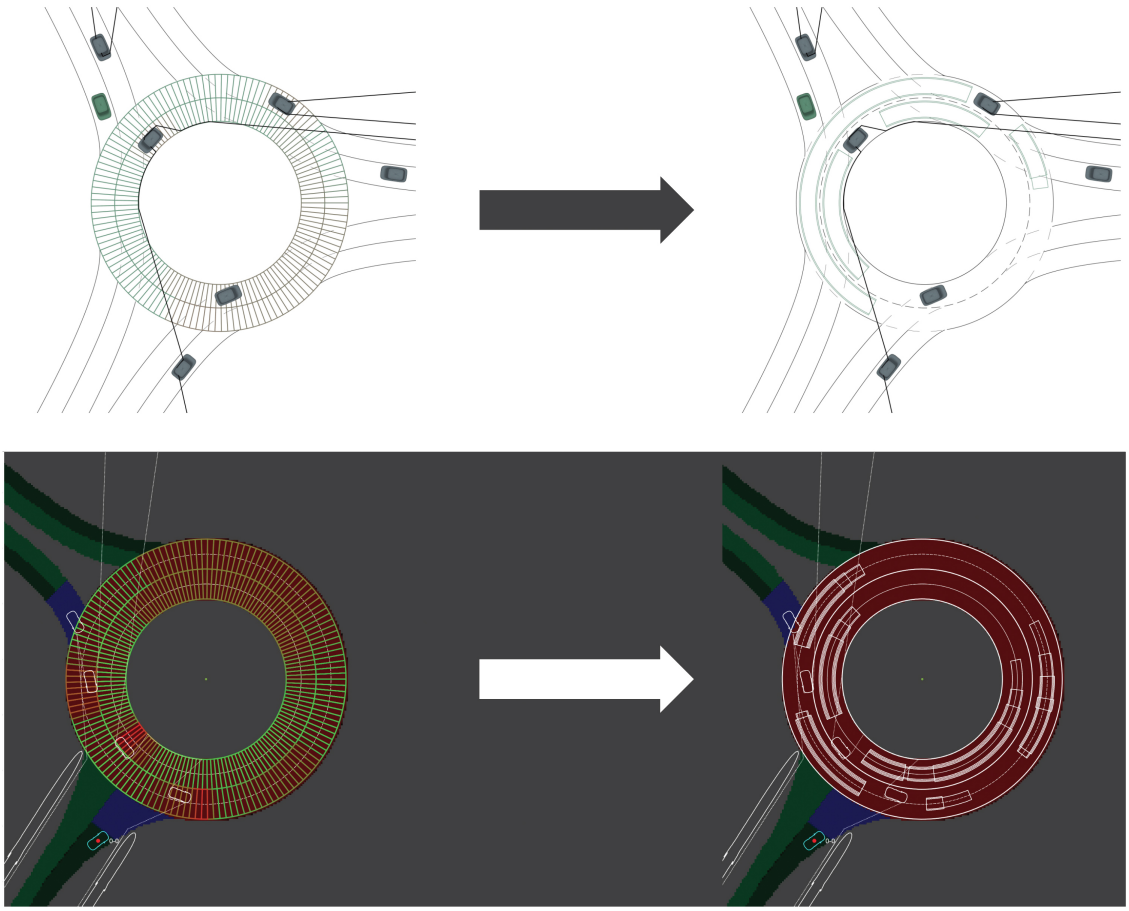

Figure 10.2 – Illustration of the contextual information provided by the proposed probably-free gaps. At the top, probably free gaps extracted in a simulated scene. At the bottom, the result obtained when the strategy is applied to a real data set.

10.1.2 Motion planning architecture

Concerning the motion planning architecture, we claimed that mixed-traffic conditions require the use of modular motion planning architectures. Among other things, in such traffic scenarios, the ego vehicle could be expected to have several interaction mechanisms available to plan maneuvers, and it should be able to consider all of them in parallel. To do so, we proposed a motion planning architecture whereby the high-level decision-making process was isolated in the so-called maneuver planner. By doing so, we would also reduce the redundancy of the sub-planing tasks that would stay the same across interaction mechanisms.

In addition to the isolation of the high-level decision-making, our planning methods build as well on the existence of a tactical planning module, which provides a set of the so-called decision spot driving maneuver. In essence, such a module was expected to choose a set of paths that could be followed to execute a targeted maneuver and encapsulate it along with the information that would be relevant to decide how to drive along the path.

The existence of the tactical planner makes the maneuver planner stay at a level of abstraction, such that the maneuver planning methods could be considered to be context agnostic.

Furthermore, our driving maneuver definition was designed to provide information relevant to perform both self-serving and cooperative maneuvers.

10.1.3 Gap-acceptance decision map

An interesting result we presented in Chapter 5 was the so-called gap-acceptance decision map (plot on the right-hand side of Fig. 10.3). Such a representation provided a very graphical and intuitive understanding of the process through which the ego vehicle would reactively accept merging gaps. In particular, such a process would account for the fact that, by the time the ego vehicle merges, it must be in a safe car-following and car-leading position w.r.t. the gap' limits.

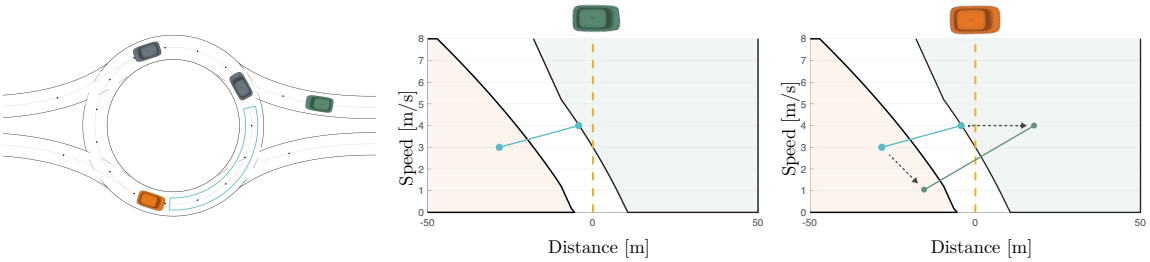

Figure 10.3 – On the left-hand side, a roundabout scenario. In the middle, gap-acceptance decision map used by the green vehicle to decide when to merge into the roundabout. On the right-hand side, the gap-acceptance decision map that the orange vehicle would use to determine if it could cooperate with the green vehicle.

Indeed, such a decision map inspired the implicitly cooperative maneuver planner presented in Chapter 7. This strategy is, to the best of our knowledge, one of the very few approaches in the literature whose objective is making the ego vehicle facilitate the maneuver of a surrounding vehicle. In essence, the method consists in making the ego vehicle change the state of the gap ahead of it, so that it could be accepted by some surrounding vehicles (plot on the right-hand side of Fig. 10.3).

10.1.4 Self-serving planning method

Regarding the self-serving maneuver planners proposed in this thesis, all the methods have revolved around the set of so-called reachable maneuver targets. Such a set was claimed to represent the decision-making solution space, in such a way that high-level decision could be understood as picking one specific maneuver to target out of the set. Hence, the three proposed self-serving maneuvers: (i) reactive, (ii) explicitly cooperative, and (ii) predictive-reactive, could be understood as three different ways of making such a decision (see Fig. 10.4).

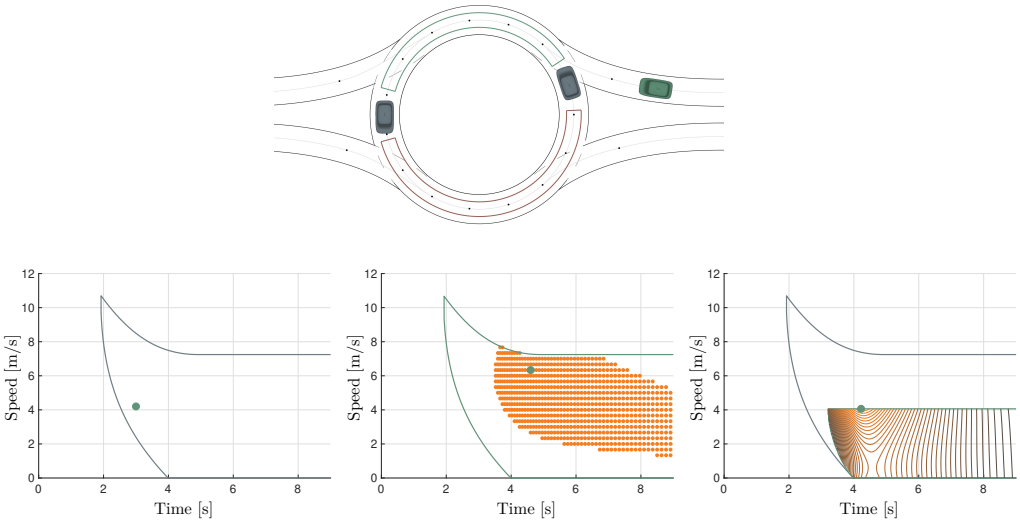

Figure 10.4 – At the top, a merging traffic scenario. At the bottom, three plots representing the decision-making process of the self-serving maneuver planner proposed in this thesis. In particular, plots at the bottom correspond, from left to right, to the: (i) reactive, (ii) explicitly cooperative, and (iii) predictive-reactive planners.

The self-serving maneuver planner (plot in the bottom-left corner of Fig. 10.4), presented in Chapter 5, presumed the existence of a maneuver template that the planner had to accept or reject depending on the state of the surrounding traffic. Thus, only one maneuver target out of the set was to be considered, and the maneuver-planner decision took the form of a go/no go decision. In this case, the only criterion leading to the MT candidate would be the acceleration the vehicle would like to apply to merge.

The self-serving explicitly cooperative planner (plot in the bottom-middle of Fig. 10.4), presented in Chapter 6, exploited a communication-based interaction mechanism to enable the ego vehicle to freely choose which maneuver target to pursue. We envisioned a virtual-vehicle based interaction mechanism that would provide a mechanism to reliably identify the maneuver targets that could be targeted, and pursue them. Any MT in the resulting subset could be safely pursued thanks to the fact that driving intent can be explicitly communicated through V2V communication. In this case, the proposed strategy to select the MT to pursue would evaluate the impact of the merging decision on the overall traffic performance.

The self-serving predictive-reactive planner (plot in the bottom-right corner of Fig. 10.4), presented in Chapter 8, aimed to take into account the full solution space without relying on V2V communication. However, the uncertainty concerning the future behavior of the surrounding vehicles was claimed to have a strongly constraining impact on the solution space. In this direction,

we have presented a strategy to identify the subset of so-called safely reachable maneuver targets. Once such a set is constructed, the MTs inside of it would be scored considering the probability distribution of the future state of the surrounding traffic. This score, in turn, would be the base for identifying the safest MT, which would be the one to pursue.

10.1.5 Validation

Finally, some of the theoretical results were applied to a more experimental and realistic setup. Specifically, we assessed the decisions generated by the proposed reactive maneuver planner when the output of a real perception layer was used as input. In particular, we used a data set (provided by our industrial partners) gathering a set of merging maneuvers performed by a human driver, as well as the object detection output of an experimental perception algorithm.

The primary motivation to compare the baseline behavior with the behavior observed in a human driver was putting into perspective all the results obtained from more advanced planners at once. Indeed, note that all the proposed maneuver planners were observed to outperform the baseline. Thus, verifying that the baseline resembles human behavior indicates that the improvement seen in simulation could potentially materialize in a real implementation—if all necessary conditions and assumptions the strategies are built upon are met.

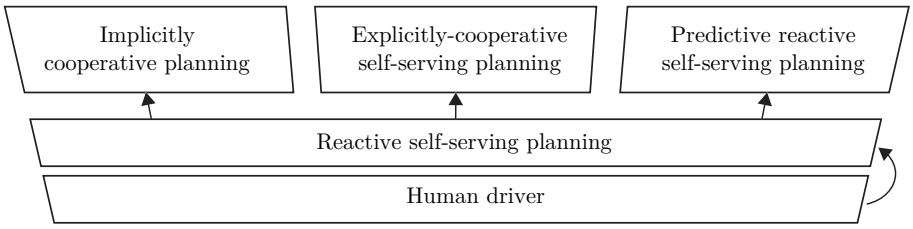

Figure 10.5 – Representation of the driving behaviors that have been compared through this thesis.

10.2 Contributions

In this thesis, we have made several contributions to the state of the art of motion planning for automated vehicles. In this section, we would summarize the most relevant ones to prevent them from being overlooked due to the number of formulated motion planners realization and implementations details provided across chapters.

Roundabouts are traffic intersections marginally studied in the literature, yet they pose significant and unprecedented challenges from the point of view of motion planning solutions. In this regard, and although some aspects remain unsolved, we have shed light on the features that a decision making approach should have for it to be efficient an safe given the particularities of the traffic interaction at this type of intersection.

Occlusions are a major issue motion planners and decision makers must handle while finding the right balance between safety and efficiency. However, the vast majority of motion planning strategies in the literature presume perfect knowledge of the surrounding objects. In this sense, we have proposed a workflow built upon an occupancy grid representation of the surrounding space, which has been shown to be a highly promising strategy to achieve reliable and efficient planning strategies. To the best of our knowledge, this approach has not being proposed in the literature before, yet we believe it represents a great step forward concerning occlusion-aware motion planning.

Finally, the last major contribution of this thesis concerns the novel decision-making solution space we exploit. Considering the explicit sequence of accelerations the ego vehicle should pursue in the future as the decision-making variables is a very convenient approach to model the decision making problem. However, it leads to vast solution spaces which cannot be fully explored due to computational constraints, which typically requires the simplification of such a space. We have proposed a high-level and low-dimensional trajectory representation based on the identification of the key locations involved in the decision that needs to be made. Such a strategy represents a powerful alternative as it provides a low-dimensional decision-making space that represents the whole set of speed profiles the vehicle can follow, simplifying the decision-making task without compromising its completeness.

The listed contributions are the foundation for the smaller and more specific contributions made in each chapter of this thesis. Several motion planning realizations that exploited different interaction mechanisms were formulated making use of the maneuver representation we propose and following a very similar workflow. Such a cohesion among methods was possible thanks to the abstraction level achieved with our proposed planning framework.

10.3 Future work

The content of this dissertation is built upon a few assumptions that might be worth revisiting for the strategies to be better suited for their practical implementations. Although several ways of extending the proposed methods have already been discussed in every chapter if this thesis, let us address some future work that could build on our investigation.

Although it might seem evident, the proposed communication-based strategy would require a reliable inter-vehicle communication system, and further research should be carried out to address problems stemming from package loss and/or the saturation of the communication channels.

Moreover, we have assumed throughout the thesis that the control layer can follow the trajectories correctly, but this assumption might not hold in all setups. Thus, a logical extension of all the proposed policies would be to take into account a certain level of error with which the vehicle is expected to meet the trajectory targets.

Furthermore, virtually all maneuver planning policies are built on the construction of the set of reachable maneuver targets, which is analytically constructed by presuming a simplified motion model. In this sense, other aspects like the curvature of the path to be followed might influence such a set, which has been disregarded and would be worth further investigating.

Additionally, our microscopic-traffic roundabout simulation environment turned out to be an excellent tool to carry out the type of analysis we intended to. In this sense, it is also our belief that such a simulation tool would also bring a great benefit to the field, and we are currently working on making the simulator available to the community.

Finally, the validation of our baseline driving behavior highly encourages us to pursue the real implementation and evaluation of the more advanced planners proposed herein.

A Appendix

A.1 Car-following

In this section, we formalize the so-called *safe car-following* (SCF) behavior that is used throughout the thesis to take into account safety considerations in the decision-making process. Specifically, we formally introduce the constraint defining a safe car-following situation, and will introduce some set of states that are of interest.

A.1.1 Safe car-leading and following constraint

Consider two vehicles L and F driving along a common path, with vehicle L being ahead of vehicle F, and their state being represented by $x_k = (s_k, v_k)$, with s_k being the position they occupy along the path, and v_k showing the speed of the vehicle along the path. In such a scenario, we consider a car-leading-following situation to be safe if the following vehicle F is driving in such a way that it is able to stop and avoid a collision with the leading vehicle L if the latter applies its maximum deceleration d. Such a condition can be referred to by stating that the vehicle F is in a safe car-following situation w.r.t. L, or equivalently, that the vehicle L is in a safe car-leading situation w.r.t. vehicle F.

For the safe car-leading-following situation to materialize, we would just have to guarantee the positivity of the distance that would separate both vehicles if vehicle L brakes with a deceleration d until being stopped and vehicle F does so as well but once a reaction time Θ_F has passed (aligned with the discussion in [75]). Such a terminal distance is given by the function

$$g_{\text{SCF}}(x_L, x_F) = (s_L + 0.5d^{-1}v_L^2) - (s_F + \Theta_F v_F + 0.5d^{-1}v_F^2). \tag{A.1}$$

Consequently, the condition for a pair of vehicles L and F to be driving safely is given by the pair of constraints

$$g_{\text{SCF}}(x_L, x_F) > 0 \qquad\qquad s_F > s_L + \underline{h}, \tag{A.2}$$

with $\underline{h}$ being the minimum headway distance that should be considered safe between the vehicles.

A.1.2 Maximum safe following speed

Given a leading vehicle L with state $x_L = (s_L, v_L)$, and a following vehicle F positioned at $s_F = s_L - \delta_F^L$ (with $\delta_F^L > \underline{h}$), we want to calculate the maximum speed $\overline{v}_F$ the following vehicle could have for it to be in a safe car-following situation w.r.t. its leading vehicle L.

The derivation only requires calculating the maximum speed for which the constraint

$$g_{\text{SCF}}(x_L, x_F) \geq 0 \tag{A.3}$$

holds, which translates in this case to

$$(s_L + 0.5d^{-1}v_L^2) - (s_F + v_F\Theta_F + 0.5d^{-1}v_F^2) \geq 0 \tag{A.4}$$
$$(s_L + 0.5d^{-1}v_L^2) - (s_L - \delta_F^L + v_F\Theta_F + 0.5d^{-1}v_F^2) \geq 0. \tag{A.5}$$

The maximum speed the vehicle F could have for the scene to be safe would be the one imposing $g_{\text{SCF}}(x_L, x_F) = 0$. That is,

$$0.5d^{-1}v_L^2 + \delta_F^L - \overline{v}_F\Theta_F - 0.5d^{-1}\overline{v}_F^2 = 0, \tag{A.6}$$
$$0.5d^{-1}\overline{v}_F^2 + \Theta_F\overline{v}_F - (\delta_F^L + 0.5d^{-1}v_L^2) = 0, \tag{A.7}$$

which leads to the expression

$$\overline{v}_F \coloneqq \texttt{MSCFV}(x_L, s_F) = -d\Theta_F + d\sqrt{\Theta_F^2 + 2d^{-1}(\delta_F^L + 0.5d^{-1}v_L^2)} = \tag{A.8}$$
$$= -d\Theta_F + \sqrt{d^2\Theta_F^2 + 2d\delta_F^L + v_L^2} \tag{A.9}$$

for the maximum safe car-following speed of vehicle F.

A.1.3 Minimum safe leading speed

The minimum speed $\underline{v}_L$ that a leading vehicle L positioned at s_L along a path of reference could have, given a following vehicle F with state $x_F = (s_F, v_F)$ (with $s_F + \delta_F^L = s_L$ and a distance $\delta_F^L > \underline{h}$) between the two vehicles, could be calculated by following a similar reasoning to the one in Section A.1.2.

In this occasion, the speed $\underline{v}_L$ is likewise the result of imposing

$$(s_L + 0.5d^{-1}\underline{v}_L^2) - (s_F + v_F\Theta_F + 0.5d^{-1}v_F^2) = 0 \tag{A.10}$$
$$\delta_F^L + 0.5d^{-1}\underline{v}_L^2 - \Theta_F v_F - 0.5d^{-1}v_F^2 = 0. \tag{A.11}$$

That is

$$\underline{v}_L = \sqrt{2d\Theta_F v_F + v_F^2 - 2d\delta_F^L}. \tag{A.12}$$

Note that the radical of the square root in (A.12) might become negative for high values of δ, which does not make physical sense. However, this artifact is due to the fact that there is a certain headway distance

$$\delta_F^{L'} = (\Theta_F v_F + 0.5d^{-1}v_F^2) \tag{A.13}$$

for which any velocity of the leading vehicle is safe, which corresponds with the minimum distance the follower vehicle needs to brake, considering a reaction time Θ_F. Thus, a more appropriate formulation for $\underline{v}_L$ would be

$$\underline{v}_L \coloneqq \texttt{mSCLV}(x_F, s_L) = \sqrt{\max\{0, 2d\Theta_F v_F + v_F^2 - 2d(s_L - s_F)\}}. \tag{A.14}$$

A.1.4 Set of safe car-following states

The results in the previous sections allow us to easily construct the set gathering the SCF states w.r.t. the state $x_L = (s_L, v_L)$ of a certain leading vehicle L.

Such a set could be constructed as

$$\mathcal{X}^{\text{SCF}}(x_L, \underline{h}) = \{x : s_L \geq s + \underline{h}, g_{\text{SCF}}(x_L, x) \geq 0\} = \tag{A.15}$$
$$= \{x : s_L \geq s + \underline{h}, v_L \leq \texttt{MSCFV}(x_L, s)\}. \tag{A.16}$$

A.1.5 Set of safe car-leading states

Similarly, we can as well construct the set of safe car-leading states containing the states that a leading vehicle can have so that it is in a safe car-leading situation w.r.t. a following vehicle F with state $x_F = (s_F, v_F)$, as

$$\mathcal{X}^{\text{SCL}}(x_F, \underline{h}) = \{x : s \geq s_F + \underline{h}, g_{\text{SCF}}(x, x_F) \geq 0\} = \tag{A.17}$$
$$= \{x : s \geq s_F + \underline{h}, v \geq \texttt{mSCLV}(x_F, s)\}. \tag{A.18}$$

A.1.6 Set of safe car-following states between two vehicles

Given the set of safe car-following and car-leading states in Section A.1.4 and Section A.1.4, we can easily define as well the set $\mathcal{X}^{\text{SCFL}}$ of states that are car-following safe w.r.t. a leading vehicle L (with state x_L), and at the same time, car-leading safe w.r.t. a following vehicle F (with state x_F).

Specifically, the set can be constructed as

$$\mathcal{X}^{\text{SCFL}}(x_L, x_F, \underline{h}) = \left\{x : x \in \mathcal{X}^{\text{SCF}}(x_L, \underline{h}), x \in \mathcal{X}^{\text{SCL}}(x_F, \underline{h})\right\} \tag{A.19}$$
$$= \{x : s \in (s_F + \underline{h}, s_L - \underline{h}), g_{\text{SCF}}(x_L, x) > 0, g_{\text{SCF}}(x, x_F) > 0\} \tag{A.20}$$
$$= \{x : s \in (s_F + \underline{h}, s_L - \underline{h}), v \in [\texttt{mSCLV}(x_F, s), \texttt{MSCFV}(x_L, s)]\} \tag{A.21}$$

A.2 Reachable states

In this section we will present the construction of some sets of interest involving reachable states, that is, those that can be reached given a certain initial position x_0 at a time t_0, and considering the sets

$$\mathcal{A} = \{a \in \mathbb{R} : a \in [a_{\text{m}}, a_{\text{M}}]\}, \tag{A.22}$$
$$\mathcal{V} = \{v \in \mathbb{R} : v \in [0, v_{\text{M}}]\}, \tag{A.23}$$
$$\mathcal{D} = \{s \in \mathbb{R} : s \geq s_0\}, \tag{A.24}$$

of, respectively, reachable accelerations, speeds, and distances.

A.2.1 Speed transition auxiliary operators

Speed transition time interval

Let us begin by introducing the operator

$$\texttt{STt}(v_a, v_b, a) = (v_b - v_a)a^{-1} \tag{A.25}$$

returning the minimum time required to reach a speed v_b, from an initial speed v_a and an acceleration a. Notice that, for the previous correlation to make sense, $a > 0$ if $v_a < v_b$, and $a < 0$ if $v_a > v_b$.

Speed transition distance

The distance needed by a vehicle to go from a speed v_a to a speed v_b with acceleration a can be calculated as

$$\texttt{STd}(v_a, v_b, a) = 0.5(v_b^2 - v_a^2)a^{-1}, \tag{A.26}$$

which is only meaningful if $a > 0$ when $v_b > v_a$, and $a < 0$ for $v_b < v_a$.

A.2.2 Time-constrained reachable distance

Minimum time-constrained reachable distance

Given an initial state $x_0 = (s_0, v_0)$ at time t_0, a minimum negative acceleration $a_1 < 0$, and the minimum speed v_m, the minimum distance that a vehicle can have driven by a time $t > t_0$ is

$$\delta_\mathrm{m}^\mathrm{tR}(x_0, t) = \begin{cases} v_0(t - t_0) + 0.5a_1(t - t_0)^2 & \text{if } (t - t_0) \leq \tau_{0,\mathrm{m}} \\ \delta_\mathrm{m}^\mathrm{tR}(x_0, \tau_{0,\mathrm{m}}) + ((t - t_0) - \tau_{0,\mathrm{m}})v_\mathrm{m} & \text{otherwise} \end{cases}, \tag{A.27}$$

with $\tau_{0,\mathrm{m}} = \texttt{STt}(v_0, v_\mathrm{m}, a_1)$.

Maximum time-constrained reachable distance

Given an initial state $x_0 = (s_0, v_0)$ at time t_0, a maximum positive acceleration $a_2 > 0$, and the maximum speed v_M, the minimum distance that a vehicle can have driven at a time $t > t_0$ is

$$\delta_\mathrm{M}^\mathrm{tR}(x_0, t) = \begin{cases} v_0(t - t_0) + 0.5a_2(t - t_0)^2 & \text{if } (t - t_0) \leq \tau_{0,\mathrm{M}} \\ \delta_\mathrm{M}^\mathrm{tR}(x_0, \tau_{0,\mathrm{M}}) + ((t - t_0) - \tau_{0,\mathrm{M}})v_\mathrm{M} & \text{otherwise} \end{cases}, \tag{A.28}$$

with $\tau_{0,\mathrm{M}} = \texttt{STt}(v_0, v_\mathrm{M}, a_2)$.

A.2.3 Time-constrained reachable speed

Minimum time-constrained reachable speed

Given an initial state $x_0 = (s_0, v_0)$ at a time t_0, a minimum negative acceleration $a_1 < 0$, and the minimum speed v_m, the minimum speed that a vehicle can reach at a time $t > t_0$ is

$$v_\mathrm{m}^\mathrm{tR}(x_0, t) = \begin{cases} v_0 + a_1(t - t_0) & \text{if } (t - t_0) \leq \tau_{0,\mathrm{m}} \\ v_\mathrm{m} & \text{otherwise} \end{cases}, \tag{A.29}$$

with $\tau_{0,\mathrm{m}} \coloneqq \mathtt{STt}(v_0, v_\mathrm{m}, a_1)$.

Maximum time-constrained reachable speed

Given an initial state $x_0 = (s_0, v_0)$ at a time t_0, a maximum positive acceleration $a_2 > 0$, and the maximum speed v_M, the maximum speed that a vehicle can reach at a time t is

$$v_\mathrm{M}^\mathrm{tR}(x_0, t) = \begin{cases} v_0 + a_2(t - t_0) & \text{if } (t - t_0) \leq \tau_{0,\mathrm{M}} \\ v_\mathrm{M} & \text{otherwise} \end{cases}, \tag{A.30}$$

with $\tau_{0,\mathrm{M}} \coloneqq \mathtt{STt}(v_0, v_\mathrm{M}, a_2)$.

A.2.4 Distance-constrained reachable speed

Minimum distance-constrained reachable speed

Given an initial state $x_0 = (s_0, v_0)$ at a time t_0, the minimum speed with which a spot located at a location $s > s_0$ can be reached is given by

$$v_m^\mathrm{dR}(x_0, s) = \begin{cases} \sqrt{v_0 + 2(s - s_0)a_1} & (s - s_0) \leq \mathtt{STd}(v_0, v_\mathrm{m}, a_1) \\ 0 & \text{otherwise} \end{cases}. \tag{A.31}$$

Maximum distance-constrained reachable speed

Given an initial state $x_0 = (s_0, v_0)$ at a time t_0, the maximum speed with which a spot located at $s > s_0$ can be reached is given by

$$v_M^\mathrm{dR}(x_0, s) = \begin{cases} \sqrt{v_0 + 2(s - s_0)a_2} & (s - s_0) \leq \mathtt{STd}(v_0, v_\mathrm{M}, a_2) \\ v_\mathrm{M} & \text{otherwise} \end{cases}. \tag{A.32}$$

A.2.5 Distance-constrained arrival time

Minimum distance-constrained arrival time

Given an initial state $x_0 = (s_0, v_0)$ at a time t_0, the minimum time interval required to reach a position $s > s_0$ is given by

$$\tau_{\mathrm{m}}^{\mathrm{R}}(x_0, s) = \begin{cases} a_2^{-1}\Big(-v_0 + \sqrt{v_0^2 + 2a_2(s - s_0)}\Big) & \text{if } (s - s_0) \leq \delta_{0,\mathrm{M}} \\ v_{\mathrm{M}}^{-1} a_2^{-1}\big(0.5(v_{\mathrm{M}} - v_0)^2 + a_2(s - s_0)\big) & \text{otherwise} \end{cases}, \tag{A.33}$$

with $\delta_{k,\mathrm{M}} = \mathtt{STd}(v_k, v_{\mathrm{M}}, a_2)$, and $\delta_{k,\mathrm{m}} = \mathtt{STd}(v_k, v_{\mathrm{m}}, a_1)$.

Maximum distance-constrained arrival time

Given an initial state $x_0 = (s_0, v_0)$ at a time t_0, the maximum time interval with which a position $s > s_0$ can be reached is given by

$$\tau_{\mathrm{M}}^{\mathrm{R}}(x_0, s) = \begin{cases} a_1^{-1}\Big(-v_0 + \sqrt{v_0^2 + 2a_1(s - s_0)}\Big) & \text{if } (s - s_0) \leq \delta_{0,\mathrm{m}} \\ \infty & \text{otherwise} \end{cases}, \tag{A.34}$$

with $\delta_{k,\mathrm{M}} = \mathtt{STd}(v_k, v_{\mathrm{M}}, a_2)$, and $\delta_{k,\mathrm{m}} = \mathtt{STd}(v_k, v_{\mathrm{m}}, a_1)$.

A.2.6 Time-distance-constrained reachable speed

Minimum time-distance-constrained reachable speed

Considering the results in [65], the auxiliary terms $\delta = s - s_0$, $\tau = t - t_0$, $\Delta a = a_2 - a_1$, $\Delta a^{-1} = a_2^{-1} - a_1^{-1}$, $\gamma = 2a_1\delta + v_0^2$, the auxiliary functions

$$\tau_{h,1}(x_0, \delta) = -v_0 a_1^{-1} + \sqrt{a_1^{-1} a_2^{-1} \gamma}\,, \tag{A.35}$$

$$\tau_{l,1}(x_0, \delta) = \Delta a^{-1} v_{\mathrm{M}} - v_0 a_2^{-1} - \sqrt{a_1^{-2}\gamma - a_1^{-1}\Delta a^{-1}(v_{\mathrm{M}}^2 - v_0^2)}, \tag{A.36}$$

$$g_1(x_0, \delta, \tau) = \max\Big\{0, v_0 + a_2\tau - \sqrt{-\Delta a(2\delta - 2v_0\tau - a_2\tau^2)}\Big\}\,, \tag{A.37}$$

$$g_2(x_0, \delta, \tau) = \max\Big\{0, v_{\mathrm{M}} - \sqrt{a_1(a_2^{-1}(v_{\mathrm{M}} - v_0)^2 + 2\delta - 2v_{\mathrm{M}}\tau)}\Big\}\,, \tag{A.38}$$

$$g_3(x_0, \delta, \tau) = \begin{cases} g_2(x_0, \delta, \tau) & \text{if } \tau \leq \tau_{l,1} \\ g_3(x_0, \delta, \tau) & \text{otherwise} \end{cases}, \tag{A.39}$$

and introducing

$$\delta_{0,\mathrm{M}} \coloneqq \mathtt{STd}(v_0, v_{\mathrm{M}}, a_2), \qquad \delta_{\mathrm{M},\mathrm{m}} \coloneqq \mathtt{STd}(v_{\mathrm{M}}, v_{\mathrm{m}}, a_1), \tag{A.40}$$

the minimum speed with which a location $s > s_0$ can be reached at a time $t > t_0$, given the initial state x_0 at a time t_0 can be expressed as

$$v_{\mathrm{m}}^{\mathrm{tdR}}(x_0, s, t) = \begin{cases} g_1(x_0, \delta, \tau) & \text{if } \delta \leq \delta_{0,\mathrm{M}} \\ g_2(x_0, \delta, \tau) & \text{if } \delta \geq \delta_{0,\mathrm{M}} + \delta_{\mathrm{M,m}} \\ g_3(x_0, \delta, \tau) & \text{otherwise} \end{cases} . \tag{A.41}$$

Maximum time-distance-constrained reachable speed

Similarly to what was done in the previous section, and again based on the results in [65], it is possible to calculate the maximum speed with which a spot positioned at $s > s_0$ can be reached at a time $t > t_0$ given an initial state x_0 at a time t_0. In particular, introducing the auxiliary terms $\delta = s - s_0$, $\tau = t - t_0$, $\Delta a = a_2 - a_1$, $\Delta a^{-1} = a_2^{-1} - a_1^{-1}$, $\gamma = 2a_1\delta + v_0^2$, the functions

$$\tau_{h,1}(x_0, \delta) = -v_0 a_1^{-1} + \sqrt{a_1^{-1} a_2^{-1} \gamma} , \tag{A.42}$$

$$\tau_{l,1}(x_0, \delta) = \Delta a^{-1} v_{\mathrm{M}} - v_0 a_2^{-1} - \sqrt{a_1^{-2}\gamma - a_1^{-1}\Delta a^{-1}(v_{\mathrm{M}}^2 - v_0^2)}, \tag{A.43}$$

$$h_1(x_0, \delta, \tau) = \min\left\{ v_{\mathrm{M}}, v_0 + a_1\tau + \sqrt{\Delta a(2\delta - 2v_0\tau - a_1\tau^2)} \right\} , \tag{A.44}$$

$$h_2(x_0, \delta, \tau) = \begin{cases} h_1(x_0, \tau, \delta) & \text{if } \tau \leq \tau_{h,1} \\ h_1(x_0, \delta, \tau_{h,1}) & \text{otherwise} \end{cases} \tag{A.45}$$

and introducing

$$\delta_{0,\mathrm{m}} \coloneqq \mathtt{STd}(v_0, v_{\mathrm{m}}, a_1), \tag{A.46}$$

the speed we are looking for can be formulated as

$$v_{\mathrm{M}}^{\mathrm{tdR}}(x_0, s, t) = \begin{cases} h_1(x_0, \delta, \tau) & \text{if } \delta \leq \delta_{0,\mathrm{m}} \\ h_2(x_0, \delta, \tau_{h,1}) & \text{otherwise} \end{cases} . \tag{A.47}$$

A.2.7 Set of reachable states

The set $\mathcal{X}^{\mathrm{tR}}(x_0)$ containing all the states that can be reached regardless of time interval required to do so, given the initial state x_0 at time t_0 can be built as

$$\mathcal{X}^{\mathrm{tR}}(x_0) = \left\{ (s, v) : s \geq s_0, v \in [v_m^{\mathrm{dR}}(x_0, s), v_M^{\mathrm{dR}}(x_0, s)] \right\}. \tag{A.48}$$

A.2.8 Set of time-constrained reachable distances

Considering the results in Section A.2.2, we can easily obtain the set $\mathcal{D}^{\mathrm{tR}}(x_0, \tau)$ gathering the distances that can be reached at a time $t > t_0$, given the initial state x_0 at a time t_0 as

$$\mathcal{D}^{\mathrm{tR}}(x_0, t) = \left\{ s \in \mathcal{D}, s \in [s_0 + \delta_{\mathrm{m}}^{\mathrm{tR}}(x_0, \tau), s_0 + \delta_{\mathrm{M}}^{\mathrm{tR}}(x_0, \tau)] \right\}. \tag{A.49}$$

A.2.9 Set of time-constrained reachable speeds

Given the results in Section A.2.3, the set $\mathcal{V}^{\mathrm{tR}}(x_0,t) \subseteq \mathcal{V}^{\mathrm{R}}$ of speeds that are reachable at a time $t > t_0$ given an initial state x_0 at a time t_0 (and w.r.t. a certain pair a_1, a_2 of, respectively, minimum and maximum accelerations the vehicle is allowed to apply) can be constructed as

$$\mathcal{V}^{\mathrm{tR}}(x_0,t) = \big\{v \in \mathcal{V} : v \in [v_{\mathrm{m}}^{\mathrm{tR}}(x_0,t), v_{\mathrm{M}}^{\mathrm{tR}}(x_0,t)]\big\}. \tag{A.50}$$

A.2.10 Set of time-constrained reachable states

Given the results in Section A.2.8 the set of states that can be reached at a certain time t can also be built as

$$\mathcal{X}^{\mathrm{tR}}(x_0,t) = \big\{x : (s-s_0) \in \mathcal{D}^{\mathrm{tR}}(x_0,t), v \in \mathcal{V}^{\mathrm{tdR}}(x_0,t,s-s_0)\big\}. \tag{A.51}$$

A.2.11 Set of distance-constrained arrival times

Considering a certain minimum and maximum acceleration $a_1 < 0$ and $a_2 > 0$ that a vehicle is allowed to apply, the set $\tau^{\mathrm{a}}(x_0,\delta)$ of arrival time intervals with which a vehicle can reach a certain distance s given its initial state x_0 at a time t_0, can be constructed, considering the results in Section A.2.5, as

$$\tau^{\mathrm{a}}(x_0,s) = \big\{\tau \in [\tau_{\mathrm{m}}^{\mathrm{R}}(x_0,s), \tau_{\mathrm{M}}^{\mathrm{R}}(x_0,s)]\big\}. \tag{A.52}$$

A.2.12 Set of time-distance-constrained reachable speed

Given the results in Section A.2.6, we can construct the set $\mathcal{V}^{\mathrm{tdR}}(x_0,t,s)$ gathering the speeds with which a spot located at $s > s_0$ can be reached at time τ, given the initial state x_0 at a time t_0, as

$$\mathcal{V}^{\mathrm{tdR}}(x_0,t,s) = \big\{v \in [v_{\mathrm{m}}^{\mathrm{tdR}}(x_0,s,t), v_{\mathrm{M}}^{\mathrm{tdR}}(x_0,s,t)]\big\}. \tag{A.53}$$

A.3 Maneuver targets

A.3.1 Set of reachable maneuver targets

In this section, we seek to find an analytical expression to characterize the set $\mathcal{T}^{\mathrm{dR}}(x_0)$ of maneuver targets (that is, of tuples $\mathcal{T} = (\tau, v)$) with which a certain spot located at a location $s_{\mathcal{T}}$ along a path (provided within the definition of $\mathcal{M}$) can be reached, given the simplified motion model $\dot{v}(t) = a(t)$, $\dot{s}(t) = v(t)$.

Profiting from the results in Section A.2.12, the set can be formulated as

$$\mathcal{T}^{\mathrm{dR}}(x_0,s_{\mathcal{T}}) = \big\{\mathcal{T}_{\mathcal{M}} : \tau \in \tau^{\mathrm{a}}(x_0,s_{\mathcal{T}}), v \in \mathcal{V}^{\mathrm{tdR}}(x_0,t,s_{\mathcal{T}})\big\}. \tag{A.54}$$

A.3.2 Set of safe car-following maneuver targets

Exploiting the definition of the set of safe car-following state, we can as well construct the set of maneuver targets $\mathcal{T} = (\tau, v)$ describing how a location $s_{\mathcal{T}}$ on the path of reference can be reached,

so that the arrival state is safe w.r.t. an obstacle $\mathcal{O}$ with state $x_{\mathcal{O}}$. In particular, note that the maneuver target $\mathcal{T}$ has associated a state $x(\tau) = (s_{\mathcal{T}}, v)$ that the vehicle would have if it meets the target. Then, we can construct the sought set as

$$\mathcal{T}^{\mathrm{SCF}}(x_{\mathcal{O}}, s_{\mathcal{T}}) = \left\{\mathcal{T} : x \in \mathcal{X}^{\mathrm{SCF}}(\hat{x}_{\mathcal{O}}(\tau), \underline{h})\right\} = \tag{A.55}$$

$$= \{\mathcal{T} : \hat{s}_{\mathcal{O}}(\tau) \geq s_{\mathcal{T}} + \underline{h}, v \leq \texttt{MSCFV}(\hat{x}_{\mathcal{O}}(\tau), s_{\mathcal{T}})\} \ , \tag{A.56}$$

where $\hat{s}_{\mathcal{O}}(\tau)$ and $\hat{x}_{\mathcal{O}}(\tau)$ show the distance and state the obstacle is expected to have at time τ, respectively.

A.3.3 Set of safely reachable maneuver targets

In this section we aim at characterizing, given an initial state x_0 at time t_0, the set $\mathcal{T}^{\mathrm{SdR}}$ of tuples $\mathcal{T} = (\tau, v)$ expressing how a location $s_{\mathcal{T}} > s_0$ can be reached while keeping a safe car-following state w.r.t. an obstacle $\mathcal{O}$ with state $x_{\mathcal{O}} = (s_{\mathcal{O}}, v_{\mathcal{O}})$ positioned ahead of the ego vehicle and on the reference, i.e. with $s_0 < s_{\mathcal{O}} < s_{\mathcal{T}}$.

The set $\mathcal{T}^{\mathrm{SdR}}$ we aim to construct can then be formulated as

$$\mathcal{T}^{\mathrm{SdR}}(x_0, x_{\mathcal{O}}, s_{\mathcal{T}}) = \mathcal{T}^{\mathrm{dR}}(x_0, s_{\mathcal{T}}) \cap \mathcal{T}^{\mathrm{SCF}}(x_{\mathcal{O}}, s_{\mathcal{T}}) \ , \tag{A.57}$$

i.e., by intersecting the set of reachable maneuver targets with the set of MTs that are car-following safe w.r.t. the predicted state of the obstacle, which, as was discussed in Section A.3.2, assumes a constant speed for the obstacle.

Note that, a priori, the fact that a certain state $x(\tau) = (s_{\mathcal{T}}, v)$ with which a certain spot is reached in a time τ is reachable and safe w.r.t. the predicted state of an obstacle, does not necessarily imply that the whole trajectory followed by the ego vehicle during the whole time interval τ to reach the terminal state is safe as well. Nonetheless, it is indeed the case, as shown in the following theorem.

Theorem 1. *Consider a vehicle with initial state $x_0 = (s_0, v_0)$ at time t_0, with a moving obstacle $\mathcal{O}$ ahead, with state $x_{\mathcal{O}} = (s_{\mathcal{O}}, v_{\mathcal{O}})$ and moving at constant speed over time. In such a scenario, states x that are (i) physically reachable by the vehicle at a time t and (ii) car-following safe w.r.t. the expected state of the obstacle—i.e. x is within the set*

$$\mathcal{X}^{SR}(x_0, x_{\mathcal{O}}, t) = \mathcal{X}^{tR}(x_0, t) \cap \mathcal{X}^{SCF}(\hat{x}_{\mathcal{O}}(t), \underline{h}) \tag{A.58}$$

—there exists at least one kinetically feasible state trajectory

$$x^T = \{x(t_0), \cdots, x(t_0 + kh), \cdots, x(t_0 + T)\} \tag{A.59}$$

with h being a certain sampling time, for which every element $x(t_0 + kh)$ is car-following safe w.r.t. the predicted state $\hat{x}_{\mathcal{O}}(t_0 + kh)$ of the obstacle. In other words, for which the constraint

$$x(t_0 + kh) \in \mathcal{X}^{SR}(x(t_0 + (k-1)h), \hat{x}_{\mathcal{O}}(t_0 + (k-1)h), t_0 + kh) \tag{A.60}$$

holds for all $\tau \in [0, H]$.

Proof. The set of safely reachable states can be consider to evolve over time as

$$\mathcal{X}^{\mathrm{SR}}(x_0, x_{\mathcal{O}}, t+h) = \mathcal{X}^{\mathrm{SCF}}(\hat{x}_{\mathcal{O}}(t+h)) \cap \left\{ \bigcup_{x' \in \mathcal{X}^{\mathrm{SR}}(x_0, x_{\mathcal{O}}, t)} \mathcal{X}^{\mathrm{tR}}(x', h) \right\} \tag{A.61}$$

for the above theorem to hold, we need to demonstrate that the growth of the set $\mathcal{X}^{\mathrm{SR}}$ over time is only limited by the safe car-following constraint at the precise time. That is, that

$$\mathcal{X}^{\mathrm{SCF}}(\hat{x}_{\mathcal{O}}(t+h)) \cap \left\{ \bigcup_{x' \in \mathcal{X}^{\mathrm{SR}}(x_0, x_{\mathcal{O}}, t)} \mathcal{X}^{\mathrm{tR}}(x', h) \right\} = \mathcal{X}^{\mathrm{SCF}}(\hat{x}_{\mathcal{O}}(t+h)) \cap \mathcal{X}^{\mathrm{tR}}(x_0, t+h) \tag{A.62}$$

One way of proving that is by showing that from any state

$$x' \in \mathcal{X}^{\mathrm{tR}}(x_0, t) \cap \partial \mathcal{X}^{\mathrm{SCF}}(\hat{x}_{\mathcal{O}}(t)) \tag{A.63}$$

that is reachable and at the boundary of the safety constraints, we can reach states

$$x'' \in \mathcal{X}^{\mathrm{tR}}(x'(t), h) \backslash \mathcal{X}^{\mathrm{SCF}}(\hat{x}_{\mathcal{O}}(t+h)) \tag{A.64}$$

that are not safe w.r.t. the obstacle progression.

We start from an arbitrary state $x(t) = (s(t), v(t))$ such that

$$s_{\mathcal{O}}(t) + 0.5 d^{-1} v_{\mathcal{O}}^2(t) = s(t) + \Theta v(t) + 0.5 d^{-1} v^2(t), \tag{A.65}$$

$$s_{\mathcal{O}}(t) > s(t) \ , \tag{A.66}$$

which also implies

$$\Theta v(t) + 0.5 d^{-1} v^2(t) - 0.5 d^{-1} v_{\mathcal{O}}^2(t) \geq 0 \tag{A.67}$$

$$2 d \Theta v(t) + v^2(t) - v_{\mathcal{O}}^2(t) \geq 0 \tag{A.68}$$

We then considering the state at $t+h$ that would be reached if the ego vehicle applied an acceleration a, that is

$$x(t+h) = (s(t+h), v(t+h)) = (s(t) + v(t)h + 0.5 a h^2, v(t) + ha). \tag{A.69}$$

Then, for the theorem to be true, such a state should violate the car-following safety constraint. Indeed, if we rewrite the safety constraint for the time $t+h$, we would have

$$s_{\mathcal{O}}(t+h) + 0.5 d^{-1} v_{\mathcal{O}}^2(t+h) \geq s(t+h) + \Theta v(t+h) + 0.5 d^{-1} v^2(t+h) \tag{A.70}$$

$$s_{\mathcal{O}}(t) + v_{\mathcal{O}}(t)h + 0.5 d^{-1} v_{\mathcal{O}}^2(t) \geq s(t) + v(t)h + 0.5 a h^2 + \Theta(v(t) + ha) + 0.5 d^{-1} (v(t) + ha)^2 \tag{A.71}$$

$$v_{\mathcal{O}}(t)h \geq v(t)h + 0.5 a h^2 + \Theta h a + 0.5 d^{-1} (h^2 a^2 + 2 v(t) h a) \tag{A.72}$$

$$v_{\mathcal{O}}(t) - v(t) \geq 0.5 a h + \Theta a + 0.5 d^{-1} (h a^2 + 2 v(t) a) \tag{A.73}$$

Furthermore, we also have that

$$s_{\mathcal{O}}(t+h) > s(t+h) \tag{A.74}$$
$$s_{\mathcal{O}}(t) + v_{\mathcal{O}}(t)h > s(t) + v(t)h + 0.5ah^2 \tag{A.75}$$
$$s_{\mathcal{O}}(t) - s(t) > h(v(t) - v_{\mathcal{O}}(t)) + 0.5ah^2 \tag{A.76}$$

which, given (A.66), leads to

$$h(v(t) - v_{\mathcal{O}}(t)) + 0.5ah^2 > 0 \tag{A.77}$$
$$v_{\mathcal{O}}(t) - v(t) < 0.5ah \tag{A.78}$$

Combining (A.73) and (A.78), we would have

$$0.5ah + \Theta a + 0.5d^{-1}(ha^2 + 2v(t)a) < 0.5ah \tag{A.79}$$
$$\Theta a + 0.5d^{-1}(ha^2 + 2v(t)a) < 0 \tag{A.80}$$

where the left-hand side of the inequality is indeed positive due to positivity of all its terms. Thus, as (A.80) does not hold, neither does (A.73). Hence, the growth of the set $\mathcal{X}^{\mathrm{SR}}$ is therefore only and uniquely limited by $\mathcal{X}^{\mathrm{SCF}}$, which proves theorem 1. ■

A.3.4 Envelope set of reachable maneuver targets

Given an initial state x_0 at a time t_0, the set containing all reachable maneuver targets $\mathcal{T} = (\tau, v)$ regardless of the distance they refer to can be constructed as well

$$\mathcal{T}^{\mathrm{R}}(x_0) = \big\{(\tau, v) : \tau \geq 0, v \in \mathcal{V}^{\mathrm{tR}}(x_0, t_0 + \tau)\big\}. \tag{A.81}$$

Bibliography

[1] Matthias Althoff and John M Dolan. Online verification of automated road vehicles using reachability analysis. *IEEE Transactions on Robotics*, 30(4):903–918, 2014.

[2] Matthias Althoff and Silvia Magdici. Set-based prediction of traffic participants on arbitrary road networks. *IEEE Transactions on Intelligent Vehicles*, 1(2):187–202, 2016.

[3] Matthias Althoff, Olaf Stursberg, and Martin Buss. Safety assessment of driving behavior in multi-lane traffic for autonomous vehicles. In *2009 IEEE Intelligent Vehicles Symposium*, pages 893–900. IEEE, 2009.

[4] Noor Hafizah Amer, Hairi Zamzuri, Khisbullah Hudha, and Zulkiffli Abdul Kadir. Modelling and control strategies in path tracking control for autonomous ground vehicles: a review of state of the art and challenges. *Journal of intelligent & robotic systems*, 86(2):225–254, 2017.

[5] Maxime Bouton, Alireza Nakhaei, Kikuo Fujimura, and Mykel J Kochenderfer. Scalable decision making with sensor occlusions for autonomous driving. In *2018 IEEE International Conference on Robotics and Automation (ICRA)*, pages 2076–2081. IEEE, 2018.

[6] Wenjing Cao, Masakazu Mukai, Taketoshi Kawabe, Hikaru Nishira, and Noriaki Fujiki. Gap selection and path generation during merging maneuver of automobile using real-time optimization. *SICE Journal of Control, Measurement, and System Integration*, 7(4):227–236, 2014.

[7] Wenjing Cao, Masakazu Mukai, Taketoshi Kawabe, Hikaru Nishira, and Noriaki Fujiki. Cooperative vehicle path generation during merging using model predictive control with real-time optimization. *Control Engineering Practice*, 34:98–105, 2015.

[8] Lei Chen and Cristofer Englund. Cooperative intersection management: a survey. *IEEE Transactions on Intelligent Transportation Systems*, 17(2):570–586, 2016.

[9] Alessandro Colombo and Domitilla Del Vecchio. Least restrictive supervisors for intersection collision avoidance: A scheduling approach. *IEEE Transactions on Automatic Control*, 60(6):1515–1527, 2015.

[10] SAE On-Road Automated Vehicle Standards Committee et al. Taxonomy and definitions for terms related to on-road motor vehicle automated driving systems. *SAE International*, 2014.

[11] Pierre De Beaucorps, Thomas Streubel, Anne Verroust-Blondet, Fawzi Nashashibi, Benazouz Bradai, and Paulo Resende. Decision-making for automated vehicles at intersections adapting human-like behavior. In *2017 IEEE Intelligent Vehicles Symposium (IV)*, pages 212–217. IEEE, 2017.

[12] Gabriel R de Campos, Adam H Runarsson, Fredrik Granum, Paolo Falcone, and Klas Alenljung. Collision avoidance at intersections: A probabilistic threat-assessment and decision-making system for safety interventions. In *17th International IEEE Conference on Intelligent Transportation Systems (ITSC)*, pages 649–654. IEEE, 2014.

[13] Gabriel Rodrigues de Campos, Paolo Falcone, Robert Hult, Henk Wymeersch, and Jonas Sjöberg. Traffic coordination at road intersections: Autonomous decision-making algorithms using model-based heuristics. *IEEE Intelligent Transportation Systems Magazine*, 9(1):8–21, 2017.

[14] Gabriel Rodrigues de Campos, Paolo Falcone, and Jonas Sjöberg. Autonomous cooperative driving: a velocity-based negotiation approach for intersection crossing. In *16th International IEEE Conference on Intelligent Transportation Systems (ITSC 2013)*, pages 1456–1461. IEEE, 2013.

[15] E. Debada, L. Makarem, and D. Gillet. A virtual vehicle based coordination framework for autonomous vehicles in heterogeneous scenarios. In *2017 IEEE International Conference on Vehicular Electronics and Safety (ICVES)*, pages 51–56, June 2017.

[16] Ezequiel Debada and Denis Gillet. Cooperative circulating behavior at single-lane roundabouts. In *2018 IEEE 21st International Conference on Intelligent Transportation Systems (ITSC)*, pages 3306–3313. IEEE, 2018.

[17] Ezequiel Debada and Denis Gillet. Virtual vehicle-based cooperative maneuver planning for connected automated vehicles at single-lane roundabouts. *IEEE Intelligent Transportation Systems Magazine*, 10(ARTICLE):35–46, 2018.

[18] Ezequiel Debada and Denis Gillet. Merging into single-lane roundabouts in the presence of uncertainty. In *2019 IEEE Intelligent Transportation Systems Conference (ITSC)*, pages 3168–3175. IEEE, 2019.

[19] Ezequiel Debada, Laleh Makarem, and Denis Gillet. A virtual vehicle based coordination framework for autonomous vehicles in heterogeneous scenarios. In *Vehicular Electronics and Safety (ICVES), 2017 IEEE International Conference on*, page in press. IEEE, 2017.

[20] Julien Diard, Pierre Bessiere, and Emmanuel Mazer. A survey of probabilistic models using the bayesian programming methodology as a unifying framework. 2003.

[21] Kurt Dresner and Peter Stone. Multiagent traffic management: A reservation-based intersection control mechanism. In *Proceedings of the Third International Joint Conference on Autonomous Agents and Multiagent Systems-Volume 2*, pages 530–537. IEEE Computer Society, 2004.

[22] Elias C Eze, Si-Jing Zhang, En-Jie Liu, and Joy C Eze. Advances in vehicular ad-hoc networks (vanets): Challenges and road-map for future development. *International Journal of Automation and Computing*, 13(1):1–18, 2016.

[23] Benjamin Fankhauser, Laleh Makarem, and Denis Gillet. Collision-free intersection crossing of mobile robots using decentralized navigation functions on predefined paths. In *Cybernetics and Intelligent Systems (CIS), 2011 IEEE 5th International Conference on*, pages 392–397. IEEE, 2011.

[24] Peter G Gipps. A model for the structure of lane-changing decisions. *Transportation Research Part B: Methodological*, 20(5):403–414, 1986.

[25] David González, Joshué Pérez, Vicente Milanés, and Fawzi Nashashibi. A review of motion planning techniques for automated vehicles. *IEEE Transactions on Intelligent Transportation Systems*, 17(4):1135–1145, 2015.

[26] Maximilian Graf, Oliver Speidel, and Klaus Dietmayer. A model based motion planning framework for automated vehicles in structured environments. In *2019 IEEE Intelligent Vehicles Symposium (IV)*, pages 201–206. IEEE, 2019.

[27] Jean Gregoire, Silvere Bonnabel, and Arnaud De La Fortelle. Priority-based coordination of robots. 2014.

[28] Michael R Hafner, Drew Cunningham, Lorenzo Caminiti, and Domitilla Del Vecchio. Cooperative collision avoidance at intersections: Algorithms and experiments. *IEEE Transactions on Intelligent Transportation Systems*, 14(3):1162–1175, 2013.

[29] MR Hafner, D Cunningham, L Caminiti, and D Del Vecchio. Automated vehicle-to-vehicle collision avoidance at intersections. In *Proceedings of world congress on intelligent transport systems*, 2011.

[30] Zehao Huang, Weichao Zhuang, Guodong Yin, Liwei Xu, and Kai Luo. Cooperative merging for multiple connected and automated vehicles at highway on-ramps via virtual platoon formation. In *2019 Chinese Control Conference (CCC)*, pages 6709–6714. IEEE, 2019.

[31] Constantin Hubmann, Marvin Becker, Daniel Althoff, David Lenz, and Christoph Stiller. Decision making for autonomous driving considering interaction and uncertain prediction of surrounding vehicles. In *Intelligent Vehicles Symposium (IV), 2017 IEEE*, pages 1671–1678. IEEE, 2017.

[32] Constantin Hubmann, Nils Quetschlich, Jens Schulz, Julian Bernhard, Daniel Althoff, and Christoph Stiller. A pomdp maneuver planner for occlusions in urban scenarios. In *2019 IEEE Intelligent Vehicles Symposium (IV)*, pages 2172–2179. IEEE, 2019.

[33] Constantin Hubmann, Jens Schulz, Gavin Xu, Daniel Althoff, and Christoph Stiller. A belief state planner for interactive merge maneuvers in congested traffic. In *2018 21st International Conference on Intelligent Transportation Systems (ITSC)*, pages 1617–1624. IEEE, 2018.

[34] Robert Hult, Gabriel R Campos, Erik Steinmetz, Lars Hammarstrand, Paolo Falcone, and Henk Wymeersch. Coordination of cooperative autonomous vehicles: Toward safer and more efficient road transportation. *IEEE Signal Processing Magazine*, 33(6):74–84, 2016.

[35] Rajendra K Jain, Dah-Ming W Chiu, and William R Hawe. A quantitative measure of fairness and discrimination. *Eastern Research Laboratory, Digital Equipment Corporation, Hudson, MA*, 1984.

[36] Andrew H Jazwinski. *Stochastic processes and filtering theory*. Courier Corporation, 2007.

[37] I Ge Jin, Bastian Schürmann, Richard M Murray, and Matthias Althoff. Risk-aware motion planning for automated vehicle among human-driven cars. In *2019 American Control Conference (ACC)*, pages 3987–3993. IEEE, 2019.

[38] Qiu Jin, Guoyuan Wu, Kanok Boriboonsomsin, and Matthew Barth. Platoon-based multi-agent intersection management for connected vehicle. In *16th International IEEE Conference on Intelligent Transportation Systems (ITSC 2013)*, pages 1462–1467. IEEE, 2013.

[39] Simon J Julier and Jeffrey K Uhlmann. New extension of the kalman filter to nonlinear systems. In *Signal processing, sensor fusion, and target recognition VI*, volume 3068, pages 182–193. International Society for Optics and Photonics, 1997.

[40] Kamal Kant and Steven W Zucker. Toward efficient trajectory planning: The path-velocity decomposition. *The international journal of robotics research*, 5(3):72–89, 1986.

[41] Arne Kesting, Martin Treiber, and Dirk Helbing. General lane-changing model mobil for car-following models. *Transportation Research Record*, 1999(1):86–94, 2007.

[42] Hanna Kurniawati and Vinay Yadav. An online pomdp solver for uncertainty planning in dynamic environment. In *Robotics Research*, pages 611–629. Springer, 2016.

[43] Joyoung Lee and Byungkyu Park. Development and evaluation of a cooperative vehicle intersection control algorithm under the connected vehicles environment. *IEEE Transactions on Intelligent Transportation Systems*, 13(1):81–90, 2012.

[44] Stéphanie Lefèvre, Dizan Vasquez, and Christian Laugier. A survey on motion prediction and risk assessment for intelligent vehicles. *ROBOMECH journal*, 1(1):1, 2014.

[45] David Lenz, Tobias Kessler, and Alois Knoll. Tactical cooperative planning for autonomous highway driving using monte-carlo tree search. In *Intelligent Vehicles Symposium (IV), 2016 IEEE*, pages 447–453. IEEE, 2016.

[46] Li Li and Fei-Yue Wang. Cooperative driving at blind crossings using intervehicle communication. *IEEE Transactions on Vehicular Technology*, 55(6):1712–1724, 2006.

[47] Li Li, Fei-Yue Wang, and Yi Zhang. Cooperative driving at lane closures. In *Intelligent Vehicles Symposium, 2007 IEEE*, pages 1156–1161. IEEE, 2007.

[48] Xiao-Yun Lu and J Karl Hedrick. Longitudinal control algorithm for automated vehicle merging. *International Journal of Control*, 76(2):193–202, 2003.

[49] Xiao-Yun Lu, Han-Shue Tan, Steven E Shladover, and J Karl Hedrick. Implementation of longitudinal control algorithm for vehicle merging. *Ann Arbor*, 2000.

[50] Kristijan Macek, Dizan Alejandro Vasquez Govea, Thierry Fraichard, and Roland Siegwart. Towards safe vehicle navigation in dynamic urban scenarios. 2009.

[51] Silvia Magdici and Matthias Althoff. Fail-safe motion planning of autonomous vehicles. In *2016 IEEE 19th International Conference on Intelligent Transportation Systems (ITSC)*, pages 452–458. IEEE, 2016.

[52] Laleh Makarem and Denis Gillet. Decentralized coordination of autonomous vehicles at intersections. *IFAC Proceedings Volumes*, 44(1):13046–13051, 2011.

[53] Laleh Makarem and Denis Gillet. Fluent coordination of autonomous vehicles at intersections. In *2012 IEEE international conference on systems, man, and cybernetics (SMC)*, pages 2557–2562. IEEE, 2012.

[54] Laleh Makarem and Denis Gillet. Model predictive coordination of autonomous vehicles crossing intersections. In *16th International IEEE Conference on Intelligent Transportation Systems (ITSC 2013)*, pages 1799–1804. IEEE, 2013.

[55] Dan Marinescu, Jan Čurn, Mélanie Bouroche, and Vinny Cahill. On-ramp traffic merging using cooperative intelligent vehicles: A slot-based approach. In *Intelligent Transportation Systems (ITSC), 2012 15th International IEEE Conference on*, pages 900–906. IEEE, 2012.

[56] Stefano Masi, Philippe Xu, and Philippe Bonnifait. Adapting the virtual platooning concept to roundabout crossing. In *2018 IEEE Intelligent Vehicles Symposium (IV)*, pages 1366–1372. IEEE, 2018.

[57] Vicente Milanés, Jorge Godoy, Jorge Villagrá, and Joshué Pérez. Automated on-ramp merging system for congested traffic situations. *IEEE Transactions on Intelligent Transportation Systems*, 12(2):500–508, 2011.

[58] Vicente Milanés, Joshué Pérez, Enrique Onieva, and Carlos González. Controller for urban intersections based on wireless communications and fuzzy logic. *IEEE Transactions on Intelligent Transportation Systems*, 11(1):243–248, 2009.

[59] Milos N Mladenovic and Montasir Abbas. Priority-based intersection control framework for self-driving vehicles: Agent-based model development and evaluation. In *Connected Vehicles and Expo (ICCVE), 2014 International Conference on*, pages 377–384. IEEE, 2014.

[60] Luis Yoichi Morales, Akai Naoki, Yuki Yoshihara, and Hiroshi Murase. Towards predictive driving through blind intersections. In *2018 21st International Conference on Intelligent Transportation Systems (ITSC)*, pages 716–722. IEEE, 2018.

[61] Hafida Mouhagir, Véronique Cherfaoui, Reine Talj, François Aioun, and Franck Guillemard. Using evidential occupancy grid for vehicle trajectory planning under uncertainty with tentacles. In *2017 IEEE 20th International Conference on Intelligent Transportation Systems (ITSC)*, pages 1–7. IEEE, 2017.

[62] Yannik Nager, Andrea Censi, and Emilio Frazzoli. What lies in the shadows? safe and computation-aware motion planning for autonomous vehicles using intent-aware dynamic shadow regions. In *2019 International Conference on Robotics and Automation (ICRA)*, pages 5800–5806. IEEE, 2019.

[63] Maximilian Naumann, Hendrik Konigshof, Martin Lauer, and Christoph Stiller. Safe but not overcautious motion planning under occlusions and limited sensor range. In *2019 IEEE Intelligent Vehicles Symposium (IV)*, pages 140–145. IEEE, 2019.

[64] Amaury Nègre, Lukas Rummelhard, and Christian Laugier. Hybrid sampling bayesian occupancy filter. In *2014 IEEE Intelligent Vehicles Symposium Proceedings*, pages 1307–1312. IEEE, 2014.

[65] Ty Nguyen and Tsz-Chiu Au. A constant-time algorithm for checking reachability of arrival times and arrival velocities of autonomous vehicles. 2019.

[66] Julia Nilsson, Mattias Brännström, Jonas Fredriksson, and Erik Coelingh. Longitudinal and lateral control for automated yielding maneuvers. *IEEE Transactions on Intelligent Transportation Systems*, 17(5):1404–1414, 2016.

[67] Enrique Onieva, Vicente Milanés, Jorge Villagra, Joshué Pérez, and Jorge Godoy. Genetic optimization of a vehicle fuzzy decision system for intersections. *Expert Systems with Applications*, 39(18):13148–13157, 2012.

[68] Piotr F Orzechowski, Annika Meyer, and Martin Lauer. Tackling occlusions & limited sensor range with set-based safety verification. In *2018 21st International Conference on Intelligent Transportation Systems (ITSC)*, pages 1729–1736. IEEE, 2018.

[69] Brian Paden, Michal Čáp, Sze Zheng Yong, Dmitry Yershov, and Emilio Frazzoli. A survey of motion planning and control techniques for self-driving urban vehicles. *IEEE Transactions on intelligent vehicles*, 1(1):33–55, 2016.

[70] Brian Paden and Emilio Frazzoli. A generalized label correcting method for optimal kinodynamic motion planning. *arXiv preprint arXiv:1607.06966*, 2016.

[71] Christian Pek and Matthias Althoff. Computationally efficient fail-safe trajectory planning for self-driving vehicles using convex optimization. In *2018 21st International Conference on Intelligent Transportation Systems (ITSC)*, pages 1447–1454. IEEE, 2018.

[72] Xiangjun Qian, Jean Gregoire, Arnaud De La Fortelle, and Fabien Moutarde. Decentralized model predictive control for smooth coordination of automated vehicles at intersection. In *Control Conference (ECC), 2015 European*, pages 3452–3458. IEEE, 2015.

[73] Xiangjun Qian, Jean Gregoire, Fabien Moutarde, and Arnaud De La Fortelle. Priority-based coordination of autonomous and legacy vehicles at intersection. In *17th international IEEE conference on intelligent transportation systems (ITSC)*, pages 1166–1171. IEEE, 2014.

[74] Jackeline Rios-Torres and Andreas A Malikopoulos. A survey on the coordination of connected and automated vehicles at intersections and merging at highway on-ramps. *IEEE Transactions on Intelligent Transportation Systems*, 18(5):1066–1077, 2017.

[75] Albert Rizaldi, Fabian Immler, and Matthias Althoff. A formally verified checker of the safe distance traffic rules for autonomous vehicles. In *NASA Formal Methods Symposium*, pages 175–190. Springer, 2016.

[76] Takeshi Sakaguchi, Atsuya Uno, and Sadayuki Tsugawa. An algorithm for merging control of vehicles on highways. In *Intelligent Robots and Systems, 1997. IROS'97., Proceedings of the 1997 IEEE/RSJ International Conference on*, volume 3, pages V15–V16. IEEE, 1997.

[77] Gunther K Schmidt and Bernd Posch. A two-layer control scheme for merging of automated vehicles. In *The 22nd IEEE Conference on Decision and Control*, pages 495–500. IEEE, 1983.

[78] Wilko Schwarting, Javier Alonso-Mora, and Daniela Rus. Planning and decision-making for autonomous vehicles. *Annual Review of Control, Robotics, and Autonomous Systems*, (0), 2018.

[79] Christoph Stiller, Georg Farber, and Soren Kammel. Cooperative cognitive automobiles. In *Intelligent Vehicles Symposium, 2007 IEEE*, pages 215–220. IEEE, 2007.

[80] Adam Stocker and Susan Shaheen. Shared automated vehicles: Review of business models. International Transport Forum Discussion Paper, 2017.

[81] Alireza Talebpour and Hani S Mahmassani. Influence of connected and autonomous vehicles on traffic flow stability and throughput. *Transportation Research Part C: Emerging Technologies*, 71:143–163, 2016.

[82] Ömer Sahin Tas, Felix Hauser, and Christoph Stiller. Decision-time postponing motion planning for combinatorial uncertain maneuvering. In *2018 21st International Conference on Intelligent Transportation Systems (ITSC)*, pages 2419–2425. IEEE, 2018.

[83] Ömer Şahin Taş and Christoph Stiller. Limited visibility and uncertainty aware motion planning for automated driving. In *2018 IEEE Intelligent Vehicles Symposium (IV)*, pages 1171–1178. IEEE, 2018.

[84] MK Tay, Kamel Mekhnacha, Cheng Chen, Manuel Yguel, and Christian Laugier. An efficient formulation of the bayesian occupation filter for target tracking in dynamic environments. *International Journal of Vehicle Autonomous Systems*, 6(1):155, 2008.

[85] Tomer Toledo, Haris N Koutsopoulos, and Moshe E Ben-Akiva. Modeling integrated lane-changing behavior. *Transportation Research Record*, 1857(1):30–38, 2003.

[86] Martin Treiber, Ansgar Hennecke, and Dirk Helbing. Congested traffic states in empirical observations and microscopic simulations. *Physical review E*, 62(2):1805, 2000.

[87] Chris Urmson, Joshua Anhalt, Drew Bagnell, Christopher Baker, Robert Bittner, MN Clark, John Dolan, Dave Duggins, Tugrul Galatali, Chris Geyer, et al. Autonomous driving in urban environments: Boss and the urban challenge. *Journal of Field Robotics*, 25(8):425–466, 2008.

[88] Jessica Van Brummelen, Marie OBrien, Dominique Gruyer, and Homayoun Najjaran. Autonomous vehicle perception: The technology of today and tomorrow. *Transportation research part C: emerging technologies*, 89:384–406, 2018.

[89] Zhen Wang, Xiaowei Shi, and Xiaopeng Li. Review of lane-changing maneuvers of connected and automated vehicles: Models, algorithms and traffic impact analyses. *Journal of the Indian Institute of Science*, pages 1–11, 2019.

[90] Erik Ward, Niclas Evestedt, Daniel Axehill, and John Folkesson. Probabilistic model for interaction aware planning in merge scenarios. *IEEE Transactions on Intelligent Vehicles*, 2(2):133–146, 2017.

[91] Moritz Werling, Sören Kammel, Julius Ziegler, and Lutz Gröll. Optimal trajectories for time-critical street scenarios using discretized terminal manifolds. *The International Journal of Robotics Research*, 31(3):346–359, 2012.

[92] Moritz Werling, Julius Ziegler, Sören Kammel, and Sebastian Thrun. Optimal trajectory generation for dynamic street scenarios in a frenet frame. In *2010 IEEE International Conference on Robotics and Automation*, pages 987–993. IEEE, 2010.

[93] Theodore L Willke, Patcharinee Tientrakool, and Nicholas F Maxemchuk. A survey of inter-vehicle communication protocols and their applications. *IEEE Communications Surveys & Tutorials*, 11(2):3–20, 2009.

[94] Jia Wu, Florent Perronnet, and Abdeljalil Abbas-Turki. Cooperative vehicle-actuator system: A sequence-based framework of cooperative intersections management. *IET Intelligent Transport Systems*, 8(4):352–360, 2013.

[95] Chairit Wuthishuwong and Ansgar Traechtler. Coordination of multiple autonomous intersections by using local neighborhood information. In *2013 international conference on connected vehicles and expo (ICCVE)*, pages 48–53. IEEE, 2013.

[96] Wenda Xu, Jia Pan, Junqing Wei, and John M Dolan. Motion planning under uncertainty for on-road autonomous driving. In *2014 IEEE International Conference on Robotics and Automation (ICRA)*, pages 2507–2512. IEEE, 2014.

[97] Yuki Yoshihara, Yoichi Morales, Naoki Akai, Eijiro Takeuchi, and Yoshiki Ninomiya. Autonomous predictive driving for blind intersections. In *2017 IEEE/RSJ International Conference on Intelligent Robots and Systems (IROS)*, pages 3452–3459. IEEE, 2017.

[98] Ming-Yuan Yu, Ram Vasudevan, and Matthew Johnson-Roberson. Occlusion-aware risk assessment for autonomous driving in urban environments. *IEEE Robotics and Automation Letters*, 4(2):2235–2241, 2019.

[99] Wei Zhan, Changliu Liu, Ching-Yao Chan, and Masayoshi Tomizuka. A non-conservatively defensive strategy for urban autonomous driving. In *2016 IEEE 19th International Conference on Intelligent Transportation Systems (ITSC)*, pages 459–464. IEEE, 2016.

Ezequiel Gonzalez Debada
PhD in Electrical Engineering

Contact

Lausanne, Switzerland.
ezgode@gmail.com
+41 788859101
10/11/1990
ezequielgdebada
www.ezgodephotography.com

Profile

Specialist in motion planning for automated vehicles. Passionated about technology, control systems, robotics, Intelligent Transportation Systems and machine learning. Methodological, creative, meticulous, problem-solver, team-player.

Aficionado to photography, sports, traveling, DIY electronic, craft projects, and digital design.

Languages

Spanish (native)
English (C2)
French (A2)

Technical & computer skills

Matlab & Simulink
Technical writing
Latex
Photoshop, Illustrator
Python
Optimal control
Machine Learning
HTML, CSS, Javascript
Git
C, C++
Catia
LabView
PLC Programming

Education

PhD. in Electrical Engineering **2015-2020**
École Politechnique Fédéral de Lausanne, Switzerland
Courses in machine learning, convex optimization, and simulation.

Master in Automatics, Robotics and Telematics **2013-2015**
Universidad de Sevilla, Spain
Courses in predictive, robust control, robotics and computer vision.

Licenciatura in Industrial Engineering **2004-2013**
Universidad de Sevilla, Spain
Specialized in Industrial Automation (class ranking: 4th out of 190).

Relevant academic projects

Motion planning for CAVs: a study on roundabouts **2015-2020**
PhD thesis, REACT group, EPFL, Lausanne, Switzerland
Collaboration with PSA Group and Safran
Development of a microscopic traffic simulator, and motion planning strategies for AVs in partially connected scenarios. Application of Bayesian Occupancy Grid and Particles Filters to handle occlusions, and MPC, quadratic optimization, machine learning, and reachability set analysis to address decision making.

Control of a battery swapping station supported by ITS **2013-2015**
Master project, Universidad de Sevilla, Spain
Design of a non-linear MPC to control the charging process of Battery Swapping Stations.

Torque vectoring design of a 4 in-wheel electric vehicle **2004-2013**
Bachelor project, Universidad de Sevilla, Spain
Implementation of an accurate dynamics car model, design of torque vectoring

Awards

Best student paper award *(IEEE ITSC 2019)* **2019**
Paper: “Merging into Single-Lane Roundabouts in the Presence of Uncertainty”.

Best modeling, simulation and optimization work *(CEA)* **2015**
Paper: “Torque distribution strategy for a four in-wheel fully electric car”.

Banco de Ideas award *(chair Telefónica)* **2013**

Work experience

Research assistant **2013-2015**
Model Predictive Control research lab, Universidad de Sevilla, Spain
Involved in the Europen project DYMASoS, focused on studying coalitional control and the applications of game theory to distributed control systems.

Tutoring university and high school students **2015-2019**
Calculus, algebra, chemistry, technical drawing.

Publications

Merging to Single-Lane Roundabouts in the Presence of Uncertainty,
E. Debada, D. Gillet., IEEE ITSC 2019.

Cooperative Circulating Behavior at SIngle-lane Roundabouts
E. Debada, D. Gillet., IEEE ITSC 2018.

VV-based cooperative maneuver planning for CAVs at Single-lane Roundabouts,
E. Debada, D. Gillet, IEEE Intelligent Transportation Systems Magazine, 2018

A Virtual Vehicle based coordination framework for AVs in heterogeneous scenarios
E. Debada, L. Makarem, D. Gillet, IEEE ICVES 2017.

Autonomous coordination of heterogeneous vehicles at roundabouts,
E. Debada, L. Makarem, D. Gillet, IEEE ITSC 2016.